ABSTRACT

Title of Document: GEOCHEMICAL AND RADIOMETRIC CONSTRAINTS ON THE REDOX HISTORY OF LATE EDIACARAN OCEANS

Sara Peek, Master of Science, 2012

Directed By: Professor Alan Jay Kaufman, Geology

Over the past decade, significant field and laboratory studies have been devoted to furthering understanding of the chemical conditions that accompanied the origin and diversification of Earth's earliest multicellular animals during the Ediacaran Period (ca. 635-542 Ma). Here, I apply geochemical methods to excellently preserved and exposed sections spanning approximately the last 10 million years of the Ediacaran Period. From Arctic Siberia, hundreds of samples were collected at high stratigraphic resolution, from which carbonate carbon and oxygen profiles have been produced, along with organic carbon and sulfur isotope data. From South China, a carbonate carbon isotope profile has been constructed. Radiometric dates constrain the timing of deposition in our sections. This work uses geochemical data and radiometric dating to inform and improve intra- and inter-basinal correlation, and serves as a preliminary study confirming the suitability of our Siberian sections to the study of oxygenation during the latest Ediacaran Period.

GEOCHEMICAL AND RADIOMETRIC CONSTRAINTS ON THE REDOX HISTORY OF LATE EDIACARAN OCEANS

By

Sara Peek

Thesis submitted to the Faculty of the Graduate School of the
University of Maryland, College Park, in partial fulfillment
of the requirements for the degree of
Master of Science
2012

Advisory Committee:
Professor Alan Jay Kaufman, Chair
Professor James Farquhar
Professor Shuhai Xiao

Dedication

To Lusann Wren Yang and Evan Murphy, who helped.

Acknowledgements

Prof. Jay Kaufman, Prof. James Farquhar, Prof. Shuhai Xiao, Prof. Aaron Martin, and Prof. Phil Piccoli provided research assistance in the preparation of this document; Craig Hebert and Yongbo Peng provided laboratory support. This work could not have been undertaken without the help of our Russian collaborators, Dr. Dmitrii Grazhdankin, Dr. Boris Kochnev, and Vladimir Rogov. Natalie Sievers, Rebecca Ohly, and Huan Cui aided in sample preparation; without their help, not nearly so much could have been accomplished.

I am also grateful for funding from the University of Maryland Geology Department, the National Science Foundation, NASA Exobiology, and the Geological Society of America.

Table of Contents

List of Tables

List of Figures

Chapter 1: Introduction

The Ediacaran Period (635-542 Ma) saw the rise and diversification of Earth's first complex organisms, the so-called Ediacara biota. Representatives of the Ediacaran biota appeared in Newfoundland as early as 575 Ma, immediately following the end of the Gaskiers glaciation at ca. 580 Ma (Narbonne and Gehling, 2003, Bowring et al, 2003). This evolutionary milestone is set against a backdrop of profound and geologically rapid environmental change: significant tectonic events, including the Pan-African orogeny (Kaufman et al, 1993), the possible reorganization of the oceanic carbon cycle (Rothman et al, 2003), and the buildup of oxygen (Canfield et al., 2006) necessary to support these complex organisms, in the atmosphere and oceans.

A large number of geochemical systems have been harnessed to provide insight into oxygen concentrations in the late Neoproterozoic. Specialized techniques, including iron speciation analysis (Canfield et al., 2008), rare earth element (REE) and trace element analysis, and molybdenum (Dahl et al., 2010) and cerium (Li et al, 2011) abundance and isotopic composition, have been developed to further understanding of ocean oxidation. Additionally, common geochemical measurements, including carbon and oxygen isotopes, carbonate-associated sulfate (CAS) isotopes, and strontium isotopes can serve as more indirect indicators of oceanic redox conditions. Application of these techniques to late Neoproterozoic rocks suggests that oxygen levels rose throughout the Ediacaran Period.

Carbon and Strontium Isotopes

Modeling of carbon and strontium isotope records for the Ediacaran Period also suggest an increase in atmospheric oxygen levels (Kaufman et al, 1993). McFadden and others (2008), working in South China, documented an example of a system in which organic carbon isotopic values were invariant at a time of wide swings in carbonate carbon isotopic values. This suggests that a large pool of dissolved organic carbon (DOC) may have buffered organic carbon isotopic values (*cf.* Rothman et al., 2003). Later in the Ediacaran Period, however, organic and inorganic carbon co-vary smoothly (McFadden et al., 2008), suggesting depletion of the DOC pool (and concomitant increase in the DIC pool) as oxygen values increased. The methods of these studies will be applied to new sections in arctic Siberia and South China in this study.

Carbonate-associated sulfate (CAS)

Historically, the concentration and isotopic composition of oceanic sulfate depended on the analysis of evaporitic deposits (see, for example, Claypool et al., 1980), which are sporadic and limited in spatial distribution, and, as soluble minerals, have a low preservation potential. More recently, Burdett et al. (1989) found that measurable amounts of sulfate (carbonate-associated sulfate (CAS)) were found within the lattice structure of carbonaceous shells of oceanic organisms. Burdett et al. (1989) showed that the concentration and isotopic composition of lattice-bound sulfate in planktonic foraminifera was representative of that of the water in which it lived. Burdett's conclusions have since been extended to carbonates precipitated inorganically.

Over the intervening time, CAS has been found to be a useful proxy for seawater sulfate concentrations and isotopic compositions, the much greater prevalence of

carbonate rock relative to evaporites has allowed great expansion of our knowledge of sulfate concentrations and compositions in the ancient ocean. However, sulfate data produced in this way is not without caveats. The original isotopic composition of CAS may be influenced by bacterial sulfate reduction or by pyrite oxidation during deposition of carbonate; the signal can also be modified by diagenesis. However, at least one study (Gill et al., 2008) has found that meteoric diagenesis results in only minor modifications of CAS signal in modern carbonates, and another (Marenco et al., 2008b) has concluded that, in at least some cases, dolomitization does not significantly degrade the signal. CAS results may also be influenced by the methods used for sulfate extraction.

Initial CAS studies used only samples uncontaminated by sulfate-bearing phases; if unaltered shells were not used (as in Burdett et al., 1989; Kampschulte et al., 2001) samples with sulfide minerals or evaporite casts were avoided. These early studies made little effort to remove soluble sulfates or sulfides, beyond sample choice. Later studies have used single or multiple washes with NaCl, NaOCl, and H_2O_2 to remove and/or oxidize soluble sulfates, organic sulfur compounds, and sulfides, respectively (McFadden et al., 2008; Kampschulte et al., 2004; Lyons et al., 2005).

Some work has been done to quantify the effects of sulfide minerals on CAS isotopic values (Marenco et al, 2008a); even small amounts of pyrite (~1 wt%) appear to influence $\delta^{34}S_{CAS}$ by several per mil. Other studies, such as one by McFadden et al. (2008), have focused their preparatory procedures on the removal of sulfides, in this case via oxidation with two rinses of 30% hydrogen peroxide, followed by a single water rinse. Notably, little work has been published quantifying the amount and isotopic composition of soluble sulfates removed by leaching CAS samples.

CAS and Oxygen

The magnitude of sulfur isotope fractionation has been related to oceanic sulfate concentration, and hence oxidation state (Fike et al., 2006; Habicht et al., 2002). Sulfur isotope studies in the Ediacaran of Oman by Fike et al. (2006) suggests that oceanic sulfate levels were below 200 μM in pre-Ediacaran time. Below this threshold, sulfate-reducing bacteria impart little to no significant fractionation to sulfates as they are converted to sulfides, which may then be deposited as pyrite if ferrous iron is available (Habicht et al, 2002). Fike et al. (2006) found that sulfur isotope fractionation between oceanic sulfate and pyrite is only ~0-10‰ at 635 Ma, gradually rising to modern values by 580 Ma, and reaches the maximum fractionation of simple bacterial sulfate reduction (-46‰) at ~549 Ma. Geochronological constraints were inferred by chemostratigraphic correlation to sections where U-Pb zircon dating was available, including the Doushantuo Formation of South China. The increasing fractionation between sulfate and sulfide suggests a gradual increase in oceanic sulfate levels. Increases in sulfate levels have been ascribed to oxidative weathering of pyrites in crustal rocks as far back as the Archean (Anbar et al, 2007).

However, there is another possible indicator of low-oxygen conditions: super-heavy pyrite. Fike et al. (2006) records $\delta^{34}S_{py}$ values of as high at +15‰ at the base of the Ediacaran in Oman. However, while $\Delta\delta^{34}S$ in that study approaches zero at the base of the Ediacaran, this data fits into the standard biological fractionation paradigm – pyrite sulfur isotopic values are always lower than those of CAS. Other workers, however, including Ries et al. (2009) and Shen et al. (2010; 2011), have recorded negative $\Delta\delta^{34}S$ values. Since research by Habicht et al. (2002) shows that under low sulfate conditions

$\Delta\delta^{34}S$ goes to zero but does not invert, these inverted values are telling us something about the conditions under which the sulfides were deposited. Ries et al. (2009) lays out a number of scenarios under which inverted $\Delta\delta^{34}S$ could be expected, including ocean stratification and sulfide reoxidation. In the former scenario, micrite is formed in the upper ocean, recording the CAS value of surface waters, and is subsequently deposited in deeper waters. Sulfides, on the other hand, may be formed via bacterial sulfate reduction acting on deeper waters with different $\delta^{34}S$ values, allowing pyrite $\delta^{34}S$ values to be heavier than $\delta^{34}S$ of CAS. Close study of local geology is required to determine the most likely depositional scenario.

Overall, there is consensus that oxygen levels rose relative to earlier levels throughout the Ediacaran Period, but that global oxygenation, especially of the deep oceans, was ongoing. None of the mentioned indicators allows absolute quantification of oxygen levels; however, modeling efforts, such as those by Kaufman et al. (1993), suggest that oxygen levels rose to near-modern levels by the end of the Ediacaran Period. The coincident rise and diversification of large, complex organisms suggests a casual evolutionary link.

In Pursuit of a Correlative Framework

Carbon, oxygen, strontium, and radiometric ages have all been used to inform and improve lithologically-based correlation schemes. Ancient sections lacking absolute dates are routinely correlated by carbon isotope excursions (see, for example, Kaufman et al., 2006 and Saylor et al., 1998). Oxygen isotopic data gives insight into potential alteration. The long residence time of strontium in the ocean (~5 million years; Broecker et al., 1982) allows correlation of sections especially in times of rapid change in strontium

isotopic composition. However, radiometric ages, when available, are the best tool for inter-basinal correlation. In this work, we will have the opportunity to use each of these data types to inform and influence correlation between our sections and worldwide.

A Focus on Siberia and China

Due to the prevalence of excellently-preserved fossil material in well-preserved stratigraphically continuous packages of carbonate rock, the late Ediacaran sedimentary successions in arctic Siberia and South China are excellent places to evaluate the influence of oxygen on evolution through geochemical methods.

Geology

Siberia

In the Khorbusuonka region of the Olenek Uplift of northeastern Siberia (Figure 1.1), Ediacaran strata sit unconformably on the Riphean Khaipakh Formation; the succession, called the Khorbusuonka Group is divided into the Mastakh, Khatyspyt, and Turkut formations. These Ediacaran strata are overlain by the Cambrian Mattaia and Erkeket formations, designated the Kessyusa Group. These strata preserve a significant record of terminal Proterozoic and basal Cambrian Earth history (Knoll et al., 1995; Pelechaty et al,. 1996ab). Latest Ediacaran (~555-541 Ma) strata consist of a very well-exposed, well-preserved, ~280-meter-thick continuous succession of carbonate platform sediments outcropping along the Khorbusuonka and Olenek rivers in northeastern Siberia.

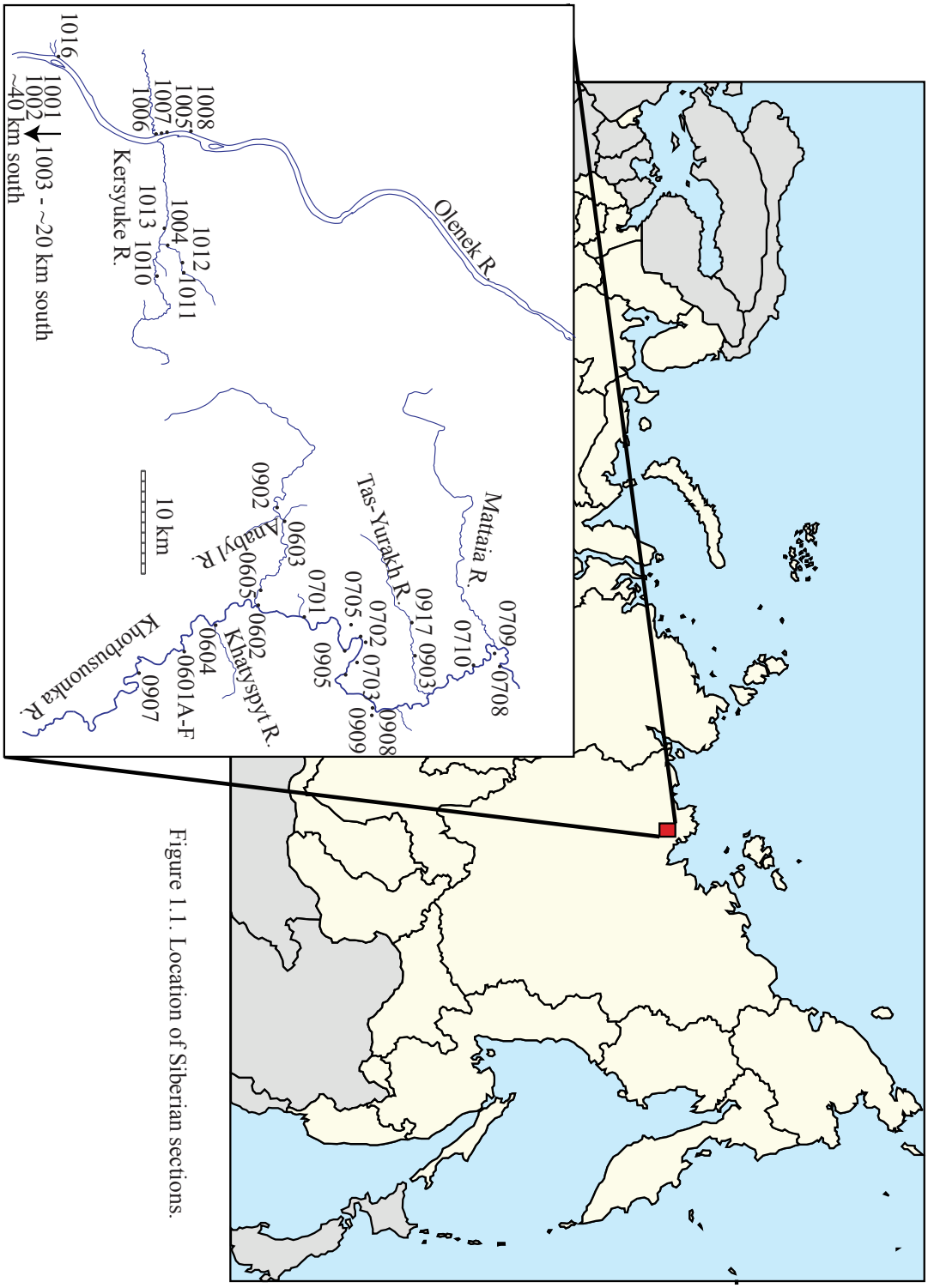

Figure 1.1. Location of Siberian sections. Khorbusuonka and Olenek River regions are shown. Sections 1001, 1002, and 1003 are located off the page as shown.

The Ediacaran Khorbusuonka River succession consists of three carbonate formations: the Mastakh, consisting of silicified peritidal dolomites with chert nodules, crossbedding, and wave ripples; the Khatyspyt, consisting of thin- to medium-bedded bituminous limestones; and the Turkut, comprising dolostones and limestones with pore space (probably secondary to dissolved evaporite minerals) filled with pyrobitumen (Bartley et al., 1998; Pelechaty et al., 1996b). The Early Cambrian Kessyusa Group, including the Mattaia Formation, on the other hand, consists largely of siliciclastic sediments. The Mattaia Formation comprises a diverse assemblage of siliciclastic, carbonate, and volcanic facies, Analysis of small shelly fossils suggests a Tommotian age for the Mattaia Formation (Grazhdankin, personal communication). (Figure 1.2).

Fossil Zones

The *Anabarites triculcatus* zone, indicative of Nemakit-Daldyn age in Siberian rocks, begins 10 m above the base of the Turkut Formation, followed by the *Purella antiqua* zone in the middle of the Mattaia Formation, and the *Nochoriocyathus sunnaginicus* zone only a few tens of meters higher in the Mattaia Formation (Grazhdankin, 2008; Figure 1.3). The Turkut Formation contains the first occurrence of the shelly invertebrates *Cambrotubulus sp*. and *Anabarites sp*. (Khomentovsky and Karlova, 1993), which conventionally have been taken to indicate basal Nemakit-Daldynian age, the beginning of the Cambrian Period in Siberia. However, the global indicator of earliest Cambrian age is the trace fossil *Treptictnus pedum* (formerly *Phycodes pedum*), which does not occur for another ~70 m, near the base of the Mattaia Formation, subsequent to diverse other trace and body fossils (Figure 1.2).

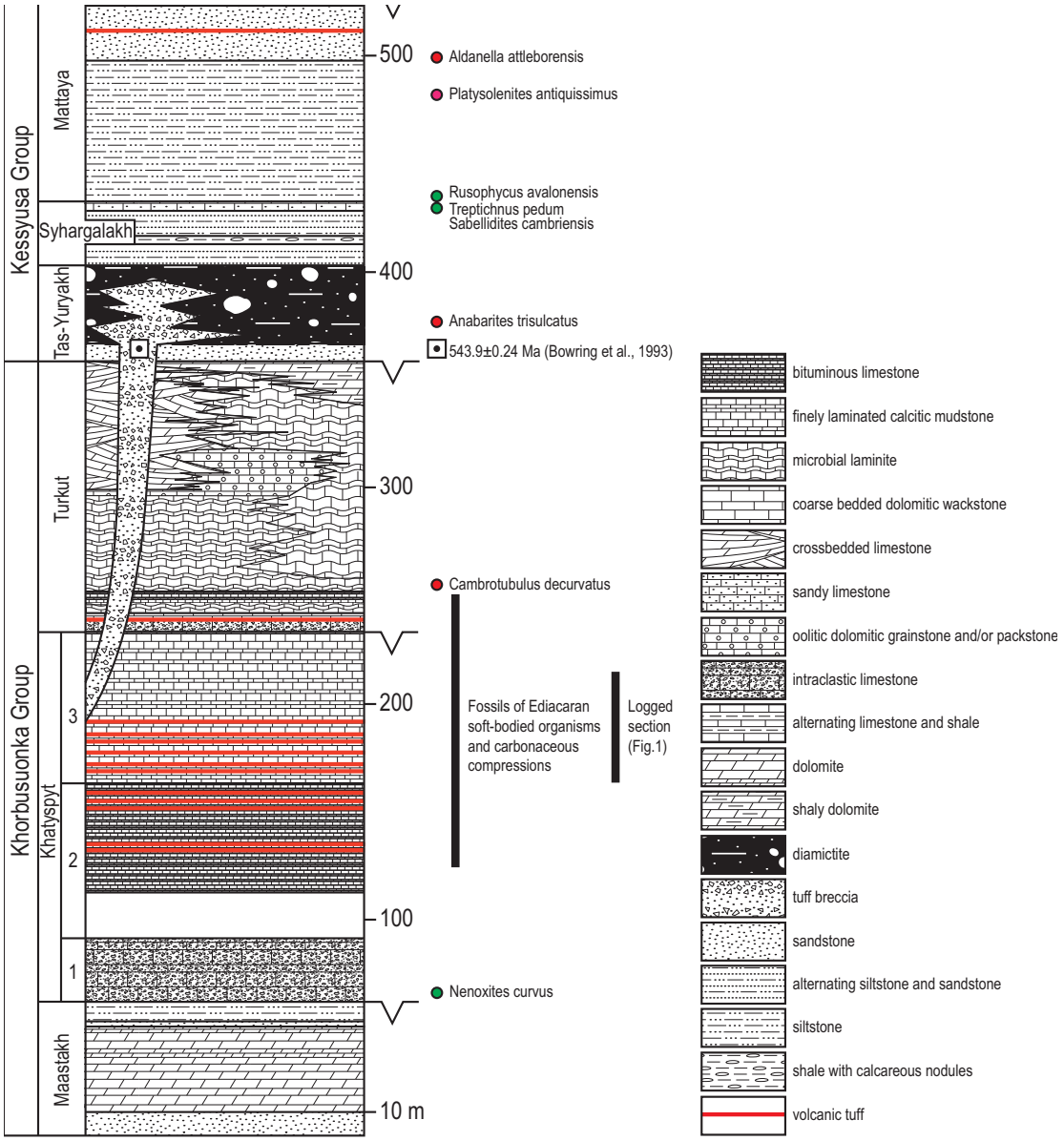

Figure 1.2. Composite section of Ediacaran and lower Cambrian strata of the Olenek Uplift in the north-eastern part of central Siberia, showing the position of the oldest small skeletal fossils (*Cambrotubulus decurvatus* and *Anabarites trisulcatus)*, the oldest ichnofabric (*Nenoxites curvus*), the index fossils that define the Precambrian/Cambrian boundary (*Sabellidites cambriensis, Treptichnus pedum, Rusophycus avalonensis, Platysolenites antiquissimus, Aldanella attleborensis*), the Ediacaran fossils and the stratigraphic position of the logged section. (Reproduced from Rogov et al., 2012.)

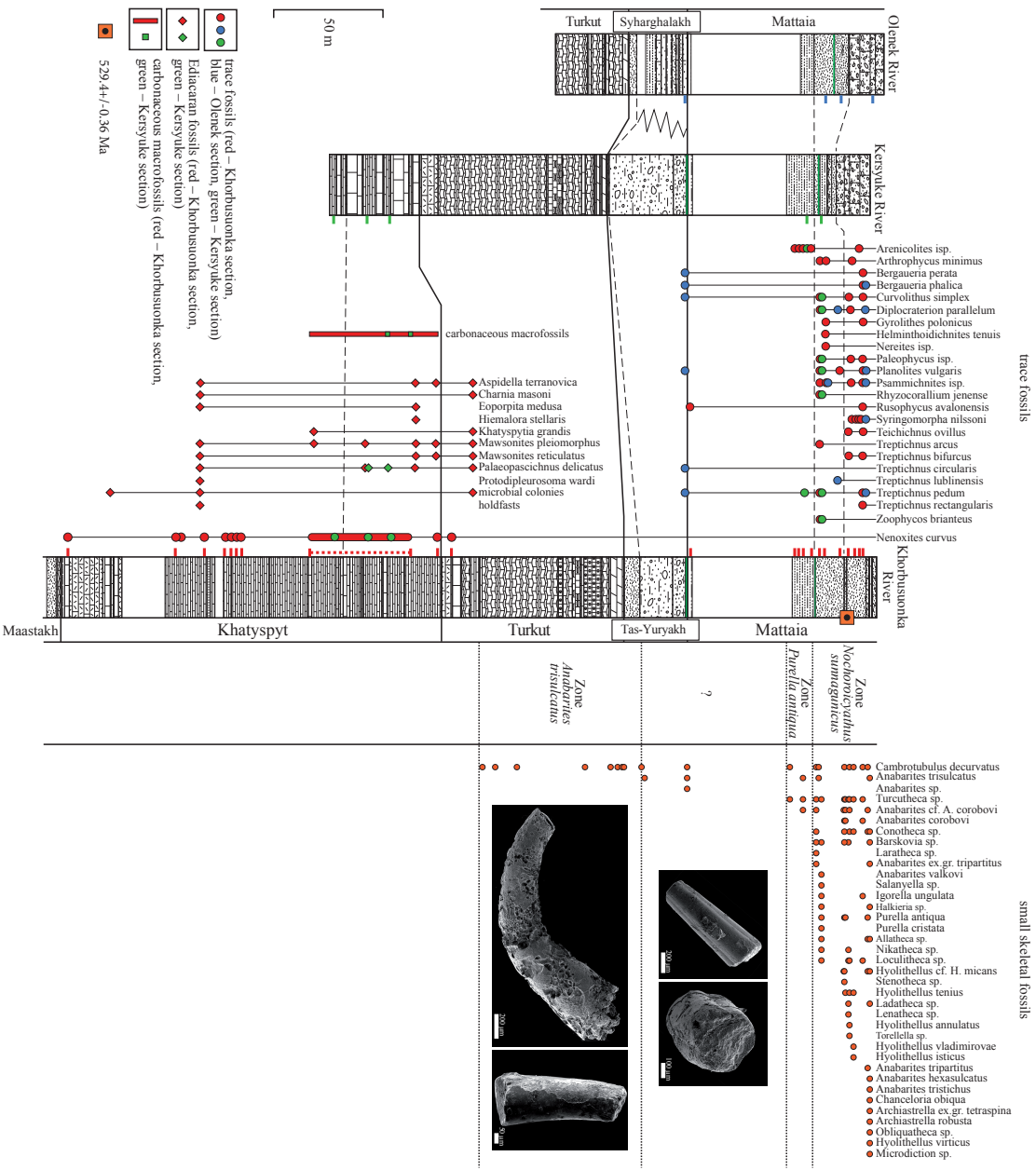

Figure 1.3. Occurrence of trace fossils and small skeletal fossils in Ediacaran Siberian sections. Courtesy Dmitrii Grazhdankin and Vladimir Rogov.

(However, it cannot be assumed that the first or last appearance of a fossil occurs at exactly the same time in different depositional settings). Any radiometric dates from the Mattaia Formation would constrain the positions of its fossils in time in a way that correlation to other sections via bio- or chemostratigraphy cannot.

The Khatyspyt Formation is an ideal setting for study of the latest Ediacaran Period, hosting an exceptional paleontological archive (Grazhdankin et al, 2008), containing a wide range of unique carbonate-hosted Ediacaran organisms, as well as carbonaceous macrofossils and trace fossils. The formation also exhibits two unusual types of preservation of the soft-bodied Ediacaran faunas, including authigenic carbonate cementation and preservation of carbonaceous films on bedding surfaces. Chemical data from this and surrounding formations can easily be placed into a biological and evolutionary context.

Given the lack of age-diagnostic fossils, reading Ediacaran time requires independent chronostratigraphic tools, such as chemostratigraphy. Low-resolution carbon and oxygen isotope data have been collected from the Khorbusuonka Group (Knoll et al., 1995; Pelechaty et al., 1996b), but the chemostratigraphic potential of these sections is largely untapped. High-resolution chemostratigraphy allows for more accurate identification of diagenetic versus secular variation, and may allow the data to better inform intra- and inter-basinal correlation. To date there have been no sulfur or strontium isotopic studies of the succession, and minimal study of organic carbon isotopes. This project will advance our chemical knowledge of the Khorbusuonka Group, adding to the compendium of chemical data for the latest Ediacaran Period.

China

The Ediacaran successions in South China are bracketed between the Cryogenian Nantuo Formation and basal Cambrian cherts, and are divided into the Doushantuo Formation (635–551 Ma) and Dengying Formation (551–542 Ma) (Xiao et al., 2011). The Doushantuo and Dengying formations outcrop extensively, providing a basin-wide record of Ediacaran sediment accumulation (Figure 1.4). High-resolution geochemical data from the fossil-rich Doushantuo Formation in South China (McFadden et al., 2008; Xiao, et al., 2011) provide paleontologic and isotopic evidence for rising oxygen levels during early Ediacaran time. However, there are caveats to understanding rates of chemical change recorded in the Doushantuo and Dengying sections. The Doushantuo varies from 40-260 meters thick, but records nearly 80 million years of sedimentation (McFadden et al, 2008; Condon et al., 2005; Kaufman et al., 2005). The Doushantuo Formation is thought to represent a very condensed Ediacaran succession with hiatuses (thought to be short in duration) associated with very slow deposition (McFadden et al., 2008). The Dengying, on the other hand, is considered to span the timeframe from 551-542 Ma, only about 10 million years, despite a thickness of over 600 meters at the studied Hujiaba locality (Figure 1.5). Radiometric constraints within the Dengying Formation are highly desired, as this information would aid in the quantification of geologic time recorded there, and constrain rates of chemical and biological change.

The Dengying Formation at Hujiaba is subdivided into three members: the Algal Dolomite Member, composed of largely microbial laminate dolostone, the Gaojiashan

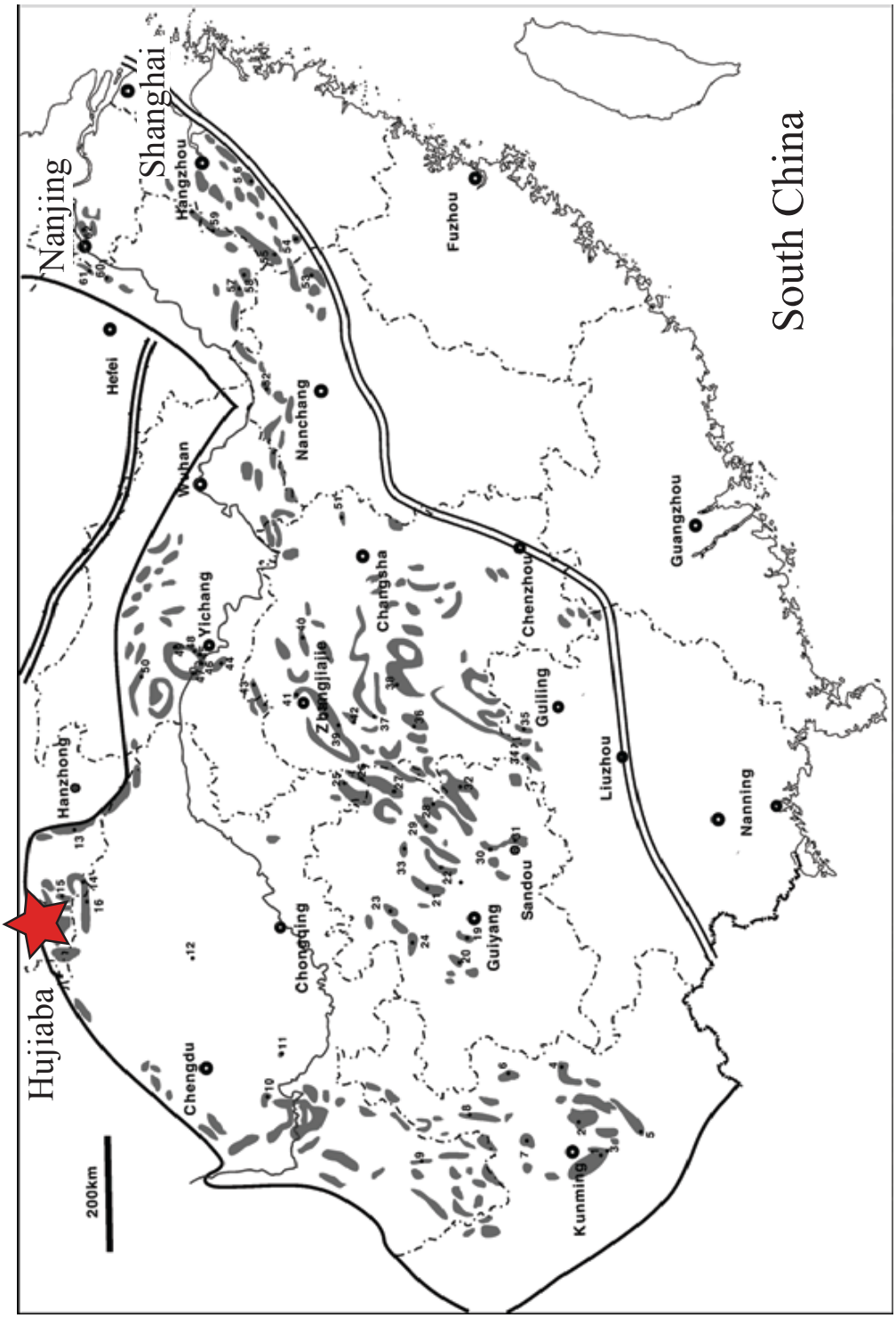

Figure 1.4. Location of Dengying section at Hujiaba. Modified from Zhu et al., 2007.

Member, composed of limestone with a variable siliciclastic component, interspersed with beds of siltstone and mudstone, and the Beiwan Member, composed of dolostone with common pyrobitumen filling vugs. The Early Cambrian limestone Kuanchuanpu Formation (not sampled) unconformably overlies the Beiwan Formation (Figure 1.5).

Paleontologically, the Dengying Formation provides a rich record of Ediacaran fossils as carbonaceous compressions and in three-dimensional preservation. The Gaojiashan Member in particular contains a rich fossil assemblage, including the first occurrences of *Cloudina, Conotubulus,* and *Shaanxilities*. Three-dimensional preservation of *Aspidella* also occurs in the Dengying Formation.

The Dengying Formation has been studied at a great number of localities throughout the basin. Carbonate carbon and oxygen studies have been carried out, but there has been no organic carbon or strontium work to date. Samples from this section, collected at one to five meter intervals, will provide new isotopic and geochronological data for the latest Ediacaran Period in South China.

Conclusion

South China and Arctic Siberia bounded separate basins during Ediacaran time (Fig.1.6; Waggoner, 2003). Nonetheless, the two successions, both deposited in tropical oceans, span the same time period, and the three members of the Dengying Formation may be considered analogous to the three formations at the Khorbusuonka River sections (Xiao et al., 2011). In both cases, the middle interval (Khatyspyt Formation; Gaojiashan Member) is considered to be of particular interest due to exceptional fossil preservation.

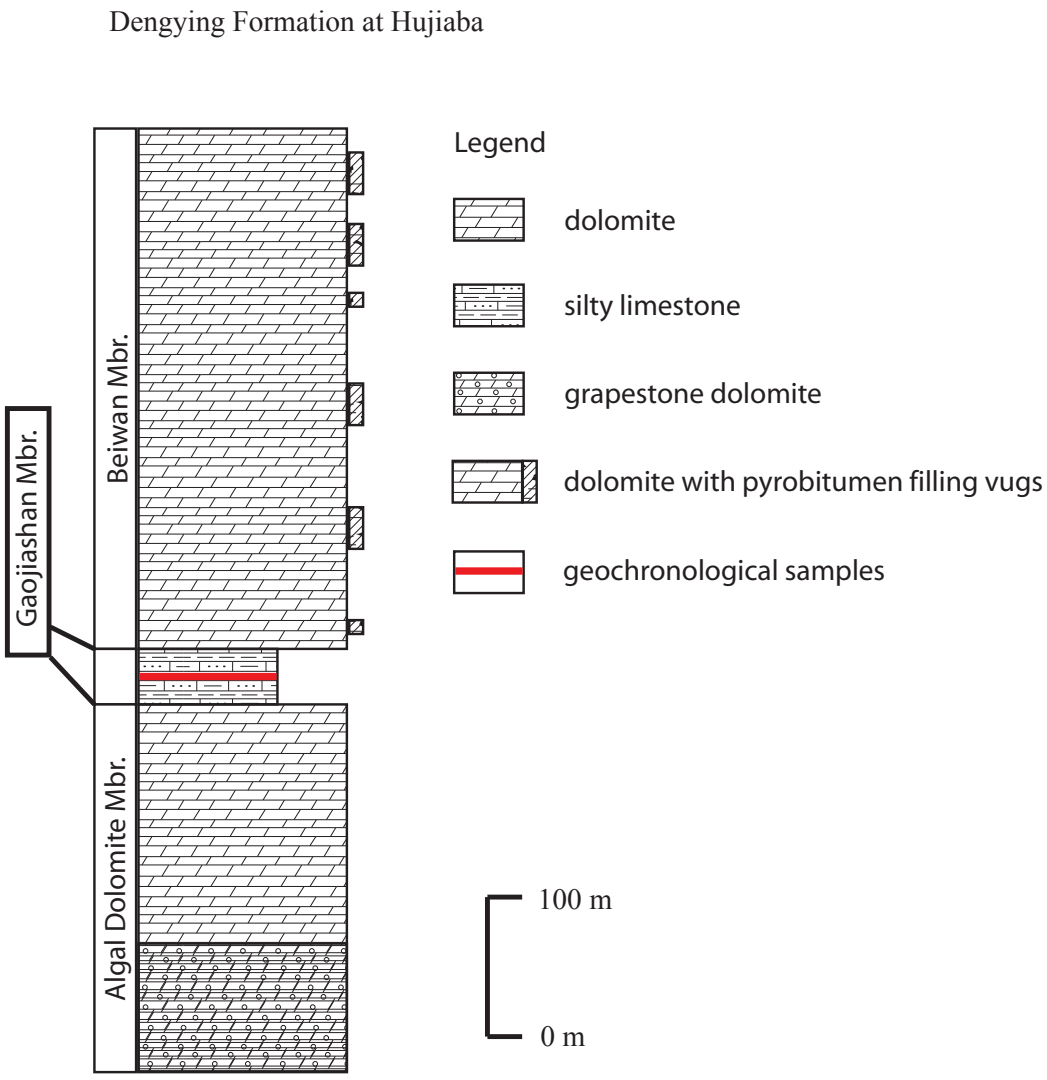

Figure 1.5. Stratigraphy for the Dengying Formation at Hujiaba Geochronological samples were collected from two closely-spaced layers in the Gaojiashan Member.

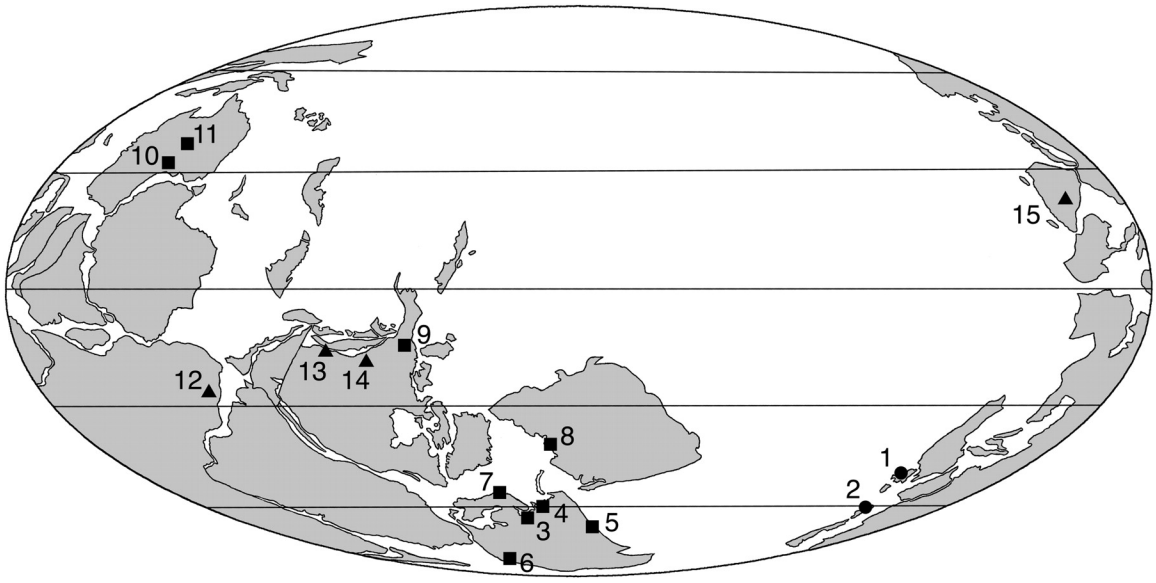

Figure 1.6. Continental Reconstruction for the early Ediacaran Period. From Waggoner, B. (2003) Integr. Comp. Biol.;43:104-113. Avalon Assemblage •: 1 = Charnwood Forest, England; 2 = Avalon Peninsula, Newfoundland (Briscal and Mistaken Point Formations). White Sea Assemblage ▪: 3 = Summer Coast, White Sea; 4 = Winter Coast, White Sea (Members 1, 9, and 11); 5 = Urals; 6 = Podolia, Ukraine; 7 = Finnmark, Norway; 8 = Olenëk Uplift, Siberia; 9 = Wernecke Mountains, Canada; 10 = Ediacara Hills, Australia (lower member and main member); 11 = Central Australia. Nama Assemblage ▲: 12 = Namibia (Kuibis and Schwartzrand Groups); 13 = Mojave Desert; 14 = British Columbia; 15 = South China

In South China, the first occurrence of *Cloudina* fossils is in the middle Gaojiashan Member, as are a number of other fossils. In Arctic Siberia, the majority of Khorbusuonka River fossils are preserved in the middle Khatyspyt Formation, as carbonaceous compression and three-dimensional forms. Additionally, the lower part of the Khatyspyt Formation contains the first occurrence of ichnofabric thought variously to represent the earliest burrowing organisms (Rogov et al., 2012), or alternatively preservation of a large, dense population of organisms as body fossils (Xiao, personal communication). This wealth of biological data, along with a continuous carbonate

record, makes these widely-separated sections an ideal laboratory for chemostratigraphic study of the effects of global and local environmental change on biological evolution.

Chapter 2: Methods

Work on this project reflects our view that high-resolution geochemical sampling and analysis is essential for understanding environmental conditions during the terminal Ediacaran Period. Our Siberian sections represent an ideal system for pursuing geochemical work; these rocks have only recently been exposed to weathering following Pleistocene post-glacial rebound, and are unmetamorphosed and undeformed. The Siberian Khorbusuonka region thus represents an important example of a remarkably-preserved carbonate platform from the terminal Ediacaran Period. The Chinese Dengying Formation, also unmetamorphosed and relatively unweathered, though uplifted and tilted, is considered (Xiao et al, 2011) to be an analogue to the Siberian Khorbusuonka Group, and provides an important basis for inter-basinal comparison.

Sampling

During fieldwork in summer 2009, latest Ediacaran outcrops along the Khorbusuonka River were sampled at high resolution (< 0.5 meter spacing) for geochemical analyses, including carbonate isotopes, organic carbon isotopes, sulfide and trace sulfur isotopes, strontium isotopes, iron speciation, and trace element analysis. To ensure adequate material for the large potential suite of analyses, samples of at least 300g were collected. Overall, approximately 900 samples were collected from over 20 localities (Figure 1.1). Russian collaborators Dr. Dmitrii Grazhdankin, Boris Kochnev, Konstantin Nagovitsin, Vladimir Rogov, and Natalia Bykova provided detailed stratigraphic logging and correlation. Over 200 oriented paleontological samples were

collected by collaborator Prof. Shuhai Xiao; approximately 140 oriented paleomagnetic samples were also collected from bedded carbonates and igneous sills.

For a comparative analysis in another terminal Ediacaran section very similar to arctic Siberia, over 170 samples for geochemical analysis were collected at the Gaojiashan locality of the Dengying Formation (Figure 1.4) in November 2009 under the supervision of Prof. Xiao, along with approximately 100 oriented paleomagnetic samples and additional paleontological samples.

Sample Processing and Export, Novosibirsk, Russia

Receipt of our Siberian samples was delayed indefinitely due to difficulties in obtaining permits for export of the materials from Russia. Accordingly, in May 2011, a team consisting of Sara Peek and undergraduates Natalie Sievers and Rebecca Ohly traveled to the Trofimuk Institute for Petroleum Geology and Geophysics in Novosibirsk, Russia, with the goal of processing large numbers of 300g samples into powders and residues more manageable for export.

Despite a lack of pre-existing laboratory facilities, space and equipment were procured, and nearly 100% of samples collected for geochemical analysis were slabbed, polished, scanned, and microdrilled. A slab was cut from each sample and polished with 40 micron grit for observation of textures. The finest and most organic carbon rich layers, believed to represent the least-altered portion of these carbonate rocks, were chosen for microdrilling (*e.g.*, Kaufman and Knoll, 1995). Microdrilling was performed with a Dremel tool with a 1 mm diameter diamond-tipped drill bit; a minimum of 20 milligrams of powder was produced from each sample.

Portions (< 100g) of each sample were crushed and acidified with 3 M HCl, with weights recorded for calculation of percent carbonate content. Additionally, a subset of samples were crushed and leached to remove soluble sulfate, then exported for completion of CAS procedures at the University of Maryland.

For isolation of total organic carbon, samples were sanded, briefly reacted with 3M HCl, or both, to remove weathered surfaces. Samples were broken in a jaw crusher to <0.5 cm, then pulverized in a Rocklabs ring and puck mill. Between samples, the two-piece ceramic mill, along with the ring and puck, were washed in running water, then dried with clean cloths. Three or more grams of powdered sample were reacted to completion with excess 6M hydrochloric acid, centrifuged, decanted, and the residue washed three times in distilled water, dried, and massed. Reaction times were typically less than 60 seconds, and rarely more than five minutes. Pre- and post-acidification sample masses allow the calculation of carbonate content and total organic carbon (TOC) from combustion yields determined during elemental analysis.

A subset of samples were prepared for extraction of carbonate-associated sulfate (CAS). Samples with high (> 90%) carbonate contents and without visible pyrite grains were chosen from three sections at 3-10 meter intervals. Approximately one hundred grams of sample powder was leached in 1L of 2% NaCl solution for 24 hours. The sample powder was filtered through a 5 micron Whatman qualitative paper filter, then a 0.45 micron Whatman cellulose nitrate membrane filter. Fifteen mL of 8% barium chloride solution was added to the supernatant. The solution was allowed to rest at least 24 hours, allowing the precipitation of any soluble sulfate as barium sulfate ($BaSO_4$),

which was filtered and retained. This process was repeated four to five times, following which the sample powders were dried and exported along with the leach precipitates.

Following these preparatory procedures, the microsamples and residues were greatly reduced in weight and bulk, from ~600 kg to <10 kg, allowing more expeditious export to the United States. A subset of the bulk powders were also exported (22 samples from key sections).

Carbonate isotopes

Stable isotope analyses were carried out at the University of Maryland Paleoclimate Colaboratory (http://one.geol.umd.edu/www/mslab/). For analysis, 100 micrograms of powder was weighed on a precision balance and placed in a Labco Exetainer® sample vial sealed with a 16.5 mm screw cap with a pierceable rubber septum. Proportionally more powder was used for samples containing less than 50% carbonate.

Utilizing a newly commissioned CF-IRMS optimized for high-throughput small sample carbonate analysis we are able to analyze 100+ samples per day; precision is ±0.043‰ for carbon and ±0.067‰ for oxygen. After loading into a 180-sample tray kept at 65°C, vials are individually flushed with a stream of UHP He carrier gas for 300 seconds, and then acidified using 0.1 ml of 100% phosphoric acid. Reactions are allowed to proceed for one hour before extraction of the evolved gas. Samples are run under continuous flow conditions with a trap current of 175μA, producing peak heights of 6 to 9 nA. Data is corrected using a two-point correction derived from both international (NBS-19) and in-house standards. Isotopic ratios are expressed in delta notation as per mil deviations from the V-PDB standard:

$$\delta^{13}C = \frac{\frac{^{13}C}{^{12}C}\text{sample} - \frac{^{13}C}{^{12}C}V - PDB}{\frac{^{13}C}{^{12}C}V - PDB} \text{ x } 1000‰$$

Organic carbon isotopes

For stable isotope analysis of post-acidification samples, approximately 500 micrograms of residue was weighed and folded into an Elementar tin cup for elemental and isotopic determinations. Isotope abundances were measured using a continuous-flow Elementar Isoprime mass spectrometer at the University of Maryland Paleoclimate Colaboratory. Samples were sequentially dropped into a 1040°C combustion column of a Eurovector elemental analyzer (EA) along with a timed pulse of O_2 and a constant flow of He carrier gas (~90 mL/min). Combustion products travel through a reaction tube packed with reduced copper wire for quantitative oxidation and O_2 resorption, then through a 660ºC chromium and cobaltous oxide reduction column. Water is removed via a 10-cm magnesium perchlorate column, and the CO_2 is separated from other gases with a 0.8 m stainless steel GC column packed with Porapak 50-80 mesh resin heated to 90°C. Maximal sample pulses appear in the mass spectrometer collectors after ~150 seconds, preceded by a 30-second reference gas injection beginning at 20 seconds into each cycle. Values are reported as per mil (‰) deviations from the V-PDB standard. Uncertainties based on multiple analyses of a standard are better than 0.12% for total organic carbon and 0.5‰ for $\delta^{13}C_{org}$.

Trace sulfate isotopes

Initial sample preparation was carried out in Novosibirsk, Russia as detailed above. Upon export to the US, bulk sample powders were re-leached one or two

additional times following the procedure detailed above, using ultrapure Milli-Q water. Fifteen mL of 8% barium chloride solution was added to the filtered supernatant, along with 1 mL of 3M HCl to prevent the precipitation of barium carbonate, as an addition to the previously-stated procedures. All samples yield visible $BaSO_4$ precipitate through the 5^{th} leach; all samples processed further continued to yield visible $BaSO_4$ on subsequent leaches. Samples were leached six to eight times in total, seven times on average. Leach precipitates were quantified at Maryland using a milligram balance, and analyzed for sulfur isotopic composition.

After leach precipitates were subjected to elemental analysis, their weights were adjusted mathematically to reflect their barium sulfate content; this is of particular importance for the leaches performed in Novosibirsk, as the slightly basic solution may have allowed for the precipitation of a small amount of barium carbonate in addition to barium sulfate. A "blank" precipitate, in which barium chloride was added to a solution of local water and salt, was also subtracted from each value.

Samples leached of soluble sulfates were dried, massed, and acidified by addition of 3M HCl. Care was taken to minimize the time spent in very low pH conditions, while reacting the sample to completion. Sample powder was placed in a large beaker, and excess 3M HCl added slowly with periodic agitation. Carbonate (non-dolomitic) samples typically reacted to completion in under 5 minutes, at which point the sample was immediately filtered through a qualitative 5 micron Whatman paper filter. The supernatant was then filtered with a 0.45 micron Whatman cellulose nitrate membrane filter, and 15 mL of 8% barium chloride solution added to precipitate sulfates freed from the carbonate lattice. The resulting barium sulfate was filtered with a 0.45 micron

Whatman filter as above, dried, quantitatively massed, and analyzed for sulfur isotopic composition. The filtered residue is retained and rinsed three times with Milli-Q water to remove acid, then dried, massed, and analyzed for organic carbon and sulfur concentration and isotopic composition.

Sulfur isotope measurements

For analysis of sulfur isotopic composition, approximately 140 micrograms of $BaSO_4$ or 1-5 mg of whole rock powder from each sample was folded into an Elementar tin cup with approximately 700 micrograms of V_2O_5. Samples were combusted using a Eurovector elemental analyzer (EA), interfaced with an Elementar Isoprime mass spectrometer. Samples are processed as the organic carbon isotopic measurements detailed above, but excluding the reduction column. SO_2 isotopic ratios are determined by integrating peak areas of m/z 66 and 64 for reference and sample pulses, relative to baseline. Isotopic ratios are expressed in delta notation as per mil deviations from the V-CDT standard:

$$\delta^{34}S = \frac{\frac{^{34}S}{^{32}S}\text{sample} - \frac{^{34}S}{^{32}S}\text{V} - \text{CDT}}{\frac{^{34}S}{^{32}S}\text{V} - \text{CDT}} \text{ x } 1000‰$$

Measurement uncertainties (typically better than ±0.3‰) were determined by interspersed analysis of standard NBS 127 (barite).

Strontium

For analysis of strontium isotopic composition, limestone samples were chosen from key intervals throughout the section. Microdrilled powders (ca. 5mg) were leached three times in 0.2 M ammonium acetate (pH ~8.2) to remove exchangeable Sr from non-

carbonate minerals (Montañez et al., 1996), then rinsed three times in Milli-Q water. The leached powder was centrifuged, decanted, and acidified with doubly-distilled 0.5 M acetic acid overnight to free strontium from the carbonate lattice. The 0.5 M acetic acid dissolves the carbonate fraction, but does not dissolve any potentially contaminating clays present in the sample (Derry et al., 1989).

The supernatant was centrifuged to remove insoluble residues and then decanted, dried, and subsequently dissolved with 200 µl of 3 M HNO_3. Strontium separation by cation exchange was carried out using a small polyethylene column containing ~1 cm of Eichrom® Sr specific resin. The column was first rinsed with 400 µl of 3 M HNO_3, then loaded with the dissolved sample. After loading, the column was sequentially eluted with 200 µl of 3 M HNO_3, 600 µl of 7 M HNO_3 and 100 µl of 3 M HNO_3 to remove the Ca, Rb and REE fractions from the sample; the Sr fraction adsorbs strongly to the resin in an acidic environment. The Sr fraction was removed by elution with ~800 µl of 0.05 M HNO_3, and the resultant eluate collected and dried. Approximately 200-300 ng of the dried sample was transferred onto a degassed and pre-baked (~4.2 A under high vacuum) high purity Re filament with 0.7 µl of Ta_2O_5 activator. The prepared filaments were measured using the VG Sector 54 thermal ionization mass spectrometer at the University of Maryland Isotope Geochemistry Laboratory (http://www.geol.umd.edu/facilities/igl.htm).

Filaments were transferred to a sample carousel within the VG Sector 54, then heated under vacuum (~10^{-7} to 10^{-8} atm) to a temperature between 1450 and 1650ºC and analyzed when a stable signal (> 0.5 V) was detected on the ion beam of mass 88. Approximately 100 $^{87}Sr/^{86}Sr$ ratios were collected for each sample. Final data are

corrected for fractionation using the standard value $^{86}Sr/^{88}Sr = 0.1194$. The fraction of ^{87}Sr resulting from *in situ* decay from ^{87}Rb was removed by measurement of rubidium abundance at mass 85. Repeated analysis of NBS SRM987 standard yields an average value of $^{87}Sr/^{86}Sr=0.71024448 \pm 0.0000111(1\sigma)$ during the analytical window.

X-ray Diffraction and X-Ray Fluorescence

X-ray Diffraction (XRD) and X-Ray Fluorescence (XRF) were carried out to identify the matrix compositions of samples from which zircons were separated. Powdered bulk samples were sent to Dr. Stan Mertzman at Franklin and Marshall College (http://www.fandm.edu/earth-and-environment/x-ray-laboratory). Samples were analyzed on a PANalytical X'pert Pro x-ray diffractometer using Cu-Kα x-rays, at 2θ angles ranging from 0-40º. Following the initial XRD analysis, samples were placed in a desiccator with ethylene glycol ($C_2H_6O_2$) until saturation, then reanalyzed. Glycol saturation affects the XRD spectra of some clays by causing changes in layer spacing.

X-ray fluorescence (XRF) measurements for major and trace elements were made on a PW2404 Panalytical, Inc. XRF vacuum spectrometer. To prepare the sample for major element analysis, crushed rock powder (0.4 grams) was mixed with lithiumtetraborate (3.6 grams), placed in a platinum crucible, and heated until molten. The molten material is transferred to a platinum casting dish and quenched. This produces a glass disk that is used for XRF analysis of SiO_2, Al_2O_3, CaO, K_2O, P_2O_5, TiO_2, Fe_2O_3, MnO, Na_2O and MgO. Analytical precision is better than ±0.15%.

To prepare the sample for trace element analysis, 7 grams of whole rock powder was mixed with 1.4 grams of high purity Copolywax powder, mixed for 10 minutes, and pressed into a briquette. Data are reported as parts per million (ppm) for Rb, Sr, Y, Zr,

Nb, Ni, Ga, Cu, Zn, U, Th, Co, Pb, Sc, Cr, V, La, Ce, and Ba. Analytical precision is better than ±5 ppm, except for Cr and Ba, where error is less than ±15 ppm.

Zircon separation and dating

To separate zircon fractions from whole rock, the sample is first crushed by hand to 200 mesh or less in an extremely clean environment. The crushed sample is placed in excess water in a ridged panning dish, and gently agitated to suspend fine particles, including clays as well as other minerals. A portion of the water is poured off, removing these particles. This process is repeated until no suspended particles are observed. The resulting sample, consisting of sand-sized grains, is separated into magnetic and non-magnetic fractions using a Frantz IsoDynamic magnetic separator. The sample is poured slowly down a tilted, vibrating tray, which passes near a strong electromagnet (up to 20 kiloGauss at 1.9 Amperes). Magnetic grains, including most mafic minerals, are diverted to a track separate from non-magnetic grains, including quartz, feldspars, and zircons. Magnetic and non-magnetic grains are collected in separate cups at the base of the machine. Separation is repeated at progressively higher electromagnet currents (0.5 A, 1.0 A, 1.5 A, and >1.9 A), and the splits saved.

After separation at the highest current, the non-magnetic fraction is subjected to heavy liquid separation. A 100 mL beaker is filled with 80 mL of methylene iodide (CH_3I), a liquid with a density of 3.3 g/cm^3. (The mineral zircon has a specific gravity of 4.6-4.7 g/cm^3, while the specific gravity of quartz is ~2.7 g/cm^3.) Less than 10 mL of sample by volume is poured into the beaker, then gently agitated for three to five minutes with a plastic stirring rod. After sufficient agitation, the base of the beaker is frozen in liquid nitrogen, and the floating grains, including quartz and feldspar, are decanted into a

funnel lined with a 5 micron Whatman paper filter, over a 1L Erlenmeyer flask. The frozen heavy fraction is partially thawed via a warm water bath, then decanted into an identical apparatus. The heavy mineral fraction, typically quite small, will contain any zircons present in the sample.

Because methylene iodide is both hazardous and expensive, both fractions are rinsed ten times with acetone and transferred to a new filter; this procedure is repeated three times, so that the methylene iodide may be completely removed from the sample and safely recovered by separation from the acetone.

Recovered zircons were poured onto carbon tape using a guide to limit their placement. The tape-mounted grains were inspected using a binocular stereomicroscope. When possible, non-zircon phases, including pyrite and rutile, were removed with fine tweezers; the remaining zircon grains were pressed down if standing on end, to provide a consistent cross-section. A row of five standard ~1 mm Sri Lankan zircon shards (563.5 ± 3.2 Ma, Gehrels et al., 2008) was added a few millimeters from the edge of the poured zircons. A one-inch-diameter ring mold was placed on the tape, containing the zircon populations, and 30-minute epoxy was poured to fill the mold. Before the epoxy set, visible bubbles were removed from the bottom surface of the mount via manipulation with a dental pick. After the 24-hour cure time, the mount was removed from the tape, and polished with 1000 grit paper until the center cross-section of an average-sized grain was visible. Subsequent polishing at 9 microns, 3 microns, 1 micron, and 0.3 microns was carried out to improve the smoothness of the surface. Little material is removed at such fine grit sizes.

Polished mounts were carbon coated to a thickness of 200-300 Angstroms using a standard thermal evaporator with a carbon electrode, then imaged in backscatter and cathodoluminescence (CL) using a JEOL JXA-8900 Superprobe with an Oxford Instruments miniCL at the University of Maryland Electron Probe Microanalyzer Laboratory (http://www.geol.umd.edu/~piccoli/probe/). The instrument was operated with an accelerating voltage of 15 kV applied to a tungsten filament and a beam current of 50 nA. Mineralogy of non-zircon grains, as well as that of discernable inclusions within grains, was identified by energy dispersive x-ray spectroscopy (EDS) using a Noran Instruments detector. Elemental peaks produced by EDS can be manually identified with high confidence by a trained operator.

For detrital samples, images were taken with a large field of view (~2 mm square) for determination of grain positions only. For igneous samples, images were taken with a large field of view, followed by high-resolution images (~50 microns square) of individual grains. Individual grain images allow recognition of inclusions within grains as well as zoning and surface imperfections.

Mounted zircons were analyzed via laser ablation ICP-MS at the LaserChron center at the University of Arizona (https://sites.google.com/a/laserchron.org/laserchron/home) using a Nu Instruments HR ICP-MS coupled to a Photon Machines Analyte G2 excimer laser. Isotopic composition and concentration data were collected for uranium, lead, and thorium. Ten standard analyses were made at the beginning of data collection, followed by a standard analysis after every five sample analyses. Grains were analyzed with a 10-micron laser spot size, allowing separate analyses for core and rim material in volcanic grains with distinguishable zoning. Inclusions were avoided when possible.

Twenty grains were analyzed from samples believed to be of volcanic origin, while over a hundred grains were analyzed from detrital samples, if available.

Sample data was reduced using a standard Excel workbook, AgeCalc, developed by George Gehrels for the Arizona LaserChron Laboratory. Sample analyses were excluded in the case high ^{204}Pb (over 100 counts per second), or over 5% error on the ratio of $^{206}Pb/^{207}Pb$ or $^{206}Pb/^{238}U$. Sample analyses were also excluded for discordance when the $^{206}Pb/^{238}U$ age divided by $^{206}Pb/^{207}Pb$ age varied more than 25% below the concordia (normal discordance), or more than 5% above the concordia (reverse discordance). The remaining samples were used to calculate radiometric ages using the calculated concordia, with best ages calculated through weighted averaging of analyses.

Chapter 3: Results

Here we present the results of our study of the abundance and isotopic composition of carbonate carbon, oxygen, and strontium, as well as organic carbon, total sulfur (TS), carbonate-associated sulfate (CAS), as well as the results of radiometric dating, in Siberia and South China during the terminal Ediacaran and early Cambrian periods. These data represent the most complete characterization of this time period on the Siberian craton, and radiometric dates augment available results from South China. High resolution, multi-site carbonate carbon and oxygen isotope data collection gives confidence in interpreting variations. These results can be used to inform the lithostratigraphic correlations of our Russian colleagues Grazhdankin and Rogov. Organic carbon, sulfur, strontium, and radiometric age analyses have been carried out on only a fraction of the available sample material, but provide additional insights as well as a base on which to build through further work. Data and supporting material can be found in Figures 3.1 to 3.42, found at the end of the section, and tabulated in Tables 3.1-3.4 and Appendix Tables A.1-A.14.

Carbon and oxygen isotopic compositions

Sections 0601-A, 0601-B, and 0601-D

Because detailed carbonate carbon and oxygen isotopic composition data was collected for a large number of sections, here we give a full description of only a small number of key sections. Following this, we give an overview of carbon and oxygen isotope variations in all sampled sections, plotted against the lithostratigraphic

correlations of Grazhdankin and Rogov, as well as our correlations modified through use of isotopic data as time markers. For sections not treated in detail, see Figures 3.5-3.22.

Samples from sections 0601-A, 0601-B, and 0601-D (see Figure 1.1) were analyzed for percent carbonate, carbonate carbon and oxygen isotopes, percent total organic carbon (% TOC), and organic carbon isotopes (Figures 3.21 and 3.23), as well as carbonate-associated sulfate (CAS) concentration and isotopes, percent total sulfur (% TS), and total sulfur isotopes ($\delta^{34}S_{TS}$) (Figures 3.22 and 3.24). See later sections for treatment of data beyond carbonate carbon and oxygen isotopic compositions.

Khatyspyt section 0601-A (Figures 3.1 and 3.2; Figures 3.21 and 3.22) consists of approximately ten meters of thinly-bedded bituminous limestone interspersed with intraclastic breccia. Carbonate concentration in this section rarely falls below 90%, and $\delta^{13}C_{carb}$ has a slight positive trend moving upsection, from +2.5‰ at the base to +4.5‰ at the top. Oxygen isotope data ($\delta^{18}O_{carb}$) exhibits greater variability; while the majority of the data trend from -4‰ to -2‰, mirroring the $\delta^{13}C_{carb}$ trend, nine data points are outliers at -5‰ or below.

The first ten meters of Khatyspyt section 0601-B samples the same stratigraphy as the upper part of section 0601-A (Figure 3.2; Figures 3.21 and 3.22). The section is composed of twenty meters of stratigraphy as described in section 0601-A; additionally, five potential tuff layers were collected as geochronological samples in the upper portion of the section. The lowest fifteen meters of section consist of nearly pure carbonate, while the uppermost five meters drops to no more than 80% carbonate. The $\delta^{13}C_{carb}$ data shows a similar trend, moving from +4‰ at the base of the section (consistent with high values in 0601-A) through zero to a negative excursion, reaching -2‰ by the top of the section.

Oxygen isotopic composition is more variable, but seems to follow a trend from -2.5‰ to -7.5‰ in the lower part of the section, then up to nearly 0‰ in the uppermost stratigraphy, correlating negatively with the $\delta^{13}C_{carb}$ trend.

Khatyspyt section 0601-D (Figure 3.2; Figures 3.23 and 3.24) consists of 60 meters of mainly bituminous, thinly-bedded limestone. Samples collected in section 0601-D are nearly pure carbonate, with the measured percent carbonate rarely falling below 90%. Carbonate carbon isotopes ($\delta^{13}C_{carb}$) range from -5‰ at the base of the section to nearly +5‰ midsection. The nadir of -5‰ at the base of 0601-D follows, with some lost time, the negative excursion at the top of 0601-B. Carbon isotope ratios smoothly rise to 0‰ over approximately fifteen meters of section. Values continue to rise over the next twenty meters; a number of samples are recorded at nearly +5‰. However, the data exhibit considerable scatter in the middle part of the section. In the upper twenty-five meters of the section, carbon isotope ratios stabilize at +2‰. Oxygen isotopes ($\delta^{18}O_{carb}$) span a range of values throughout the section. Nonetheless, it is clear that oxygen isotope ratios negatively covary with $\delta^{13}C_{carb}$: from an apex of 0‰ at the base of the section, values fall to -8‰ within fifteen meters, continue invariant through the thirty meters of the section, then rise to -2‰ in the uppermost portion of the section.

Intra-basinal correlation of results

Based on similarly detailed analysis of each of the sampled sections, we identify a large number of positive, invariant, and negative intervals in the carbon isotopic composition of our Ediacaran and early Cambrian sections from arctic Siberia (see data in Table A.1). Beginning at the base of our studied interval, where the Mastakh Formation overlies the Kaipakh Formation at an angular unconformity surface, carbon

isotopic composition is observed at +2‰, rising to +6‰ over ~40 m of section; this is designated P1 (positive interval 1) (Figure 3.1).

A sandstone level overlies an unconformity surface at the top of the Mastakh Formation (Figure 3.1), marking the base of the Khatyspyt Formation. The lowest carbonate level in the Khatyspyt Formation has a carbon isotope composition of 0‰, down from +6‰ in the upper Mastakh; this negative excursion is not preserved in the rock record. From 0‰, the carbon isotopic composition of the lower Khatyspyt sections rises to +4‰ (designated P2; Figure 3.1 and 3.2), then falls to -5‰ (designated N1; negative interval 1). Carbon isotopic compositions rise to nearly +5‰ by the middle of section 0601-D (P3), then undergo a significant negative excursion, as low as -7‰, in equivalent sections 0603 and 0605 (N2). These values rebound to 0‰ before a second negative excursion of similar magnitude is seen in the lower part of 0701-B (N3), although isotopic compositions in correlated sections 0601-E and 0602-A only reach as low as -3‰. Above N3, an invariant interval (I2) is observed at 0‰ in 0701 and 0602-A. A final positive excursion (P4) is observed at the top of the Khatyspyt Formation in 0602-A, 0602-B, and the upper part of 0701, with carbon isotopic compositions rising to nearly +5‰ before returning to 0‰ for the remainder of the Khatyspyt Formation and the lower part of the Turkut Formation (I3, Figures 3.3-3.4). Invariant interval I3 continues to the middle of the Turkut Formation, until values cross into negative territory, reaching values as low as -2‰ in some sections (N4). It is notable that the negative carbon isotope values begin in a range of lithologies, including pisolite in 0703-A, microbialaminate in 0702-B, and thick-bedded dolomite in 0710.

An unknown interval passes between the upper Turkut Formation and the sampled portions of the Mattaia Formation (sections 1002, 0705, and 0709; Figure 3.5). Section 1002 begins with carbon isotope values of as low as -4‰ (N5), rising rapidly through 0‰ to a +5‰ excursion (P5), which is also seen in section 0705.

Detailed results for carbon and oxygen isotopic composition and percent carbonate can be seen for each section in Figure 3.6 (Mastakh Fm.), Figures 3.7-3.10 (Khatyspyt Fm.), Figures 3.11-3.19 (Turkut Fm.), and Figures 3.7 and 3.20 (Mattaia Fm.). The geochemical data are also presented in Table A.1.

From these figures, it can be seen that the Turkut Formation has persistently more positive $\delta^{18}O$ relative to the Mastakh, Khatyspyt, and Mattaia Formations, with values as enriched as -2‰ (see sections 0908 and 0909, in Figure 3.13, as well as 1001A-B, in Figure 3.14). On the other hand, $\delta^{18}O$ in 0703-A (Figure 3.12) is more negative than other Turkut sections at around -8‰ to -10‰, undergoing a positive shift at the top of the section to values as enriched as 0‰, coincident with the negative shift in carbon isotopic composition (N4).

Figures 3.21-3.24 provide detailed results for Khatyspyt sections 0601-A, 0601-B, and 0601-D, including organic and inorganic carbon isotopic composition and concentration as well as carbonate-associated sulfate and total sulfur isotopic composition and concentration.

Organic carbon content and isotopic composition

Organic carbon data was collected from sections 0601-A, 0601-B, and 0601-D (Figures 3.21 and 3.23; Table A.3). All samples in 0601-A and 0601-B contain less than 0.5 weight percent total organic carbon (TOC); most samples contain less than 0.2%.

Typical samples from 0601-D contain ~0.3% TOC, though several samples containing a relatively low percent carbonate have TOC levels of up to 1.5%.

In section 0601-A, $\delta^{13}C_{org}$ is nearly invariant at approximately -31‰; the differential between carbonate and organic carbon isotopes ($\Delta\delta^{13}C_{carb\text{-}org}$) is similarly invariant at ~35‰. Organic carbon data from section 0601-B exhibits more variability, mirroring 0601-A in the bottom half of the section, then moving noisily in a generally positive direction, with values as high as -27‰ at the top of the section. The broad negative covariance between $\delta^{13}C_{carb}$ and $\delta^{13}C_{org}$ results in a generally negative trend in $\Delta\delta^{13}C_{carb\text{-}org}$; the differential is as high as 35‰ at the base of the section, and as low as 27‰ at the top.

In section 0601-D, organic carbon isotopic compositions vary widely over much shorter time periods than $\delta^{13}C_{carb}$, moving smoothly from -40‰ at the base of the section to -35‰ and back to -40‰ in the first ten meters of section. Similarly, the next thirty meters of section show smooth variation from -40‰ to -30‰, then back to -42‰. Organic carbonate isotopic composition data is unavailable for the uppermost part of 0601-D. Calculated values for $\Delta\delta^{13}C_{carb\text{-}org}$ also vary rapidly but smoothly. Because of the relative invariance in $\delta^{13}C_{carb}$ above the first fifteen meters of section, variations in $\delta^{13}C_{org}$ largely control the shape of the $\Delta\delta^{13}C_{carb\text{-}org}$ curve. The two values are offset by as little as 32‰ and as much as 45‰.

Carbonate-associated sulfate (CAS) and total sulfur (TS)

In overlapping Khatyspyt sections 0601-A and 0601-B, four and five samples, respectively, were analyzed for carbonate-associated sulfate (CAS) concentration and isotopic composition, percent total sulfur (% TS), and total sulfur isotopic composition

($\delta^{34}S_{TS}$) (see Figure 3.22, Tables 3.1 and A.4); see Figure 3.2 for correlation of sections). In both sections, CAS concentration rises from ~500 ppm to higher values moving upsection. While $\delta^{34}S_{CAS}$ values are generally high (> 40‰), some samples from each section have lower values. Low sampling resolution precludes the identification of trends in this dataset. Total sulfur (TS) concentrations are typically very low (< 0.05%) in both sections. In 0601-A, $\delta^{34}S_{TS}$ values fall between -10‰ and 0‰, while in 0601-B, variation from -12‰ to +9‰ is observed. In both sections, $\Delta\delta^{34}S_{CAS\text{-}TS}$ values are typically between 40‰ and 50‰, values typical of the late Ediacaran; however, values as low as 20‰ and 33‰ are observed in 0601-A and 0601-B respectively.

Table 3.1. CAS and TS concentration and isotope data

Section	Number	ppm CAS	%TS	$\delta^{34}S_{CAS}$	$\delta^{34}S_{TS}$	$\Delta\delta^{34}S_{CAS\text{-}TS}$
0601-A	0	558	0.138	39.94	-6.37	46.31
0601-A	3.5	578	0.029	18.7	-1.1	19.8
0601-A	6.1	895	0.014	41.16	-3.02	44.18
0601-A	7.7	1118	0.029	37.06	-3.13	40.19
0601-B	0	454	0.004	40.78	3.74	37.04
0601-B	4	379	0.016	44.58	11.82	32.76
0601-B	7	1079	0.394	31.15	-12.86	44.01
0601-B	10.7	120	0.013	41.58	-3.36	44.94
0601-B	13.7	805	0.035	31.16	-9.13	40.29
0601-D	-2.5	1969	0.090	46.94	14.71	32.23
0601-D	-0.6	1529	0.220	44.77	2.14	42.63
0601-D	4.9	1078	0.007	47.74	23.75	23.99

Section	Number	ppm CAS	%TS	$\delta^{34}S_{CAS}$	$\delta^{34}S_{TS}$	$\Delta\delta^{34}S_{CAS-TS}$
0601-D	6	676	0.000	45.68	34.1	11.58
0601-D	9.5	73	0.010	34.46	31.88	2.58
0601-D	11.5	382	0.070	41.4	31.82	9.58
0601-D	17	454	0.030	36.36	28.69	7.67
0601-D	20	1	0.010	NA	NA	NA
0601-D	26.5	7	0.050	31.01	34.23	-3.22
0601-D	28.5	11	0.070	35.8	42.72	-6.92
0601-D	34	162	0.070	42.7	26.63	16.07
0601-D	44	390	0.060	42.08	30	12.08
0601-D	54	12	0.020	31.4	31.32	0.08

In the Khatyspyt section 0601-D thirteen samples were analyzed for carbonate-associated sulfate (CAS) concentration and isotopic composition, percent total sulfur (% TS), and total sulfur isotopic composition ($\delta^{34}S_{TS}$) (see Figure 3.24; Table 3.1). In the first ten meters of section, CAS concentrations are high, but fall rapidly from ~2000 ppm to ~500 ppm. Samples from the upper part of the section contain low concentrations of CAS, in one case yielding too little precipitate to analyze (< 0.0001 g). No discernable trend was found in the CAS isotope ratios ($\delta^{34}S_{CAS}$), with values ranging between +40‰ and +50‰. The total sulfur isotope ratios ($\delta^{34}S_{TS}$), on the other hand, undergo a shift of 25‰, from +10‰ to +35‰. This shift occurs over only ~5 meters of section, and is coincident with the reduction of CAS concentration below 500 ppm. Accordingly, the $\Delta\delta^{34}S_{CAS-TS}$ curve is controlled by $\delta^{34}S_{TS}$ values, with large fractionations near the base of

the section, and small or negative fractionations in the upper section. The $\Delta\delta^{34}S_{CAS\text{-}TS}$ values appear anti-correlated with CAS concentration. Above 500 ppm, CAS concentrations are associated with large fractionations, whereas lower concentrations are associated with smaller fractionations, and the lowest measurable concentrations, less than 10 ppm, with negative fractionations. Variability in total sulfur concentration, on the other hand, is not correlated with changes in $\delta^{34}S_{TS}$ or $\Delta\delta^{34}S_{CAS\text{-}TS}$.

Referencing the carbonate carbon isotope curve, the shift in carbon isotope values from -5‰ to 0‰ in the lowest part of the section is coincident with shifts in sulfur isotope values.

Leach Precipitates

Isotopic compositions were also measured for the leach precipitates (Figures 3.26 and 3.27). As seen in Figure 3.26, $\delta^{34}S$ values for leach precipitates span a wide range, from approximately +40‰ to -10‰, although values are somewhat more consistent over multiple leaches of the same sample. Values for 0601-A and 0601-B tend to be lower than those for 0601-D, though isotopic compositions of leach precipitates span a range of values in all three sections.

Figure 3.27 compares the isotopic compositions of leaches, CAS, and residues for each sample, plotted against composite stratigraphic heights. A distinction can be drawn between the lower and upper stratigraphy. In the lower portion of the stratigraphy (0601-A, 0601-B, and the lower part of 0601-D), isotopic compositions of residues are lower than those of leaches, which are lower than those of CAS. On the other hand, in the upper part of 0601-D, leaches have the lowest isotopic compositions, while residues are heavier. CAS isotopic compositions for this portion of the stratigraphy are typically

higher than residue isotopic compositions, but are lower in two cases. These changes correspond to decreasing CAS concentrations in 0601-D, appearing to initiate as CAS concentrations dip below 500 ppm.

To allow visual evaluation of potential correlations between data derived from the CAS process, a series of crossplots (Figures 3.28-A-F, 3.29-A-E, Table 3.2) was created, including concentrations and isotopic compostions of CAS and total sulfur and total leach precipitate weights. In some cases, the small sample size of individual sections allow the suggestion of correlation between data types (see, for example, Figure 3.29-A). However, when considering the overall sample set, the correlations appear to be of the opposite polarity, or disappear completely. The plotted data can also be compared statistically by calculating the coefficient of determination (r^2, Table 3.2). These values suggest that there is little correlation between most of the data types compared. The only exception is the comparison between CAS concentration and the difference in isotopic compositions of CAS and TS for each sample. This comparison has both a visually-discernable correlation and a relatively high r^2 value (0.35, Table 3.2).

Table 3.2. r^2 values for determining correlation between factors.

Sample Set	x values	y values	r^2	Figure
0601-A, B, D	total leach wt.	$\delta^{34}S_{CAS}$	0.04	3.31-A
0601-A, B, D	total leach wt.	$\Delta\delta^{34}S_{CAS-TS}$	0.09	3.31-B
0601-A, B, D	total leach wt.	ppm CAS	0.01	3.31-C
0601-A, B, D	total leach wt.	% TS	0.02	3.31-D
0601-A, B, D	$\Delta\delta^{34}S_{CAS-TS}$	% TS	0.11	3.31-E
0601-A, B, D	$\Delta\delta^{34}S_{CAS-TS}$	ppm CAS	0.35	3.31-F

0601-A, B, D	$\delta^{34}S_{TS}$	$\delta^{34}S_{CAS}$	0.02	3.32-A
0601-A, B, D	ppm CAS	$\delta^{34}S_{CAS}$	0.11	3.32-B
0601-A, B, D	% TS	$\delta^{34}S_{CAS}$	0.01	3.32-C
0601-A, B, D	% TS	ppm CAS	0.16	3.32-D
0601-A, B, D	% TS	$\delta^{34}S_{TS}$	0.12	3.32-E

Strontium Isotopic Composition

Strontium isotope ratios ($^{87}Sr/^{86}Sr$) were measured in ten carbonate samples from the Khatyspyt, Turkut, and Mattaia formations. Six of the samples were from the Khatyspyt Formation, three from the Turkut Formation, and one from the Mattaia Formation. These samples span approximately 350 meters of the original lithological correlation scheme devised by Grazhdankin and Rogov (seen in Figures 3.1-3.3). Sample selection was influenced by the limited occurrence of non-dolomitized carbonate rocks in the Turkut and Mastakh formations. Four of the six Khatyspyt samples (K601A-7.6, K601C-18.3, K605-10.1, K701B-6.25) and the single Mattaia sample (K705-4.0) were chosen for stratigraphic proximity to one or more selected geochronological samples (Figure 3.30). Strontium isotope ratios range from 0.7079 to 0.7087 (Table 3.3), not including the value of K604-1.9, an outlier at 0.7093. The Khatyspyt and Turkut samples show a slight positive trend moving up section, while the single Mattaia sample far up section gives a slightly lower value.

Table 3.3. $^{87}Sr/^{86}Sr$ measurement data. Correlated stratigraphic height is constructed from the original correlation scheme of Grazhdankin and Rogov.

Name	Correlated Stratigraphy (m)	$^{87}Sr/^{86}Sr$	% uncertainty	2σ uncertainty
K705-4.0	402	0.70818	0.0029	0.000021
T710-10.0	273	0.70866	0.0040	0.000028
T901-7.8	262	0.70835	0.0023	0.000016
K601C-71.0	212	0.70794	0.0031	0.000022
K701B-6.25	208	0.70845	0.0027	0.000019
1004-1056	184	0.70814	0.0037	0.000026
K605-10.1	133	0.70821	0.0028	0.000020
K601C-18.3	91	0.70793	0.0007	0.000005
K601A-7.7	61	0.70786	0.0029	0.000021
K604-1.9	46	0.70930	0.0027	0.000019

Radiometric Dating

Mattaia Formation

In the 2010 field season, Grazhdankin and company collected a volcanic ash from the upper part of the Mattaia Formation in the Kessyusa Group, in section 0709. The ash bed is 20 cm in thickness, bright white in the lower part, grading upward to greenish-yellow to brownish gray. The lower part of the layer was sampled.

X-ray diffraction (XRD) and x-ray fluorescence (XRF) analyses were performed on the sample matrix. XRD analysis yielded spectra for gypsum, high-layer charge

corrensite (a mixed-layer clay), and muscovite (Figure 3.31, Tables A.5 and A.6). Notably, the spectra do not suggest the presence of quartz or calcite, reducing the likelihood of a detrital origin for the rock.

Elemental analysis of the sample matrix shows that the total concentration of sulfur in the sample is less than 1%, permitting a gypsum concentration of no more than 3%. Mass spectrometric analysis of the bulk sample gives a $\delta^{34}S$ of +16‰, a value broadly similar to that of bulk sample $\delta^{34}S$ in other Khorbusuonka sections.
The XRF analysis (Table 3.4) is consistent with the interpretation that the layer is igneous in origin. The trace element analyses reveal that zircon concentrations (3400 ppm) are especially high, as are a number of other rare earth elements. However, the XRF data suggests that the identification of large gypsum peaks in the XRD analysis corresponds to only small amounts of this highly reflective phase.

The bulk sample was sent to a lab in Irkutsk for separation, yielding tens of thousands of zircon grains ranging up to 150 microns in sieve size. The zircons were sieved to 80 microns at UMD to decrease inconsistency in grain size, and mounts were made for the large and small fractions. Pyrite grains were removed from each mount. Electron dispersive spectroscopy (EDS) analyses were used to determine the mineralogy of anomalous grains and inclusions. In the small size fraction, barite, monazite, and titanite grains were observed. Inclusions of apatite, rutile, and pyrite were observed, especially in the large size fraction.

Electron backscatter diffraction (EBSD) and cathodoluminescence (CL) microprobe images of twenty grains were taken to map differences in composition within

Table 3.4. Major and trace element composition of Mattaia sample 0709-60.

Sample: 0709-60				
Major element comp. (%)			**Trace element comp. (ppm)**	
SiO_2	54.32		**Rb**	104.7
TiO_2	0.63		**Sr**	396
Al_2O_3	23.94		**Y**	204
Fe_2O_3T	4.96		**Zr**	3442
MnO	0.07		**V**	28
MgO	2.78		**Ni**	4
CaO	3.42		**Cr**	2
Na2O	0.41		**Nb**	317.1
K_2O	6.98		**Ga**	51.2
P_2O_5	0.09		**Cu**	228
SO_3	1.74		**Zn**	46
Total	**99.34**		**Co**	19
LOI	**10.09**		**Ba**	395
%SO_3	2.33		**La**	206
			Ce	397
			U	8.2
			Th	98.1
			Sc	8
			Pb	25

each grain. Over half of the imaged zircon grains contained a discernable rim and core, and oscillatory zoning was commonly observed (for example, Figure 3.33). Inclusions within grains were ubiquitous.

To date the sample, each of the twenty imaged grains imaged were subjected to laser ablation using a 10 micron spot size. The small spot size allowed distinct measurements to be derived from zircon cores, rims, and any intermediate layers. A total of 41 measurements were taken, of which 29 were accepted. The remaining measurements were rejected due to high Pb-204, high Pb-206/Pb-207 error, or discordance. A concordia plot of accepted measurements can be seen in Figure 3.34. Accepted measurements are tabulated in Table A.7.

Rims, cores, and intermediate layer ages were indistinguishable within error. The weighted mean of all accepted measurements is 528 ± 11 Ma (2σ) (Figure 3.35). The error encompasses both that which results from the distribution of sample measurements as well as the systematic error, principally derived from the variability of standard analyses, along with the uncertainty on the correct age of the standard, and the uncertainty on the decay constant.

Dengying Formation

Carbon and Oxygen Isotopic Composition

One hundred and seventy-one samples from a single section of the Dengying Formation were analyzed for carbonate carbon and oxygen isotopic composition (Figure 3.25, Table A.2). Here, the base of the Algal Dolomite Member has a carbon isotopic composition of +2‰; values trend more positive upsection to +4‰ (P1), with an excursion up to +5.5‰. After a brief stabilization at 0‰ (I1), another, more significant

positive excursion to +6‰ (P2) occurs upsection, coincident with facies change from microbialaminate of the Algal Dolomite to carbonaceous siltstone and shale of the Gaojiashan Member. A generally positive isotopic composition dominates for the next 200 meters (P3), reaching as high as +4‰, then trends negative for the next 100 meters, reaching -1‰ by the top of the section (N1).

Oxygen isotope data was also collected for the Dengying Formation. Generally heavy (up to 0‰) but variable isotopic compositions are recorded in the lower part of the section. Values fall to -5‰ during carbon isotope excursion P2, then exhibit variability between -4‰ and -2‰ during P3. Oxygen isotopic composition mirrors that of carbon for the uppermost part of the section, reaching -10‰ by the top of the section.

Radiometric Dating

Two samples collected from the Gaojiashan Member of the Dengying Formation in South China have also been separated to yield zircons. The layers are separated by approximately two meters, and vary in lithology both between themselves and the surrounding carbonate strata. The lower layer (sample 09G-35.3) is lithified, about 3 cm thick, consisting of 3 mm greenish layers on the top and bottom grading into a yellowish middle portion. The upper layer (sample 09G-37.9) is ~2 cm thick, consisting of gray-green to white clay, which is soft and easily crumbled.

Matrix material from the two Dengying samples was sent to Dr. Stan Mertzman at Franklin and Marshall College for XRD analysis. Data resulting from XRD analysis indicates that the Dengying samples lack the montmorillonite and bentonite clays considered indicators of volcanic origin. Sample 09G-35.3 is a mix of dolomite, calcite and quartz (Figure 3.36, Tables A.8 and A.9). 09G-37.9 consists predominantly of quartz,

with calcite and a small amount of a 10 Angstrom phase, most likely muscovite (Figure 3.37, Tables A.11 and A.12). This data supports a detrital origin for the Dengying geochronological samples.

From sample 09G-35.3, only ~60 zircon grains were separated. The grains were uniformly small (up to 100 microns across) and rounded. Concentric zoning is observed in cathodoluminescence microprobe images (Figure 3.37). Fifty grains were mounted and analyzed; 24 analyses were excluded due to discordance, high ^{204}Pb, or high error on the ratio of $^{206}Pb/^{208}Pb$. The results of 26 analyses are shown in Figure 3.40 (Table A.13-1 and A.13-2). None of the grains has an age younger than 600 Ma, but there are too few analyses to be confident that this absence represents depositional exclusion rather than undersampling. No maximum depositional age was calculated for this sample.

On the other hand, thousands of zircons were separated from 09G-37.9. While most grains are similar in size to those found in 09G-35.3, grains range up to three times that size (300 microns). Most grains are rounded, but 5-10% of grains retain their original elongate shape, and a few unrounded grains are observed (Figure 3.38). Several hundred grains were mounted, from which 175 were analyzed. Eighty-three analyses were excluded, leaving 92 interpretable analyses, shown in Figures 3.41 and 3.42 (Table A.14-1 and A.14-2). Grain ages in this sample range from the Ediacaran to the Archean. The population of youngest grains (N = 4) has an average age of 548 ± 8.1 Ma (2σ). The maximum depositional age for this sample is 560 Ma, consistent with deposition during the Ediacaran Period.

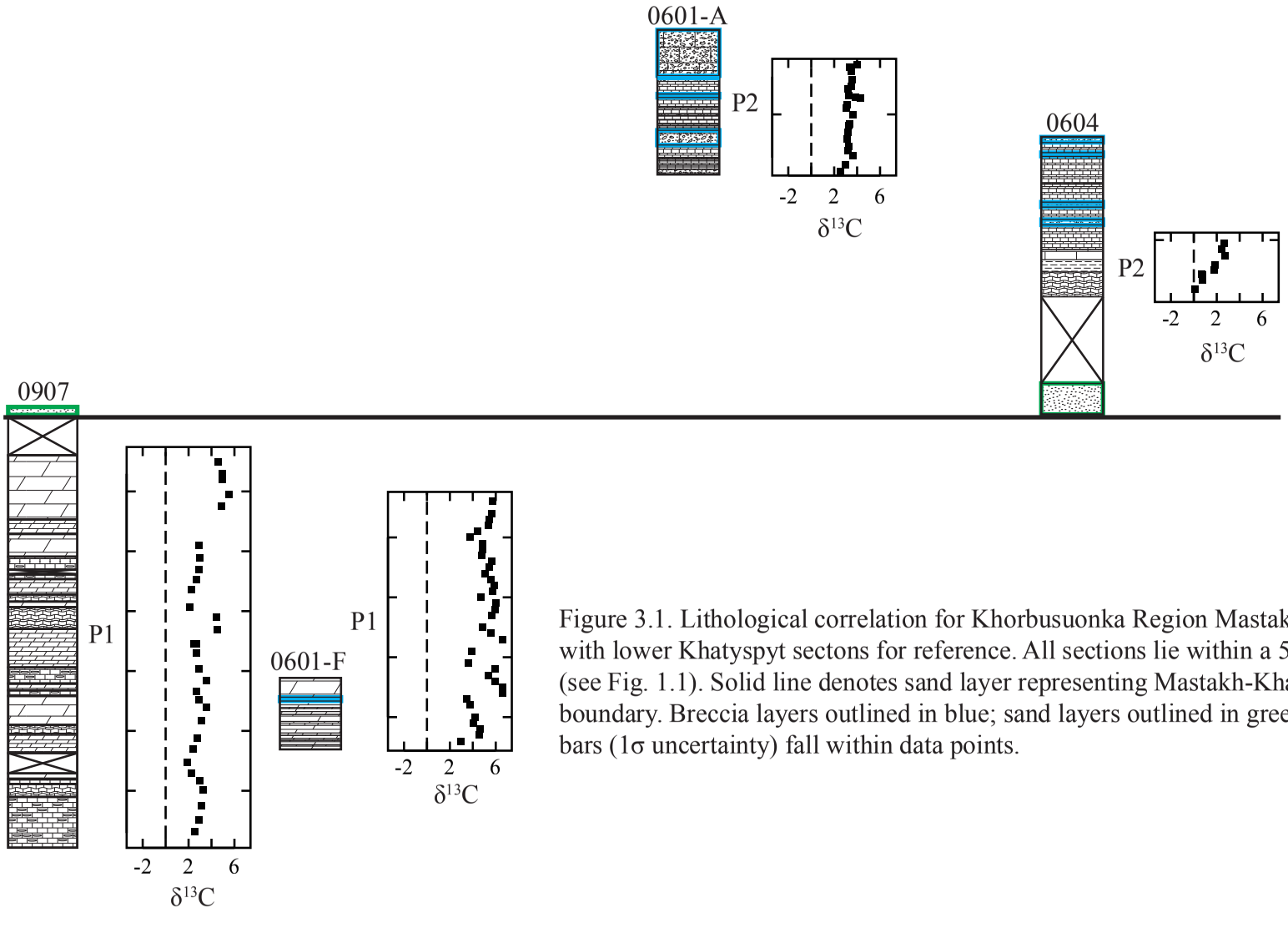

Figure 3.1. Lithological correlation for Khorbusuonka Region Mastakh sections, with lower Khatyspyt sectons for reference. All sections lie within a 5 km radius (see Fig. 1.1). Solid line denotes sand layer representing Mastakh-Khatyspyt boundary. Breccia layers outlined in blue; sand layers outlined in green. Error bars (1σ uncertainty) fall within data points.

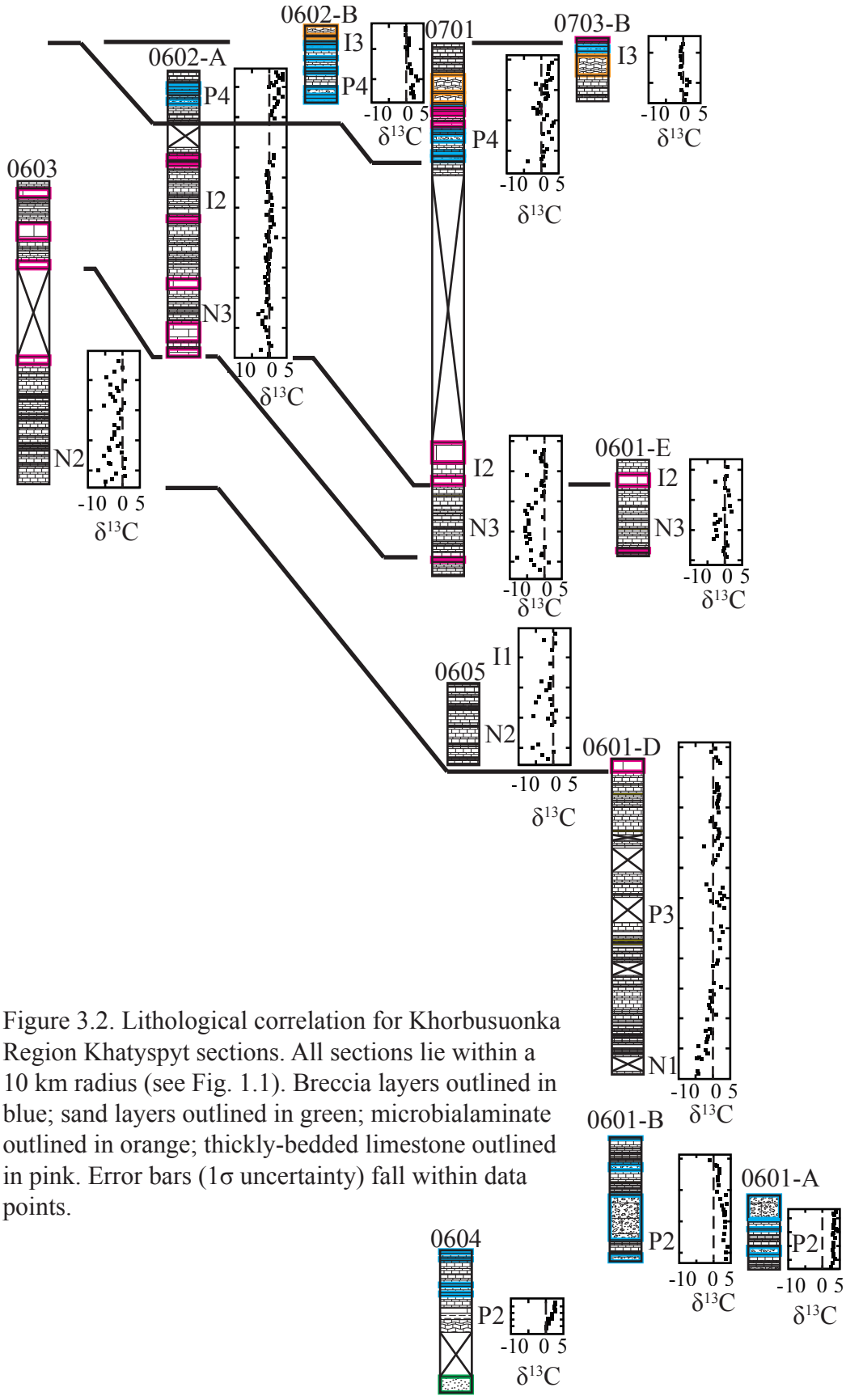

Figure 3.2. Lithological correlation for Khorbusuonka Region Khatyspyt sections. All sections lie within a 10 km radius (see Fig. 1.1). Breccia layers outlined in blue; sand layers outlined in green; microbialaminate outlined in orange; thickly-bedded limestone outlined in pink. Error bars (1σ uncertainty) fall within data points.

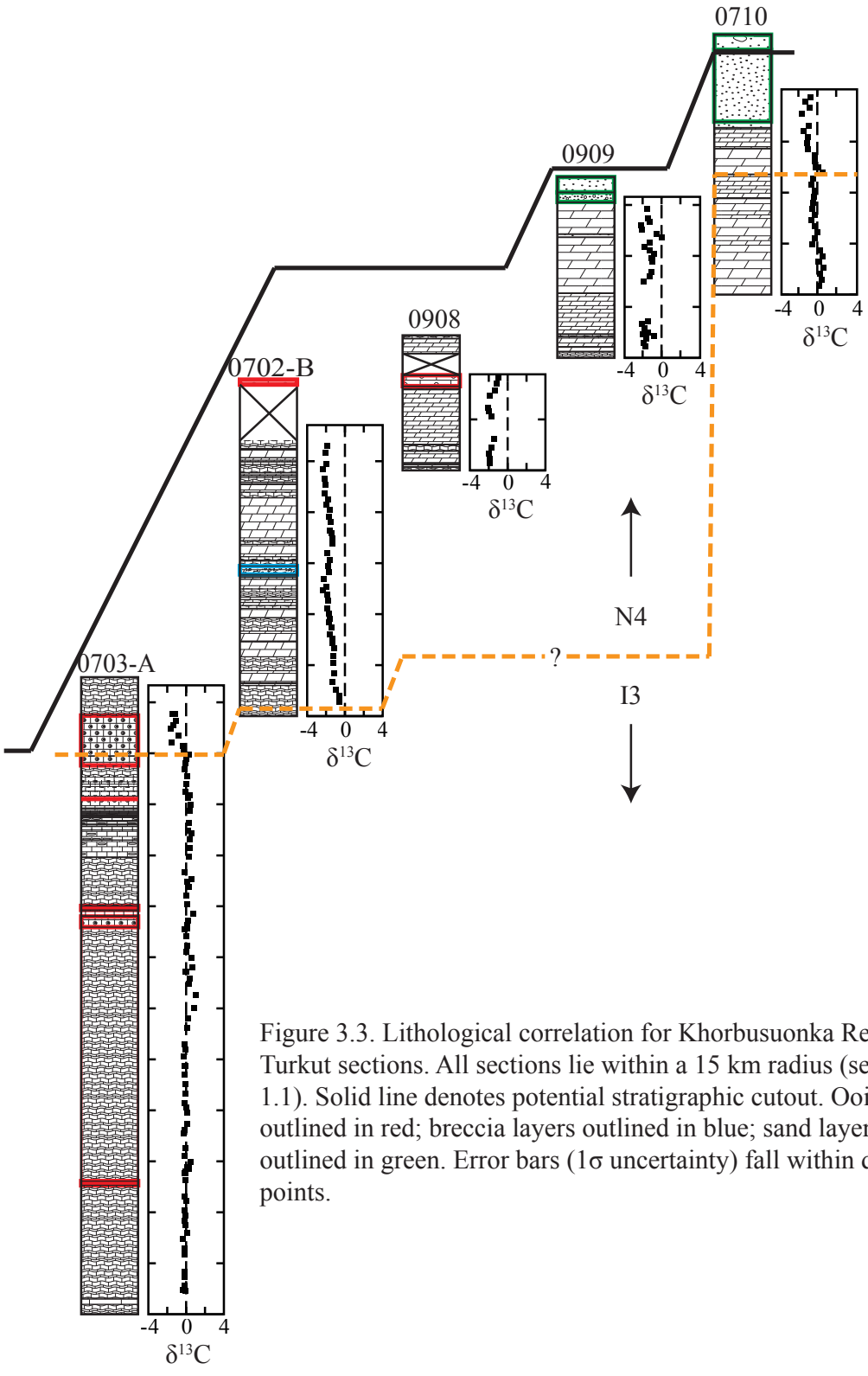

Figure 3.3. Lithological correlation for Khorbusuonka Region Turkut sections. All sections lie within a 15 km radius (see Fig. 1.1). Solid line denotes potential stratigraphic cutout. Ooid layers outlined in red; breccia layers outlined in blue; sand layers outlined in green. Error bars (1σ uncertainty) fall within data points.

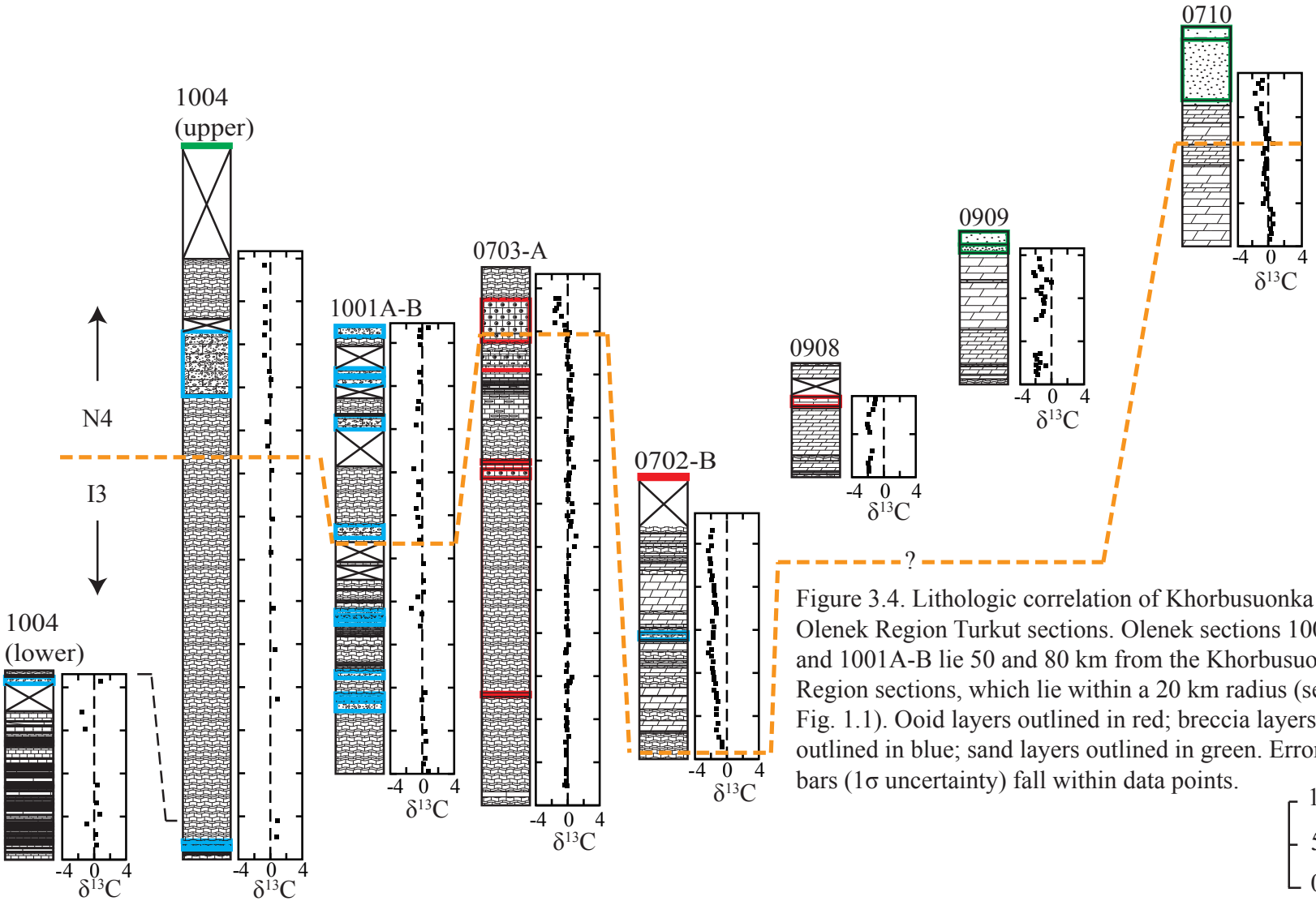

Figure 3.4. Lithologic correlation of Khorbusuonka and Olenek Region Turkut sections. Olenek sections 1004 and 1001A-B lie 50 and 80 km from the Khorbusuonka Region sections, which lie within a 20 km radius (see Fig. 1.1). Ooid layers outlined in red; breccia layers outlined in blue; sand layers outlined in green. Error bars (1σ uncertainty) fall within data points.

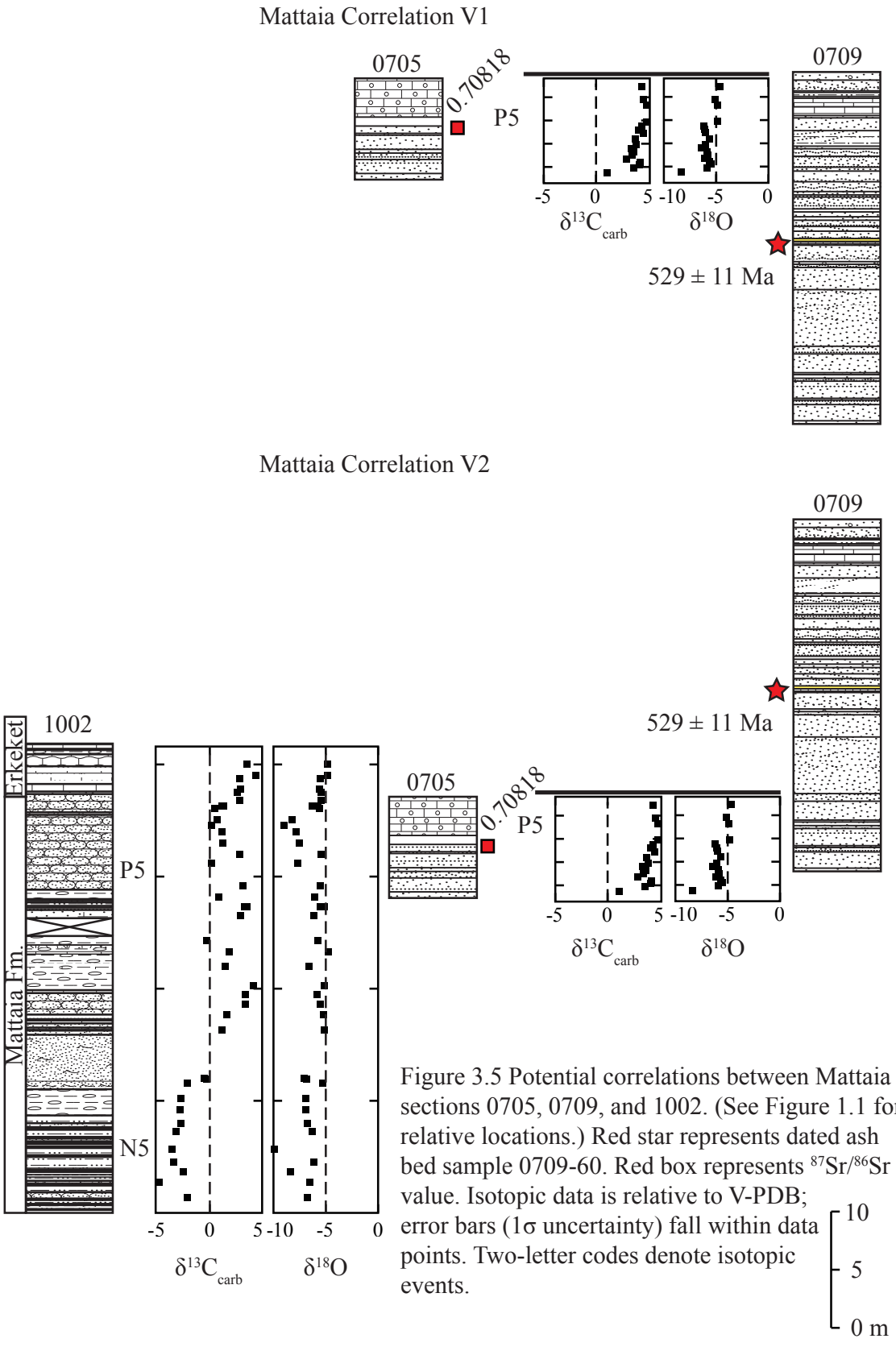

Figure 3.5 Potential correlations between Mattaia sections 0705, 0709, and 1002. (See Figure 1.1 for relative locations.) Red star represents dated ash bed sample 0709-60. Red box represents $^{87}Sr/^{86}Sr$ value. Isotopic data is relative to V-PDB; error bars (1σ uncertainty) fall within data points. Two-letter codes denote isotopic events.

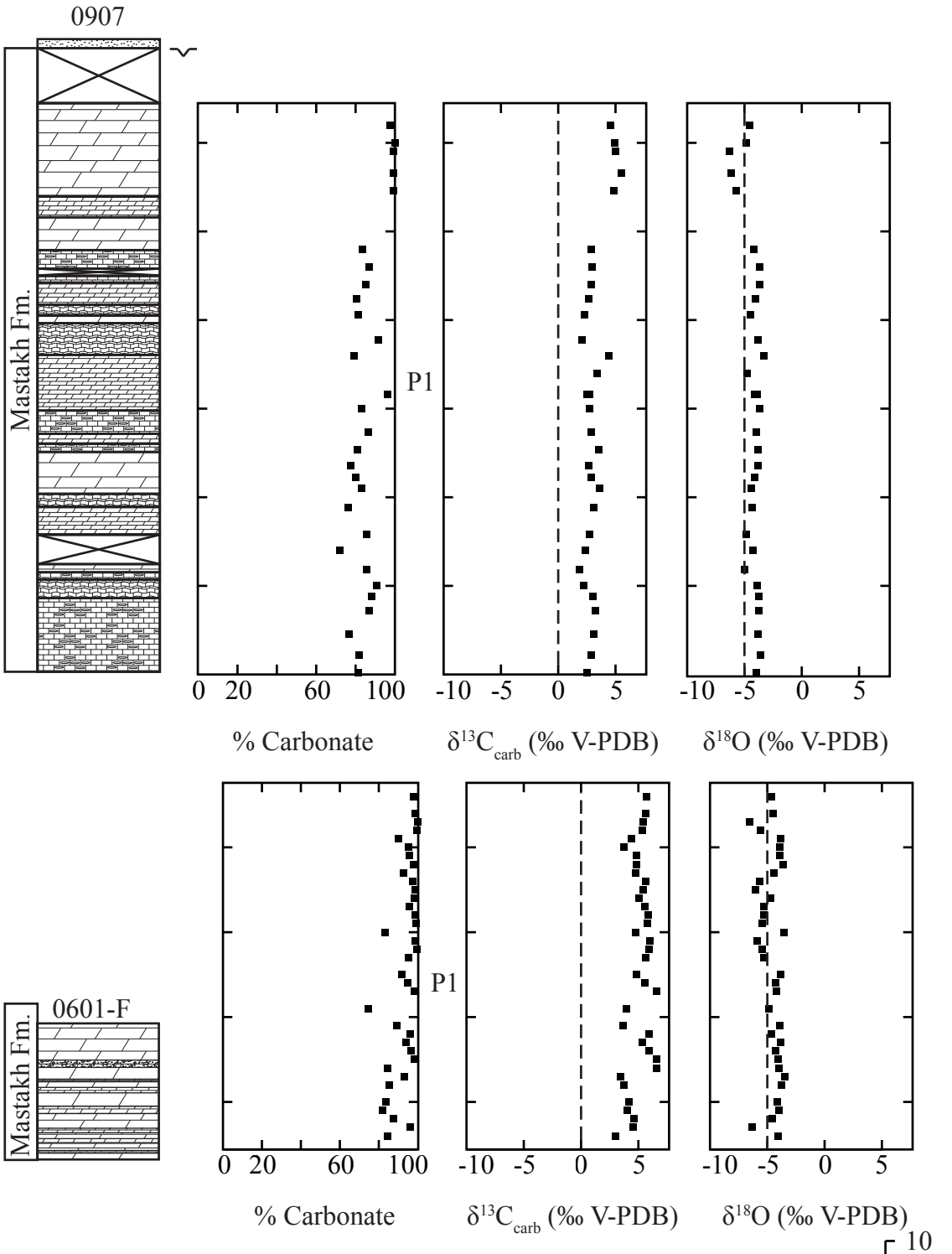

Figure 3.6. Percent carbonate and carbon and oxygen istotope data for Mastakh sections 0907 and 0601-F (Khorbusuonka region, see Figure X). See Figure 1.1 for potential correlations. Error bars (1σ uncertainty) fall within data points. Sandstone at top of 0907 represents basal Khatyspyt. Two-letter codes denote isotopic events.

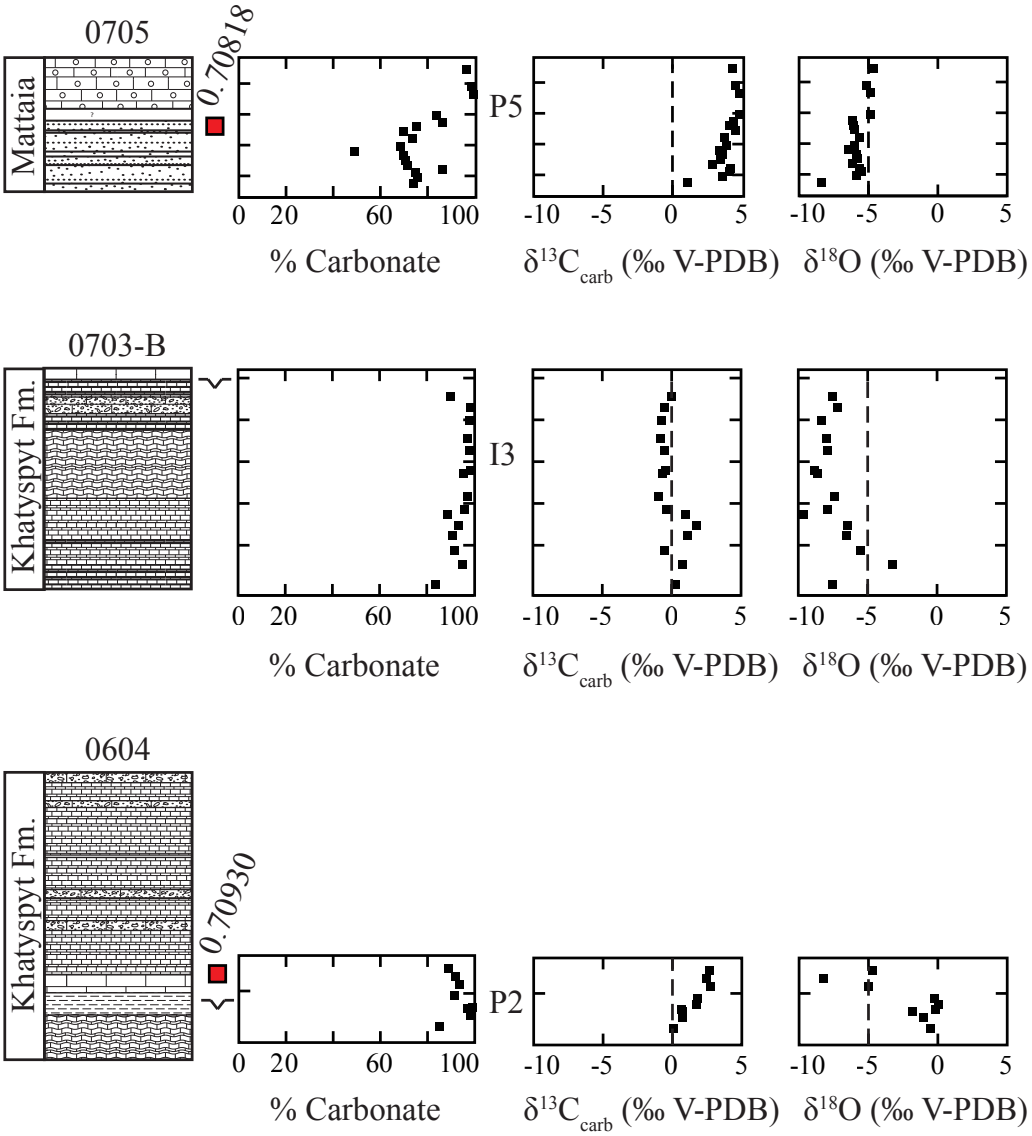

Figure 3.7. Percent carbonate and carbon and oxygen istotope data for Khatyspyt sections 0604 and 0703-B and Mattaia section 0705 (Khorbusuonka Region, see Figure 1.1). See Figure 3.2 for potential correlations. Error bars (1σ uncertainty) fall within data points. Red boxes represent $^{87}Sr/^{86}Sr$ values. Two-letter codes denote isotopic events.

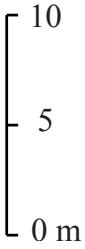

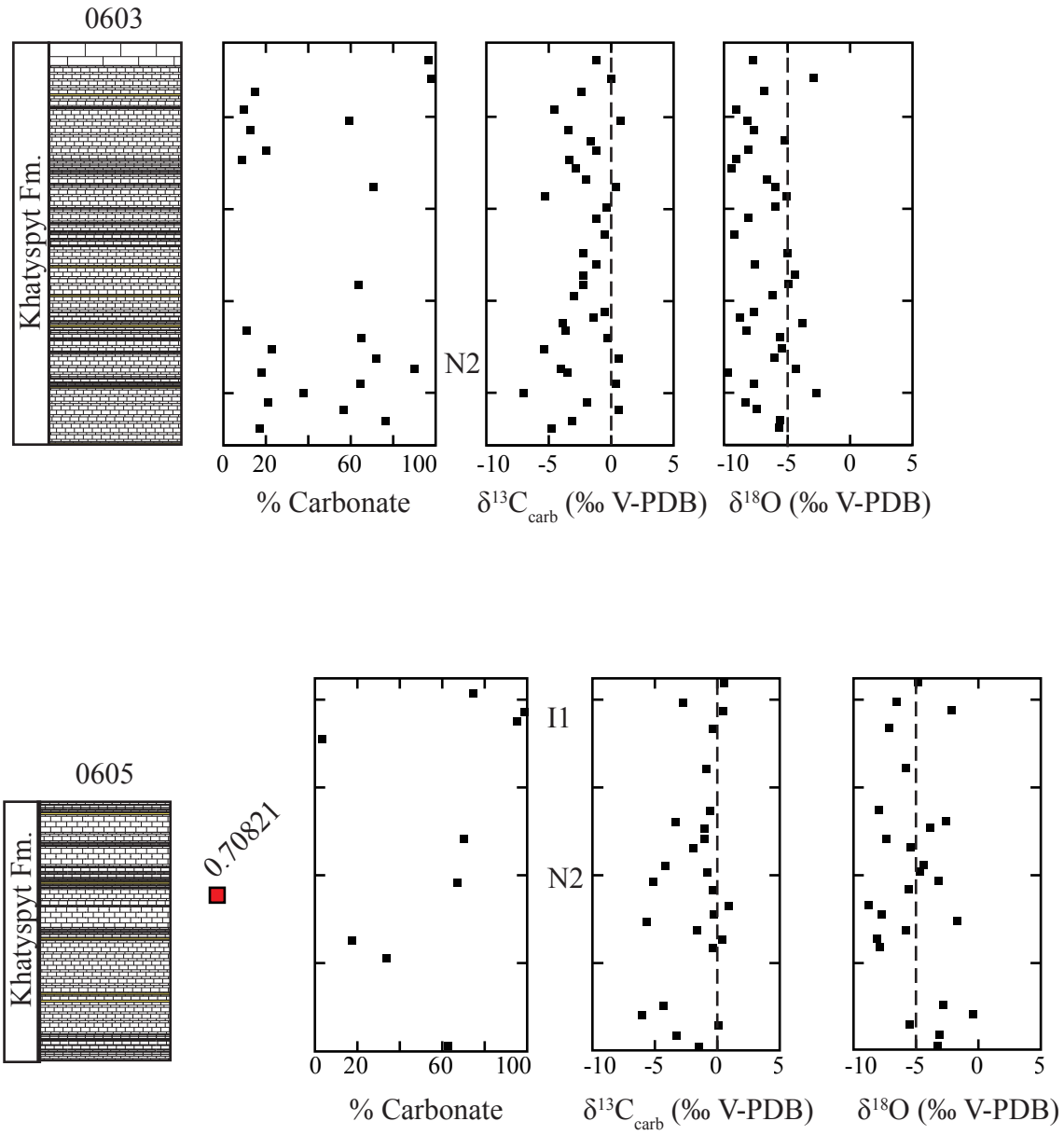

Figure 3.8. Percent carbonate and carbon and oxygen isotope data for Khatyspyt sections 0603 and 0605 (Khorbusuonka Region, see Figure 1.1). See Figure Y for potential correlations. Error bars (1σ uncertainty) fall within data points. Red box represents $^{87}Sr/^{86}Sr$ value. Two-letter codes denote isotopic events.

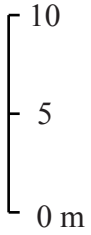

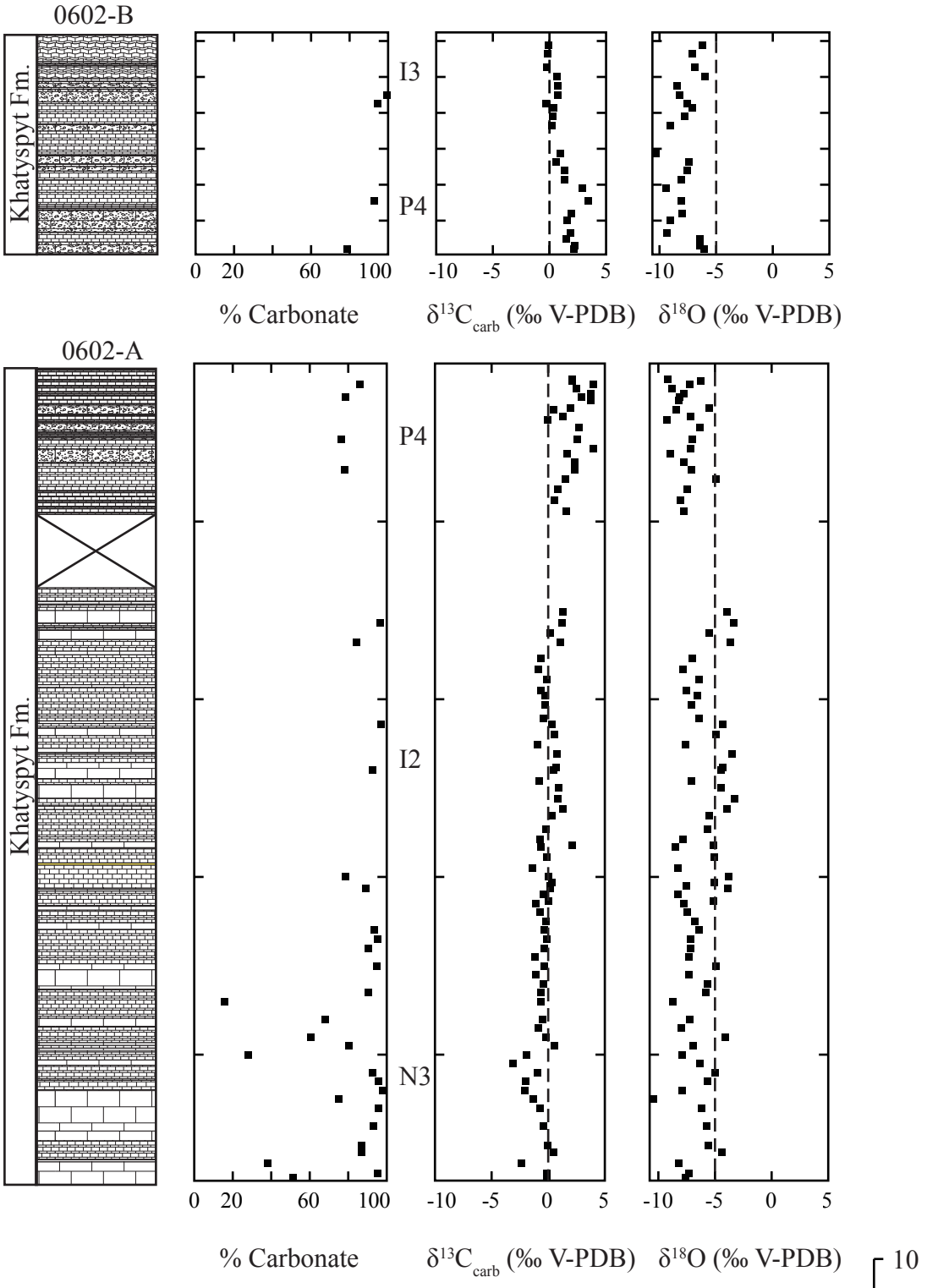

Figure 3.9. Percent carbonate and carbon and oxygen isotope data for upper and lower portions of Khatyspyt section 0602 (Khorbusuonka Region, see Figure 1.1). For relation of upper and lower section, see Figure 3.2. Error bars (1σ uncertainty) fall within data points. Two-letter codes denote isotopic events.

Figure 3.1. Lithological correlation for Khorbusuonka Region Mastakh sections, with lower Khatyspyt sections for reference. All sections lie within a 5 km radius (see Fig. 1.1). Solid line denotes sand layer representing Mastakh-Khatyspyt boundary. Breccia layers outlined in blue; sand layers outlined in green. Error bars (1σ uncertainty) fall within data points.

Figure 3.2. Lithological correlation for Khorbusuonka Region Khatyspyt sections. All sections lie within a 10 km radius (see Fig. 1.1). Breccia layers outlined in blue; sand layers outlined in green; microbialaminate outlined in orange; thickly-bedded limestone outlined in pink. Error bars (1σ uncertainty) fall within data points.

Figure 3.3. Lithological correlation for Khorbusuonka Region Turkut sections. All sections lie within a 15 km radius (see Fig. 1.1). Solid line denotes potential stratigraphic cutout. Ooid layers outlined in red; breccia layers outlined in blue; sand layers outlined in green. Error bars (1σ uncertainty) fall within data points.

Figure 3.4. Lithological correlation of Khorbusuonka and Olenek Region Turkut sections. Olenek sections 1004 and 1001A-B lie 50 and 80 km from the Khorbusuonka Region sections, which lie within a 20 km radius (see Fig. 1.1). Ooid layers outlined in red; breccia layers outlined in blue; sand layers outlined in green. Error bars (1σ uncertainty) fall within data points.

Figure 3.5. Potential correlations between Mattaia sections 0705, 0709, and 1002. (See Figure 1.1 for relative locations.) Red star represents dated ash bed sample 0709-60. Red box represents $^{87}Sr/^{86}Sr$ value. Isotopic data is relative to V-PDB; error bars (1σ uncertainty) fall within data points. Two-letter codes denote isotopic events.

Figure 3.6. Percent carbonate and carbon and oxygen isotope data for Mastakh sections 0907 and 0601-F (Khorbusuonka region; see Figure 1.1). See Figure 3.1 for potential correlations. Error bars (1σ uncertainty) fall within data points. Sandstone at top of 0907 represents basal Khatyspyt. Two-letter codes denote isotopic events.

Figure 3.7. Percent carbonate and carbon and oxygen isotope data for Khatyspyt sections 0604 and 0703-B and Mattaia section 0705 (Khorbusuonka Region, see Figure 1.1). See Figure 3.2 for potential correlations. Error bars (1σ uncertainty) fall within data points. Red boxes represent $^{87}Sr/^{86}Sr$ values. Two-letter codes denote isotopic events.

Figure 3.8. Percent carbonate and carbon and oxygen isotope data for Khatyspyt sections 0603 and 0605 (Khorbusuonka Region, see Figure 1.1). See Figure 3.2 for potential correlations. Error bars (1σ uncertainty) fall within data points. Red box represents $^{87}Sr/^{86}Sr$ value. Two-letter codes denote isotopic events.

Figure 3.9. Percent carbonate and carbon and oxygen isotope data for upper and lower portions of Khatyspyt section 0602 (Khorbusuonka Region, see Figure 1.1). For relation of upper and lower section, see Figure 3.2. Error bars (1σ uncertainty) fall within data points. Two-letter codes denote isotopic events.

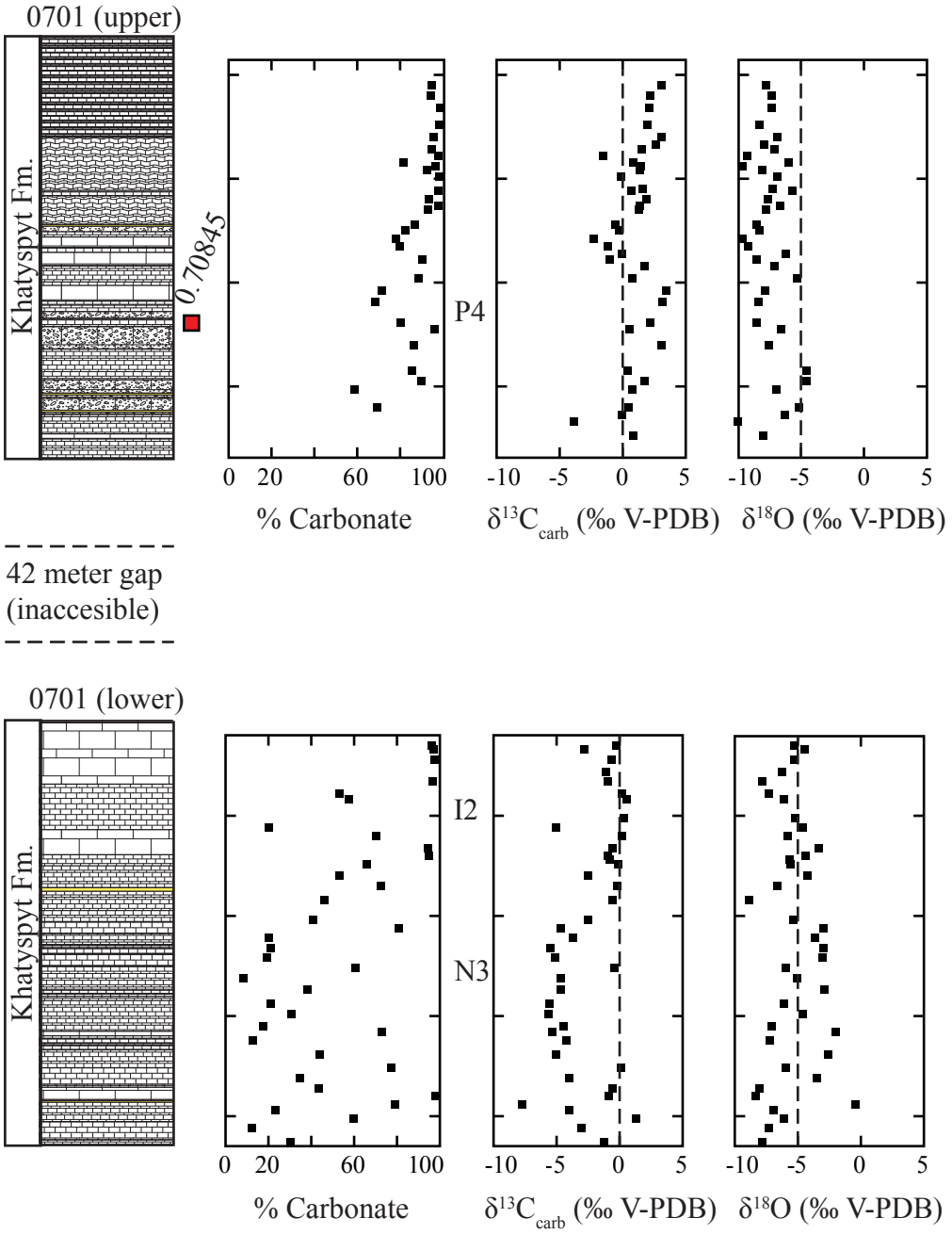

Figure 3.10. Percent carbonate and carbon and oxygen isotope data for upper and lower portions of Khatyspyt section 0701 (Khorbusuonka Region, see Figure 1.1). Lower section lies 42 m below upper section (see Figure 3.2). Error bars (1σ uncertainty) fall within data points. Red box represents $^{87}Sr/^{86}Sr$ value. Two-letter codes denote isotopic events.

10
5
0 m

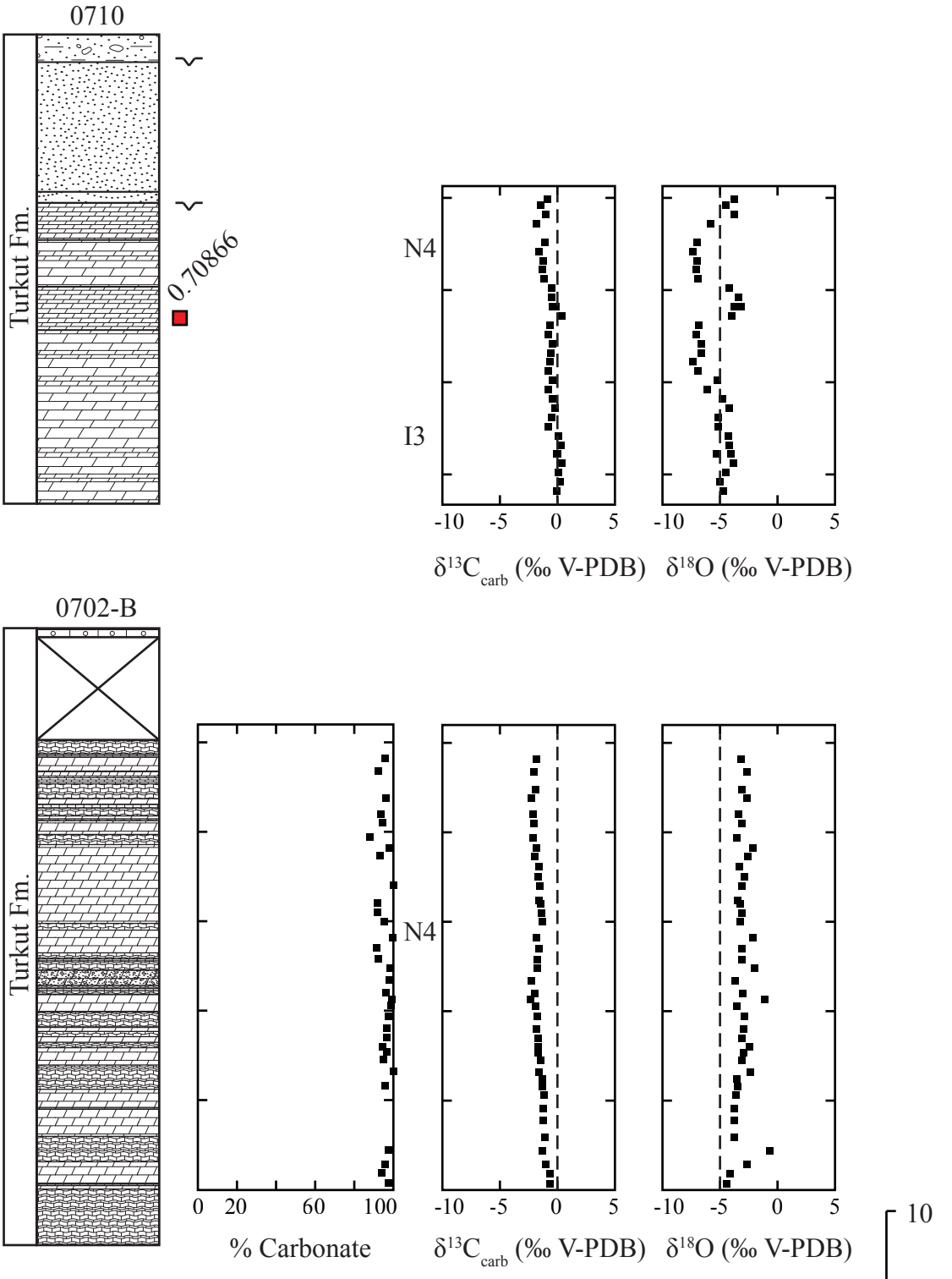

Figure 3.11. Percent carbonate and carbon and oxygen isotope data for Turkut sections 0710 and 0702-B (Khorbusuonka Region, see Figure 1.1). See Figure 3.3 for potential correlations. Error bars (1σ uncertainty) fall within data points. Percent carbonate data unavailable for 0710. Red box represents $^{87}Sr/^{86}Sr$ value.Two-letter codes denote isotopic events.

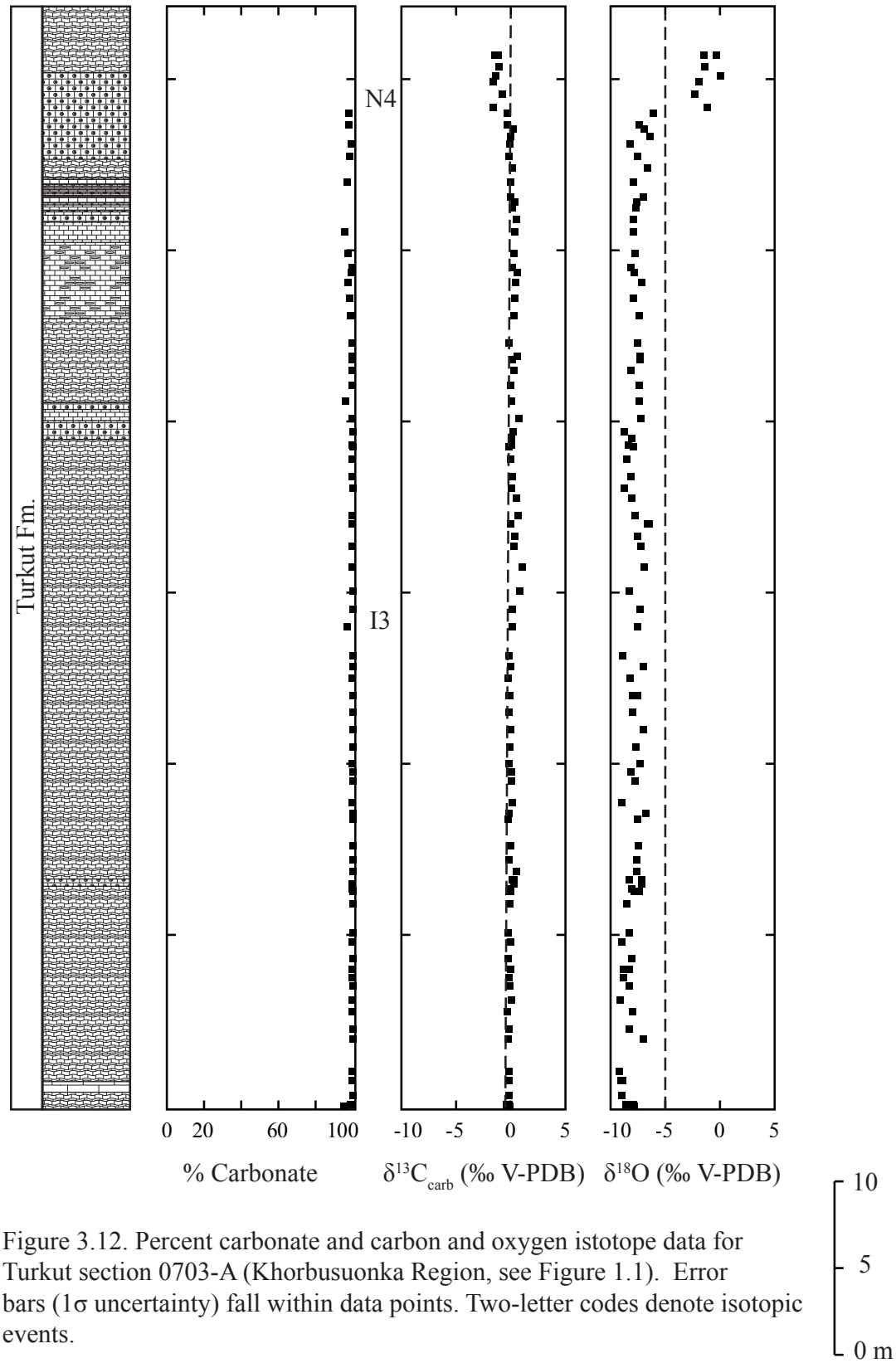

Figure 3.12. Percent carbonate and carbon and oxygen isotope data for Turkut section 0703-A (Khorbusuonka Region, see Figure 1.1). Error bars (1σ uncertainty) fall within data points. Two-letter codes denote isotopic events.

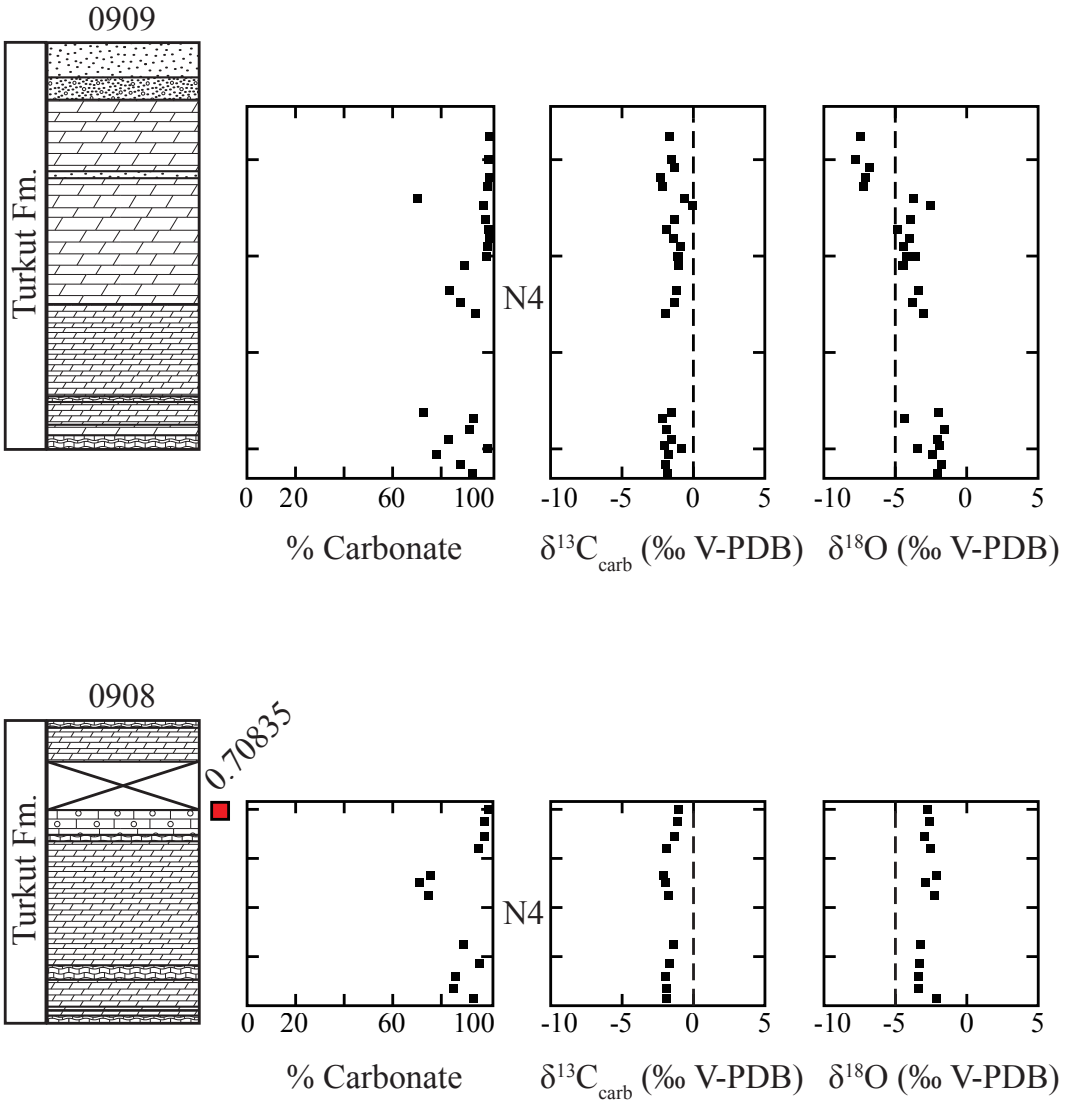

Figure 3.13. Percent carbonate and carbon and oxygen istotope data for Turkut sections 0908 and 0909 (Khorbusuonka Region, see Figure 1.1). See Figure Y for potential correlations. Error bars (1σ uncertainty) fall within data points. Red box represents $^{87}Sr/^{86}Sr$ value. Two-letter codes denote isotopic events.

10
5
0 m

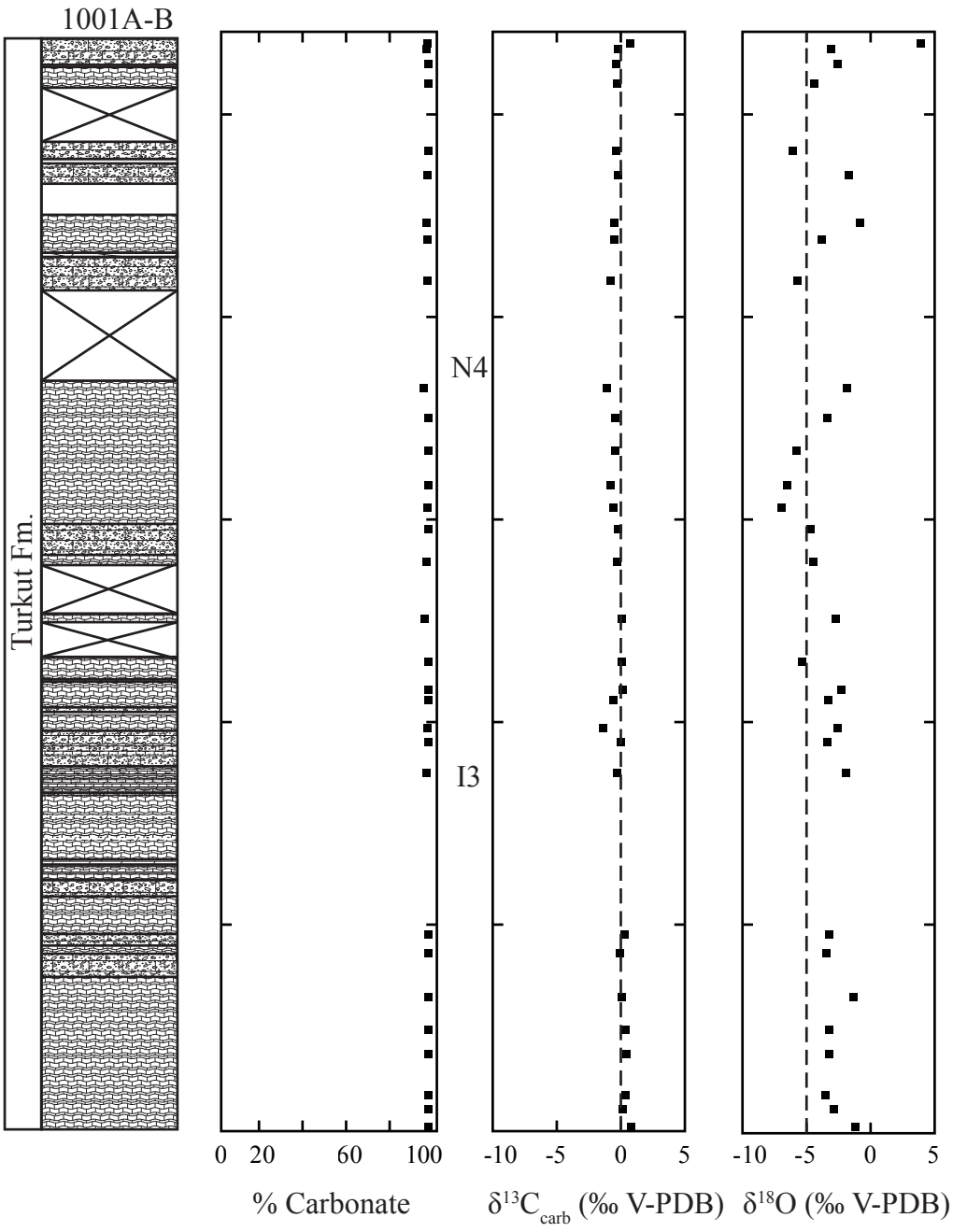

Figure 3.14. Percent carbonate and carbon and oxygen isotope data for Turkut section 1001A-B (Olenek Region; see Figure 1.1). Error bars (1σ uncertainty) fall within data points. Two-letter codes denote isotopic events.

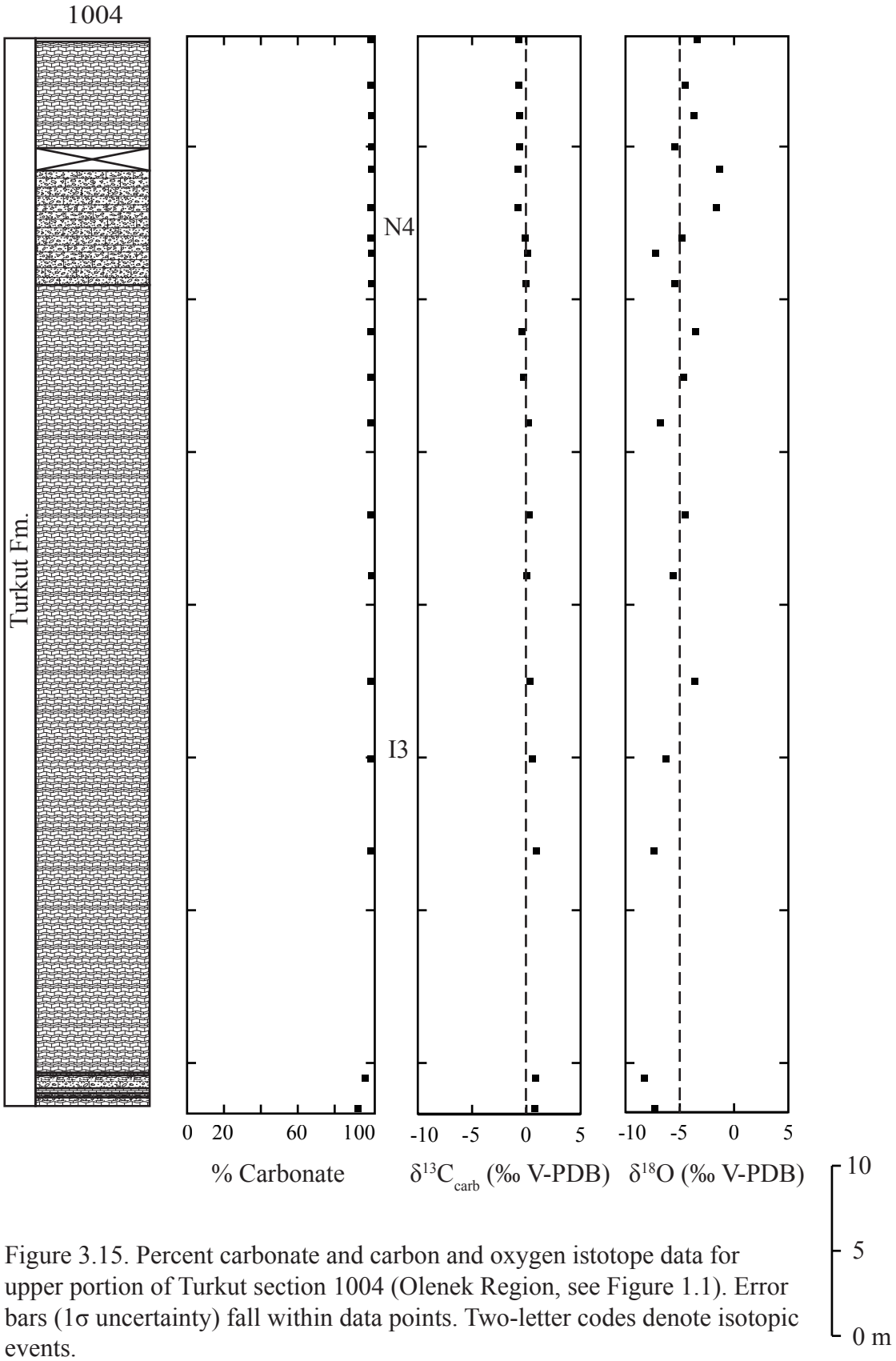

Figure 3.15. Percent carbonate and carbon and oxygen isotope data for upper portion of Turkut section 1004 (Olenek Region, see Figure 1.1). Error bars (1σ uncertainty) fall within data points. Two-letter codes denote isotopic events.

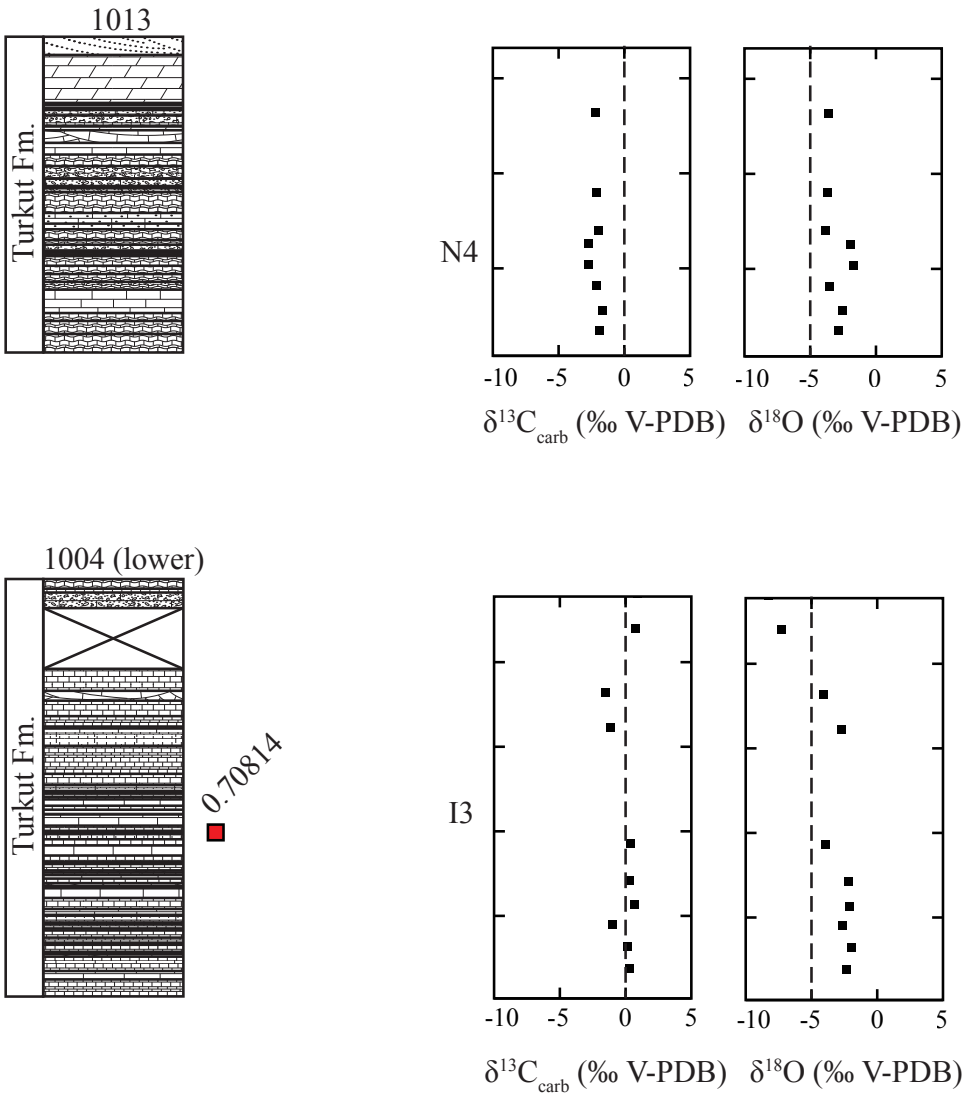

Figure 3.16. Carbon and oxygen istotope data for Turkut sections 1013 and 1004 (lower portion) (Olenek Region, see Figure 1.1). For potential correlations, see Figures X and Y. Error bars (1σ uncertainty) fall within data points. Percent carbonate data unavailable. Red box represents $^{87}Sr/^{86}Sr$ value. Two-letter codes denote isotopic events. See upper portion of 1004 in figure 3.15.

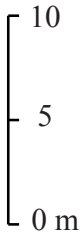

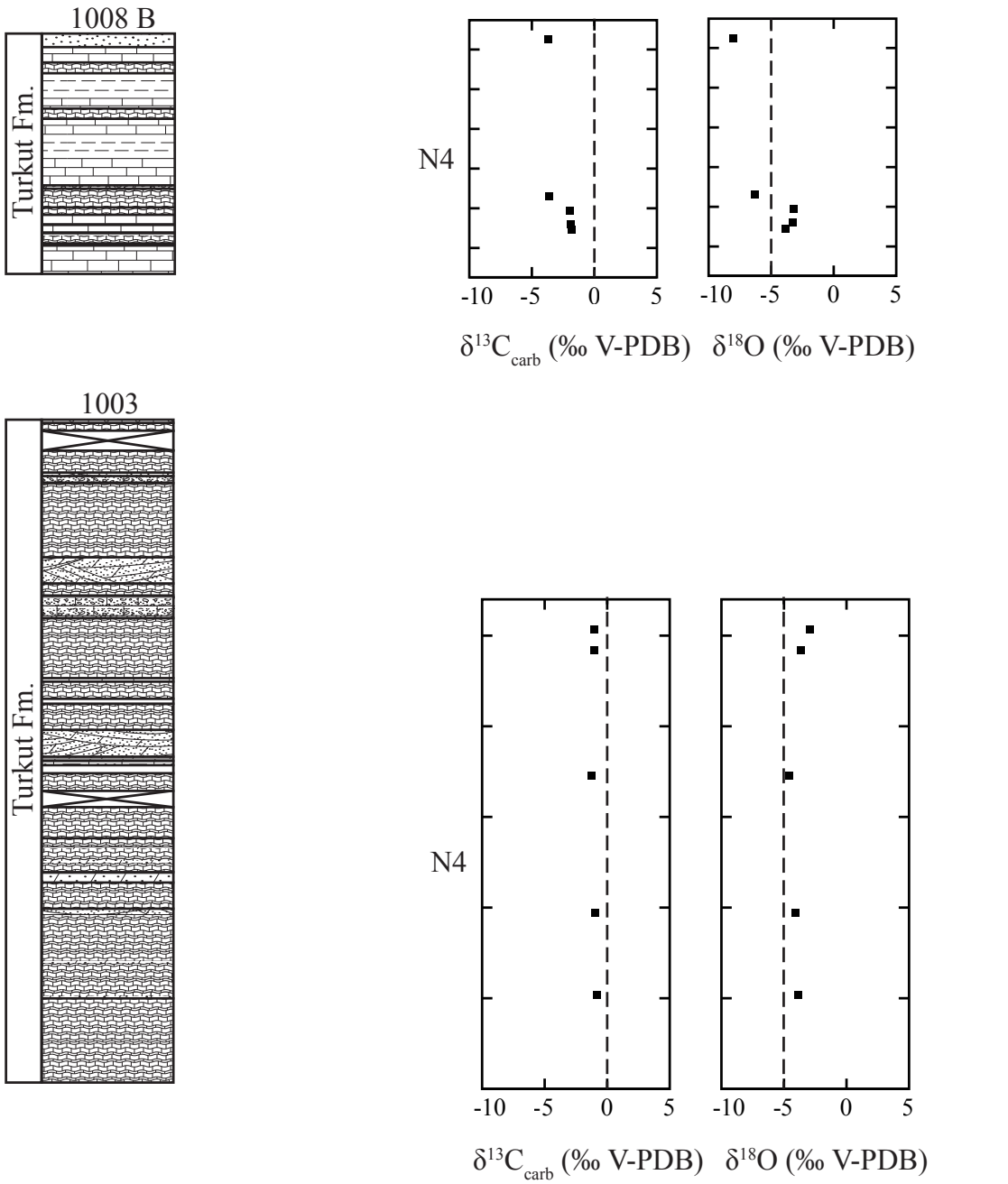

Figure 3.17. Carbon and oxygen isotope data for Turkut sections 1008-B and 1003 (Olenek Region, see Figure 1.1). Error bars (1σ uncertainty) fall within data points. Percent carbonate data unavailable. Two-letter codes denote isotopic events.

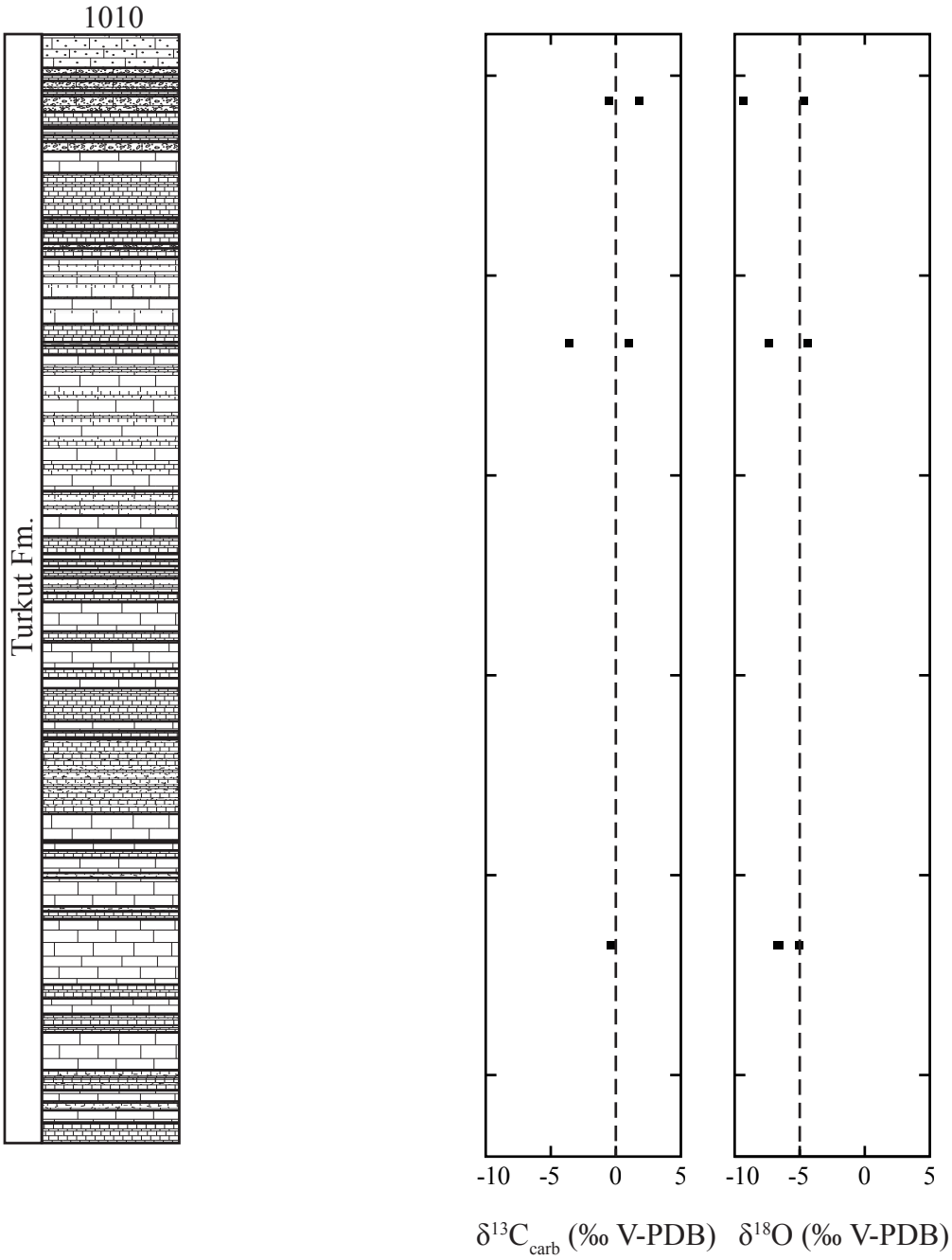

Figure 3.18. Carbon and oxygen istotope data for Turkut section 1010 (Olenek Region, see Figure 1.1). Error bars (1σ uncertainty) fall within data points. Percent carbonate data unavailable.

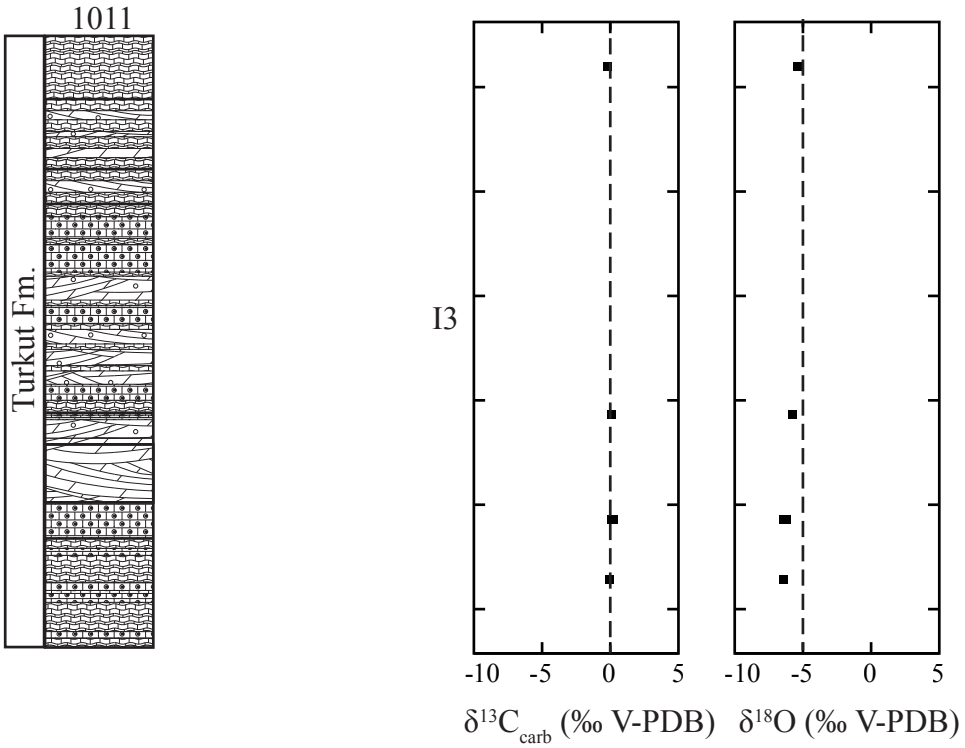

Figure 3.19. Carbon and oxygen istotope data for Turkut section 1011 (Olenek Region, see Figure 1.1). Error bars (1σ uncertainty) fall within data points. Percent carbonate data unavailable. Two-letter codes denote isotopic events.

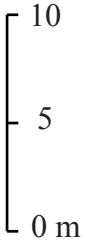

Figure 3.10. Percent carbonate and carbon and oxygen isotope data for upper and lower portions of Khatyspyt section 0701 (Khorbusuonka Region, see Figure 1.1). Lower section lies 42 m below upper section (see Figure 3.2). Error bars (1σ uncertainty) fall within data points. Red box represents $^{87}Sr/^{86}Sr$ value. Two-letter codes denote isotopic events.

Figure 3.11. Percent carbonate and carbon and oxygen isotope data for Turkut sections 0710 and 0702-B (Khorbusuonka Region, see Figure 1.1). See Figure 3.3 for potential correlations. Error bars (1σ uncertainty) fall within data points. Percent carbonate data unavailable for 0710. Red box represents $^{87}Sr/^{86}Sr$ value.Two-letter codes denote isotopic events.

Figure 3.12. Percent carbonate and carbon and oxygen isotope data for Turkut section 0703-A (Khorbusuonka Region, see Figure 1.1). Error bars (1σ uncertainty) fall within data points. Two-letter codes denote isotopic events.

Figure 3.13. Percent carbonate and carbon and oxygen isotope data for Turkut sections 0908 and 0909 (Khorbusuonka Region, see Figure 1.1). See Figure 3.3 for potential correlations. Error bars (1σ uncertainty) fall within data points. Red box represents $^{87}Sr/^{86}Sr$ value. Two-letter codes denote isotopic events.

Figure 3.14. Percent carbonate and carbon and oxygen isotope data for Turkut section 1001A-B (Olenek Region; see Figure 1.1). Error bars (1σ uncertainty) fall within data points. Two-letter codes denote isotopic events.

Figure 3.15. Percent carbonate and carbon and oxygen isotope data for upper portion of Turkut section 1004 (Olenek Region, see Figure 1.1). Error bars (1σ uncertainty) fall within data points. Two-letter codes denote isotopic events.

Figure 3.16. Carbon and oxygen isotope data for Turkut sections 1013 and 1004 (lower portion) (Olenek Region, see Figure 1.1). For potential correlations, see Figures 3.3 and 3.4. Error bars (1σ uncertainty) fall within data points. Percent carbonate data unavailable. Red box represents $^{87}Sr/^{86}Sr$ value. Two-letter codes denote isotopic events. See upper portion of 1004 in Figure 3.15.

Figure 3.17. Carbon and oxygen isotope data for Turkut sections 1008-B and 1003 (Olenek Region, see Figure 1.1). Error bars (1σ uncertainty) fall within data points. Percent carbonate data unavailable. Two-letter codes denote isotopic events.

Figure 3.18. Carbon and oxygen isotope data for Turkut section 1010 (Olenek Region, see Figure 1.1). Error bars (1σ uncertainty) fall within data points. Percent carbonate data unavailable.

Figure 3.19. Carbon and oxygen isotope data for Turkut section 1011 (Olenek Region, see Figure 1.1). Error bars (1σ uncertainty) fall within data points. Percent carbonate data unavailable. Two-letter codes denote isotopic events.

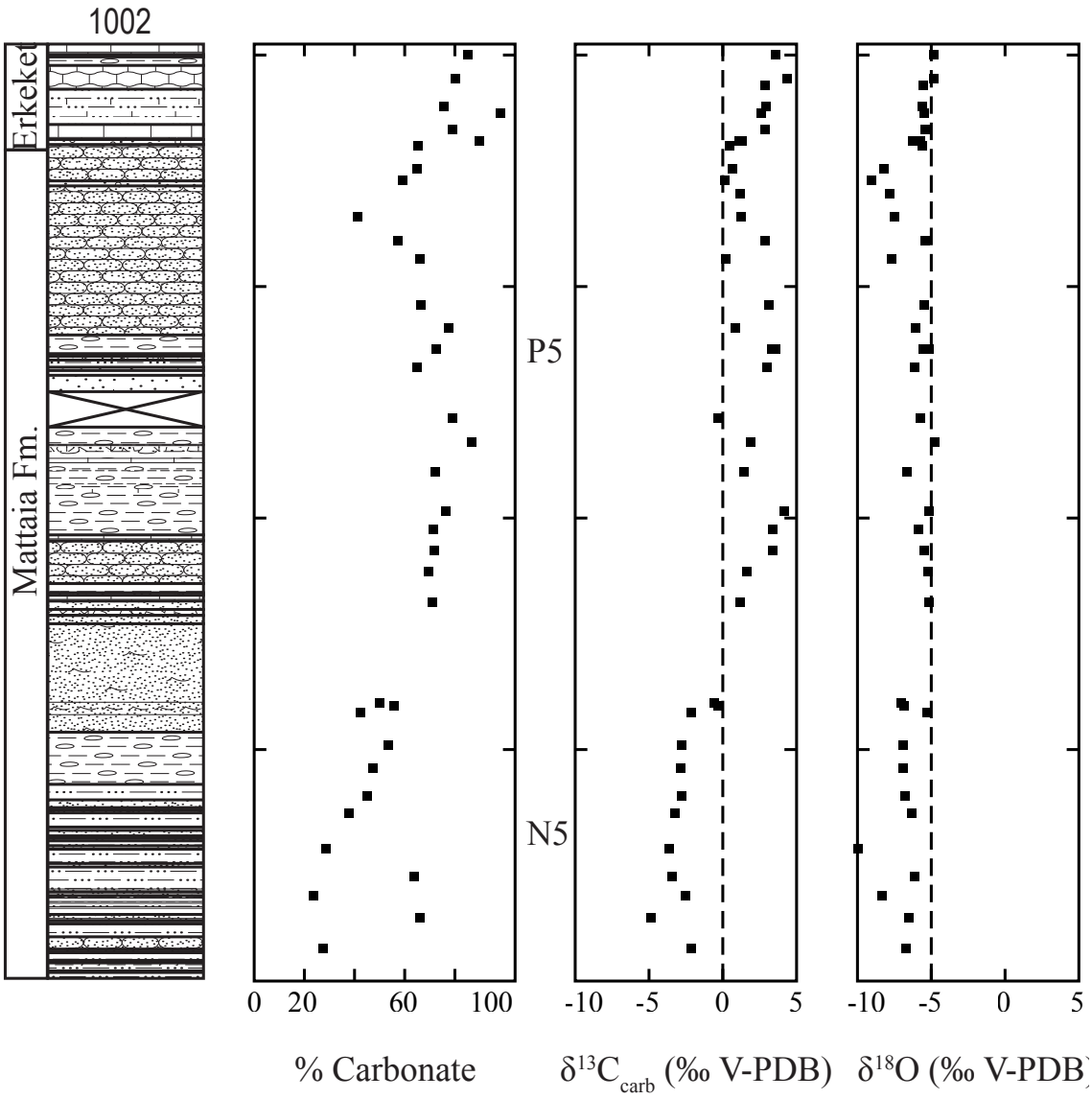

Figure 3.20. Percent carbonate and carbon and oxygen istotope data for Mattaia section 1002 (Olenek Region, see Figure 1.1). Error bars (1σ uncertainty) fall within data points.Two-letter codes denote isotopic events.

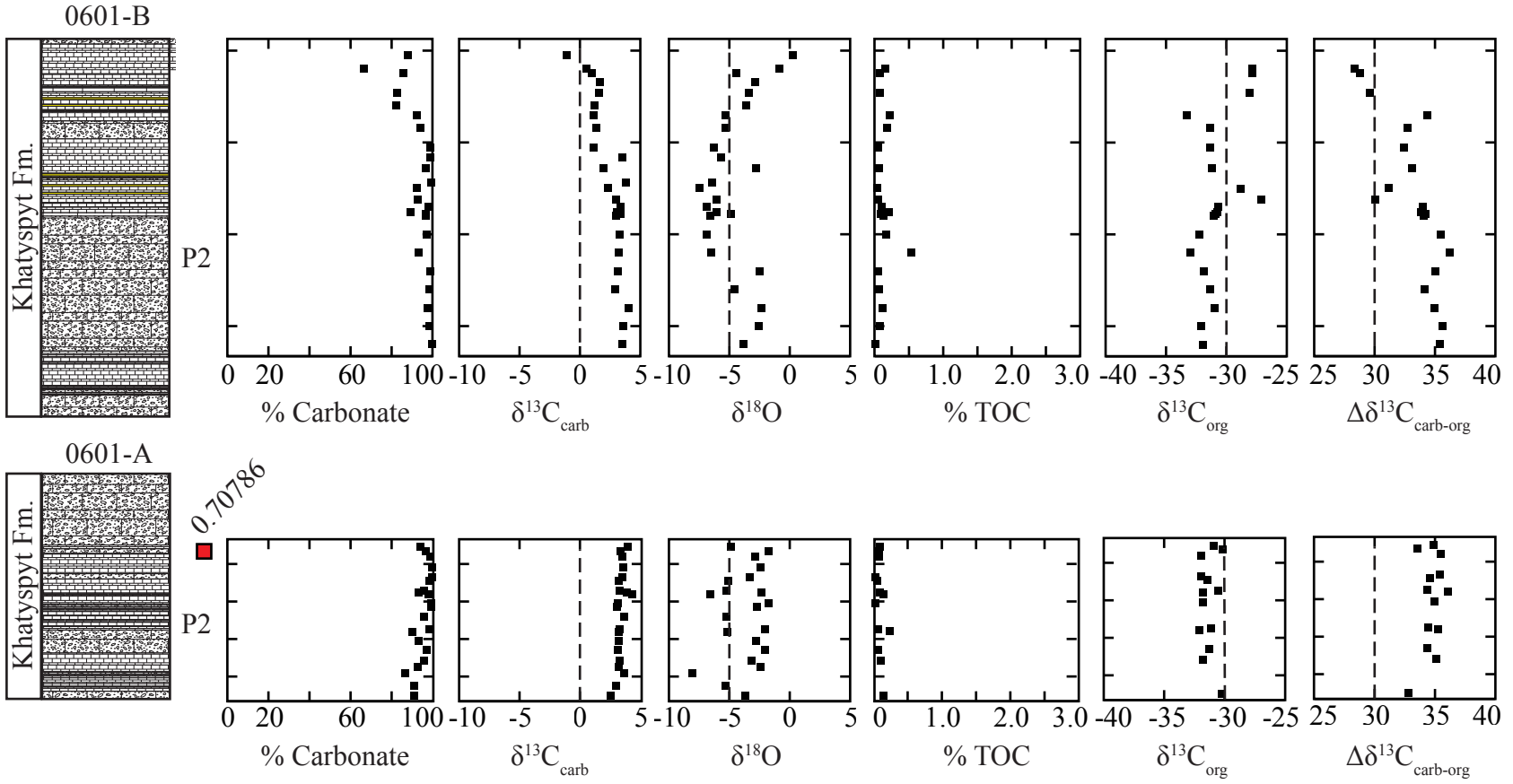

Figure 3.21. Carbon and oxygen data for Khatyspyt sections 0601-A and 0601-B. All isotope data in ‰ V-PDB. Uncertainty on carbonate measurements is less than 0.1‰; uncertainty on C_{org} measurements is less than 0.5‰. Red box represents $^{87}Sr/^{86}Sr$ value; yellow layers represent potential volcanic ash layers. Recall overlap of 0601-A with the lowerportion of 0601-B, as in Figure X. Two-letter codes denote isotopic events.

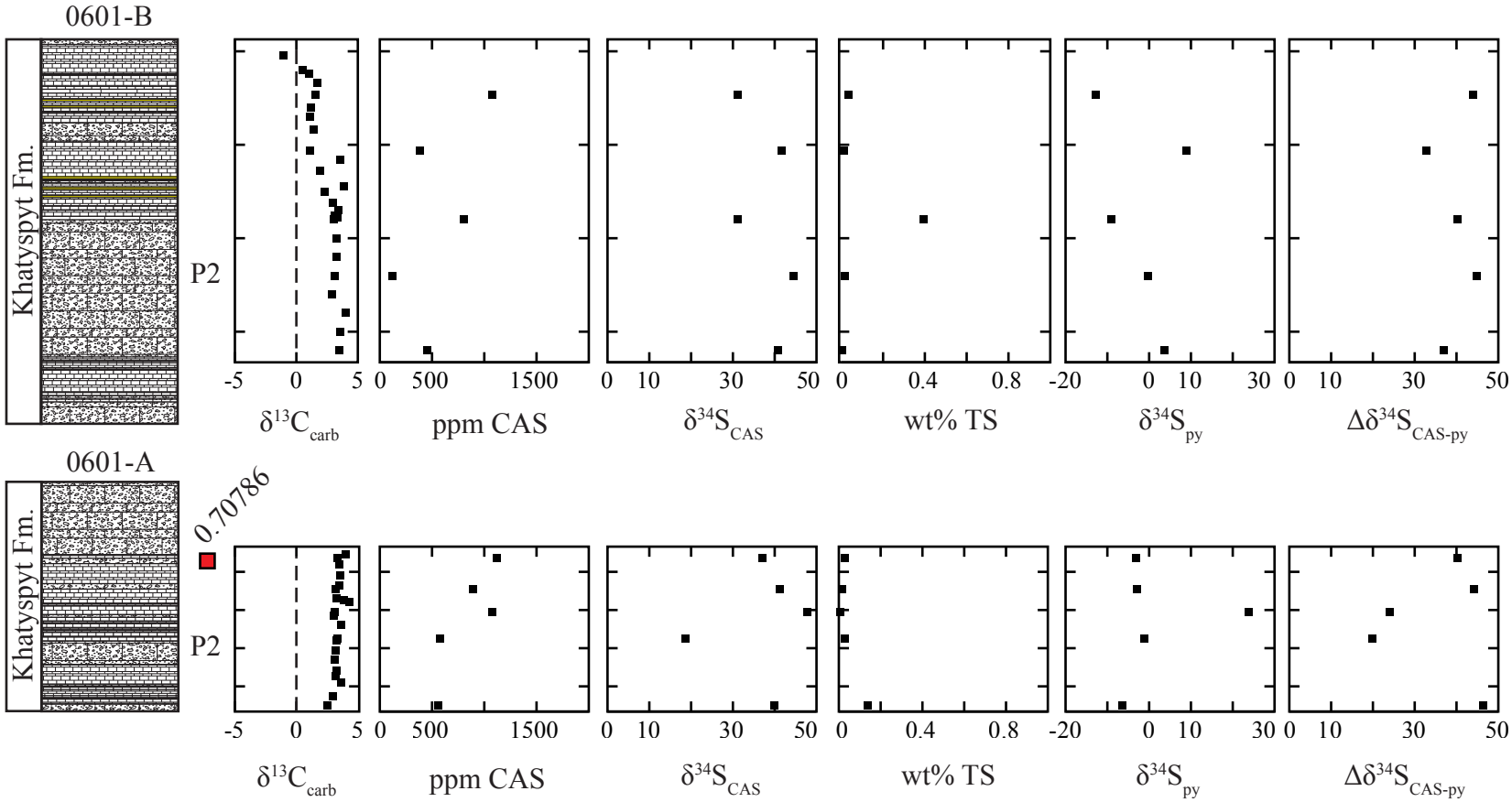

Figure 3.22. Sulfur data for Khatyspyt sections 0601-A and 0601-B, with carbonate carbon data for reference. All sulfur isotope data in ‰ V-CDT; $\delta^{13}C_{carb}$ data in ‰ V-PDB. Uncertainty on sulfur measurements is less than 0.8‰; uncertainty on carbon measurements is less than 0.1‰. CAS concentration data represents lower bound.Red box represents $^{87}Sr/^{86}Sr$ value; yellow layers represent potential volcanic ash layers. Recall overlap of 0601-A with the lower portion of 0601-B, as in Figure X. Two-letter codes denote isotopic events.

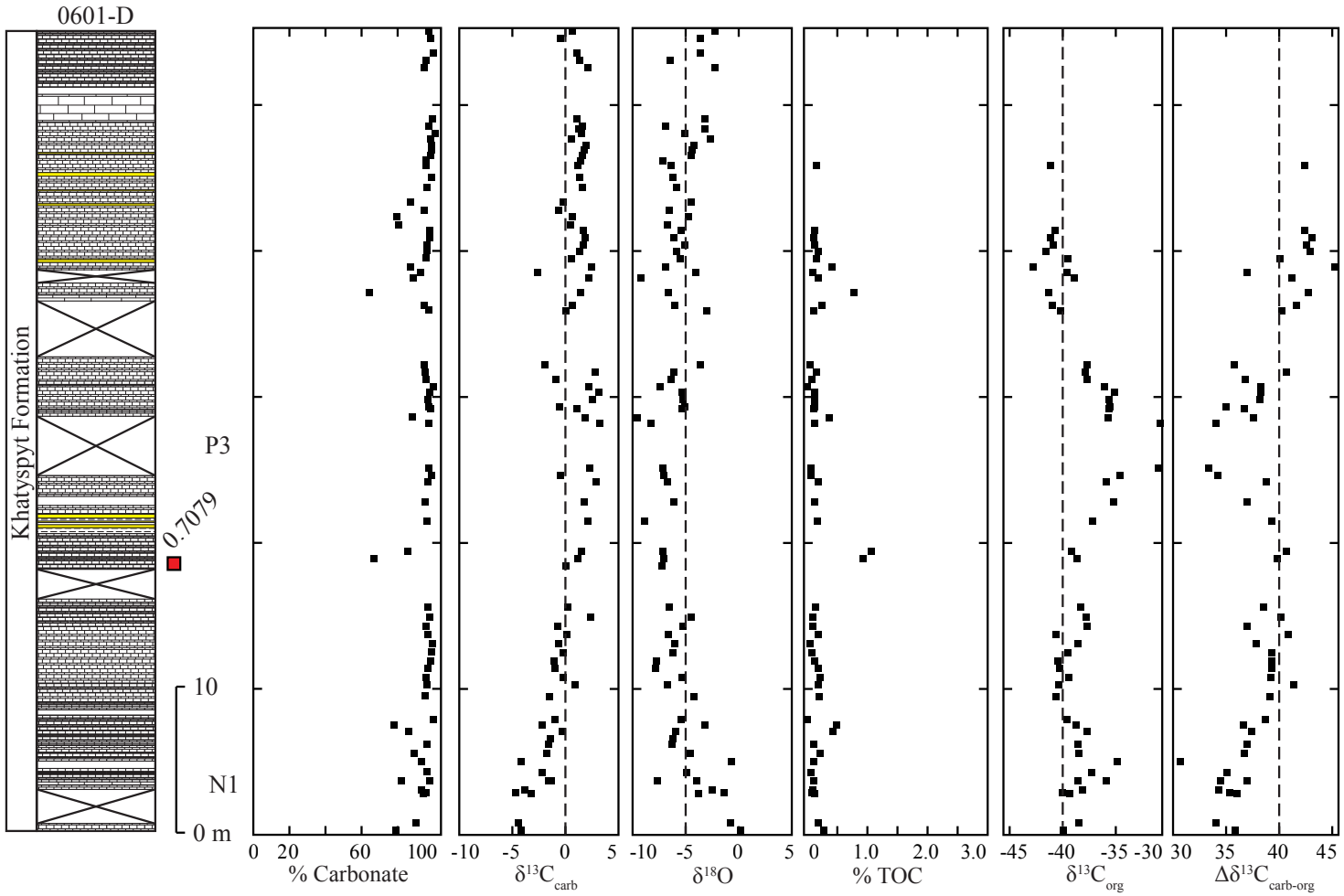

Figure 3.23. Carbon and oxygen data for Khatyspyt section 0601-D. All isotope data in ‰ V-PDB. Uncertainty on carbonate measurements is less than 0.1‰; uncertainty on C_{org} measurements is less than 0.5‰. Red box represents $^{87}Sr/^{86}Sr$ value; yellow layers represent potential volcanic ash layers. Two-letter codes denote isotopic events.

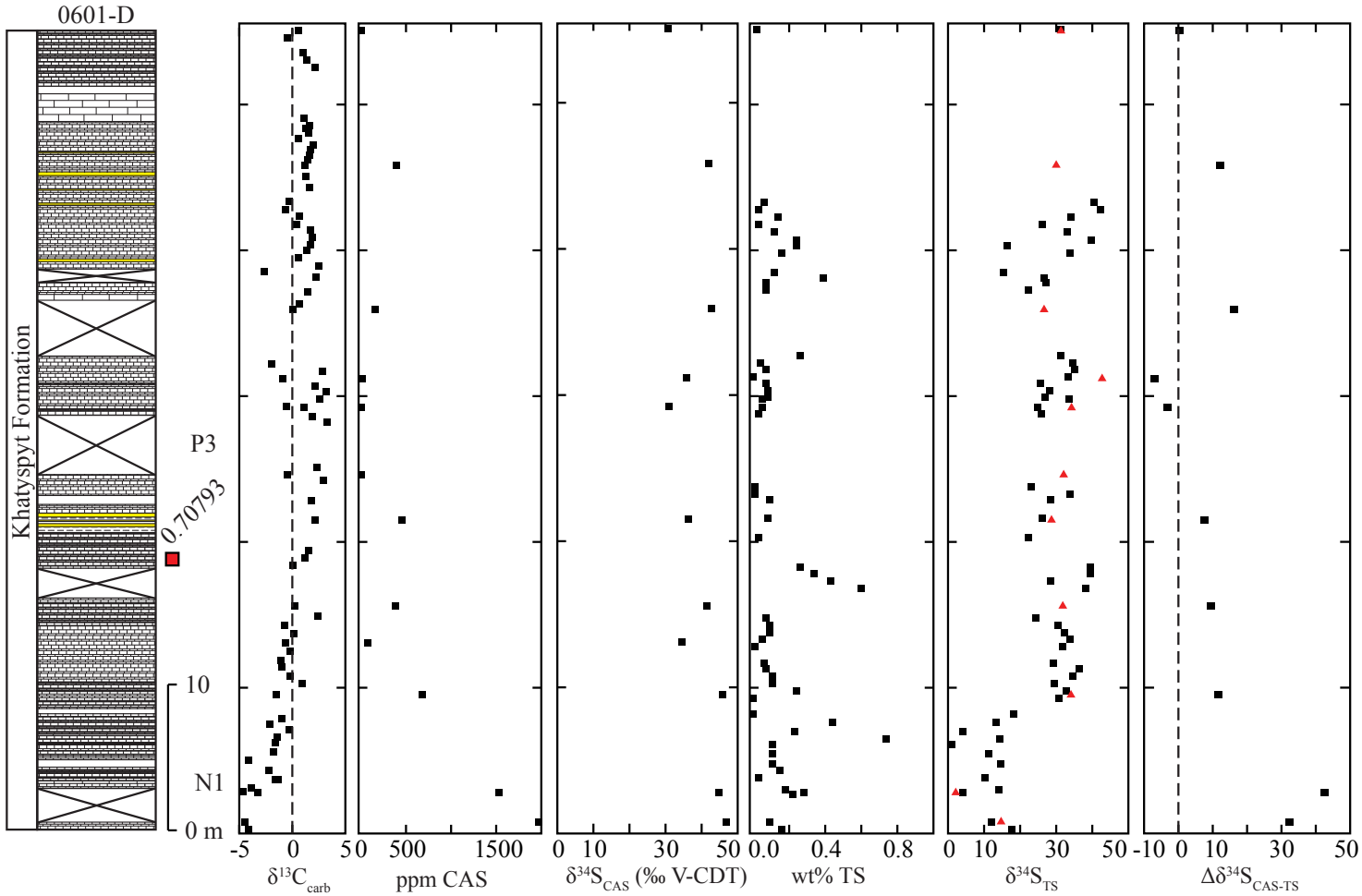

Figure 3.24. Sulfur data for Khatyspyt section 0601-D, with $\delta^{13}C_{carb}$ for reference. All sulfur isotope data in ‰ V-CDT; $\delta^{13}C_{carb}$ data in ‰ V-PDB. Uncertainty on sulfur measurements is less than 0.8‰; uncertainty on carbon measurements is less than 0.1‰. CAS concentration data represents lower bound. Red triangles in pyrite plot represent analyses of residues resulting from CAS. Red box represents $^{87}Sr/^{86}Sr$ value; yellow layers represent potential volcanic ash layers. Two-letter codes denote isotopic events.

Figure 3.20. Percent carbonate and carbon and oxygen isotope data for Mattaia section 1002 (Olenek Region, see Figure 1.1). Error bars (1σ uncertainty) fall within data points. Two-letter codes denote isotopic events.

Figure 3.21. Carbon and oxygen data for Khatyspyt sections 0601-A and 0601-B. All isotope data in ‰ V-PDB. Uncertainty on carbonate measurements is less than 0.1‰; uncertainty on C_{org} measurements is less than 0.5‰. Red box represents $^{87}Sr/^{86}Sr$ value; yellow layers represent potential volcanic ash layers. Recall overlap of 0601-A with the lower portion of 0601-B, as in Figure 3.2. Two-letter codes denote isotopic events.

Figure 3.22. Sulfur data for Khatyspyt sections 0601-A and 0601-B, with carbonate carbon data for reference. All sulfur isotope data in ‰ V-CDT; $\delta^{13}C_{carb}$ data in ‰ V-PDB. Uncertainty on sulfur measurements is less than 0.8‰; uncertainty on carbon measurements is less than 0.1‰. CAS concentration data represents lower bound.Red box represents $^{87}Sr/^{86}Sr$ value; yellow layers represent potential volcanic ash layers. Recall overlap of 0601-A with the lower portion of 0601-B, as in Figure 3.2. Two-letter codes denote isotopic events.

Figure 3.23. Carbon and oxygen data for Khatyspyt section 0601-D. All isotope data in ‰ V-PDB. Uncertainty on carbonate measurements is less than 0.1‰; uncertainty on C_{org} measurements is less than 0.5‰. Red box represents $^{87}Sr/^{86}Sr$ value; yellow layers represent potential volcanic ash layers. Two-letter codes denote isotopic events.

Figure 3.24. Sulfur data for Khatyspyt section 0601-D, with $\delta^{13}C_{carb}$ for reference. All sulfur isotope data in ‰ V-CDT; $\delta^{13}C_{carb}$ data in ‰ V-PDB. Uncertainty on sulfur measurements is less than 0.8‰; uncertainty on carbon measurements is less than 0.1‰. CAS concentration data represents lower bound. Red triangles in pyrite plot represent analyses of residues resulting from CAS. Red box represents $^{87}Sr/^{86}Sr$ value; yellow layers represent potential volcanic ash layers. Two-letter codes denote isotopic events.

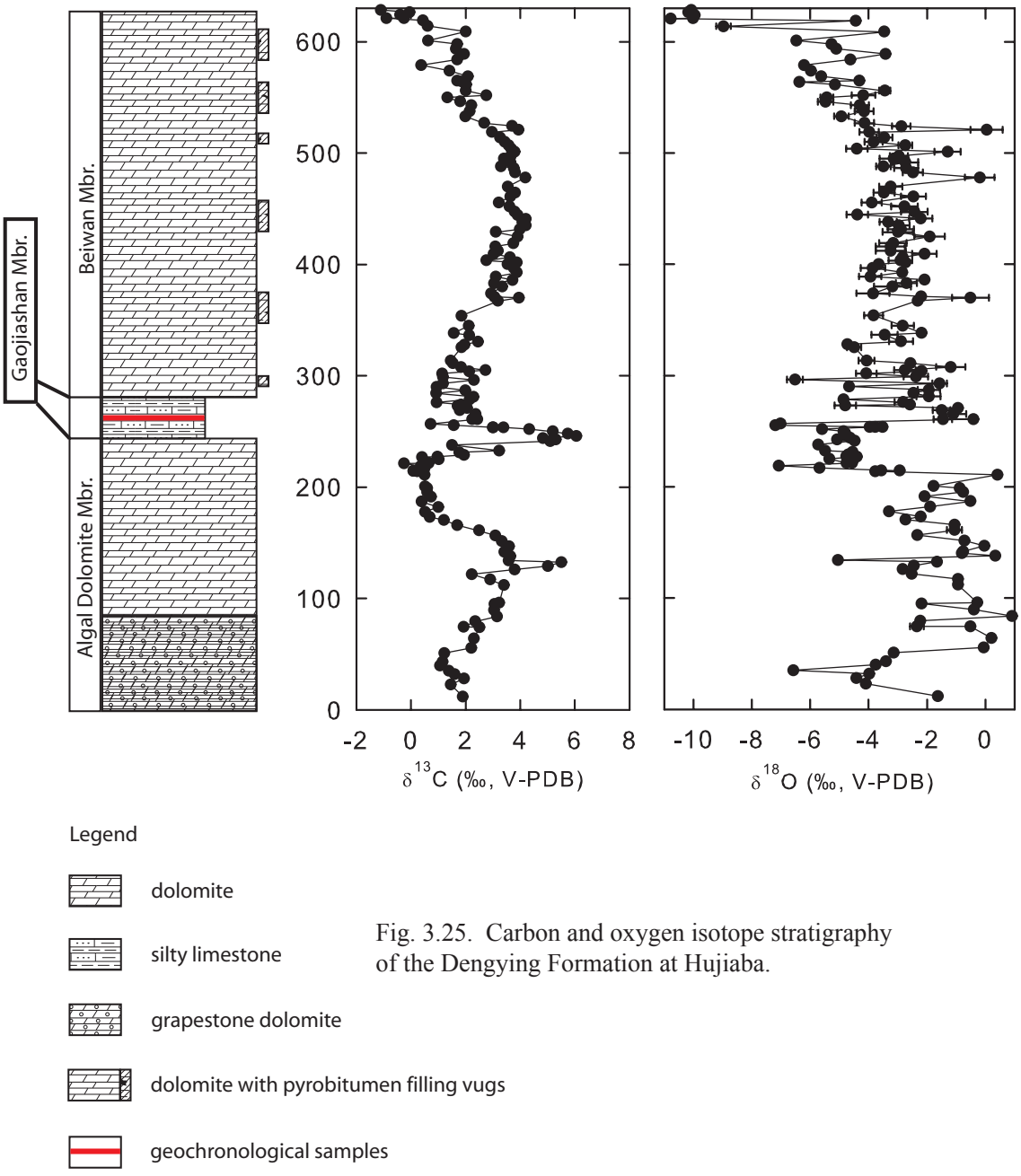

Fig. 3.25. Carbon and oxygen isotope stratigraphy of the Dengying Formation at Hujiaba.

Figure 3.25. Carbon and oxygen isotope stratigraphy of the Dengying Formation at Hujiaba. Error bars represent 1σ error; when not visible, error bars fall within symbol.

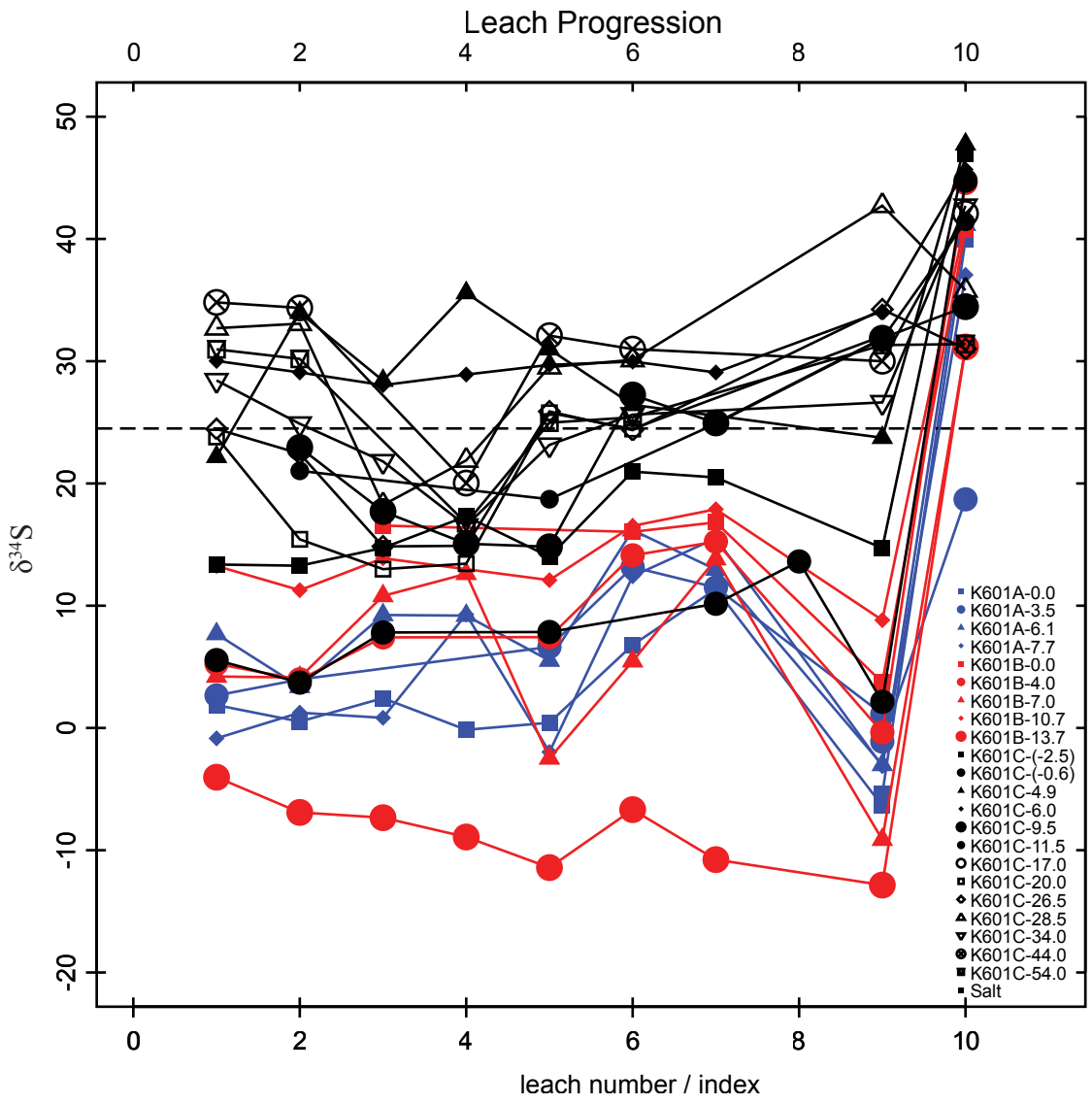

Figure 3.26. Progression of $\delta^{34}S$ values for leaches (indices 1-8), residues (index 9), and CAS (index 10) for samples from sections 0601-A (K601A), 0601-B (K601B), and 0601-D (K601C). Horizontal dotted line represents value for salt and water blank.

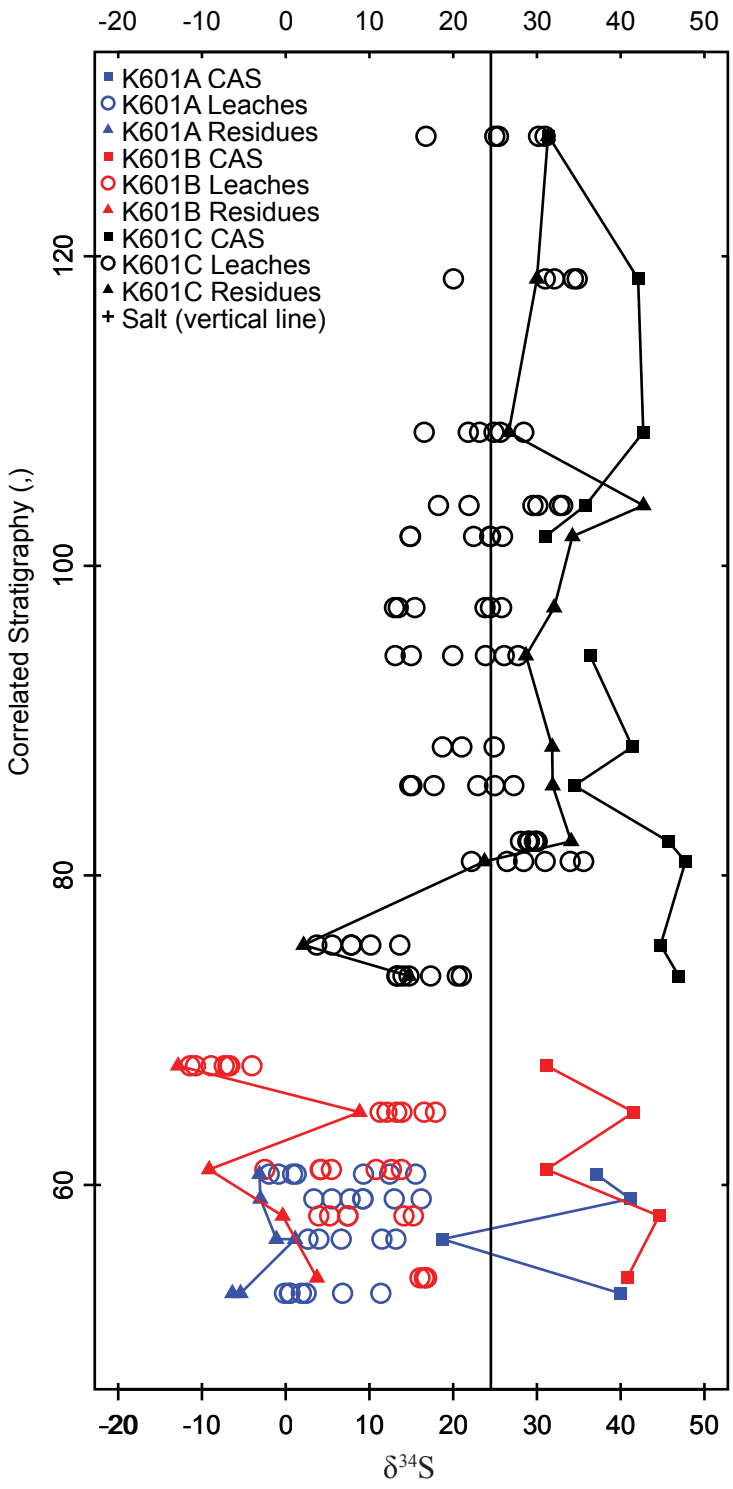

Figure 3.27. Progression of $\delta^{34}S$ values for leaches, residues, and CAS for samples from sections 0601-A (K601A), 0601-B (K601B), and 0601-D (K601C). Vertical dotted line represents value for salt and water blank.

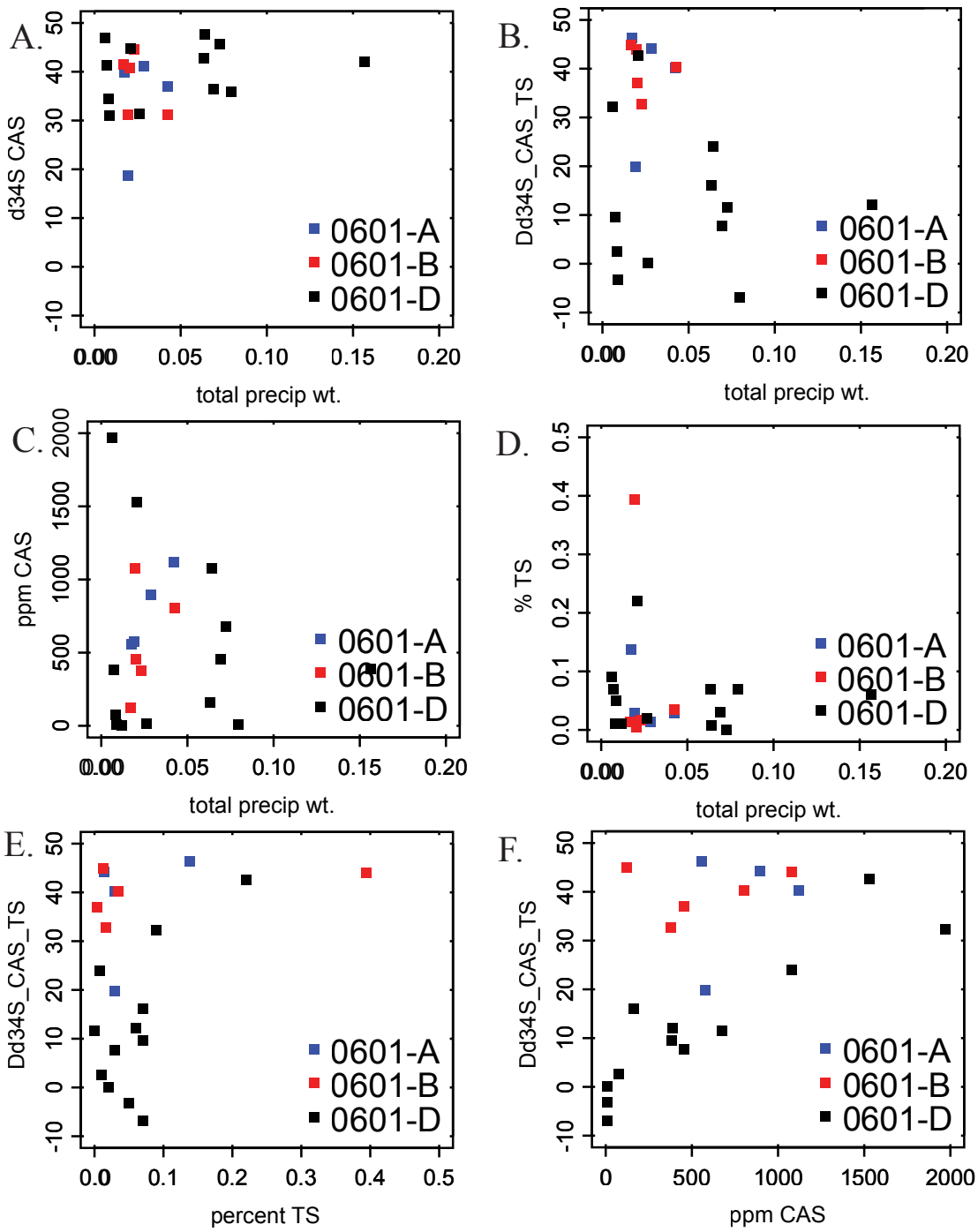

Figure 3.28, A-F. Crossplots of CAS extraction data, including CAS and TS concentrations and isotopic compositions, for 22 samples, as well as the total amount of soluble sulfate removed from each sample. R^2 values for crossplots can be found in Table 3.2.

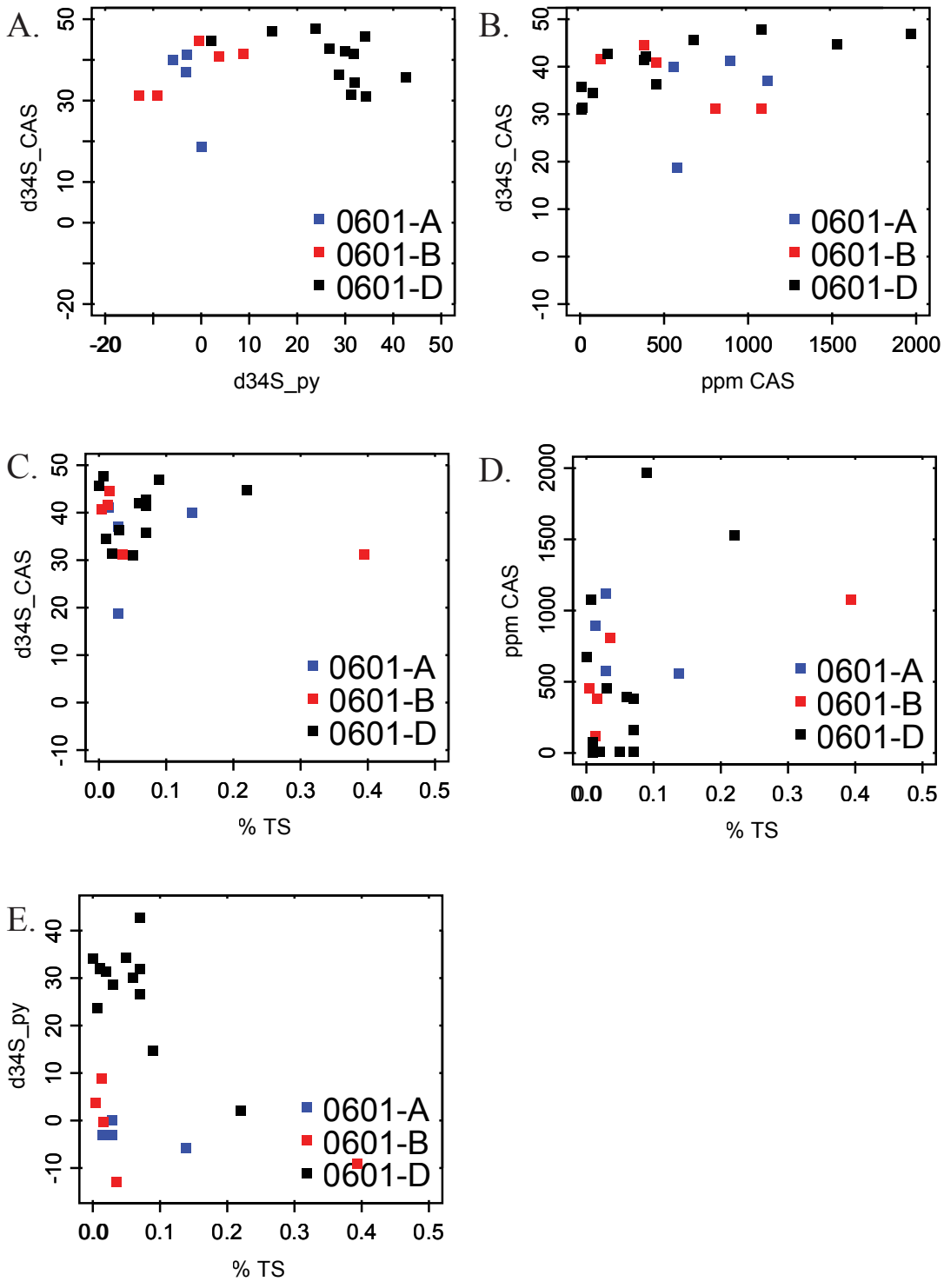

Figure 3.29, A-E. Crossplots of CAS extraction data, including CAS and TS concentrations and isotopic compositions, for 22 samples, as well as the total amount of soluble sulfate removed from each sample. R^2 values for crossplots can be found in Table 3.2.

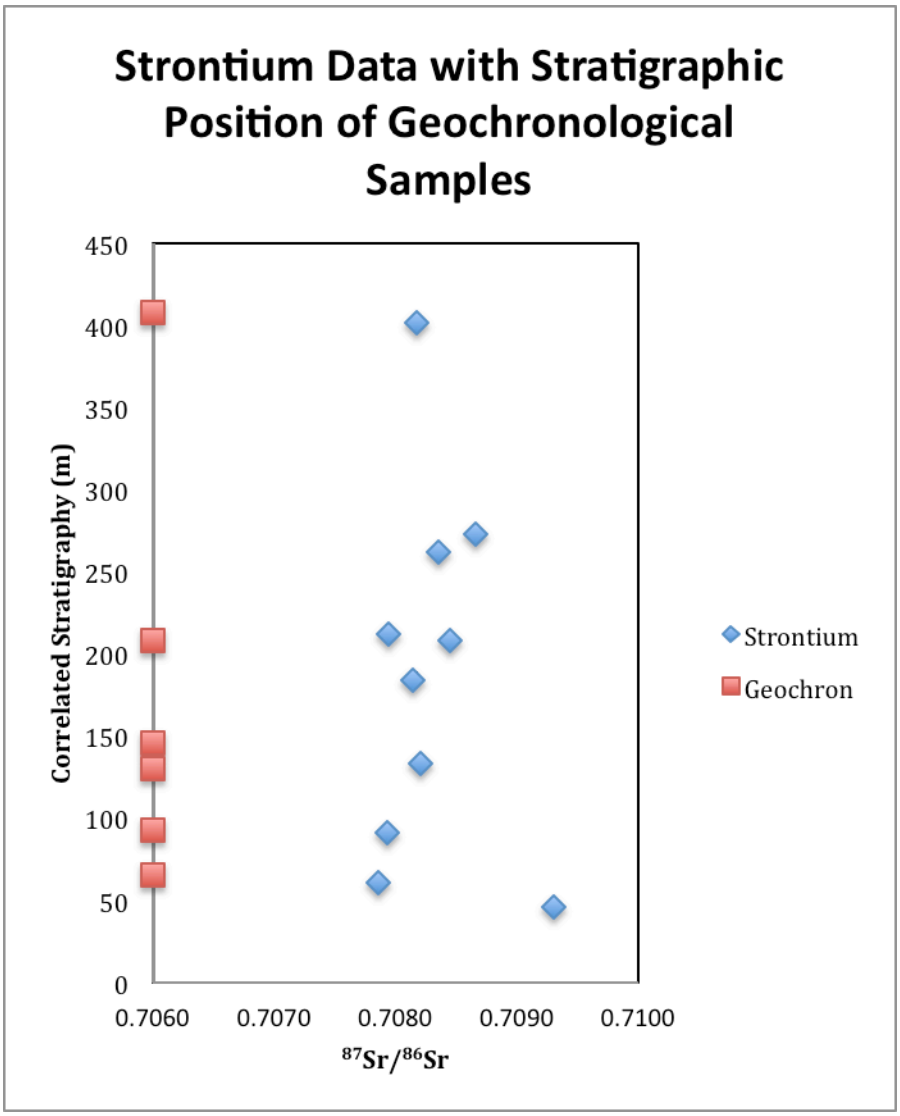

Figure 3.30. Strontium data with stratigraphic position of geochronological samples. Geochronological data points are intended to show only stratigraphic positions. Error bars fall within data points.

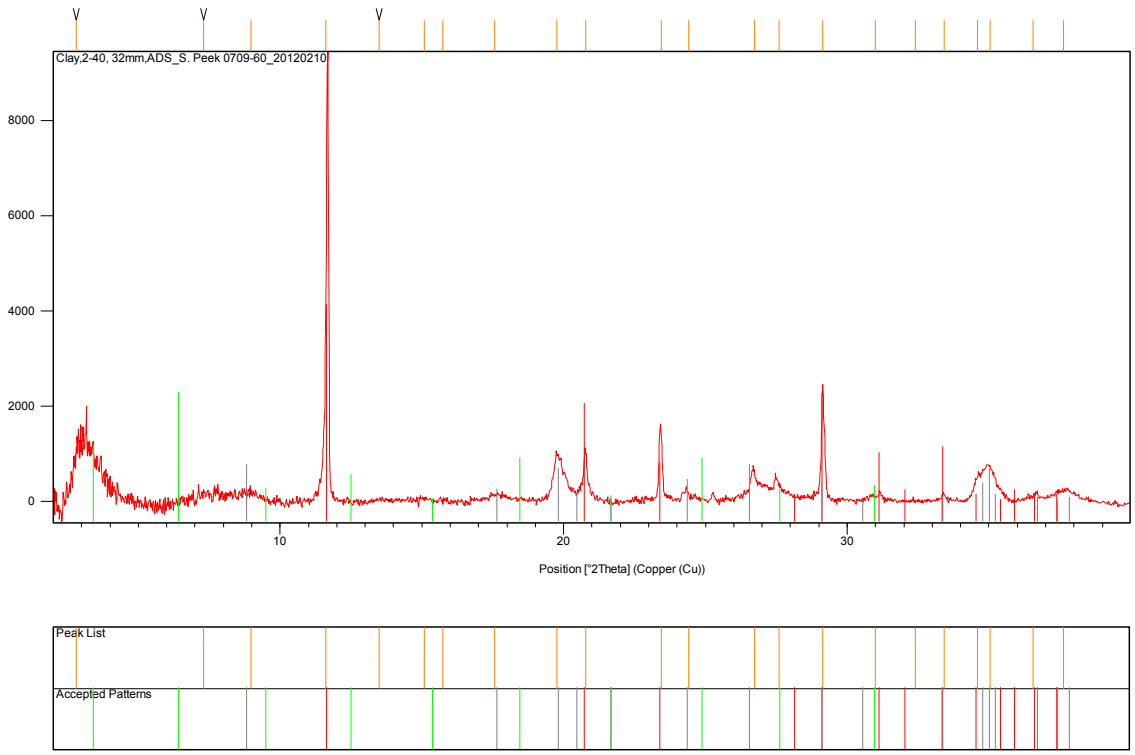

Figure 3.31. XRD spectrum of Mattaia sample 0709-60. Pattern and peak lists can be found in appendix tables A.5 and A.6.

Figure 3.32. Magnified photograph of zircons extracted from Mattaia sample 0709-60.

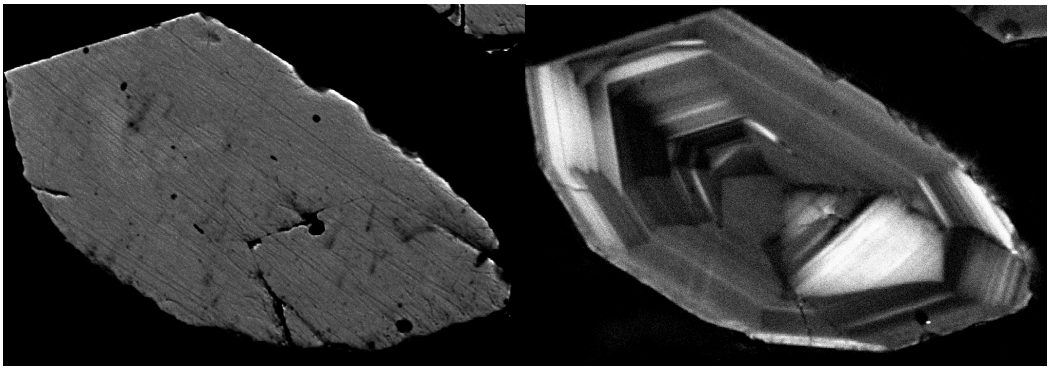

Figure 3.33. EBSD (left) and CL image of typical zircon grain showing oscillatory zoning

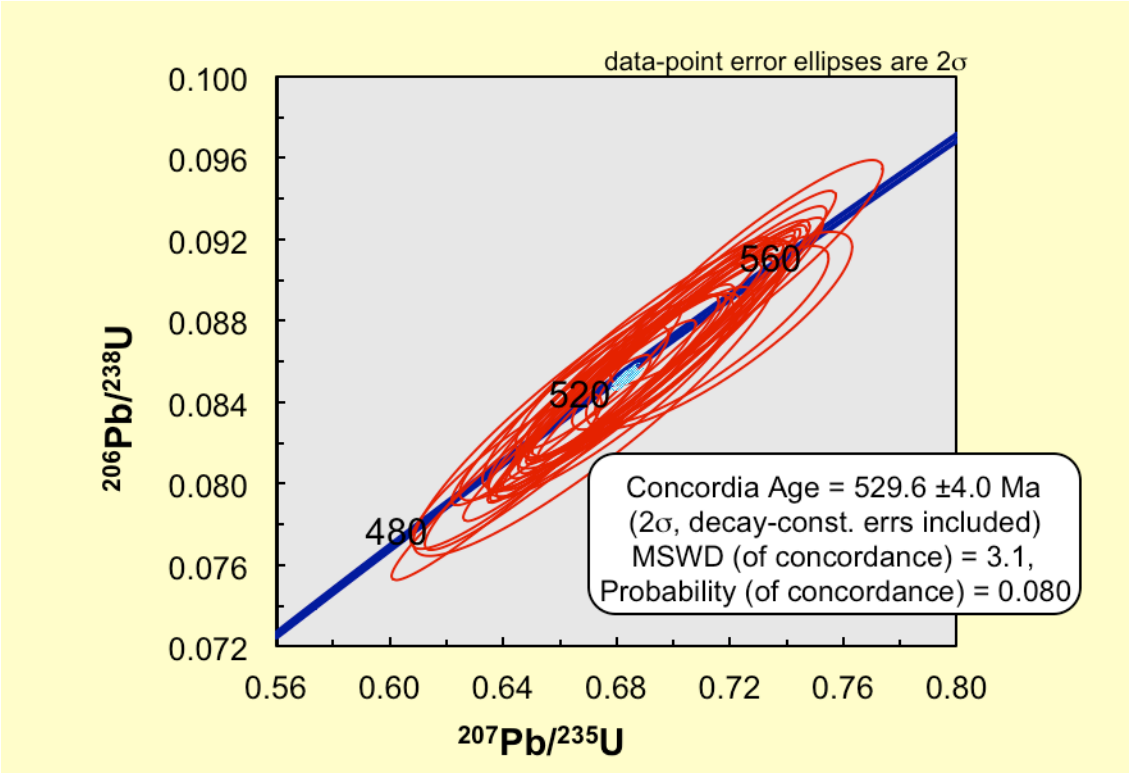

Figure 3.34. Concordia plot for U-Pb geochronology for Mattaia sample 0709-60.

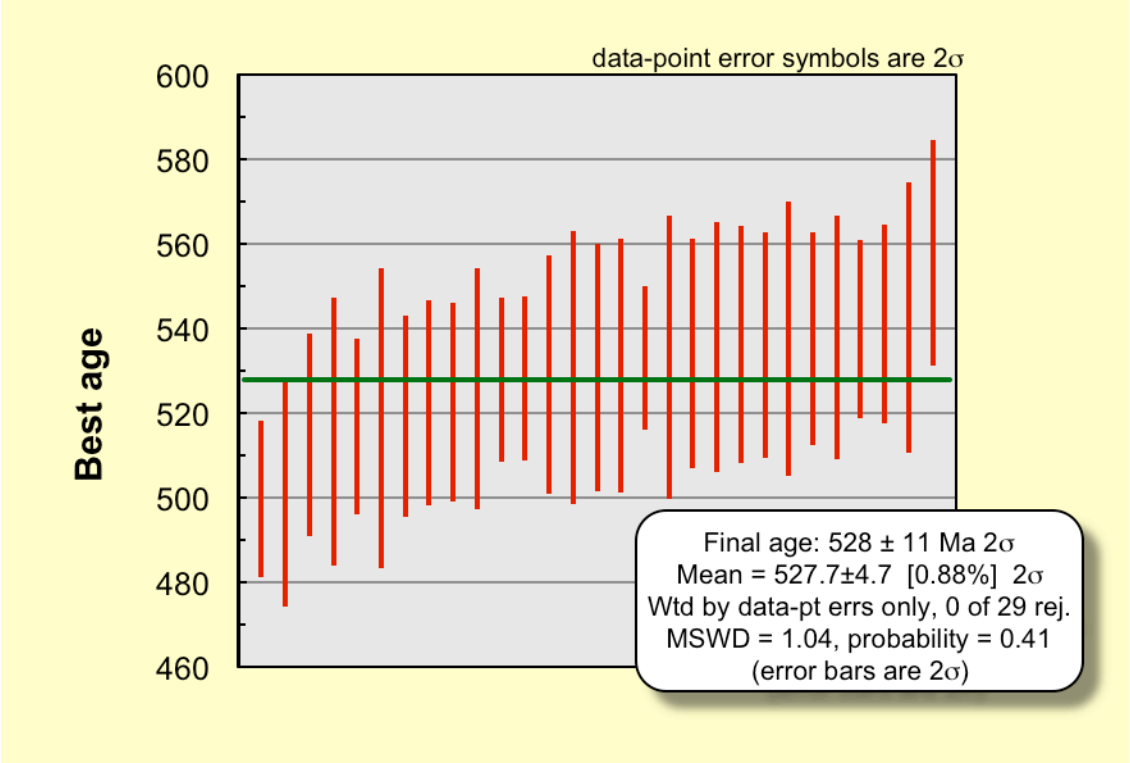

Figure 3.35. Weighted mean of all ages derived from U-Pb geochronology for Mattaia sample 0709-60.

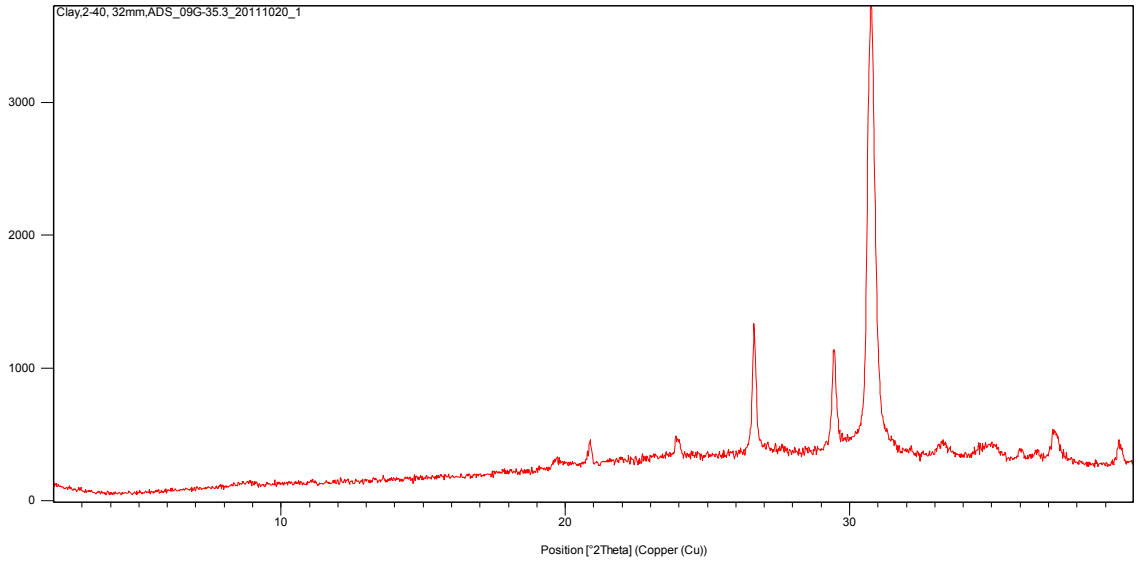

Figure 3.36-A – XRD spectrum for Dengying sample 09G-35.3 (unglycolated); counts vs 2Θ angle.

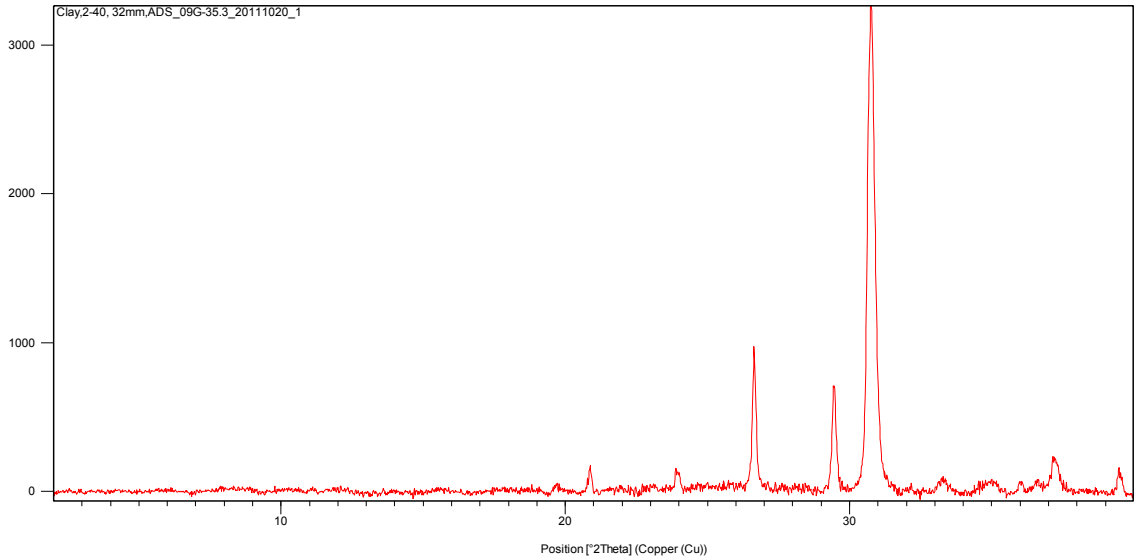

Figure 3.36-B – XRD spectrum for Dengying sample 09G-35.3 (glycolated); counts vs 2Θ angle.

-

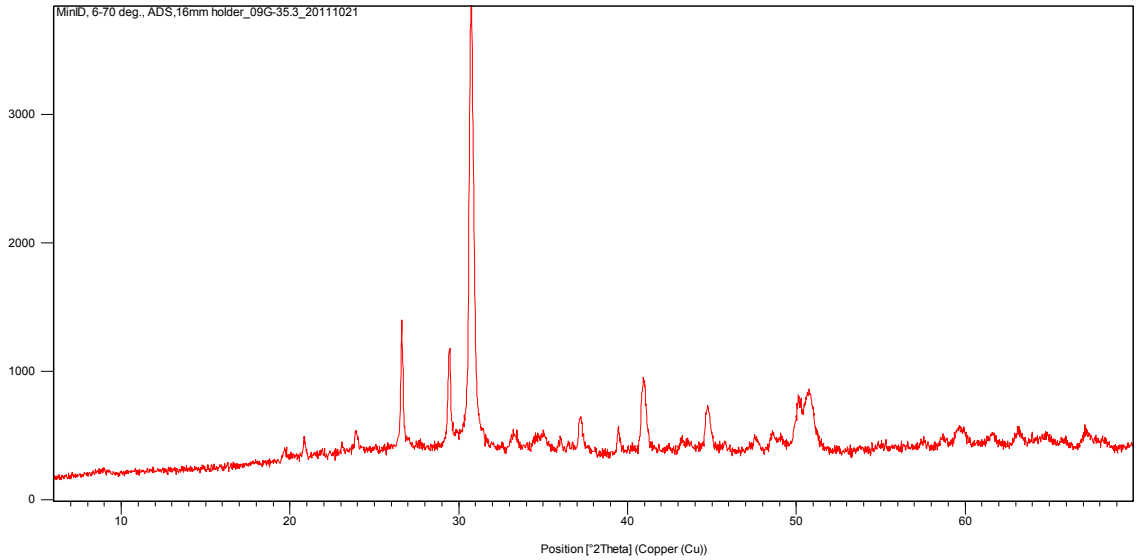

Figure 3.37-A – XRD spectrum for Dengying sample 09G-37.9 (unglycolated); counts vs 2Θ angle.

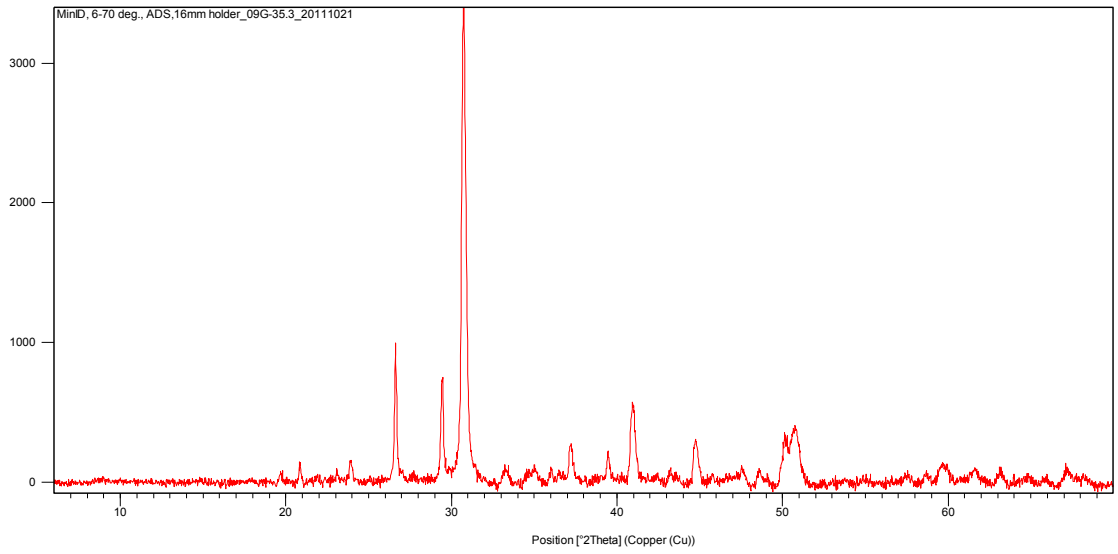

Figure 3.37-B – XRD spectrum for Dengying sample 09G-37.9 (glycolated); counts vs 2Θ angle

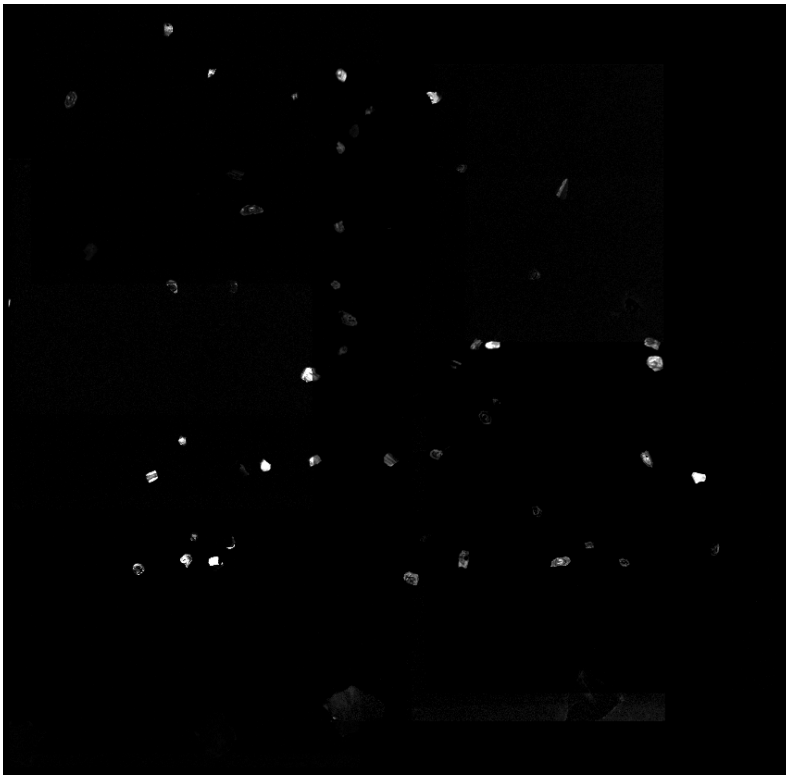

Figure 3.38. Cathodoluminescent image of Dengying sample 09G-35.3. Image is approximately 2 mm in width.

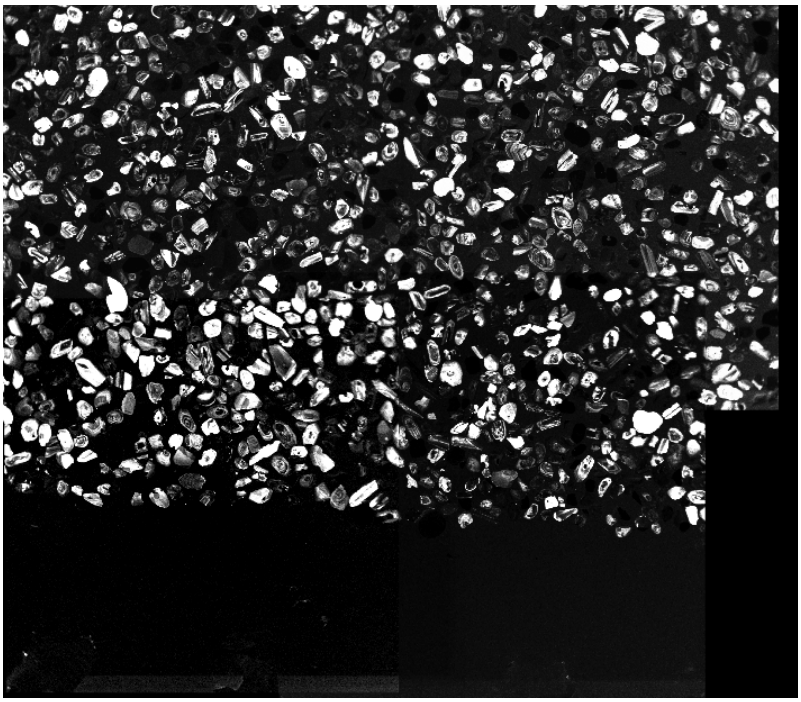

Figure 3.39. Cathodoluminescent image of Dengying sample 09G-37.9. Image is approximately 2 mm in width.

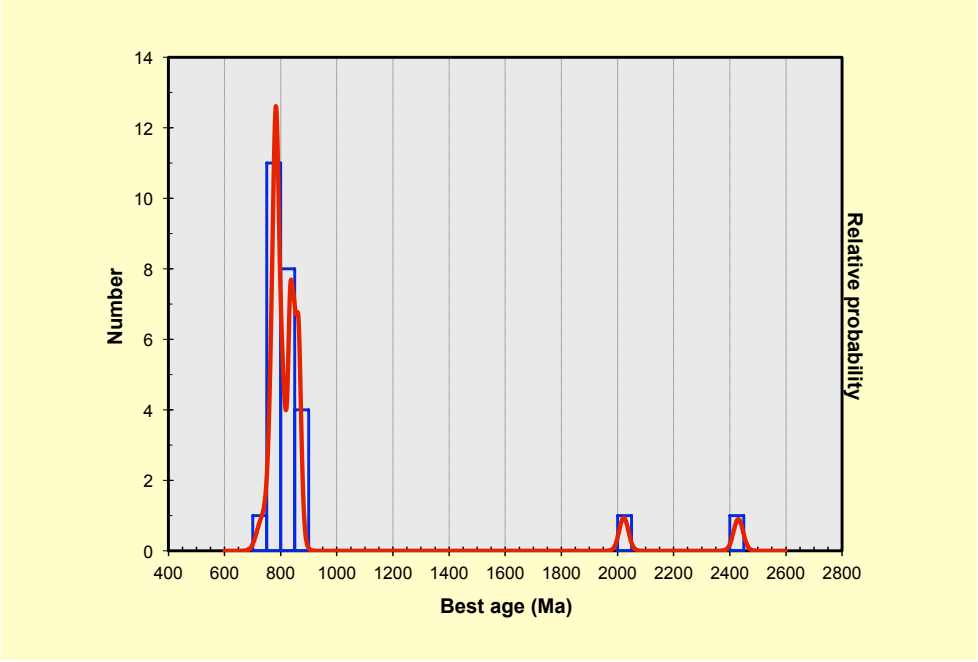

Figure 3.40. Age distribution of 26 grains from Dengying sample 09G-35.3 dated using U-Pb geochronology.

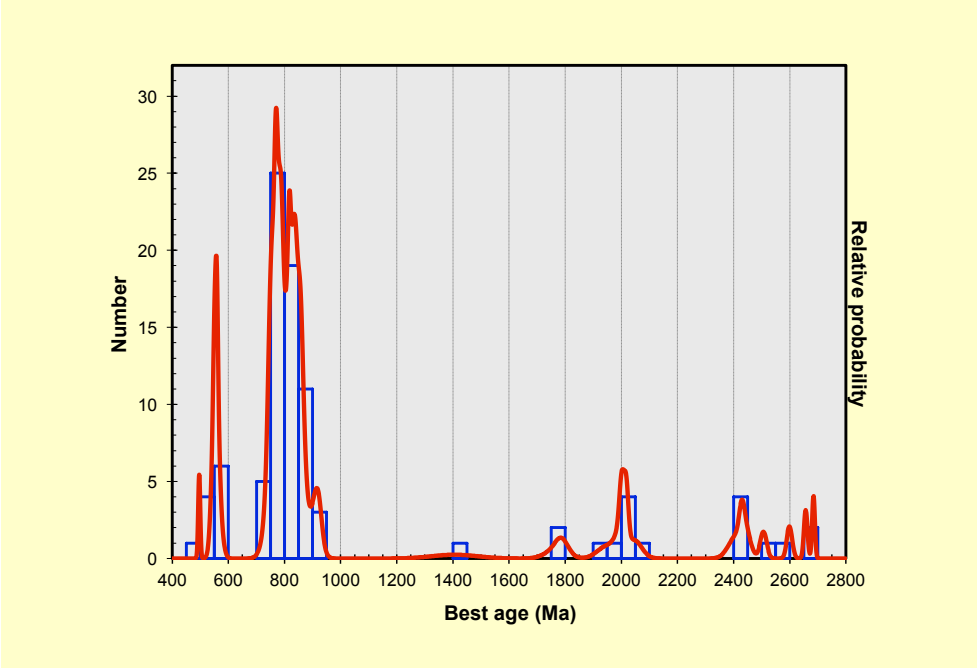

Figure 3.41. Age distribution of 92 grains from Dengying sample 09G-37.9 dated using U-Pb geochronology.

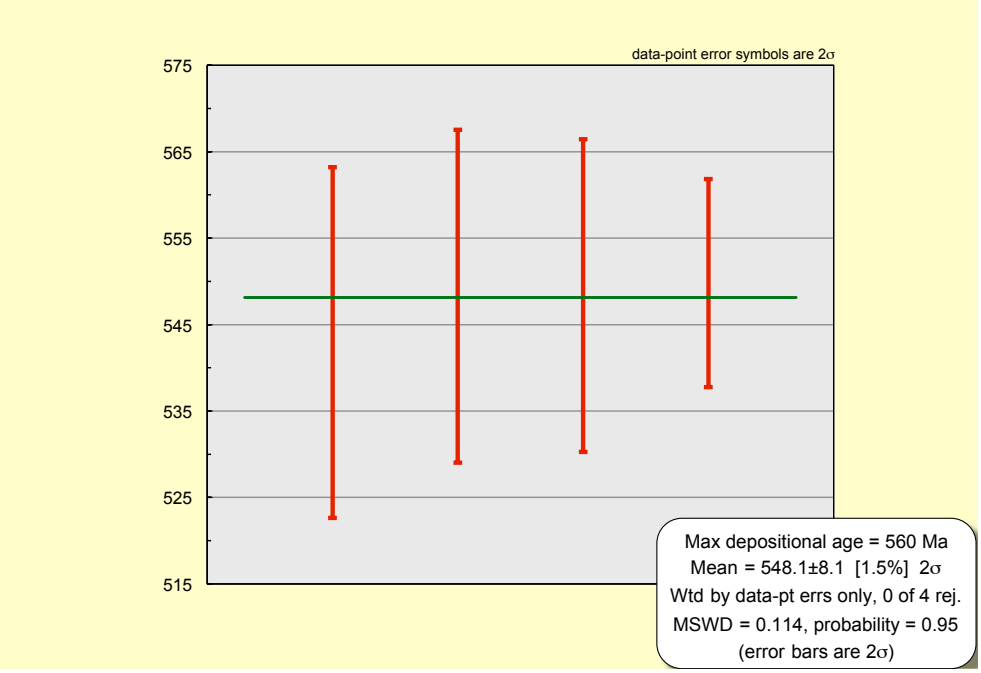

Figure 3.42. Maximum depositional age, derived from the youngest population of grains (N = 4) from Dengying sample 09G-37.9.

Chapter 4: Discussion

Our goals in this study of Ediacaran Period sections include evaluation of intra- and inter-basinal correlations. We aim to augment the lithologic intra-basinal correlations of our collaborators with information from a number of isotopic systems, including carbon, oxygen, and sulfur, in addition to directly addressing the issue of timing of deposition using radiometric dating. Additionally, we aim to use isotopic information to inform inter-basinal correlations, particularly between studied sections in Russia and China. Ultimately, we hope to use isotopic information to understand paleoenvironmental conditions in the latest Ediacaran Period.

Evaluating Alteration

Our confidence in our isotopic data must be based on evidence that the data represents an original, unaltered signal. Alteration can be evaluated on a number of grounds. First, oxygen isotopic values can serve as an indicator of alteration; very light values (-10‰ or lower) can indicate alteration by meteoric or metamorphic fluids. However, relatively little of our oxygen isotopic data falls below -5‰, while significant portions of the data fall near 0‰ or even in the positive range. Such heavy values are not typically associated with alteration.

Our high-resolution data set also allows us to evaluate alteration based on the consistency of our isotopic data. Because our sections were typically sampled at a density of several analyses per meter, outlier points can be clearly identified, while "potential outliers" can be supported by the surrounding data, suggesting that they are not the product of alteration.

Another attribute of our large data set is the ability to evaluate whether excursions occur in a single facies, or throughout a range of facies. Excursions that only occur in a single facies could suggest that that facies was particularly susceptible to alteration, particularly if the facies was rich in organic carbon. Such high-TOC facies could provide a source for light carbon, potentially leading to an artificial lightness of carbon isotopic values in the surrounding carbonate rock. However, our large data set allows us to identify similar, correlated excursions in separated sections and in different facies types, greatly reducing the likelihood that all resulted from alteration. For example, excursion N4 in the Turkut Formation occurs across a large number of sampled sections in a wide variety of facies (overview: Figures 3.3-3.4; Figures 4.5-4.6; detail: Figures 3.11-3.15)

Organic-carbon mediated alteration can be evaluated in sections for which we have both carbonate carbon and organic carbon isotopic data. We have this data for sections 0601-A, 0601-B, and 0601-D (Figures 3.21 and 3.23). Two negative excursions occur in these sections, N1 at the base of 0601-D, and a negative trend immediately below N1 at the top of 0601-B. Do these negative excursions correlate with higher TOC concentrations? Figure 4.1 shows crossplots for each section of percent TOC with $\Delta\delta^{13}C_{carb\text{-}org}$, which reaches its lowest values during the negative excursions. None of these crossplots suggest that high TOC is correlated with lower $\Delta\delta^{13}C_{carb\text{-}org}$ values. Thus, in this case there is no evidence that higher TOC concentration resulted in greater alteration in these sections.

In our Khatyspyt sections, low carbonate content is potentially associated with a high level of bioturbation, which could result in more easily-altered rock. Bioturbation is recorded by traces replaced with microcrystalline silica, comprising nearly 100% of some

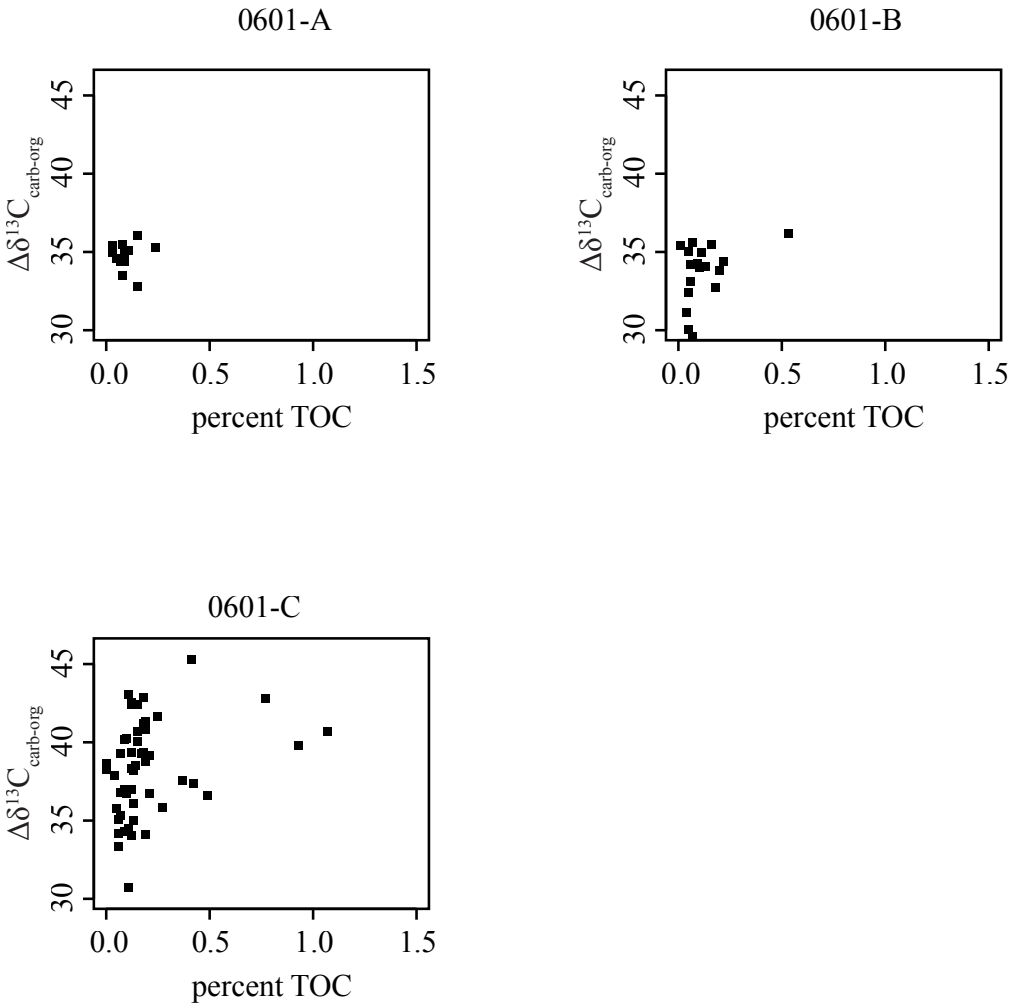

Figure 4.1. Crossplots of $\Delta\delta^{13}C_{carb\text{-}org}$ vs. percent TOC for sections 0601-A, 0601-B, and 0601-D.

layers in the upper Khatyspyt Formation (Rogov et al., 2012). A rock with lower carbonate content is proportionally easier to alter, especially if the ratio of TOC to carbonate rises. Additionally, the sediment mixing that is produced by bioturbation may increase the magnitude of any early diagenetic alteration to the remaining carbonate. Overall, the upper member of the Khatyspyt Formation (including, for example, sections

0605 and 0603; Figure 3.8) appears to be moderately to intensely bioturbated (Rogov et al, 2012), indicating that we should exercise care in evaluating these strata.

In Figure 3.2, for example, negative excursions of very similar character are seen in Khatyspyt sections 0605, 0603, and 0701. However, the oxygen data for these three sections (Figure 3.8; Figure 3.10) is significantly scattered, ranging from -5‰ to nearly -10‰ in 0605, and from nearly 0‰ to -10‰ in both 0603 and the lower part of 0701. This could suggest that alteration played a role in producing the carbon isotopic signatures in these sections. Also notable in all three sections is a wide range of carbonate contents, from nearly 100% to almost 0%, suggesting that bioturbation may have played a role.

On the other hand, negative excursion N1 in the lower Khatyspyt (0601-B and 0601-D, Figures 3.2, 3.21, and 3.23) is associated with smooth negative covariance in $\delta^{18}O$, from ~-5‰ up to 0‰ at the lowest sampled portions of the $\delta^{13}C$ excursion. Carbonate contents also fall slightly in both sections during N1, but rarely reach values lower than 80%. This smooth covariance seems less likely to be indicative of alteration.

Alteration of carbon isotope values can also be evaluated within the "lithification" paradigm of Knauth and Kennedy (2009). Figure 4.2A-E crossplots carbon and oxygen for Siberian sections 0601-A, 0601-B, and 0601-D. Figure 4.3 crossplots carbon and oxygen for Siberian (left) and Chinese samples (right). Symbols indicate stratigraphic subdivisions of each region. Dotted line encloses "lithification trend." Siberian data appear to be bounded to the left by a vertical line, indicating alteration of $\delta^{18}O$ independent of $\delta^{13}C$ without application of the lithification trend. On the other hand, the

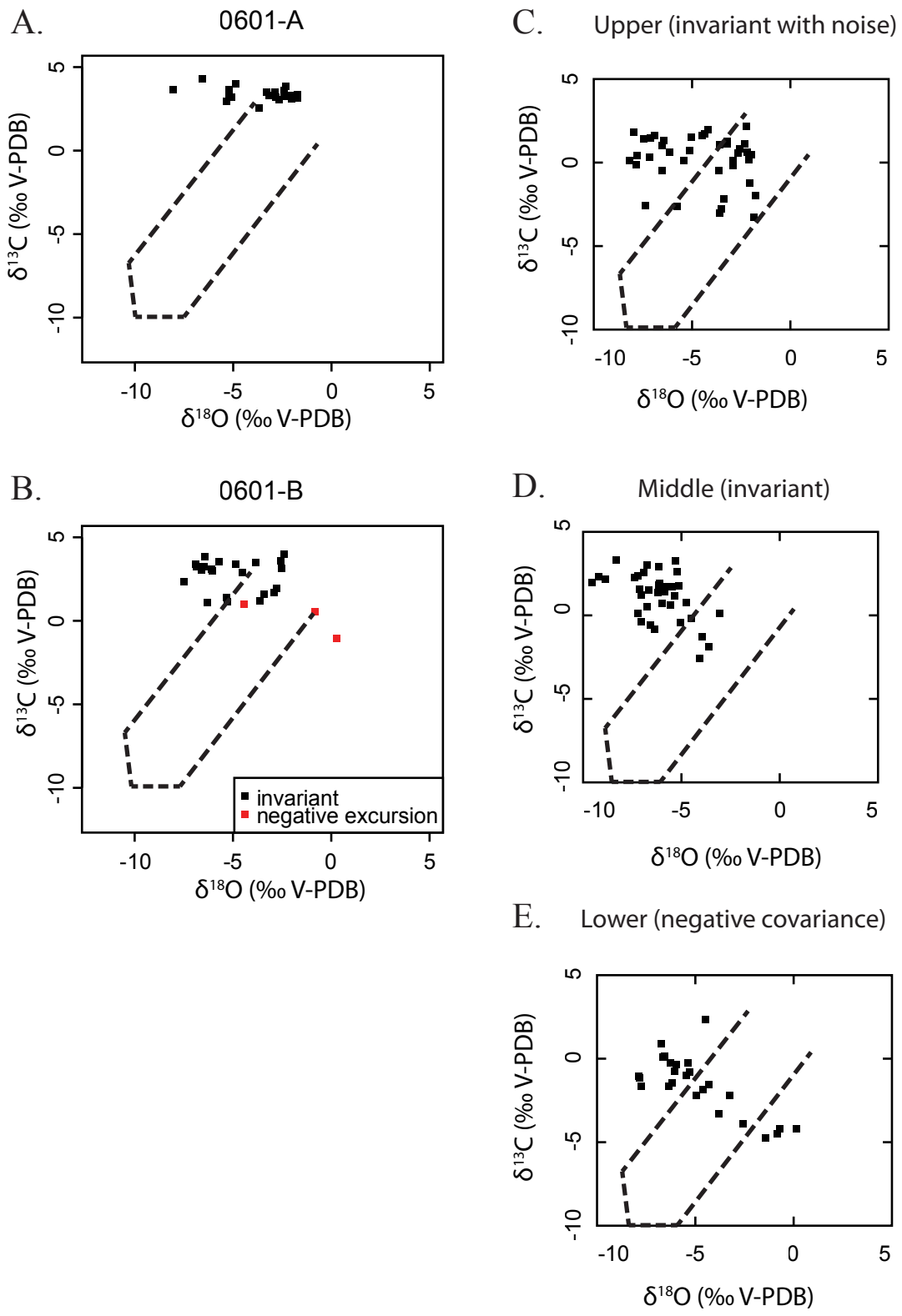

Figure 4.2. Crossplots of carbon and oxygen isotopic data for sections 0601-A, 0601-B, and 0601-D (C-E).

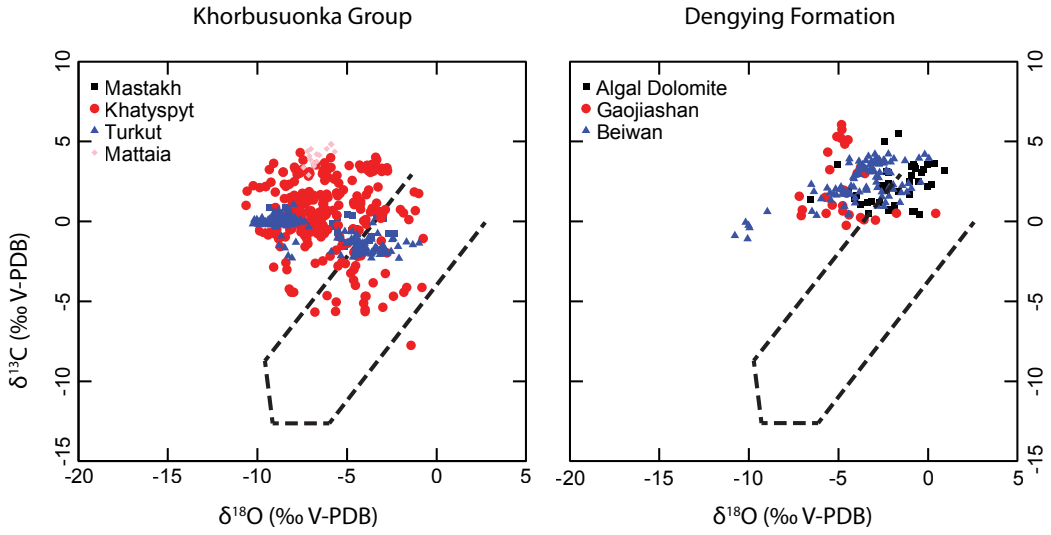

Figure 4.3. Crossplots of carbon and oxygen data from Siberia and South China.

Chinese data appear to be bounded to the left by a line approximately parallel to Knauth and Kennedy's lithification trend, potentially indicating alteration first by lithification followed by secondary alteration of $\delta^{18}O$ independent of $\delta^{13}C$. Little variability can be distinguished between members, although the negative excursion at the top of the section is represented as a spur of values more negative in both carbon and oxygen isotopic compositions.

Intra-basinal Correlation

If we are confident that the majority of our carbonate data analyses were performed on unaltered samples, the nearly 1000 analyses that were made of $\delta^{13}C$ and $\delta^{18}O$ allow us a new window into intra- and inter-basinal correlation in the latest Ediacaran. As noted in Chapter 3, we have taken the lithological correlations of

Grazhdankin and Rogov (seen governing section positions in Figure 4.4), and modified them in light of the carbon isotope stratigraphy.

One modification is to assume that the negative trend in the upper Turkut Formation can be correlated. In Figures 3.3 and 3.4, for example, the Turkut Formation is correlated lithologically, while in Figures 4.5 and 4.6, the sections are correlated by the point at which the carbon isotopic value crosses the zero point. The difference between these two correlations could be considered in the paradigm of erosive cutdown.

The most important thing we could learn by modifying correlations to fit isotope trends is where sections lie relative to potential or confirmed dateable beds. Potentially-dateable beds are found throughout the Khatyspyt, and a single bed in the Mattaia Formation has been found to contain zircons and dated. Correlation of key fossil beds, including the first appearance of bioturbation, with radiometric dates is highly desirable.

Inter-basinal Correlation

In addition to intra-basinal correlations, we can attempt to use our carbon isotope trends to correlate our sections to other latest Ediacaran sections worldwide. However, we have produced some of the most high-resolution data to date for the latest Ediacaran. For example, an overview paper (Saylor et al, 1998) suggests that most of our stratigraphy lies in what is considered an invariant interval. Saylor records only the positive excursion in the Mastakh ("c," "P1"), a single nadir in the mid-Khatyspyt ("b," corresponding perhaps to our N1, N2, or N3), and a zero crossing in the Turkut ("a," "N4"). However, sampling in other sections is relatively low resolution, due largely to unavailability of suitable carbonate facies. This suggests that the previous work could easily fail to capture the rapid excursions that we see in Siberia.

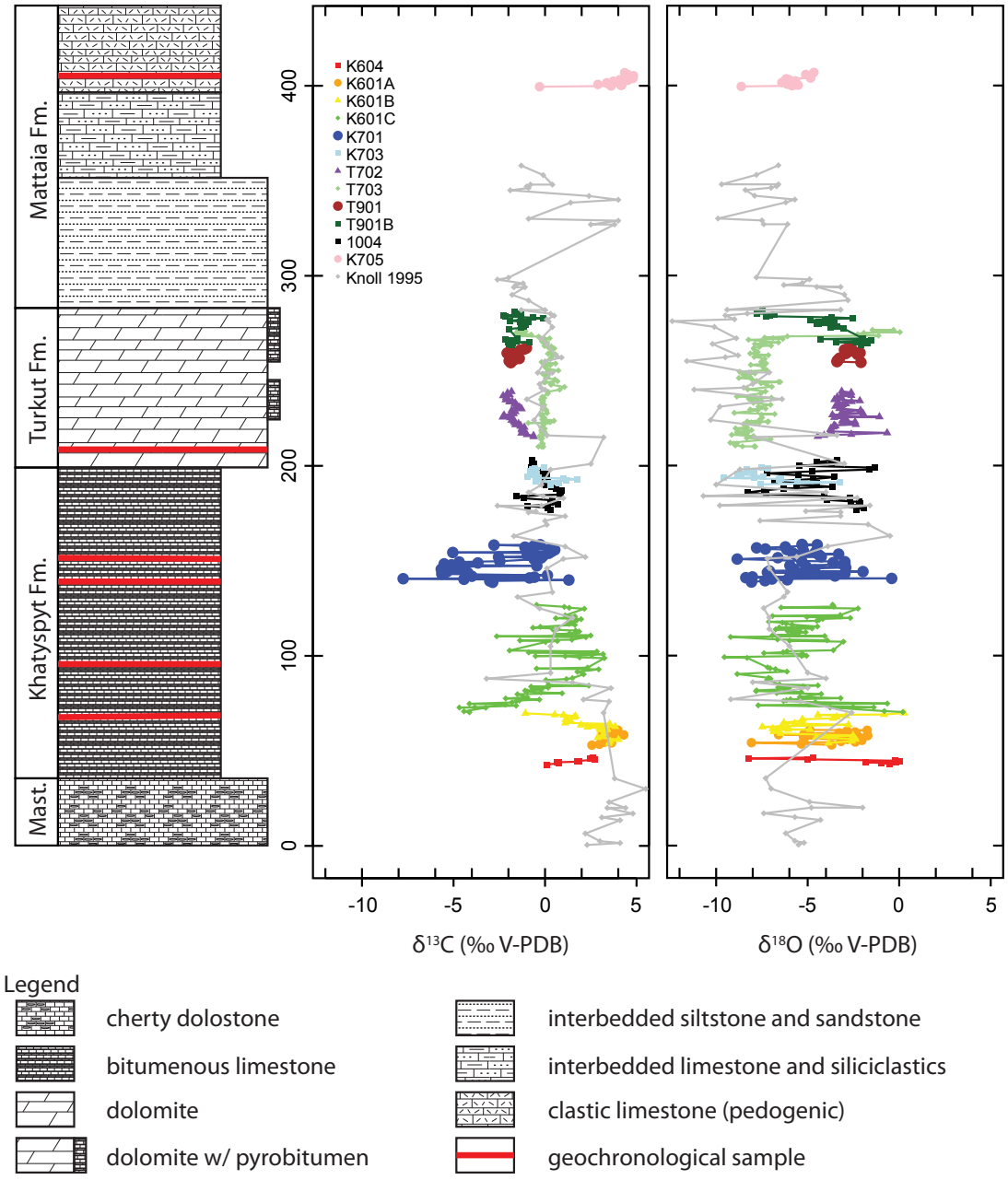

Figure 4.4. Composite carbon and oxygen isotope stratigraphy of the Khorbusuonka Group, correlation after Grazhdankin and Rogov. "Mast." stands for Mastakh Fm. Data from Knoll et al., 1995 in gray for comparison.

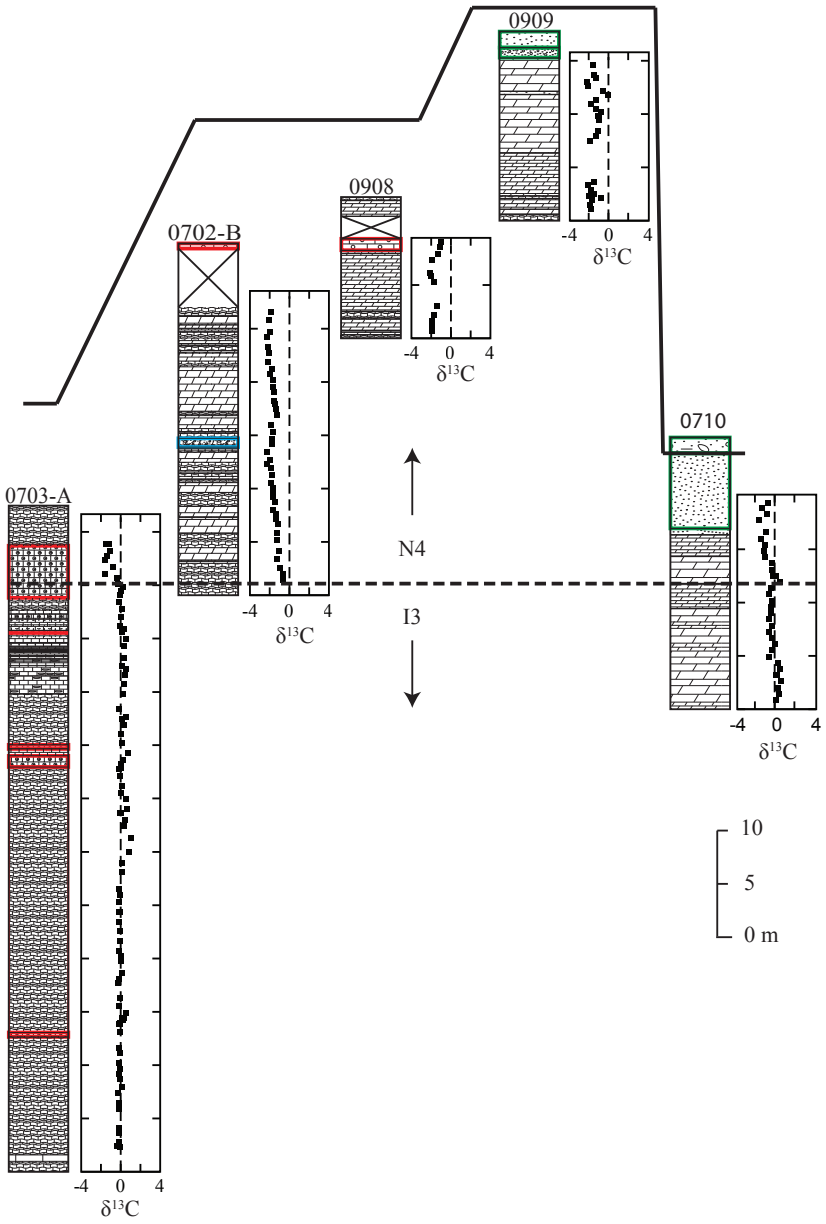

Figure 4.5. Isotopic correlation for Khorbusuonka Region Turkut sections. All sections lie within a 15 km radius (see Fig. 1.1). Dashed line denotes crossover of carbon isotopes into negative values. Solid line denotes potential stratigraphic cutout. Sections 0908 and 0909 are correlated lithologically. Ooid layers outlined in red; breccia layers outlined in blue; sand layers outlined in green. Error bars (1σ uncertainty) fall within data points.

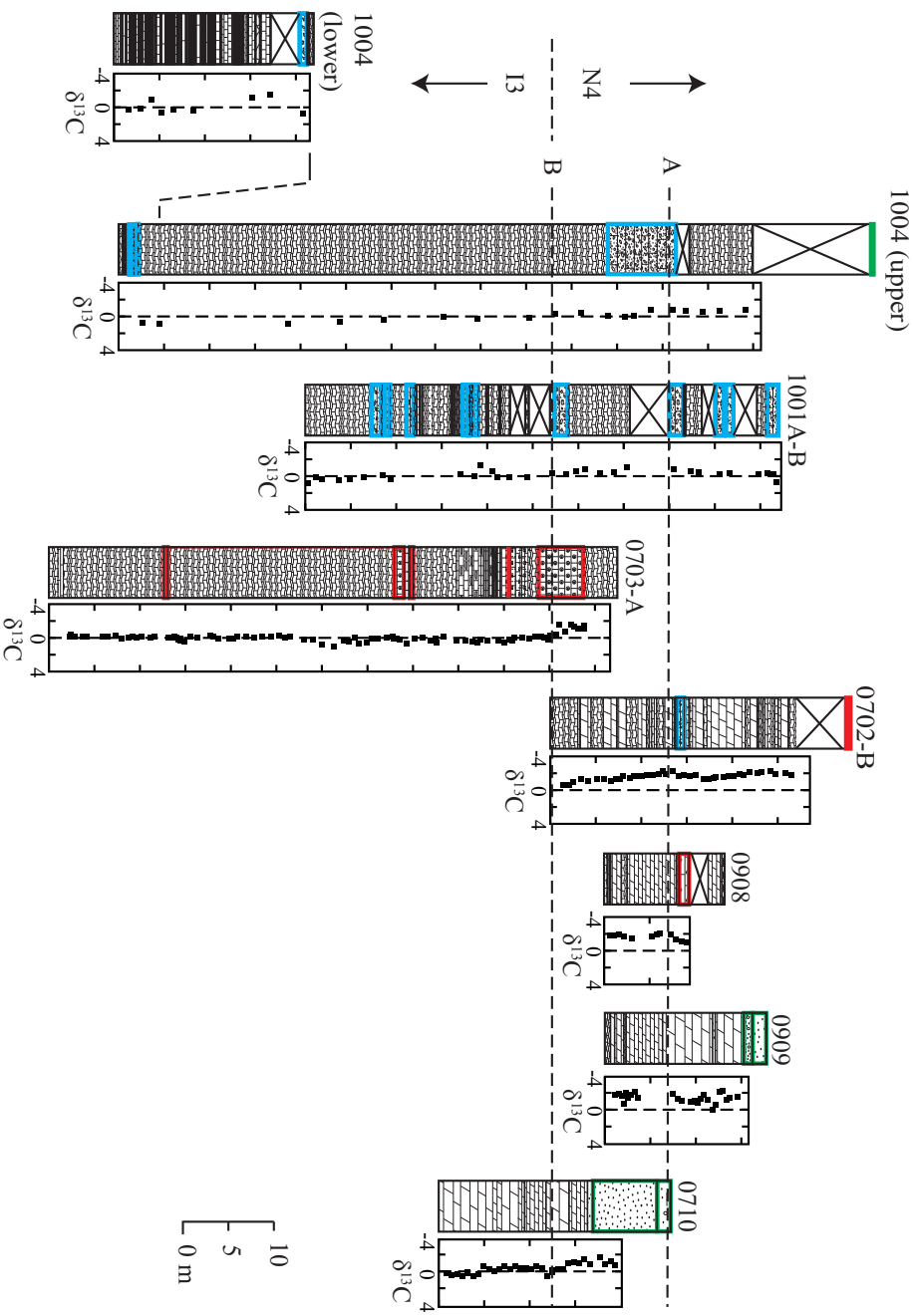

Figure 4.6. Isotopic correlation of Khorbusuonka and Olenek Region Turkut sections. Olenek sections 1004 and 1001A-B lie 50 and 80 km from the Khorbusuonka Region sections, which lie within a 20 km radius (see Fig. 1.1). Upper dashed line marks inflection point from negative to positive trend; lower dashed line marks crossover point between positive and negative values. Ooid layers outlined in red; breccia layers outlined in blue; sand layers outlined in green. Error bars (1σ uncertainty) fall within data points.

Alternatively, is there any reason to suspect that these rapid high-magnitude variations are confined to this basin? Kaufman et al (2006) produced a stable isotope record of the terminal Neoproterozoic Krol platform in northern India, which did record a number of rapid high-magnitude carbon isotopes variations. However, the composite carbon isotope stratigraphy is very noisy, and is consistent with Saylor's definition of only a few isotope zones in the terminal Ediacaran.

A focus on South China yields a similar conclusion. The terminal Ediacaran Dengying section at Hujiaba (Figure 3.25) also contains far fewer excursions than our Siberian sections. Similar to the excursions detailed in Saylor et al., the Dengying Formation at Hujiaba begins with a positive trend, moving through a negative excursion to a long invariant interval, then a zero crossing near the top of the section. Superimposed on this general framework are two more rapid excursions, neither of which has an analogue in our Siberian sections. The lower excursion is a zig-zag of four points, with no analogue in nearby sections; it seems possible that the feature resulted from localized alteration. However, it is difficult to explain the upper excursion by alteration. This feature consists of a relatively smooth, 13-point spike from 0‰ to +6‰; negative covariance with oxygen isotopic data is observed. The excursion is observed in some form in other South China sections (for example, Jiang et al., 2007; Zhu et al, 2007). This suggests that the excursion is original, and has intra-basinal, if not worldwide, correlative potential.

A crossplot of our Dengying carbon and oxygen isotopic data can be seen in Figure 4.3B, alongside that of the Khorbusuonka region.

Organic Carbon

Organic carbon data was collected in three sections representing the lower Khatyspyt Formation. Organic carbon data can be seen in Figures 3.21 and 3.23. Organic carbon isotope values fall near -30‰ for most of 0601-A and 0601-B, representing a 30-35‰ offset from carbonate carbon isotope values. Organic carbon isotopic composition, like that of inorganic carbon, is seen to vary on relatively rapid scales. However, while instances of negative covariance are observed, the two measurements largely appear to vary independently. Rapid variations in the organic carbon record are notable in the context of other organic carbon data in the Ediacaran Period where the lack of variation in organic carbon isotopic composition in the Doushantuo Formation relative to inorganic carbon has been construed as evidence for a large pool of dissolved organic carbon (DOC; McFadden et al., 2008). This pool would buffer the isotopic composition of buried organic carbon against changes in the isotopic composition of dissolved inorganic carbon (DIC). While we do not typically observe covariance in our limited dataset, it is also clear that this highly-variable data did not result from a buffered system.

The maximum biological fractionation between dissolved inorganic carbon (DIC) and organic carbon is approximately 32-35‰. However, the typical offset observed between inorganic and organic carbon is approximately 28‰ for the Neoproterozoic, and 22‰ in the modern day (Knoll et al., 1986).

While we can understand reduction in fractionation in terms of carbon limitation, our organic carbon data almost exclusively reflect greater fractionations (up to 45‰ in 0601-D), suggesting a more complex origin for the sampled organic carbon.

Methanogenesis combined with methanotropy (anaerobic oxidation of methane) could explain these larger fractionations. Methanogenic bacteria produce methane in anoxic bottom waters. While the majority of this methane escapes to be oxidized in the upper ocean or in the atmosphere, a fraction may be captured by methanotrophic bacteria, metabolized, and ultimately buried (Hayes, 1994). Notably, methanogenic metabolic pathways produce a much greater fractionation between inorganic carbon and methane output. This greater fractionation is compounded when methanotrophs preferentially intake ^{12}C from the already-light methane, ultimately resulting in storage of very light biomass.

An alternative hypothesis draws on the oxidation of transported organic matter, termed "fossil C_{org}" (Kaufman et al., 2007; Johnston et al., 2012). If fossil organic carbon is present, sea level drawdown could expose the reservoir to available oxidants, resulting in the release of bicarbonate ion (HCO_3^{2-}). This weathering product would have the isotopic signature of its parent organic matter, likely much lighter than the local DIC pool. The incorporation of this lighter material could cause negative excursions in $\delta^{13}C_{carb}$, potentially resulting in short records of supra-maximum fractionation.

However, we would expect this effect to be accompanied by additional evidence of sea level drawdown. While sections 0601-A and 0601-B each contain a few meters of intraclastic breccia, the most extreme $\Delta\delta^{13}C_{carb\text{-}org}$ values (up to 45‰) are seen in section 0601-D, for which available lithostratigraphy suggests deep water.

Carbonate-associated sulfate leaching

Stirred leaching over twenty-four hours was carried out five to eight times on twenty-two samples from Siberian sections 0601-A, 0601-B, and 0601-D. In sum,

leaching removed significant amounts of soluble sulfate from nearly all samples. Table A.4 shows the amount of soluble sulfate removed by leaching, alongside the total amount of sulfate derived from acidification (CAS). The total leach precipitate weight is typically a significant fraction of the total sulfate removed from the sample. While leach precipitates account for ~25% of total sulfate in 0601-A, the fraction varies up to 60% in 0601-B, and to nearly 100% in the upper part of 0601-D. These high values underscore the need for leaching.

Table 4.1. Amount of soluble sulfate removed by leaching. Weights are adjusted for sulfur content, and given in grams.

Section	Number	ppm CAS	CAS precipitate weight	Total leach precipitate weight	Leach wt. as % of total SO_4^{2-}
0601-A	0	558	0.0500	0.0173	25.75
0601-A	3.5	578	0.0667	0.0193	22.39
0601-A	6.1	895	0.0990	0.0287	22.44
0601-A	7.7	1118	0.1262	0.0423	25.09
0601-B	0	454	0.0525	0.0203	27.86
0601-B	4	379	0.0434	0.0230	34.67
0601-B	7	1079	0.0997	0.0196	16.41
0601-B	10.7	120	0.0124	0.0169	57.69
0601-B	13.7	805	0.0651	0.0427	39.60
0601-D	-2.5	1969	0.2361	0.0061	2.52
0601-D	-0.6	1529	0.1692	0.0209	10.98
0601-D	4.9	1078	0.1046	0.0641	38.01
0601-D	6	676	0.0790	0.0725	47.87

Section	Number	ppm CAS	CAS precipitate weight	Total leach precipitate weight	Leach wt. as % of total SO_4^{2-}
0601-D	9.5	73	0.0082	0.0083	50.40
0601-D	11.5	382	0.0507	0.0074	12.67
0601-D	17	454	0.0411	0.0693	62.79
0601-D	20	<1	0.0000	0.0118	100.00
0601-D	26.5	7	0.0001	0.0089	98.67
0601-D	28.5	11	0.0007	0.0796	99.14
0601-D	34	162	0.0172	0.0633	78.67
0601-D	44	390	0.0417	0.1565	78.95
0601-D	54	12	0.0004	0.0263	98.39

Figure 4.7 shows the amount of barium sulfate precipitated from each leach step alongside the CAS precipitate. While the majority of leaches precipitated very little barium sulfate, taken together, they represent a significant fraction of the total sulfate removed from the sample. Notably, for most samples, the majority of the soluble sulfate was not removed on the first one to two leaches. Most CAS studies (McFadden et al., 2008; Fike et al., 2006; and others) are performed using only one or two leach steps. While leaching procedures vary widely in both leachate solution and duration, it is clear that under some conditions, one to two leaches would not be sufficient to remove the influence of soluble sulfate on CAS isotopic composition.

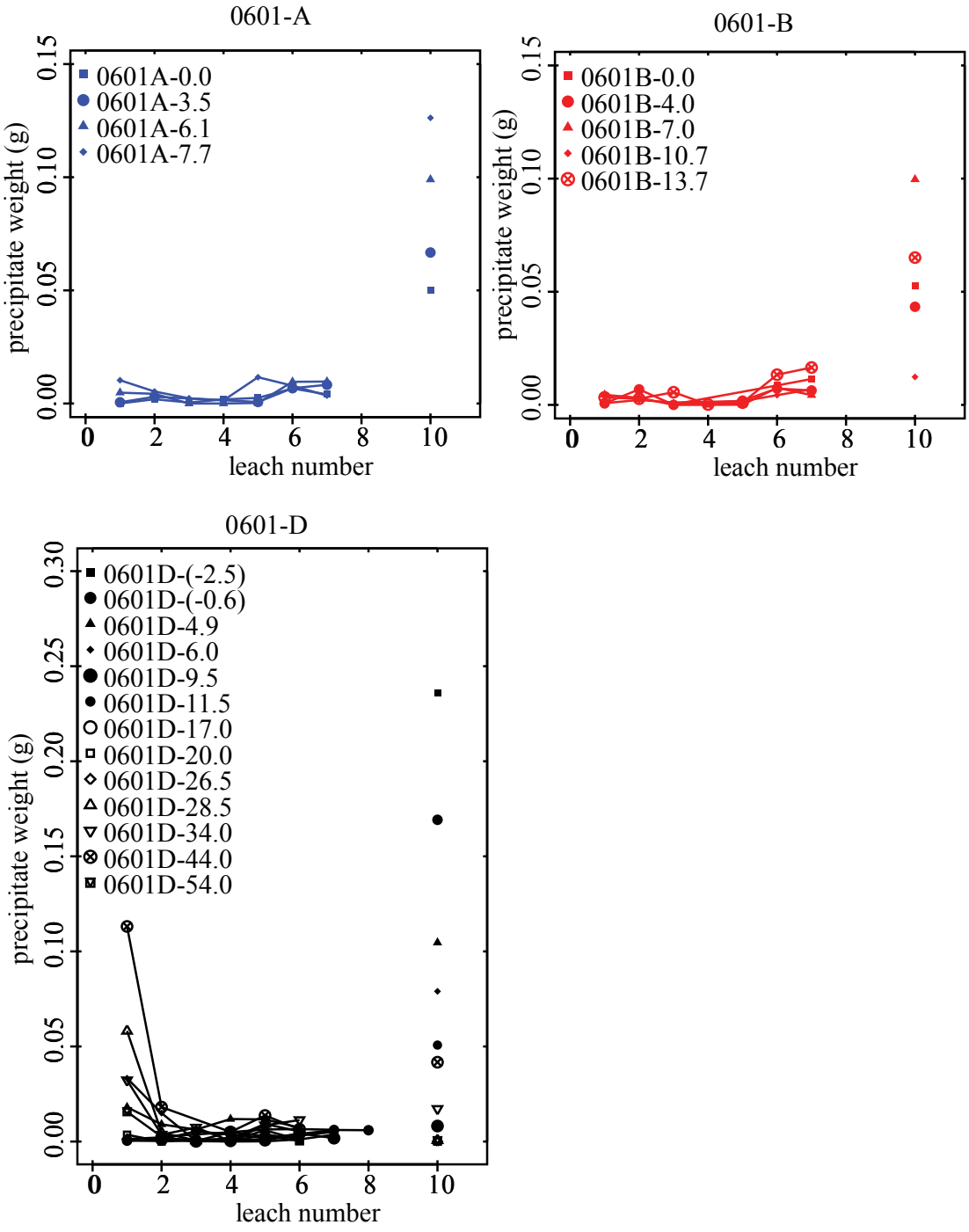

Figure 4.7. Progression of leach precipitate weight with repeated leaching. Leach numbers 1-8 denote leach precipitates; leach number 10 denotes precipitate weight following acidification (CAS precipitate weight). Precipitate weights are adjusted to reflect only the weight of barium sulfate, if other compounds were precipitated.

On the other hand, how do we know that we have removed all soluble sulfate from our samples, or at least enough to significantly diminish its influence? In some cases, our latter leaches have removed more soluble sulfate that the earlier ones. In Figure 4.7, this pattern can be seen in samples from both 0601-A and 0601-B. While this could represent an unaccounted-for artifact of performing the leach procedure in two separate countries, we have attempted to account for differences, as detailed in Chapter 2. Additionally, this pattern is not seen in samples from section 0601-D. Because soluble sulfate removal was observed through the last leach step for most samples, only half of each sample (50 grams) was acidified to extract CAS. The other half of the sample was reserved for further leaching, to be followed by acidification to extract CAS. Any differences in these replicates can be attributed to the removal of soluble sulfate during subsequent leaches.

Another possibility in accounting for greater amounts of sulfate removed in later leaches is that our leaching or drying procedures allow for the oxidation of TS sulfides to sulfate, which is then removed by leaching. However, in 0601-A and 0601-B, the isotopic composition of the sulfate removed during leaching, particularly during the later leaches, is typically 5-10‰ more positive than the $\delta^{34}S_{TS}$ for the same sample. On the other hand, many samples in 0601-D have leach precipitates 5-10‰ more *negative* than $\delta^{34}S_{TS}$. In both of these cases, oxidized TS would require mixing with either a large amount of material near the isotopic composition of the leach material, or a lesser amount of material of more greatly differing isotopic composition. This suggests that only a small fraction (if any) of the soluble sulfate could result from laboratory-based oxidation of TS sulfides.

Does leaching significantly influence $\delta^{34}S_{CAS}$? Table 4.2 gives both the measured $\delta^{34}S_{CAS}$ and a calculated "unleached $\delta^{34}S_{CAS}$": the value that would have been measured if no leaches were performed on the sample. This value is calculated by taking the weighted average of all leach precipitate isotopic compositions with the measured CAS isotopic composition. The "leach differential" column gives the value by which $\delta^{34}S_{CAS}$ would have been lowered if no leach steps were carried out. The numbers can be large, ranging up to -15‰ in 0601-B; all are outside measurement uncertainty, making it clear that a lack of soluble sulfate removal would significantly influence results. Since "unleached" CAS isotopic compositions are lighter in every case, non-removal of soluble sulfate could significantly affect how we consider the relationship between the isotopic composition of CAS and TS. In 0601-D especially, non-leached CAS samples would have produced apparent inversion (wherein TS is heavier that CAS) in a number of cases in the upper portion of the section.

Table 4.2 Influence of leaching on $\delta^{34}S_{CAS}$. "Unleached $\delta^{34}S_{CAS}$" is calculated based on quantity and isotopic composition of soluble sulfates removed during leaching. "Leach differential" is the difference between measured $\delta^{34}S_{CAS}$ and calculated unleached $\delta^{34}S_{CAS}$.

Section	Number	ppm CAS	%carb	post-leach $\delta^{34}S_{CAS}$ (‰)	unleached $\delta^{34}S_{CAS}$ (‰)	leach differential (‰)
0601-A	0	558	90.9	39.94	31.05	-8.89
0601-A	3.5	578	98.5	18.7	16.86	-1.84
0601-A	6.1	895	98.6	41.16	34.54	-6.62
0601-A	7.7	1118	96.7	37.06	28.60	-8.46
0601-B	0	454	99.9	40.78	34.01	-6.77
0601-B	4	379	99.0	44.58	32.80	-11.78

Section	Number	ppm CAS	%carb	post-leach $\delta^{34}S_{CAS}$ (‰)	unleached $\delta^{34}S_{CAS}$ (‰)	leach differential (‰)
0601-B	7	1079	96.9	31.15	27.15	-4.00
0601-B	10.7	120	98.8	41.58	26.63	-14.95
0601-B	13.7	805	82.8	31.16	15.54	-15.62
0601-D	-2.5	1969	90.1	46.94	46.24	-0.70
0601-D	-0.6	1529	94.0	44.77	40.94	-3.83
0601-D	4.9	1078	99.9	47.74	40.62	-7.12
0601-D	6	676	99.9	45.68	38.00	-7.68
0601-D	9.5	73	99.3	34.46	29.44	-5.02
0601-D	11.5	382	96.9	41.4	39.12	-2.28
0601-D	17	454	96.0	36.36	29.53	-6.83
0601-D	20	<1	99.0	NA	23.58	NA
0601-D	26.5	7	98.4	31.01	24.39	-6.62
0601-D	28.5	11	95.7	35.8	31.89	-3.91
0601-D	34	162	97.4	42.7	29.72	-12.98
0601-D	44	390	95.9	42.08	35.61	-6.47
0601-D	54	12	97.1	31.4	27.58	-3.82

Total Sulfur

Total sulfur (TS) isotopic and composition data were collected for sections 0601-A, 0601-B, and 0601-D (Figures 3.22 and 3.24). The vast majority of samples in these sections have total sulfur concentrations under 0.2% by weight, although a few samples range up to 0.8% in 0601-D. This relatively low TS concentration decreases the

likelihood that our carbonate-associated sulfate (CAS) isotopic composition has been significantly influenced by TS isotopic values (Marenco et al., 2008).

In both modern and most ancient sediments, TS isotopic values are typically less than 0‰. TS deposition usually occurs subsequent to the reduction of oceanic sulfate by bacterial sulfate reduction (BSR) or similar metabolisms, resulting in fractionations of -46‰ or more (Fike et al., 2006). In our sections, TS isotopic values are uniformly negative throughout 0601-A, variably negative and positive in 0601-B, and highly positive (up to +40‰) in 0601-D. These positive values are the result of two factors: first, the oceanic sulfate pool in the Ediacaran was highly positive (up to +50‰, this study; many others; Claypool, 1980). Secondly, low sulfate conditions in 0601-B and especially the upper part of 0601-D may have resulted in lesser fractionations during bacterial reduction of sulfate (Habicht et al, 2002; Fike et al, 2006).

However, even minimal fractionations resulting from BSR cannot explain the two inverted $\Delta\delta^{34}S_{CAS\text{-}TS}$ points in the middle part of section 0601-D. Explanation of these values, where TS is isotopically heavier than CAS, requires multiple sulfate reservoirs, or recycling of sulfate (for example, as in Ries et al, 2006; Shen et al, 2010).

Low-resolution data in sections 0601-A seem to indicate relative invariance, while those in 0601-B do not show a significant trend. However, high-resolution TS data in section 0601-D shows a clear trend: values jump from ~+10‰ to ~+35‰ approximately 10 meters from the base of the section. Notably, this jump is coincident with the fall of CAS concentration to ~500 ppm. This reinforces the idea that highly positive TS isotopic compositions are correlated with low oceanic sulfate conditions.

The offset in TS isotopic composition in 0601-D is also coincident with the return of $\delta^{13}C_{carb}$ to positive values following negative excursion N1, underscoring the idea of perturbation of oceanic chemistry.

Comparison with Oman CAS data

In the lowest part of the Ara Formation in Oman, CAS isotopes record the beginning of a positive shift of over +20‰, from +20‰ to +40‰ (Fike and Grotzinger, 2008). This shift, recorded in evaporitic deposits, has no equivalent pyrite isotope data. However, pyrite data is available before and after the interval in which the shift is seen, and records an analogous shift, from nearly -20‰ to above +10‰. Collectively, these shifts in isotopic values are referred to as the Ara anomaly.

Our CAS data span approximately the same interval as the Ara Formation. Our data also record a strong shift in pyrite isotopes, from about +10‰ to nearly +40‰ (Figure 3.24). However, it is notable that this shift in pyrite isotopes is not accompanied by a similar shift in CAS isotopes. Rather, CAS isotopes typically higher than +40‰ throughout the section, similar to the post-shift values seen in the Ara Formation.

The Khatyspyt Formation CAS data does not record a shift to higher positive values alongside the shifting pyrite values (Figures 3.22 and 3.24). What could lead the pyrite isotopes to vary independently of the CAS isotopes?

The data from the Khatyspyt Formation and the Ara Formation also differ strongly in the fractionation between CAS and pyrite isotopic values. While Fike and Grotzinger's (2008) values for fractionation are widely variable, they vary between +25‰ and +50‰. Fractionation in the Khatyspyt Formation, on the other hand, is

typically near +50‰ in the lower section, but falls to +10‰ or below in the upper section after the shift in pyrite values. In two samples, negative fractionation is observed.

The pyrite isotopic values observed in the Khatyspyt Formation are extremely heavy. Pyrite values below zero are more typical for most of Earth history. Fike and Grotzinger (2008) suggest that higher isotopic values would be required for oceanic sulfur inputs, on the basis of their CAS and pyrite data from the Ara Formation. The Khatyspyt Formation records even higher values in both CAS and pyrite, with no evidence of restriction, as is seen in the Ara Formation.

The differences in the sulfur isotopic compositions recorded in these two coeval sections preclude the identification of a single causal event. However, dramatic shifts in CAS and/or pyrite isotopes in both sections suggest instability in the global sulfur cycle, and the highly positive sulfur isotopic values seen in both sections require more positive values for oceanic sulfur inputs.

Strontium Isotopic Composition

Strontium isotopic composition was measured in ten samples spaced throughout the stratigraphy of our Siberian sections (Figure 3.30, Table 3.3). Samples were chosen both for spacing and for stratigraphy proximity to collected geochronological samples. Not including the value of K604-1.9, an outlier at 0.7093, the Khatyspyt and Turkut samples show a slight positive trend moving up section, while the single Mattaia sample far up section gives a slightly lower value.

The anomalously high value seen in sample K604-1.9 can be attributed to the incorporation of clay into the rock during deposition. Clay is typically enriched in ^{87}Rb and the inclusion of even small amounts of clay in carbonate rock will raise the $^{87}Sr/^{86}Sr$

ratio over time as ^{87}Rb decays to ^{87}Sr. The morphology of the lower part of the Khatyspyt Formation, with its thinly-bedded, bituminous carbonates, supports the supposition that clay could have been incorporated into this sample during deposition, providing a mechanism for influencing the $^{87}Sr/^{86}Sr$ ratio of the rock. For this reason we will not include sample K604-1.9 in further discussions.

Additional data from the same sections collected by other workers in Russia (Figure 4.8) suggest near-invariance through the Khatyspyt Formation at ~0.7080, with some enrichment in ^{87}Sr occurring in the Turkut Formation. As only dolomite samples are available in most of the Turkut Formation, it is possible that this enrichment is a result of alteration.

Because enrichment in ^{87}Sr can occur as a result of alteration or of ingrowth via ^{87}Rb found in clay minerals, it is important to constrain the potential alteration of samples. Our samples for strontium analysis were microdrilled from the darkest, finest-textured portions of samples high percent carbonate chosen to reflect low levels of alteration (Figure 4.9). However, particularly in the Khatyspyt Formation, it is difficult to completely exclude trace amounts of clay minerals; this provides a potential avenue for minor modification of the ^{87}Sr content of a sample. Thus we must consider the possibility that the slightly lower values found by our Russian colleagues represent a more accurate

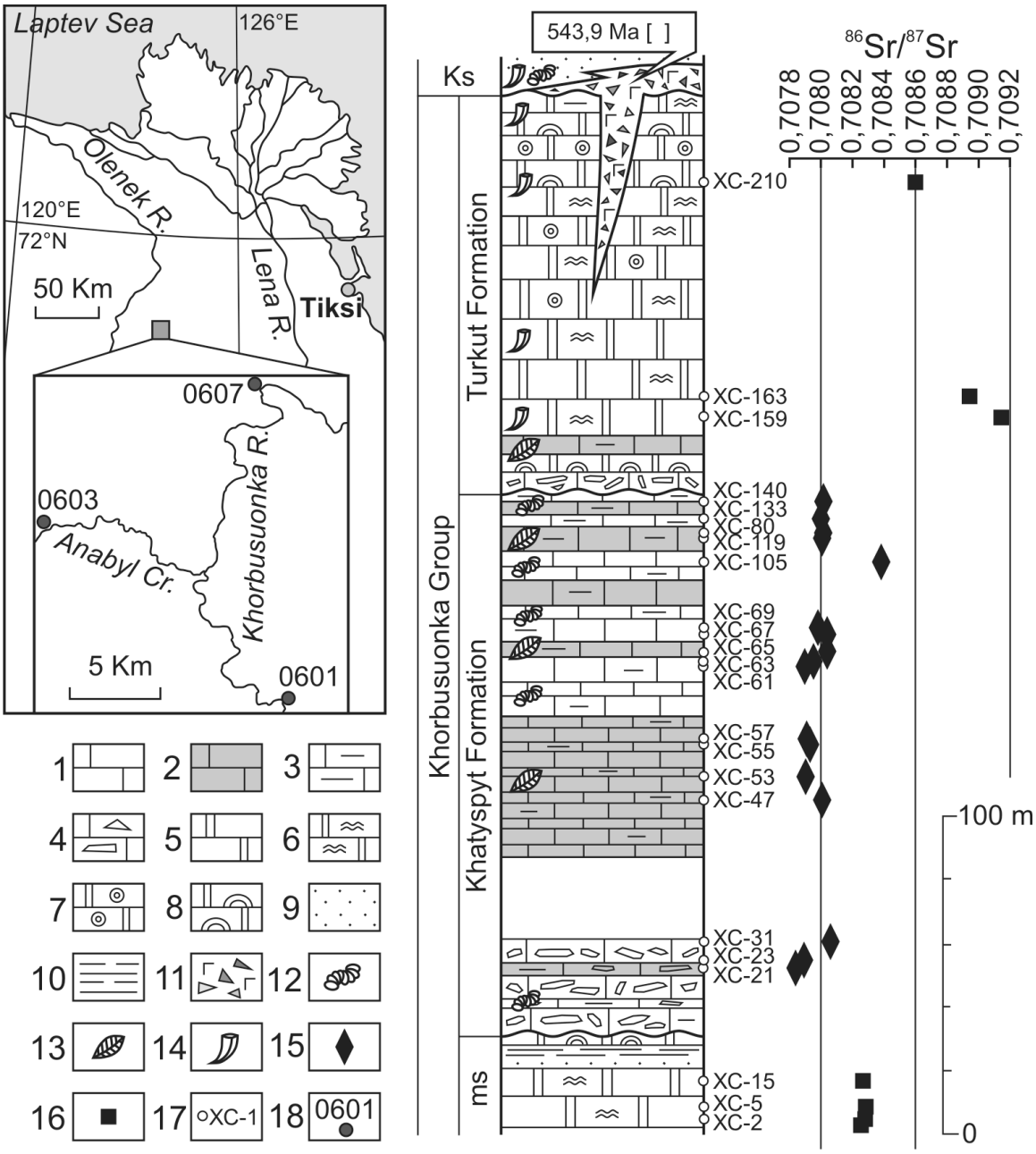

Figure 4.8. Strontium data produced from our Khorbusuonka Region sections by Irina Vishnevskaya and others. Square data points represent dolomitic samples; diamond points represent limestone samples.

Figure 4.9. Photo of hand sample of 0701B-6.25, with box around area specified for microdrilling. Note avoidance of visible cracks and discontinuities. Sample is approximately 4 cm in width.

determination of the original strontium isotopic composition of our samples. On the other hand, a separate study (Halverson et al., 2007) measured strontium values in the latest Ediacaran and found them to be falling; a nadir of 0.7085 is reached at the Precambrian-Cambrian boundary, measured in Namibia (Kaufman et al, 1993). Other workers (Derry et al. 1994, Montañez et al., 1996; reprinted in review by Halverson et al., 2007) have also found steep positive trends in strontium isotopic composition in the earliest Cambrian in both Siberia and other localities.

The bulk of our small dataset defines a comparatively rapidly-rising $^{87}Sr/^{86}Sr$ isotopic composition throughout the latest Ediacaran, which directly conflicts with the datasets generated by our Russian colleagues and those reprinted in the review of Halverson et al. (2007). This pattern suggests a rise in continental weathering through latest Ediacaran. This would be consistent with a rise in atmospheric oxygen content or a fall in sea level (Kaufman et al, 1993). However, the invariant trend found by our Russian

colleagues is not consistent with this inference, nor is the negative trend evident in Halverson's review. Overall, the lack of consistency in strontium isotopic composition measurements for this time period precludes meaningful interpretation. The datasets compiled by Halverson et al. (2007) contain samples from several widely-separated sections, of which some are assigned ages by relatively low-confidence correlations. On the other hand, we have the opportunity to make further narrowly-spaced measurements, which will aid in the identification of outliers, increasing confidence in the trend.

Our single Mattaia value, at 0.70818, is consistent with mid-to-late Tommotian time according to data collected in other Siberian sections by Kaufman et al. (1996). However, samples from the mid-to-upper Nemakit-Daldyn, analyzed for the same paper, define a negative trend, in opposition to the positive trend seen in our sample set. A better match for our data is found in the lower portion of the Nemakit-Daldyn, where sample $^{87}Sr/^{86}Sr$ values trend from ~0.7085 to ~0.7087. This suggests that the 120 meter gap in our analyses is coincident with the mid-to-upper Nemakit-Daldyn as delineated in Kaufman et al. (1996). On the other hand, the 0.7080 values found by our Russian colleagues are found nowhere in Kaufman et al. data from the Nemakit-Daldyn. Further analysis of available samples could give more confidence in the determination of whether our positively-trending samples represent outliers.

Radiometric Dating

Siberia

Radiometric dating was performed on zircons separated from a single sample from the early Cambrian Mattaia Formation in the Khorbusuonka region of northeastern Siberia (Figures 3.31-3.35; Table A.7). No carbon isotope data is available from the

section containing the dated layer; however, correlated sections exhibit carbon isotope values of approximately +5‰ (Figure 3.5; Table A.1). Based on established time-series chemostratigraphy of the Lower Cambrian interval in Siberia (Kouchinsky et al, 2007; Kouchinsky et al., 2011) and worldwide (Maloof et al., 2010), this value is distinct enough that it could be useful for inter-basinal correlation, allowing our radiometric date to gain wider applicability. The weighted mean of all accepted measurements is 528 ± 11 Ma (2σ) (Figure 3.35).

Our measurement carries a large uncertainty due to the trade-offs made during initial age determination. Measurements made via LA-ICPMS, as this one was, carry uncertainties between ±5 and ±11 years, depending on laser spot size (Martin, personal communication). Larger (20 micron) spot sizes ablate greater quantities of material, resulting in greater measurement precision. However, in the case of small, visibly zoned zircons, it is imperative that a single region be sampled to avoid mingling material of potentially differing ages. In our work, a smaller (10 micron) spot size was used, allowing independent sampling of visible core, mid-grain, and rim material. Analysis of these layers, distinct under cathodoluminescent imaging, allowed us to determine that the zones have no significant age differences.

Because all zones of all grains fall within uncertainty of one another, we can be reasonably confident that the zircons have a single source. Grains from a single source can be subjected to dating via thermal ionization mass spectrometry (TIMS), which requires the dissolution of a number of grains. Because the sample solutions utilized in TIMS dating can be spiked, instrumental fractionation can be accounted for, allowing much greater precision in determination of radiometric dates. Our sample is currently

undergoing TIMS dating in the laboratory of Prof. Sam Bowring at the Massachusetts Institute of Technology.

Our date from the Mattaia Formation could potentially have an impact on how evolutionary rates are viewed. Maloof and others (2010) have constructed an age model based on five Moroccan radiometric dates coupled with local $\delta^{13}C$ chemostratigraphy (Figure 4.10). Sections from around the world are correlated to the Moroccan strata via $\delta^{13}C$ tie points. In this way fossil appearance is tied to radiometric dates, allowing analysis of first-appearance data. From this constructed correlation, Maloof observes three pulses of early animal diversification. In Maloof's correlative paradigm, only two excursions, 5p and 6p, contain measurements with carbon isotope values high enough to match our +5‰ values at our dated layer. However, these two excursions are placed at ~531 (middle Nemakit-Daldyn) and ~526 Ma (latest Nemakit-Daldyn), respectively, neatly bracketing our radiometric measurement.

At the current level of precision, each of the noted excursions falls well within the uncertainty of our radiometric date. However, if a more precise measurement is obtained via TIMS dating, our sample may inform Maloof's correlation, in turn affecting the placement of fossil first appearances in time. Preliminary reports from Bowring indicate a weighted mean $^{206}Pb/^{238}U$ date of 529.45 ± 0.39 Ma (Bowring, personal communication). This date falls between the 5p and 6p excursions delineated in Maloof et al. (2010). Because the dated strata are located near or within a +5‰ carbon isotope excursions, one of the large positive excursions described by Maloof et al. must have occurred at this time. Moving these excursions in time, along with their associated fossil appearances,

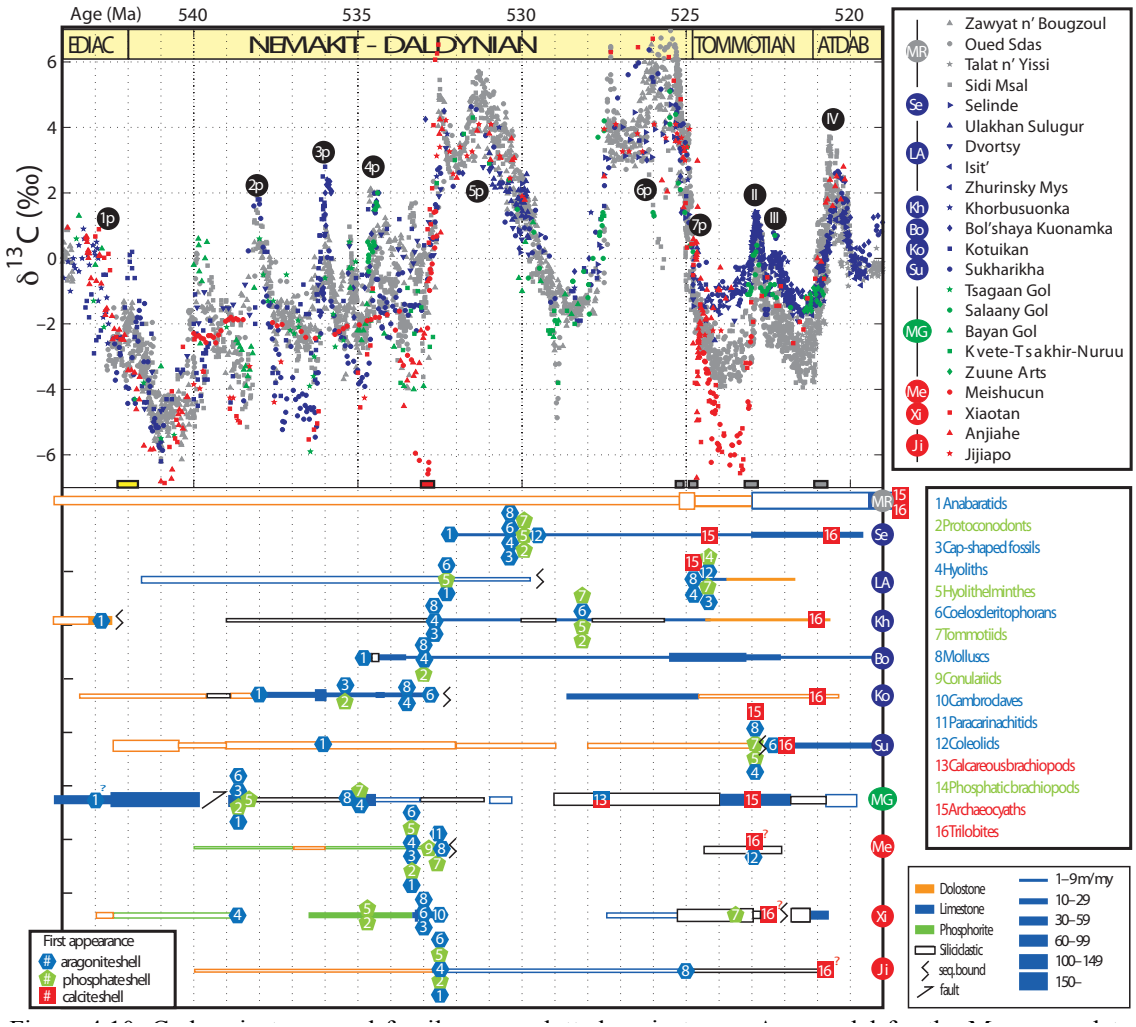

Figure 4.10. Carbon isotopes and fossil ranges plotted against age. Age model for the Moroccan data (gray shapes: Zawyat n' Bougzoul, Oued Sdas, and Talat n' Yissi [Maloof et al., 2005], and Sidi M'sal [Maloof et al., 2010a]) assumes constant sediment accumulation rates between U/Pb zircon tie points. U/ Pb tie points are illustrated as gray (Morocco: Maloof et al., 2005, 2010a), red (China: Brooks et al., 2006), and yellow (Oman: Bowring et al., 2007) rectangles, the centers and widths of which represent the ages and 2σ error bars, respectively, of each analysis. Each group of colored shapes represents $\delta^{13}C_{CaCO3}$ data from a different stratigraphic section. Siberia (blue)—Selinde River (Kouchinsky et al., 2005), Ulakhan Sulugur (Aldan River; Brasier et al., 1993), Dvortsy (Aldan River; Magaritz et al., 1986; Brasier et al., 1993), Isit' and Zhurinsky Mys (Lena River; Magaritz et al., 1991; Kirschvink et al., 1991), Khorbusuonka River (Olenek Uplift; Knoll et al., 1995a), Bol'shaya Kuonamka (Anabar Uplift; Kouchinsky et al., 2001), Kotuikan River (Anabar Uplift; Knoll et al., 1995b; Kaufman et al., 1996), Sukharikha River (Kouchinsky et al., 2007). Mongolia (green)—Tsagaan Gol, Salaany Gol, Bayan Gol, Kvete-Tsakhir-Nuruu, and Zuune Arts (Brasier et al., 1996). China (red)—Meishucun (Brasier et al., 1990), Xiaotan (Zhou et al., 1997), Anjiahe (Ishikawa et al., 2008), and Jijiapo (M. Zhu, 2010, personal commun.). The labeled $\delta^{13}C_{CaCO3}$ peaks

(1p–7p and II–IV) were named in Siberia (e.g., Kouchinsky et al., 2007). Sections for which both $\delta^{13}C_{CaCO3}$ and biostratigraphy are available are plotted below, with line-width representing sedimentation rates inferred from the age model in meters per million years (m/ m.y.), and line color representing dominant lithology (dolostone, limestone, phosphorite, or mixed siliciclastics). The lines are filled if they represent a fossiliferous interval, and they are hollow if they are unfossiliferous. Blue hexagons, green pentagons, and red squares depict the first appearance of organism and calcite skeletons respectively. (Figure reproduced from Maloof et al., 2010.)

would lengthen or shorten the fuse to the Cambrian excursion, with implications for evolutionary rates.

The successful determination of a radiometric age for this single available geochronological sample is made more significant by the availability of >10 additional geochronological samples spaced throughout the Khatyspyt Formation. Though these samples have not been subjected to XRD or XRF, they are similar in color and texture to the dated Mattaia sample.

Within both the paradigm of Maloof's correlation and that of trace and body fossil occurrence in the Khatyspyt and Mattaia formations, our samples may prove influential in understanding the timing of evolutionary milestones.

China

Detrital zircons were extracted from two closely-spaced layers in the Gaojiashan Member of the Dengying Formation at Hujiaba in South China, and dated via LA-ICPMS (Figures 3.38-3.42; Tables A.13 and A.14). Little can be concluded from sample 09G-35.3; only a very small number of very small zircons were extracted from the sample. The majority of the <50 dated grains fall within a population with ages ranging from 700-900 Ma, with two grains with ages of over 2000 Ma. This suggests that the source material for this layer samples igneous rock with an age of 700-900 Ma.

On the other hand, thousands of zircons were separated from sample 09G-37.9. These grains recorded a wider range of populations (Figure 3.41). The 700-900 Ma population, unsurprisingly, comprises the bulk of the extracted zircons, and several grains older than 2000 Ma are observed. However, this layer also contains a substantial population of younger zircons, with radiometric ages ranging from ~550-600 Ma. The four youngest grains have an average age of 548.1 ± 8.1 Ma (Figure 3.42), and a maximum depositional age of 560 Ma. Since these rocks are known to predate the pre-Cambrian-Cambrian boundary, their depositional window is small. Additionally, it is notable that these youngest grains were incorporated into the dated layer at most a few million years after their formation, suggesting shallow emplacement if not surficial deposition as volcanic ash.

Chapter 5: Conclusions

The initial aim of this work was to understand the evolution of oxygen concentrations in the latest Ediacaran ocean. Some of the work detailed in this study forms a basis for a continuing effort to understand Ediacaran oxygenation. The initial CAS work, and the combination of organic and inorganic carbon data, could be expanded to give a time-resolved picture of fractionation by bacterial metabolism. Additionally, our initial determination of a positively-sloping strontium curve provides circumstantial evidence for increased continental weathering, consistent with a rise in oxygen.

However, constraints on time, induced in no small part through difficulties in sample export from Russia, have required that the scope of the work be redefined. Several ideas were pursued: carbon and oxygen isotopic compositions were measured in a large number of sections at high resolution with the aim of informing intra- and inter-basinal correlation; the small available set of powdered samples from key sections were subjected to CAS extraction, allowing us to evaluate both isotopic composition and our CAS methodology; and radiometric dating was performed on suitable samples. Other measurements, including organic carbon and strontium isotopic compositions, may also be used to inform correlations.

The most notable feature of our high-resolution carbon and oxygen data is the highly variable nature of the carbon isotope curve. While major features are recorded worldwide, a large number of small, rapid excursions are observed in our data, both in Siberia and South China. More high resolution work could show similar excursions in sections in similar paleo-locations. Our Siberian sections are currently associated with a radiometric date from the Mattaia Formation, and additional dates may be obtained from

the Khatyspyt Formation. If correlation to our Siberian sections is possible with the use of carbon isotope variations, more localities could be tied to absolute time. On the other hand, it may be found that these rapid variations are unique to the Khorbusuonka region; in this case, reasons for high variability can be evaluated in light of the chemical changes unfolding throughout the Ediacaran Period.

Our CAS data can also be evaluated in relation to Ediacaran chemical changes. More importantly, however, CAS concentration and isotopic data is associated with data on soluble sulfate removal. This level of detail is not reached in many previous studies; often, adequate soluble sulfate removal is assumed without evaluation. Our data make clear the importance of adequate soluble sulfate removal; at minimum, removed soluble sulfate should be quantified in multiple steps to determine whether a significant amount is likely to remain.

However, potentially the most significant portion of this study is radiometric dates derived from U-Pb geochronology. A single date in the Siberian Mattaia Formation is well-positioned to influence understanding of evolutionary rates in the early Cambrian Period. Perhaps more importantly, the successful dating of this sample increases the probability that additional dates will be derived from similar samples collected throughout the fossil-rich Khatyspyt Formation.

In this work, only a small subset of the available Siberian material has been analyzed. Additional total sulfur and organic carbon sample have been prepared and only require analysis. Microdrilled powders from each collected geochemical sample have the potential to be analyzed for trace element composition as well as additional resolution in

the strontium isotope curve. If additional samples can be exported from Russia, higher-resolution CAS curves could be obtained, augmenting promising initial results.

Overall, this work serves as an initial study of the Siberian Khorbusuonka region, and confirms that this region has the potential to yield interesting geochemical results.

Appendices

Table A.1. Carbonate data for Siberia.

TA.1	Name	Section Height(m)	Correlated Height (m)	$\delta^{13}C$	$\delta^{18}O$	%carb
1	0907-0.1	0.1	0.1	2.53	-3.99	81.47
2	0907-1.1	1.1	1.1	2.87	-3.57	81.98
3	0907-2.3	2.3	2.3	3.12	-3.79	76.5
4	0907-3.6	3.6	3.6	3.26	-3.73	86.82
5	0907-4.4	4.4	4.4	3.01	-3.78	88.27
6	0907-5.0	5	5	2.22	-3.89	90.61
7	0907-5.9	5.9	5.9	1.86	-4.98	85.8
8	0907-7.0	7	7	2.37	-4.29	71.85
9	0907-7.9	7.9	7.9	2.73	-4.83	85.53
10	0907-9.4	9.4	9.4	3.1	-4.35	76.26
11	0907-10.5	10.5	10.5	3.58	-4.38	83.19
12	0907-11.1	11.1	11.1	2.87	-4.09	80.24
13	0907-11.8	11.8	11.8	2.66	-3.83	77.69
14	0907-12.7	12.7	12.7	3.54	-3.84	80.96
15	0907-13.7	13.7	13.7	2.9	-3.98	86.38
16	0907-15.0	15	15	2.7	-3.68	83.15
17	0907-15.8A	15.8	15.8	2.49	-3.89	96.24
18	0907-15.8B	15.8	15.8	2.71	-4.11	96.24
19	0907-17-0	17	17	4.5	-4.38	NA
20	0907-18.0	18	18	4.45	-3.28	79.09
21	0907-18.9	18.9	18.9	2.1	-3.82	91.48
22	0907-20.3	20.3	20.3	2.27	-4.5	81.25
23	0907-21.2	21.2	21.2	2.67	-4.02	80.52
24	0907-22.0	22	22	2.89	-3.7	85.32
25	0907-23.0	23	23	2.98	-3.7	86.9
26	0907-24.0	24	24	2.88	-4.18	83.38
27	0907-27.3	27.3	27.3	4.89	-5.72	99.26
28	0907-28.3	28.3	28.3	5.54	-6.16	99.08
29	0907-29.5	29.5	29.5	4.97	-6.3	99.15
30	0907-30.0	30	30	4.92	-4.81	99.9
31	0907-31.0	31	31	4.57	-4.57	97.39
32	0601F-0.0	0	8	2.98	-4.05	84.35
33	0601F-0.5	0.5	8.5	4.56	-6.35	96.11
34	0601F-1.0	1	9	4.62	-4.57	87.57
35	0601F-1.5	1.5	9.5	4.06	-3.99	81.76
36	0601F-2.0	2	10	4.17	-4.11	83.82

TA.1	Name	Section Height(m)	Correlated Height (m)	$\delta^{13}C$	$\delta^{18}O$	%carb
37	0601F-3.0	3	11	3.73	-3.74	85.22
38	0601F-3.5	3.5	11.5	3.44	-3.5	92.98
39	0601F-4.0	4	12	6.57	-3.99	84.57
40	0601F-4.5	4.5	12.5	6.6	-4.05	98.08
41	0601F-5.0	5	13	5.96	-4.3	96.6
42	0601F-5.5	5.5	13.5	5.35	-3.83	93.86
43	0601F-6.0	6	14	5.91	-4.64	95.92
44	0601F-6.5	6.5	14.5	3.65	-3.91	89.39
45	0601F-7.5	7.5	15.5	3.93	-4.88	74.46
46	0601F-8.5	8.5	16.5	6.61	-4.18	98.11
47	0601F-9.0	9	17	5.55	-4.31	94.86
48	0601F-9.5	9.5	17.5	4.86	-3.87	91.83
49	0601F-10.5	10.5	18.5	5.66	-5.3	95.21
50	0601F-11.0	11	19	5.93	-5.48	99.74
51	0601F-11.5	11.5	19.5	6.04	-5.88	98.83
52	0601F-12.0	12	20	4.73	-3.56	83.02
53	0601F-12.5	12.5	20.5	5.75	-5.42	99.34
54	0601F-13.0	13	21	5.88	-5.33	98.69
55	0601F-13.5	13.5	21.5	5.56	-5.29	95.87
56	0601F-14.0	14	22	5.04	-4.75	98.42
57	0601F-14.5	14.5	22.5	5.45	-6.02	98.72
58	0601F-15.0	15	23	5.62	-5.66	97.2
59	0601F-15.5	15.5	23.5	4.79	-4.44	92.62
60	0601F-16.0	16	24	4.83	-3.63	97.97
61	0601F-16.5	16.5	24.5	4.86	-3.94	95.72
62	0601F-17.0	17	25	3.73	-3.89	95.29
63	0601F-17.5	17.5	25.5	4.41	-3.85	90.13
64	0601F-18.0	18	26	5.35	-5.62	99.46
65	0601F-18.5	18.5	26.5	5.4	-6.57	99.9
66	0601F-19.0	19	27	5.62	-4.5	98.66
67	0601F-20.0	20	28	5.69	-4.66	97.98
68	0604-neg1.2	-1.2	42.8	0.11	-0.53	85.13
69	0604-neg0.5	-0.5	43.5	0.74	-1	98.13
70	0604-neg0.1	-0.1	43.9	0.74	-1.84	96.93
71	0604-0.0	0	44	0.67	-0.17	99.17
72	0604-0.3	0.3	44.3	1.74	0.02	NA
73	0604-0.7	0.7	44.7	1.84	-0.23	91.54
74	0604-1.4	1.4	45.4	2.74	-5.02	93.56
75	0604-1.9	1.9	45.9	2.45	-8.22	92.01
76	0604-2.4	2.4	46.4	2.64	-4.69	88.89
77	0601A-0	0	53	2.56	-3.69	90.88

TA.1	Name	Section Height(m)	Correlated Height (m)	$\delta^{13}C$	$\delta^{18}O$	%carb
78	0601A-0.5	0.5	53.5	2.97	-5.35	90.78
79	0601A-1.18	1.18	54.18	3.63	-8.07	86.76
80	0601A-1.53	1.53	54.53	3.23	-2.4	92.9
81	0601A-1.83	1.83	54.83	3.3	-3.18	95.59
82	0601A-2.4	2.4	55.4	3.12	-2.04	97.18
83	0601A-2.9	2.9	55.9	3.19	-2.82	93.15
84	0601A-3.4	3.4	56.4	3.24	-5.19	90.07
85	0601A-3.5	3.5	56.5	3.32	-2.04	98.49
86	0601A-4.2	4.2	57.2	3.66	-5.23	95.63
87	0601A-4.7	4.7	57.7	3.06	-2.68	99.37
88	0601A-4.9	4.9	57.9	3.15	-1.72	99.41
89	0601A-5.4	5.4	58.4	4.3	-6.59	97.81
90	0601A-5.5	5.5	58.5	3.85	-2.32	93.18
91	0601A-5.6	5.6	58.6	3.3	-5.21	95.79
92	0601A-6.1	6.1	59.1	3.21	-5.08	98.55
93	0601A-6.3	6.3	59.3	3.52	-3.28	99.69
94	0601A-6.8	6.8	59.8	3.59	-2.41	99.71
95	0601A-7.4	7.4	60.4	3.51	-2.86	98.97
96	0601A-7.7	7.7	60.7	3.35	-1.75	96.7
97	0601A-7.9	7.9	60.9	3.98	-4.89	94.17
98	0601B-0	0	54	3.49	-3.86	99.9
99	0601B-1	1	55	3.57	-2.58	98.18
100	0601B-2	2	56	4.01	-2.38	97.73
101	0601B-3	3	57	2.88	-4.54	98.56
102	0601B-4	4	58	3.13	-2.52	99.04
103	0601B-5	5	59	3.25	-6.48	92.98
104	0601B-6	6	60	3.26	-6.86	97.05
105	0601B-7	7	61	3.02	-6.6	96.86
106	0601B-7.1	7.1	61.1	3.37	-4.87	96.47
107	0601B-7.2	7.2	61.2	3.1	-6.08	89.19
108	0601B-7.5	7.5	61.5	3.39	-6.91	98.05
109	0601B-7.9	7.9	61.9	2.99	-6.05	92.9
110	0601B-8.5	8.5	62.5	2.32	-7.48	92.22
111	0601B-8.8	8.8	62.8	3.83	-6.43	99.34
112	0601B-9.6	9.6	63.6	1.96	-2.77	96.49
113	0601B-10.2	10.2	64.2	3.53	-5.71	99.03
114	0601B-10.7	10.7	64.7	1.11	-6.3	98.82
115	0601B-11.8	11.8	65.8	1.39	-5.32	93.88
116	0601B-12.5	12.5	66.5	1.13	-5.28	92.06
117	0601B-13	13	67	1.19	-3.61	82.35
118	0601B-13.7	13.7	67.7	1.59	-3.42	82.82

TA.1	Name	Section Height(m)	Correlated Height (m)	$\delta^{13}C$	$\delta^{18}O$	%carb
119	0601B-14.3	14.3	68.3	1.67	-2.9	305.76
120	0601B-14.8	14.8	68.8	1.01	-4.44	85.63
121	0601B-15	15	69	0.53	-0.83	66.35
122	0601B-15.77	15.77	69.77	-1.07	0.27	87.75
123	0601C-neg3.0	-3	70.3	-4.13	0.2	79.25
124	0601C-neg2.5	-2.5	70.8	-4.43	-0.81	90.12
125	0601C-neg0.6	-0.6	72.8	-3.24	-3.77	94
126	0601C-neg0.5	-0.5	72.9	-4.68	-1.39	95.85
127	0601C-neg0.3	-0.3	73.1	-3.84	-2.52	93.23
128	0601C-0.5	0.5	73.7	-1.58	-7.7	97.54
129	0601C-1.0	1	74.3	-2.17	-4.92	96.05
130	0601C-1.5	1.5	75	-4.13	-0.65	93.09
131	0601C-2.2	2.2	75.6	-1.8	-4.58	88.97
132	0601C-2.8	2.8	76.2	-1.58	-6.32	96.42
133	0601C-3.2	3.2	76.6	-1.4	-6.16	NA
134	0601C-3.7	3.7	77.1	-0.31	-5.94	85.88
135	0601C-4.3	4.3	77.5	-2.15	-3.2	78.09
136	0601C-4.9	4.9	77.9	-0.97	-5.43	99.9
137	0601C-6.5	6.5	79.5	-1.51	-4.26	95.28
138	0601C-7.0	7	80.3	0.93	-6.69	96.28
139	0601C-7.5	7.5	80.8	-0.22	-5.35	95.76
140	0601C-8.0	8	81.4	-0.98	-7.82	96.9
141	0601C-8.4	8.4	81.9	-1.09	-7.79	98.05
142	0601C-9.0	9	82.5	-0.2	-6.24	98.71
143	0601C-9.5	9.5	83.1	-0.68	-6.03	99.31
144	0601C-10.0	10	83.7	0.17	-6.61	96.78
145	0601C-10.5	10.5	84.3	-0.76	-5.24	95.75
146	0601C-11.0	11	84.9	2.39	-4.44	97.89
147	0601C-11.5	11.5	85.6	0.19	-6.54	96.86
148	0601C-14.0	14	88.4	0.05	-7.21	NA
149	0601C-14.5	14.5	88.9	1.17	-7.03	66.77
150	0601C-15.0	15	89.4	1.5	-7.14	85.84
151	0601C-17.0	17	91.5	2.11	-8.85	96.01
152	0601C-18.3	18.3	92.8	1.77	-6.13	95.2
153	0601C-19.6	19.6	94.2	2.93	-6.76	96.88
154	0601C-20.0	20	94.6	-0.46	-7.05	99.01
155	0601C-20.5	20.5	95.1	2.32	-7.19	97.4
156	0601C-25.5	25.5	98.2	3.24	-8.31	97.23
157	0601C-25.9	25.9	98.6	1.89	-9.55	88.13
158	0601C-26.5	26.5	99.2	1.1	-5.33	98.44
159	0601C-26.6	26.6	99.3	-0.52	-5.06	97.16

TA.1	Name	Section Height(m)	Correlated Height (m)	$\delta^{13}C$	$\delta^{18}O$	%carb
160	0601C-27.10	27.1	99.8	2.56	-5.22	96.61
161	0601C-27.6	27.6	100.3	3.17	-5.31	97.91
162	0601C-28.0	28	100.7	2.19	-7.39	99.9
163	0601C-28.5	28.5	101.2	-0.89	-6.34	95.74
164	0601C-29.0	29	101.7	2.83	-6.13	95.03
165	0601C-29.5	29.5	102.2	-1.94	-3.6	94.84
166	0601C-34.0	34	105.93	0.03	-3.05	97.35
167	0601C-34.5	34.5	106.3	0.67	-5.99	94.89
168	0601C-34.8	34.8	73.7	-1.37	-3.94	81.94
169	0601C-35.2	35.2	107.15	1.47	-6.65	64.53
170	0601C-36.5	36.5	108.15	2.23	-9.21	88.59
171	0601C-37.0	37	108.55	-2.64	-4.07	92.73
172	0601C-37.4	37.4	108.9	2.49	-6.92	87.06
173	0601C-38.0	38	109.5	0.56	-5.54	95.82
174	0601C-38.5	38.5	110	1.34	-5.85	96.18
175	0601C-39.0	39	110.4	1.7	-5.11	96.45
176	0601C-39.5	39.5	110.9	1.86	-6.09	97.55
177	0601C-40.0	40	111.4	1.67	-5.46	97.7
178	0601C-40.5	40.5	111.8	0.44	-6.75	80.72
179	0601C-41.0	41	112.35	0.69	-4.76	79.7
180	0601C-41.5	41.5	112.8	-0.66	-6.55	94.72
181	0601C-42.0	42	113.35	-0.25	-4.47	87.2
182	0601C-43.0	43	114.33	1.63	-5.85	96.07
183	0601C-43.5	43.5	115.05	1.31	-6.18	98.68
184	0601C-44.0	44	115.84	1.21	-6.38	95.86
185	0601C-44.5	44.5	116.2	1.46	-7.12	95.87
186	0601C-45.0	45	116.55	1.6	-4.5	98.2
187	0601C-45.5	45.5	116.9	1.74	-4.37	98.89
188	0601C-46.0	46	117.25	1.97	-4.18	99.01
189	0601C-46.5	46.5	117.65	0.59	-2.67	98.44
190	0601C-47.0	47	118.05	1.5	-5.04	99.98
191	0601C-47.3	47.3	118.35	1.25	-3.22	99.98
192	0601C-47.5	47.5	118.55	1.63	-6.92	97.26
193	0601C-48.0	48	119.05	1.1	-3.22	99.03
194	0601C-51.5	51.5	122.55	2.15	-2.25	94.94
195	0601C-52.0	52	123.05	1.32	-6.45	95.79
196	0601C-52.5	52.5	123.55	1.05	-3.58	99.68
197	0601C-53.5	53.5	124.55	-0.46	-3.64	98.26
198	0601C-54.0	54	125.05	0.61	-2.2	97.06
199	0601C-69.0	69	210.5	0.45	-1.99	94.59
200	0601C-69.5	69.5	211	0.12	-2.93	92.68

TA.1	Name	Section Height(m)	Correlated Height (m)	$\delta^{13}C$	$\delta^{18}O$	%carb
201	0601C-70.0	70	211.5	-0.46	-6.51	59.59
202	0601C-70.5	70.5	212	-0.13	-7.86	NA
203	0601C-71.0	71	212.5	0.81	-2.58	96.05
204	0601C-71.5	71.5	213	0.19	-2.09	97.51
205	0601C-72.0	72	213.5	-3.26	-1.84	97.26
206	0601C-72.5	72.5	214	-2.19	-3.39	83.65
207	0601C-73.0	73	214.5	0.32	-7.17	NA
208	0601C-73.5	73.5	215	-2.58	-7.39	56.76
209	0601C-74.1	74.1	215.6	0.4	-7.81	73.52
210	0601C-74.5	74.5	216	-3.01	-3.59	71.01
211	0601C-74.8	74.8	216.3	-1.97	-1.75	76.14
212	0601C-75.3	75.3	216.8	-1.22	-2.07	97.66
213	0601C-76.0	76	217.5	-2.77	-3.5	89.74
214	0601C-76.6	76.6	218.1	1.83	-7.98	54.36
215	0601C-77.0	77	218.5	-0.18	-2.9	63.19
216	0601C-77.5	77.5	219	1.42	-7.47	NA
217	0601C-79.2	79.2	220.7	1.14	-2.33	96.24
218	0601C-80.0	80	221.5	1.04	-6.51	98.67
219	0601C-80.5	80.5	222	0.13	-5.41	99.7
220	0601C-81.5	81.5	223	-2.62	-5.75	98.46
221	0601C-82.0	82	223.5	0.1	-8.18	99.98
222	0601C-82.5	82.5	224	0.62	-6.13	NA
223	0601C-84.0	84	225.5	0.71	-5.12	81.99
224	0602-0.1	0.1	163.1	-0.16	-7.58	51.3
225	0602-0.3	0.3	163.3	-0.15	-7.33	95.45
226	0602-0.9	0.9	163.9	-2.35	-8.2	38.01
227	0602-1.5	1.5	164.5	0.5	-4.38	86.87
228	0602-1.9	1.9	164.9	-0.05	-5.62	86.82
229	0602-3.0	3	166	-0.45	-5.7	93.29
230	0602-4.0	4	167	-0.74	-6.15	95.86
231	0602-4.5	4.5	167.5	-1.35	-10.46	74.87
232	0602-5.0	5	168	-2.04	-7.89	97.95
233	0602-5.5	5.5	168.5	-2.01	-5.64	95.81
234	0602-6.0	6	169	-0.97	-5.01	92.72
235	0602-6.5	6.5	169.5	-3.11	-6.33	NA
236	0602-7.0	7	170	-1.92	-7.91	27.85
237	0602-7.5	7.5	170.5	0.57	-6.96	80.12
238	0602-8.0	8	171	-0.18	-4.11	60.77
239	0602-8.5	8.5	171.5	-0.84	-7.99	NA
240	0602-9.0	9	172	-0.48	-7.24	68.04
241	0602-10.0	10	173	-0.61	-8.72	15.81

TA.1	Name	Section Height(m)	Correlated Height (m)	$\delta^{13}C$	$\delta^{18}O$	%carb
242	0602-10.5	10.5	173.5	-0.66	-5.79	90.48
243	0602-11.0	11	174	-0.41	-5.66	NA
244	0602-11.5	11.5	174.5	-1.07	-7.33	NA
245	0602-12.0	12	175	-0.33	-4.94	94.66
246	0602-12.5	12.5	175.5	-1.18	-7.32	NA
247	0602-13.0	13	176	-0.32	-7.16	90.28
248	0602-13.5	13.5	176.5	-0.11	-7.12	95.42
249	0602-14.0	14	177	-0.33	-6.43	93.49
250	0602-14.5	14.5	177.5	-0.18	-6.79	NA
251	0602-15.0	15	178	-0.7	-7.49	NA
252	0602-15.5	15.5	178.5	-1.1	-7.73	NA
253	0602-15.65	15.65	178.65	0.03	-5.13	NA
254	0602-16.0	16	179	-0.39	-8.3	NA
255	0602-16.35	16.35	179.35	0.17	-3.88	89
256	0602-16.5	16.5	179.5	0.21	-7.55	NA
257	0602-16.67	16.67	179.67	0.33	-5.09	NA
258	0602-17.0	17	180	0.01	-3.81	78.69
259	0602-17.5	17.5	180.5	-1.39	-8.3	NA
260	0602-18.1	18.1	181.1	-0.12	-5.04	NA
261	0602-18.7	18.7	181.7	-0.63	-8.48	NA
262	0602-18.80	18.8	181.8	2.09	-5.11	NA
263	0602-19.1	19.1	182.1	-0.73	-7.85	NA
264	0602-19.70	19.7	182.7	-0.18	-5.69	NA
265	0602-20.47	20.47	183.47	0.3	-5.51	NA
266	0602-20.85	20.85	183.85	1.32	-3.95	NA
267	0602-21.41	21.41	184.41	0.86	-3.27	NA
268	0602-22.00	22	185	0.89	-4.45	NA
269	0602-22.41	22.41	185.41	-0.79	-7.06	NA
270	0602-23.00	23	186	0.49	-4.43	92.68
271	0602-23.15	23.15	186.15	0.71	-4.32	NA
272	0602-23.90	23.9	186.9	0.76	-3.53	NA
273	0602-24.43	24.43	187.43	-0.92	-7.62	NA
274	0602-25.00	25	188	0.55	-4.92	NA
275	0602-25.57	25.57	188.57	0.29	-4.35	97.03
276	0602-25.92	25.92	188.92	-0.44	-6.39	NA
277	0602-26.70	26.7	189.7	-0.31	-7.07	NA
278	0602-27.20	27.2	190.2	-0.27	-6.59	NA
279	0602-27.50	27.5	190.5	-0.65	-7.56	NA
280	0602-28.10	28.1	191.1	-0.14	-6.4	NA
281	0602-28.70	28.7	191.7	-0.85	-7.79	NA
282	0602-29.30	29.3	192.3	-0.62	-7.04	NA

TA.1	Name	Section Height(m)	Correlated Height (m)	$\delta^{13}C$	$\delta^{18}O$	%carb
283	0602-30.20	30.2	193.2	1.05	-3.63	84.12
284	0602-30.72	30.72	193.72	0.2	-5.54	NA
285	0602-31.30	31.3	194.3	1.23	-3.35	96.74
286	0602-31.90	31.9	194.9	1.31	-3.95	NA
287	0602-37.60	37.6	200.6	1.61	-7.76	NA
288	0602-38.20	38.2	201.2	0.56	-8.04	NA
289	0602-38.80	38.8	201.8	0.83	-7.42	NA
290	0602-39.40	39.4	202.4	1.54	-4.9	NA
291	0602-39.90	39.9	202.9	2.31	-7.09	78.32
292	0602-40.35	40.35	203.35	2.36	-7.72	NA
293	0602-40.80	40.8	203.8	1.64	-8.94	NA
294	0602-41.10	41.1	204.1	3.97	-7.15	NA
295	0602-41.65	41.65	204.65	2.58	-7.02	76.19
296	0602-42.30	42.3	205.3	2.7	-6.3	NA
297	0602-42.70	42.7	205.7	-0.07	-9.25	NA
298	0602-42.90	42.9	205.9	1.26	-7.14	NA
299	0602-43.30	43.3	206.3	0.44	-8.44	NA
300	0602-43.40	43.4	206.4	1.99	-5.5	NA
301	0602-43.80	43.8	206.8	3.76	-8.19	NA
302	0602-44.0	44	207	2.93	-8.09	78.62
303	0602-44.20	44.2	207.2	3.79	-7.75	NA
304	0602-44.50	44.5	207.5	2.49	-8.79	NA
305	0602-44.70	44.7	207.7	3.97	-7.2	86.16
306	0602-44.90	44.9	207.9	2.09	-6.24	NA
307	0602-45.0	45	208	2.08	-9.19	NA
308	0602-45.40	45.4	248.4	2.16	-6.04	78.87
309	0602-45.6	45.6	248.6	2.24	-6.46	NA
310	0602-46.0	46	249	1.46	-6.4	NA
311	0602-46.30	46.3	249.3	1.82	-9.33	NA
312	0602-47.00	47	250	1.54	-9.05	NA
313	0602-47.40	47.4	250.4	1.95	-7.99	NA
314	0602-48.10	48.1	251.1	3.43	-8.09	92.98
315	0602-48.8	48.8	251.8	2.88	-9.46	NA
316	0602-49.30	49.3	252.3	1.36	-8.1	NA
317	0602-49.80	49.8	252.8	1.35	-7.52	NA
318	0602-50.26	50.26	253.26	0.56	-7.44	NA
319	0602-50.75	50.75	253.75	0.99	-10.32	NA
320	0602-52.30	52.3	255.3	0.18	-9.03	NA
321	0602-52.80	52.8	255.8	0.27	-7.76	NA
322	0602-53.30	53.3	256.3	0.39	-7.09	NA
323	0602-53.50	53.5	256.5	-0.28	-7.55	94.37

TA.1	Name	Section Height(m)	Correlated Height (m)	$\delta^{13}C$	$\delta^{18}O$	%carb
324	0602-54.00	54	257	0.71	-8.21	99.39
325	0602-54.50	54.5	257.5	0.71	-8.42	NA
326	0602-55.0	55	258	0.66	-6.02	NA
327	0602-55.55	55.55	258.55	-0.25	-6.89	NA
328	0602-56.30	56.3	259.3	-0.15	-7.1	NA
329	0602-56.75	56.75	259.75	-0.09	-6.2	NA
330	0603-0.1	0.1	118.1	-4.81	-5.68	17.27
331	0603-0.5	0.5	118.5	-3.11	-5.6	76.51
332	0603-1.1	1.1	119.1	0.64	-7.5	56.56
333	0603-1.5	1.5	119.5	-1.95	-8.34	21.02
334	0603-2.0	2	120	-7.05	-2.7	37.64
335	0603-2.5	2.5	120.5	0.37	-7.71	64.44
336	0603-3.1	3.1	121.1	-3.52	-9.79	17.81
337	0603-3.3	3.3	121.3	-4.02	-4.32	90.1
338	0603-3.9	3.9	121.9	0.59	-6.03	71.84
339	0603-4.4	4.4	122.4	-5.38	-5.47	22.85
340	0603-5.0	5	123	-0.27	-5.63	64.9
341	0603-5.4	5.4	123.4	-3.68	-8.3	10.78
342	0603-5.8	5.8	123.8	-3.88	-3.84	NA
343	0603-6.1	6.1	124.1	-1.38	-8.82	NA
344	0603-6.4	6.4	124.4	-0.51	-7.72	NA
345	0603-7.3	7.3	125.3	-2.99	-6.24	NA
346	0603-7.9	7.9	125.9	-2.25	-4.96	63.49
347	0603-8.4	8.4	126.4	-2.23	-4.45	NA
348	0603-9	9	127	-1.21	-7.64	NA
349	0603-9.6	9.6	127.6	-2.22	-4.99	NA
350	0603-10.6	10.6	128.6	-0.55	-9.3	NA
351	0603-11.5	11.5	129.5	-1.17	-8.13	NA
352	0603-12.1	12.1	130.1	-0.38	-5.98	NA
353	0603-12.7	12.7	130.7	-5.28	-5.09	NA
354	0603-13.2	13.2	131.2	0.41	-6	70.91
355	0603-13.6	13.6	131.6	-2.03	-6.64	NA
356	0603-14.2	14.2	132.2	-2.8	-9.48	NA
357	0603-14.7	14.7	132.7	-3.39	-9.11	8.7
358	0603-15.2	15.2	133.2	-1.18	-8.18	20.39
359	0603-15.7	15.7	133.7	-1.64	-5.2	NA
360	0603-16.3	16.3	134.3	-3.46	-7.72	12.69
361	0603-16.8	16.8	134.8	0.73	-8.21	59.39
362	0603-17.4	17.4	135.4	-4.57	-9.13	9.6
363	0603-18.4	18.4	136.4	-2.35	-6.86	14.99
364	0603-19.1	19.1	137.1	-0.01	-2.95	97.96

TA.1	Name	Section Height(m)	Correlated Height (m)	$\delta^{13}C$	$\delta^{18}O$	%carb
365	0603-20.1	20.1	138.1	-1.19	-7.76	96.41
366	0605-0.2	0.2	123.2	-1.51	-3.27	NA
367	0605-0.8	0.8	123.8	-3.25	-3.09	62.77
368	0605-1.4	1.4	124.4	0.07	-5.52	NA
369	0605-2	2	125	-6.01	-0.45	NA
370	0605-2.5	2.5	125.5	-4.28	-2.79	NA
371	0605-5.8	5.8	128.8	-0.36	-7.92	33.81
372	0605-6.3	6.3	129.3	0.36	-8.09	NA
373	0605-6.8	6.8	129.8	-1.59	-5.8	17.36
374	0605-7.3	7.3	130.3	-5.68	-1.68	NA
375	0605-7.7	7.7	130.7	-0.25	-7.72	NA
376	0605-8.2	8.2	131.2	0.93	-8.76	NA
377	0605-9.1	9.1	132.1	-0.33	-5.55	NA
378	0605-9.6	9.6	132.6	-5.13	-3.17	NA
379	0605-10.1	10.1	133.1	-0.77	-4.69	67.29
380	0605-10.5	10.5	133.5	-4.14	-4.36	NA
381	0605-11.5	11.5	134.5	-1.93	-5.4	NA
382	0605-12	12	135	-1.01	-7.34	NA
383	0605-12.6	12.6	135.6	-1.02	-3.85	70.02
384	0605-13	13	136	-3.36	-2.57	NA
385	0605-13.6	13.6	136.6	-0.57	-7.97	NA
386	0605-16	16	139	-0.86	-5.84	NA
387	0605-18.3	18.3	141.3	-0.35	-7.12	3.27
388	0605-19.3	19.3	142.3	0.48	-2.14	95.36
389	0605-19.8	19.8	142.8	-2.72	-6.53	98.8
390	0605-20.9	20.9	143.9	0.58	-4.81	74.82
391	0701-0-2	0.2	138.7	-1.21	-7.8	30.36
392	0701-0.9	0.9	139.4	-3.02	-7.33	12.41
393	0701-1.4	1.4	139.9	1.3	-6.11	59.62
394	0701-1.8	1.8	140.3	-3.97	-6.92	23.17
395	0701-2.1	2.1	140.6	-7.75	-0.41	78.95
396	0701-2.5	2.5	141	-0.85	-8.38	97.81
397	0701-2.9	2.9	141.4	-0.58	-8.02	43.49
398	0701-3.4	3.4	141.9	-4	-3.51	34.66
399	0701-3.9	3.9	142.4	0.13	-5.95	77.31
400	0701-4-6	4.6	143.1	-5.03	-2.6	44.07
401	0701-5.3	5.3	143.8	-4.23	-7.2	12.75
402	0701-5.7	5.7	144.2	-5.37	-1.98	73.02
403	0701-6.0	6	144.5	-4.43	-7.09	17.43
404	0701-6.6	6.6	145.1	-5.63	-4.62	30.59
405	0701-7.1	7.1	145.6	-5.53	-6.1	21.28

TA.1	Name	Section Height(m)	Correlated Height (m)	$\delta^{13}C$	$\delta^{18}O$	%carb
406	0701-7.8	7.8	146.3	-4.68	-2.92	38.28
407	0701-8.4	8.4	146.9	-4.64	-5.09	8.19
408	0701-8.9	8.9	147.4	-0.45	-5.97	60.74
409	0701-9.4	9.4	147.9	-5.11	-3.05	19.16
410	0701-9.9	9.9	148.4	-5.51	-2.97	20.88
411	0701-10.4	10.4	148.9	-3.67	-3.61	20.26
412	0701-10.9	10.9	149.4	-4.69	-2.97	80.95
413	0701-11.3	11.3	149.8	-2.47	-5.33	40.92
414	0701-12.3	12.3	150.8	-0.59	-8.85	46.2
415	0701-13.0	13	151.5	-0.21	-6.63	72.32
416	0701-13.5	13.5	152	-2.54	-4.26	53.02
417	0701-14.1	14.1	152.6	-0.1	-5.58	65.7
418	0701-14.3	14.3	152.8	-0.76	-5.63	NA
419	0701-14.5	14.5	153	-0.97	-4.39	94.88
420	0701-14.9	14.9	153.4	-0.55	-3.31	94.38
421	0701-15.5	15.5	154	0.21	-5.82	70.39
422	0701-15.9	15.9	154.4	-5.04	-4.58	20.2
423	0701-16.4	16.4	154.9	0.36	-5.22	NA
424	0701-17.3	17.3	155.8	0.53	-6.14	57.46
425	0701-17.6	17.6	156.1	0.22	-7.31	53.02
426	0701-18.2	18.2	156.7	-0.96	-7.79	96.62
427	0701-18.7	18.7	157.2	-1.1	-6.22	NA
428	0701-19.3	19.3	157.8	-0.62	-5.28	97.74
429	0701-19.8	19.8	158.3	-2.79	-4.48	97.07
430	0701-20.0	20	158.5	-0.27	-5.31	96.41
431	0701B-1.15	1.15	202.65	0.86	-7.97	NA
432	0701B-1-80	1.8	203.3	-3.87	-10	NA
433	0701B-2.15	2.15	203.65	-0.06	-6.26	NA
434	0701B-2.5	2.5	204	0.44	-5.15	69.2
435	0701B-3.35	3.35	204.85	0.75	-6.93	58.74
436	0701B-3.75	3.75	205.25	1.77	-4.56	90.03
437	0701B-4.25	4.25	205.75	0.38	-4.55	85.71
438	0701B-5.5	5.5	207	3.08	-7.54	86.48
439	0701B-6.25	6.25	207.75	0.52	-6.57	96.02
440	0701B-6.55	6.55	208.05	2.18	-8.51	80.34
441	0701B-8.7	8.7	210.2	0.74	-5.32	88.69
442	0701B-7.55	7.55	209.05	3.17	-8.38	68.62
443	0701B-8.1	8.1	209.6	3.47	-7.82	71.3
444	0701B-9.3	9.3	210.8	1.75	-7.13	NA
445	0701B-9.6	9.6	211.1	-1.01	-8.5	90.38
446	0701B-9.9	9.9	211.4	-0.08	-6.17	NA

TA.1	Name	Section Height(m)	Correlated Height (m)	$\delta^{13}C$	$\delta^{18}O$	%carb
447	0701B-10.25	10.25	211.75	-1.19	-9.21	79.86
448	0701B-10.6	10.6	212.1	-2.28	-9.63	78.25
449	0701B-11.0	11	212.5	-0.27	-8.32	82.59
450	0701B-11.3	11.3	212.8	-0.57	-8.49	86.89
451	0701B-12.0	12	213.5	1.28	-7.74	92.9
452	0701B-12.2	12.2	213.7	1.35	-6.65	97.89
453	0701B-12.5	12.5	214	1.89	-7.65	93.44
454	0701B-12.9	12.9	214.4	0.65	-5.64	97.74
455	0701B-13.0	13	214.5	1.59	-7.28	NA
456	0701B-13.6	13.6	215.1	-0.12	-6.87	98.11
457	0701B-13.9	13.9	215.4	1.38	-8.08	92.41
458	0701B-14.1	14.1	215.6	1.44	-9.66	96.32
459	0701B-14.3	14.3	215.8	0.85	-6	81.38
460	0701B-14.6	14.6	216.1	-1.55	-9.27	97.69
461	0701B-14.9	14.9	216.4	1.54	-7.12	94.84
462	0701B-15.15	15.15	216.65	2.66	-7.93	NA
463	0701B-15.5	15.5	217	3.07	-6.85	95.64
464	0701B-16.1	16.1	217.6	1.96	-8.28	98.31
465	0701B-16.9	16.9	218.4	2.1	-7.31	98.72
466	0701B-17.5	17.5	219	2.19	-7.29	94.48
467	0701B-18.0	18	219.5	3.09	-7.77	94.7
468	0703-0.1	0.1	190.1	0.3	-7.55	83.67
469	0703-1.1	1.1	191.1	0.76	-3.22	95.22
470	0703-1.75	1.75	191.75	-0.52	-5.55	91.62
471	0703-2.45	2.45	192.45	1.15	-6.55	91.08
472	0703-2.95	2.95	192.95	1.76	-6.47	93.56
473	0703-3.45	3.45	193.45	1	-9.61	89
474	0703-3.7	3.7	193.7	-0.35	-7.93	96.08
475	0703-4.35	4.35	194.35	-0.97	-7.42	97.41
476	0703-5.45	5.45	195.45	-0.68	-8.65	95.58
477	0703-5.6	5.6	195.6	-0.47	-8.83	98.57
478	0703-6.55	6.55	196.55	-0.51	-7.9	98.18
479	0703-7.1	7.1	197.1	-0.79	-7.99	97.39
480	0703-7.95	7.95	197.95	-0.71	-8.33	98.01
481	0703-8.6	8.6	198.6	-0.54	-7.17	98.48
482	0703-9.1	9.1	199.1	-0.03	-7.54	90.14
483	0702-0.35	0.35	215.35	-0.62	-4.45	97.28
484	0702-0.91	0.91	215.91	-0.63	-4.1	93.84
485	0702-1.42	1.42	216.42	-0.99	-2.62	95.58
486	0702-2.20	2.2	217.2	-1.29	-0.66	97.57
487	0702-2.95	2.95	217.95	-1.1	-3.73	NA

TA.1	Name	Section Height(m)	Correlated Height (m)	$\delta^{13}C$	$\delta^{18}O$	%carb
488	0702-3.90	3.9	218.9	-1.27	-3.76	NA
489	0702-4.55	4.55	219.55	-1.27	-3.73	NA
490	0702-5.30	5.3	220.3	-1.13	-3.59	NA
491	0702-5.80	5.8	220.8	-1.33	-3.48	95.83
492	0702-6.2	6.2	221.2	-1.34	-3.56	NA
493	0702-6.60	6.6	221.6	-1.62	-2.37	99.9
494	0702-7.25	7.25	222.25	-1.45	-3.08	94.68
495	0702-7.7	7.7	222.7	-1.66	-2.98	96.56
496	0702-8.0	8	223	-1.64	-2.41	94.29
497	0702-8.50	8.5	223.5	-1.7	-3.12	96.42
498	0702-9.00	9	224	-1.83	-2.93	96.75
499	0702-9.70	9.7	224.7	-1.74	-2.91	97.27
500	0702-10.30	10.3	225.3	-1.9	-3.55	98.86
501	0702-10.65	10.65	225.65	-2.31	-1.08	99.13
502	0702-11.0	11	226	-1.95	-3.02	96.21
503	0702-11.70	11.7	226.7	-2.24	-3.65	98.01
504	0702-12.4	12.4	227.4	-1.72	-1.97	98.17
505	0702-12.9	12.9	227.9	-1.75	-3.12	92.18
506	0702-13.5	13.5	228.5	-1.62	-3.11	91.25
507	0702-14.1	14.1	229.1	-1.83	-2.11	99.86
508	0702-15.0	15	230	-1.28	-3.27	95.12
509	0702-15.5	15.5	230.5	-1.35	-3.1	92.03
510	0702-16.0	16	231	-1.43	-3.21	92
511	0702-17.0	17	232	-1.55	-3.07	99.9
512	0702-17.5	17.5	232.5	-1.66	-2.91	NA
513	0702-16.2	16.2	231.2	-1.59	-3.49	NA
514	0702-18.1	18.1	233.1	-1.63	-3.32	NA
515	0702-18.65	18.65	233.65	-1.95	-2.6	93.13
516	0702-19.1	19.1	234.1	-1.8	-2.15	97.94
517	0702-19.7	19.7	234.7	-2.15	-3.54	87.95
518	0702-20.5	20.5	235.5	-2.04	-3.13	94.64
519	0702-21.0	21	236	-2.13	-3.39	93.43
520	0702-21.9	21.9	236.9	-2.29	-2.62	96.36
521	0702-22.4	22.4	237.4	-1.93	-3.13	NA
522	0702-23.4	23.4	238.4	-2.05	-2.62	92.49
523	0702-24.1	24.1	239.1	-1.83	-3.14	95.68
524	0703-0.0	0	210	-0.1	-7.86	95.11
525	0703-0.10A	0.1	210.1	-0.36	-7.92	98.63
526	0703-0.10B	0.1	210.1	-0.19	-8.56	NA
527	0703-0.60	0.6	210.6	-0.17	-8.95	99.9
528	0703-1.50A	1.5	211.5	-0.13	-9.04	99.85

TA.1	Name	Section Height(m)	Correlated Height (m)	$\delta^{13}C$	$\delta^{18}O$	%carb
529	0703-1.50B	1.5	211.5	-0.14	-8.87	99.74
530	0703-2.00	2	212	-0.16	-9.23	99.81
531	0703-3.90	3.9	213.9	-0.21	-7.02	99.94
532	0703-4.50	4.5	214.5	-0.16	-8.33	99.94
533	0703-5.50	5.5	215.5	-0.32	-7.97	99.83
534	0703-6.20	6.2	216.2	0.1	-9.15	99.7
535	0703-7.00	7	217	-0.06	-8.3	99.94
536	0703-7.50	7.5	217.5	-0.18	-8.86	99.89
537	0703-8.0A	8	218	-0.04	-8.8	99.89
538	0703-8.0B	8	218	-0.04	-8.26	NA
539	0703-8.60	8.6	218.6	-0.21	-8.07	99.94
540	0703-9.60	9.6	219.6	-0.02	-8.94	99.83
541	0703-10.10	10.1	220.1	-0.21	-8.31	99.94
542	0703-11.80	11.8	221.8	-0.06	-8.5	99.93
543	0703-12.55A	12.55	222.55	-0.15	-7.86	99.94
544	0703-12-55B	12.55	222.55	-0.04	-7.36	NA
545	0703-12.70	12.7	222.7	-0.03	-8.08	99.82
546	0703-13.00	13	223	0.26	-7.19	99.54
547	0703-13.2A	13.2	223.2	0.31	-7.15	NA
548	0703-13.2B	13.2	223.2	0.14	-8.3	NA
549	0703-13.70	13.7	223.7	0.49	-7.64	99.94
550	0703-14.40	14.4	224.4	-0.15	-7.59	99.94
551	0703-15.2	15.2	225.2	-0.03	-7.49	99.93
552	0703-16.75	16.75	226.75	-0.24	-7.53	99.93
553	0703-17.10	17.1	227.1	-0.15	-6.8	99.93
554	0703-17.75	17.75	227.75	0.11	-9.01	99.88
555	0703-19.0	19	229	0.07	-7.73	99.93
556	0703-19.50	19.5	229.5	0.05	-8.14	99.94
557	0703-20.00	20	230	-0.14	-7.3	99.85
558	0703-21.00	21	231	-0.11	-7.69	99.93
559	0703-22.00	22	232	-0.04	-7.03	99.93
560	0703-23.00	23	233	-0.16	-7.97	99.92
561	0703-24.00.A1	24	234	-0.13	-7.52	99.93
562	0703-24.00.A2	24	234	-0.11	-7.72	NA
563	0703-24.00.B	24	234	-0.13	-8	NA
564	0703-25.00	25	235	-0.22	-8.2	99.68
565	0703-25.70	25.7	235.7	-0.04	-6.98	99.93
566	0703-26.3	26.3	236.3	-0.15	-8.87	99.92
567	0703-28.0	28	238	0.15	-7.56	97.21

TA.1	Name	Section Height(m)	Correlated Height (m)	$\delta^{13}C$	$\delta^{18}O$	%carb
568	0703-29.0	29	239	0.17	-7.31	99.93
569	0703-30.10	30.1	240.1	0.8	-8.28	99.93
570	0703-31.50	31.5	241.5	1.06	-6.96	99.55
571	0703-32.70	32.7	242.7	0.32	-7.26	99.73
572	0703-33.30	33.3	243.3	0.39	-7.55	NA
573	0703-34.0	34	244	0.01	-6.59	99.77
574	0703-34.50	34.5	244.5	0.68	-7.79	99.7
575	0703-35.50	35.5	245.5	0.54	-8.05	NA
576	0703-36.1	36.1	246.1	0.04	-8.76	99.9
577	0703-36.80	36.8	246.8	0.14	-8.17	99.82
578	0703-37.80	37.8	247.8	-0.02	-8.53	99.86
579	0703-38.50	38.5	248.5	-0.13	-7.88	99.93
580	0703-38.6	38.6	248.6	0.08	-8.38	99.78
581	0703-39.0	39	249	0.08	-8.08	NA
582	0703-39.4	39.4	249.4	0.23	-8.72	99.9
583	0703-40.15	40.15	250.15	0.73	-7.23	99.68
584	0703-41.20	41.2	251.2	0.1	-7.4	96.1
585	0703-42.1	42.1	252.1	-0.01	-7.42	99.84
586	0703-43.0	43	253	0.29	-8.11	99.69
587	0703-43.6	43.6	253.6	0.11	-7.3	99.79
588	0703-43.8	43.8	253.8	0.57	-7.28	99.7
589	0703-44.6	44.6	254.6	-0.19	-7.54	99.87
590	0703-46.2	46.2	256.2	0.28	-7.35	98.57
591	0703-47.2	47.2	257.2	0.35	-7.92	98.54
592	0703-48.1	48.1	258.1	0.43	-7.15	97.37
593	0703-48.7	48.7	258.7	0.56	-7.84	99.22
594	0703-49.0	49	259	0.16	-8.14	99.5
595	0703-49.8	49.8	259.8	0.29	-7.73	97.25
596	0703-51.1	51.1	261.1	0.34	-7.92	95.63
597	0703-51.8	51.8	261.8	0.5	-7.95	NA
598	0703-52.5	52.5	262.5	0.16	-7.65	NA
599	0703-52.8	52.8	262.8	0.34	-7.61	NA
600	0703-53.1	53.1	263.1	-0.03	-7	NA
601	0703-54.0	54	264	0	-7.88	97.07
602	0703-54.8	54.8	264.8	0.11	-6.6	NA
603	0703-55.5	55.5	265.5	-0.17	-7.53	98.28
604	0703-56.2	56.2	266.2	-0.1	-8.23	99.16
605	0703-56.65	56.65	266.65	-0.01	-6.36	NA
606	0703-57.1	57.1	267.1	0.25	-6.89	NA
607	0703-57.35	57.35	267.35	-0.29	-7.35	97.73
608	0703-58.0	58	268	-0.35	-6.11	97.89

TA.1	Name	Section Height(m)	Correlated Height (m)	$\delta^{13}C$	$\delta^{18}O$	%carb
609	0703-58.35	58.35	268.35	-1.57	-1.13	NA
610	0703-59.1	59.1	269.1	-0.76	-2.27	NA
611	0703-59.85	59.85	269.85	-1.59	-1.93	NA
612	0703-60.20	60.2	270.2	-1.36	0.04	NA
613	0703-60.7	60.7	270.7	-1.07	-1.4	NA
614	0703-61.4A	61.4	271.4	-1.46	-0.31	NA
615	0703-61.4B	61.4	271.4	-1.14	-1.46	NA
616	0710-0.5	0.5	264.1	-0.04	-4.71	NA
617	0710-1	1	264.6	0.23	-4.99	NA
618	0710-1.5	1.5	265.1	0.12	-4.53	NA
619	0710-2	2	265.6	0.4	-3.84	NA
620	0710-2.5A	2.5	266.1	0	-4.03	NA
621	0710-2.5B	2.5	266.1	-0.07	-5.32	NA
622	0710-3	3	266.6	0.34	-4.22	NA
623	0710-3.5	3.5	267.1	0.11	-4.27	NA
624	0710-4	4	267.6	-0.79	-5.16	NA
625	0710-4.5	4.5	268.1	-0.5	-5.13	NA
626	0710-5	5	268.6	-0.18	-4.23	NA
627	0710-5.5	5.5	269.1	-0.46	-4.79	NA
628	0710-6	6	269.6	-0.83	-6.09	NA
629	0710-6.5	6.5	270.1	-0.44	-5.25	NA
630	0710-7	7	270.6	-0.78	-6.94	NA
631	0710-7.5	7.5	271.1	-0.61	-7.38	NA
632	0710-8	8	271.6	-0.57	-6.6	NA
633	0710-8.5	8.5	272.1	-0.45	-6.64	NA
634	0710-9	9	272.6	-0.83	-7.04	NA
635	0710-9.5	9.5	273.1	-0.62	-6.85	NA
636	0710-10	10	273.6	0.35	-3.99	NA
637	0710-10.5A	10.5	274.1	-0.11	-3.18	NA
638	0710-10.5B	10.5	274.1	-0.4	-3.78	NA
639	0710-11	11	274.6	-0.5	-3.4	NA
640	0710-11.5	11.5	275.1	-0.51	-4.21	NA
641	0710-12	12	275.6	-1.17	-6.95	NA
642	0710-12.5	12.5	276.1	-1.28	-7.08	NA
643	0710-13	13	276.6	-1.23	-6.98	NA
644	0710-13.5	13.5	277.1	-1.63	-7.39	NA
645	0710-14	14	277.6	-1.07	-7.01	NA
646	0710-15	15	278.6	-1.84	-5.78	NA
647	0710-15.5	15.5	279.1	-1.03	-3.77	NA
648	0710-16	16	279.6	-1.46	-4.53	NA
649	0710-16.35	16.35	279.95	-0.9	-3.78	NA

TA.1	Name	Section Height(m)	Correlated Height (m)	$\delta^{13}C$	$\delta^{18}O$	%carb
650	0901-0.1	0.1	254.3	-1.87	-2.09	93.39
651	0901-0.5	0.5	254.7	-1.87	-3.4	85.17
652	0901-1.0	1	255.2	-1.96	-3.38	85.85
653	0901-1.5	1.5	255.7	-1.71	-3.33	95.79
654	0901-2.3	2.3	256.5	-1.41	-3.26	89.33
655	0901-4.3	4.3	258.5	-1.75	-2.28	74.87
656	0901-4.8	4.8	259	-1.99	-2.91	71.12
657	0901-5.1	5.1	259.3	-2.07	-2.14	75.51
658	0901-6.2	6.2	260.4	-1.9	-2.53	95.11
659	0901-6.7	6.7	260.9	-1.36	-2.99	97.92
660	0901-7.3	7.3	261.5	-1.12	-2.61	97.72
661	0901-7.8	7.8	262	-1.02	-2.77	99.44
662	0901B-0.0	0	263.7	-1.83	-2.06	93.01
663	0901B-0.5	0.5	264.2	-1.97	-1.74	87.88
664	0901B-1.0	1	264.7	-1.75	-2.38	78.01
665	0901B-1.3	1.3	265	-0.84	-3.43	99.19
666	0901B-1.5	1.5	265.2	-2.03	-1.89	NA
667	0901B-1.8	1.8	265.5	-1.55	-2.01	82.95
668	0901B-2.3	2.3	266	-1.88	-1.52	91.51
669	0901B-2.9	2.9	266.6	-2.15	-4.32	93.43
670	0901B-3.2	3.2	266.9	-1.52	-1.98	72.78
671	0901B-8.3	8.3	272	-1.98	-3.02	94.07
672	0901B-8.9	8.9	272.6	-1.32	-3.77	87.89
673	0901B-9.5	9.5	273.2	-1.15	-3.37	83.28
674	0901B-10.8A	10.8	274.5	-1.05	-4.52	89.47
675	0901B-10.8B	10.8	274.5	-1.04	-4.4	NA
676	0901B-11.3A	11.3	275	-1.07	-3.57	98.64
677	0901B-11.3B	11.3	275	-1.13	-4.24	NA
678	0901B-11.8	11.8	275.5	-0.89	-4.42	99.05
679	0901B-12.2	12.2	275.9	-1.38	-4.03	99.72
680	0901B-12.7	12.7	276.4	-1.9	-4.86	99.44
681	0901B-13.2	13.2	276.9	-1.31	-3.92	98.43
682	0901B-13.9	13.9	277.6	-0.09	-2.54	97.32
683	0901B-14.3	14.3	278	-0.65	-3.69	70.4
684	0901B-14.9	14.9	278.6	-2.15	-7.26	98.87
685	0901B-15.4	15.4	279.1	-2.29	-7.05	99.9
686	0901B-15.9	15.9	279.6	-1.31	-6.83	NA
687	0901B-16.3	16.3	280	-1.52	-7.77	99.62
688	0901B-17.5	17.5	281.2	-1.66	-7.45	99.9
689	1001-1	0	220	0.8	-1.19	99.9
690	1001-2	0.9	220.9	0.14	-2.89	99.9

TA.1	Name	Section Height(m)	Correlated Height (m)	$\delta^{13}C$	$\delta^{18}O$	%carb
691	1001-3	1.6	221.6	0.33	-3.55	99.9
692	1001-5	3.6	223.6	0.45	-3.26	99.9
693	1001-6	4.8	224.8	0.39	-3.21	99.9
694	1001-7	6.4	226.4	0.09	-1.34	99.9
695	1001-9	8.6	228.6	-0.08	-3.43	99.9
696	1001-12	9.5	229.5	0.32	-3.22	99.9
697	1001-21	17.5	237.5	-0.28	-1.94	99.28
698	1001-22	19	239	-0.03	-3.41	99.9
699	1001-23	19.7	239.7	-1.35	-2.54	99.7
700	1001-24	21.1	241.1	-0.6	-3.3	99.9
701	1001-25	21.6	241.6	0.12	-2.27	99.9
702	1001-26	23	243	0.11	-5.38	99.9
703	1001-27	25.1	245.1	0.11	-2.75	98.51
704	1001-28	27.9	247.9	-0.32	-4.46	99.38
705	1001-29	29.54	249.54	-0.21	-4.68	99.9
706	1001-30	30.6	250.6	-0.59	-6.92	99.72
707	1001-31	31.7	251.7	-0.78	-6.53	99.9
708	1001-32	33.4	253.4	-0.41	-5.82	99.9
709	1001-33	35	255	-0.46	-3.35	99.9
710	1001-34	36.5	256.5	-1.09	-1.82	97.75
711	1001-35	41.8	261.8	-0.79	-5.7	99.71
712	1001-37	43.8	263.8	-0.53	-3.8	99.6
713	1001-38	44.64	264.64	-0.5	-0.79	99.13
714	1001-40	47	267	-0.25	-1.68	99.64
715	1001-42	48.21	268.21	-0.38	-6.06	99.9
716	1001-43	51.5	271.5	-0.28	-4.4	99.9
717	1001-45	52.5	272.5	-0.39	-2.61	99.9
718	1001-47	53.25	273.25	-0.22	-3.12	99.41
719	1001-48	53.5	273.5	0.76	3.88	99.69
720	1002-1	0.4	371.4	-2.12	-6.74	27.63
721	1002-5	4.7	375.7	-3.65	-9.93	28.47
722	1002-11	11	382	-0.55	-7.03	50
723	1002-2	1.75	372.75	-4.87	-6.53	65.89
724	1002-3	2.7	373.7	-2.52	-8.35	23.81
725	1002-4	3.5	374.5	-3.43	-6.13	63.9
726	1002-6	6.25	377.25	-3.23	-6.32	37.78
727	1002-7	7	378	-2.77	-6.79	44.95
728	1002-8	8.2	379.2	-2.83	-6.89	47.16
729	1002-9	9.2	380.2	-2.77	-6.9	53.57
730	1002-10	10.6	381.6	-2.12	-5.3	42.36
731	1002-12	10.9	381.9	-0.32	-6.87	55.76

TA.1	Name	Section Height(m)	Correlated Height (m)	$\delta^{13}C$	$\delta^{18}O$	%carb
732	1002-13	15.35	386.35	1.17	-5.17	71.2
733	1002-14	16.7	387.7	1.6	-5.24	69.57
734	1002-15	17.6	388.6	3.38	-5.51	71.67
735	1002-16	18.5	389.5	3.36	-5.87	71.29
736	1002-17	19.3	390.3	4.14	-5.14	76.36
737	1002-18	21	392	1.44	-6.62	72
738	1002-19	22.3	393.3	1.88	-4.79	86.79
739	1002-20	23.3	394.3	-0.3	-5.75	79.14
740	1002-21	25.5	396.5	2.97	-6.14	64.89
741	1002-22A	26.3	397.3	3.58	-5.52	72.65
742	1002-22B	26.3	397.3	3.31	-5.16	NA
743	1002-23	27.2	398.2	0.84	-6.04	77.37
744	1002-24	28.2	399.2	3.13	-5.51	66.31
745	1002-25	30.2	401.2	0.18	-7.67	66.23
746	1002-26	31	402	2.84	-5.43	57.29
747	1002-27	32	403	1.24	-7.51	41.38
748	1002-28	33	404	1.2	-7.84	NA
749	1002-29	33.6	404.6	0.14	-9.03	59.16
750	1002-30	34.1	405.1	0.67	-8.23	65.07
751	1002-31	35.1	406.1	0.44	-5.63	65.37
752	1002-32A	35.3	406.3	1.32	-6.28	89.58
753	1002-32B	35.3	406.3	1.13	-5.75	NA
754	1002-33	35.8	406.8	2.87	-5.42	79.17
755	1002-34	36.8	407.8	2.93	-5.63	75.69
756	1002-35A	36.5	407.5	2.63	-5.48	98.14
757	1002-35B	37.7	408.7	2.86	-5.52	NA
758	1002-36	38	409	4.39	-4.85	80.21
759	1002-37	39	410	3.58	-4.86	85
760	1003-1	4.2	250.2	-0.84	-3.89	NA
761	1003-2	8.7	254.7	-0.97	-4.09	NA
762	1003-3	16.28	262.28	-1.28	-4.6	NA
763	1003-4	23.18	269.18	-1	-3.68	NA
764	1003-5	24.33	270.33	-1.06	-2.93	NA
765	1004-1051	1	176.9	0.28	-2.34	72.38
766	1004-1052	2.3	178.2	0.15	-1.95	79.05
767	1004-1053	3.6	179.5	-0.96	-2.62	90.97
768	1004-1054	4.77	180.67	0.68	-2.12	95.9
769	1004-1055	6.2	182.1	0.31	-2.2	94.23
770	1004-1056	8.4	184.3	0.4	-3.94	94.67
771	1004-1059	15.23	191.13	-1.17	-2.7	93.01
772	1004-1060	17.3	193.2	-1.54	-4.11	89.59

TA.1	Name	Section Height(m)	Correlated Height (m)	$\delta^{13}C$	$\delta^{18}O$	%carb
773	1004-1061	21.1	197	0.78	-7.28	92.72
774	1004-1062	23.13	199.03	0.87	-8.29	96.65
775	1004-1063	38	213.9	0.89	-7.39	99.68
776	1004-1065	44	219.9	0.58	-6.3	99.6
777	1004-1066B	49.1	225	0.35	-3.65	99.72
778	1004-1067	56	231.9	0.07	-5.62	99.9
779	1004-1068	60	235.9	0.26	-4.52	99.63
780	1004-1070	66	241.9	0.16	-6.81	99.66
781	1004-1071	69	244.9	-0.29	-4.68	99.38
782	1004-1073	72	247.9	-0.42	-3.53	99.41
783	1004-1074	75.1	251	-0.03	-5.49	99.9
784	1004-1076	77.1	253	0.09	-7.24	99.9
785	1004-1077	78.1	254	-0.12	-4.77	99.64
786	1004-1078	80.1	256	-0.74	-1.65	99.7
787	1004-1080	82.6	258.5	-0.74	-1.31	99.9
788	1004-1082	84.1	260	-0.66	-5.47	99.9
789	1004-1083	86.1	262	-0.6	-3.71	99.9
790	1004-1085	88.1	264	-0.7	-4.51	99.66
791	1004-1086	91.1	267	-0.73	-3.41	99.67
792	1008B-1001	2.2	271.2	-1.92	-3.3	NA
793	1008B-1002	1.9	270.9	-1.81	-3.83	NA
794	1008B-1003	2.85	271.9	-1.94	-3.19	NA
795	1008B-1005	3.6	272.6	-3.6	-6.31	NA
796	1008B-1008	11.5	280.5	-3.71	-8	NA
797	1010-1005	50.75	198.75	1.77	-9.36	NA
798	1010-1006	50.75	198.75	-0.56	-4.69	NA
799	1010-1008	38.6	186.6	-3.6	-4.42	NA
800	1010-1009	38.6	186.6	1.02	-7.35	NA
801	1010-1010	8.5	156.5	-0.38	-5.01	NA
802	1010-1012	8.5	156.5	-0.23	-6.6	NA
803	1010-1013	8.5	156.5	-0.35	-6.7	NA
804	1011-1005	2.4	226.4	-0.05	-6.43	NA
805	1011-1006	5.3	229.3	0.27	-6.21	NA
806	1011-1007	10.3	234.3	0.1	-5.77	NA
807	1011-1008	5.3	229.3	0.07	-6.4	NA
808	1011-1009	27	251	-0.18	-5.38	NA
809	1013-1001-2	0.75	266.75	-1.88	-2.83	NA
810	1013-1004	1.8	267.8	-1.63	-2.54	NA
811	1013-1005	3.1	269.1	-2.15	-3.56	NA
812	1013-1006-7	4.2	270.2	-2.73	-1.7	NA
813	1013-1008-9	5.3	271.3	-2.7	-1.9	NA

TA.1	Name	Section Height(m)	Correlated Height (m)	$\delta^{13}C$	$\delta^{18}O$	%carb
814	1013-1010-1	6	272	-1.95	-3.82	NA
815	1013-1012-4	8	274	-2.13	-3.68	NA
816	1013-1015	12.2	278.2	-2.17	-3.62	NA

Table A.2. Carbonate data, South China. Isotopic data is given as the average of replicates, if applicable.

TA.2	Formation	Height (m)	$\delta^{13}C$	$\delta^{18}O$	Replicates
1	Algal Dol.	12	1.89	-1.63	3
2	Algal Dol.	23	1.45	-4.10	3
3	Algal Dol.	28	1.95	-4.43	3
4	Algal Dol.	32	1.60	-3.98	3
5	Algal Dol.	35.2	1.38	-6.58	3
6	Algal Dol.	40	1.07	-3.76	3
7	Algal Dol.	43.3	1.15	-3.40	3
8	Algal Dol.	51	1.23	-3.15	3
9	Algal Dol.	55.6	2.21	-0.06	2
10	Algal Dol.	64	2.30	0.21	3
11	Algal Dol.	74.4	2.51	-0.52	3
12	Algal Dol.	74.5	1.92	-2.35	3
13	Algal Dol.	79.5	2.34	-2.24	1
14	Algal Dol.	84	3.15	0.91	1
15	Algal Dol.	89.8	3.04	-0.39	1
16	Algal Dol.	95	3.06	-2.19	1
17	Algal Dol.	96	3.23	-0.28	1
18	Algal Dol.	112	3.41	-0.95	1
19	Algal Dol.	117	2.89	-0.93	1
20	Algal Dol.	122	2.22	-2.52	1
21	Algal Dol.	126	3.80	-2.84	1
22	Algal Dol.	129	5.00	-2.45	1
23	Algal Dol.	132.5	5.50	-1.67	1
24	Algal Dol.	134.2	3.57	-5.06	1
25	Algal Dol.	138	3.63	0.34	1
26	Algal Dol.	140.4	3.55	-0.81	1
27	Algal Dol.	142	3.41	-0.77	1
28	Algal Dol.	147	3.58	-0.03	1
29	Algal Dol.	151.5	3.33	-0.72	1
30	Algal Dol.	156.6	3.09	-2.34	1
31	Algal Dol.	161.1	2.48	-1.06	2
32	Algal Dol.	166	1.69	-1.05	1
33	Algal Dol.	170.5	1.20	-2.74	1

TA.2	Formation	Height (m)	$\delta^{13}C$	$\delta^{18}O$	Replicates
34	Algal Dol.	173.4	0.69	-2.22	1
35	Algal Dol.	178	0.51	-3.31	1
36	Algal Dol.	182.1	1.01	-1.89	1
37	Algal Dol.	187	0.40	-0.51	1
38	Algal Dol.	191.5	0.73	-2.09	1
39	Algal Dol.	195.4	0.60	-0.76	1
40	Algal Dol.	199	0.60	-0.88	1
41	Algal Dol.	200.7	0.51	-1.77	1
42	Gaojiashan	211	0.50	0.42	1
43	Gaojiashan	214	0.24	-3.77	1
44	Gaojiashan	214.5	0.10	-3.58	3
45	Gaojiashan	214.5	0.08	-2.94	3
46	Gaojiashan	217	0.50	-5.69	3
47	Gaojiashan	219	0.36	-7.08	3
48	Gaojiashan	221.4	-0.25	-4.57	3
49	Gaojiashan	221.5	0.65	-4.76	3
50	Gaojiashan	225	1.02	-5.35	3
51	Gaojiashan	226.9	0.41	-4.41	3
52	Gaojiashan	227.3	0.98	-4.77	3
53	Gaojiashan	229	1.95	-4.70	3
54	Gaojiashan	231.3	1.76	-4.55	3
55	Gaojiashan	232.6	3.23	-5.49	3
56	Gaojiashan	237.8	1.51	-5.73	3
57	Gaojiashan	241.3	5.10	-4.47	3
58	Gaojiashan	242.7	5.30	-5.09	3
59	Gaojiashan	244	4.83	-4.65	3
60	Gaojiashan	246	6.05	-4.83	3
61	Gaojiashan	248.1	5.74	-4.81	3
62	Gaojiashan	250	5.19	-4.85	3
63	Gaojiashan	252	4.33	-5.60	3
64	Gaojiashan	253.8	3.39	-3.77	3
65	Gaojiashan	253.8	2.99	-3.53	3
66	Gaojiashan	253.8	3.01	-3.96	3
67	Gaojiashan	255.5	1.57	-7.19	3
68	Gaojiashan	256.8	0.72	-7.02	3
69	Gaojiashan	260.9	2.44	-0.41	1
70	Gaojiashan	260.9	2.24	-1.45	2
71	Beiwan	265.5	2.36	-1.10	2
72	Beiwan	269	1.79	-1.50	2
73	Beiwan	271	2.06	-0.94	1
74	Beiwan	273.2	1.70	-4.80	2

TA.2	Formation	Height (m)	$\delta^{13}C$	$\delta^{18}O$	Replicates
75	Beiwan	274	1.84	-2.59	1
76	Beiwan	276	0.94	-2.81	2
77	Beiwan	278.7	2.15	-4.86	1
78	Beiwan	281.1	2.29	-1.95	2
79	Beiwan	284.4	0.93	-2.46	1
80	Beiwan	287	2.00	-1.94	2
81	Beiwan	290	0.94	-4.67	1
82	Beiwan	293	1.18	-1.57	2
83	Beiwan	296.2	2.31	-6.52	2
84	Beiwan	299	1.17	-2.38	2
85	Beiwan	302	1.15	-4.08	2
86	Beiwan	304	2.13	-2.18	1
87	Beiwan	305	2.73	-2.76	2
88	Beiwan	307.7	1.83	-1.19	2
89	Beiwan	311.2	1.54	-2.58	1
90	Beiwan	313.5	1.46	-4.07	2
91	Beiwan	325.5	1.85	-4.50	2
92	Beiwan	328	1.96	-4.73	1
93	Beiwan	330.6	2.45	-2.89	2
94	Beiwan	336.5	2.13	-3.45	2
95	Beiwan	338.4	1.57	-2.19	1
96	Beiwan	344.9	2.11	-2.83	2
97	Beiwan	354	1.84	-3.83	2
98	Beiwan	367.2	3.18	-2.33	1
99	Beiwan	370	3.95	-0.51	2
100	Beiwan	371	3.06	-2.20	1
101	Beiwan	374	2.93	-3.85	2
102	Beiwan	380	3.34	-3.18	3
103	Beiwan	383	3.05	-2.71	2
104	Beiwan	386	3.71	-2.09	1
105	Beiwan	389	3.11	-3.94	2
106	Beiwan	392.7	3.87	-2.85	1
107	Beiwan	396.7	3.76	-3.86	2
108	Beiwan	400.2	3.54	-3.66	1
109	Beiwan	401.8	3.88	-2.74	1
110	Beiwan	403.5	2.76	-2.91	2
111	Beiwan	406.5	3.63	-2.83	1
112	Beiwan	409.5	3.03	-2.09	2
113	Beiwan	412.1	3.18	-3.24	2
114	Beiwan	416	3.09	-3.25	2
115	Beiwan	419	3.75	-3.16	2

TA.2	Formation	Height (m)	$\delta^{13}C$	$\delta^{18}O$	Replicates
116	Beiwan	425	3.91	-1.91	2
117	Beiwan	429	3.11	-3.00	2
118	Beiwan	431.5	3.98	-2.89	2
119	Beiwan	435	4.20	-2.97	2
120	Beiwan	438	4.07	-3.33	2
121	Beiwan	441	4.21	-2.22	2
122	Beiwan	444.5	3.91	-4.39	2
123	Beiwan	447.2	3.79	-2.43	2
124	Beiwan	452	3.60	-2.77	2
125	Beiwan	455.5	3.21	-3.90	2
126	Beiwan	461	3.64	-2.47	2
127	Beiwan	464.5	3.80	-3.47	2
128	Beiwan	469.7	3.54	-3.24	2
129	Beiwan	478	4.19	-0.19	2
130	Beiwan	482.5	3.82	-2.49	2
131	Beiwan	486.5	3.76	-2.71	2
132	Beiwan	488	3.29	-3.49	2
133	Beiwan	491.7	3.63	-2.75	2
134	Beiwan	495	3.39	-3.14	2
135	Beiwan	497.5	3.65	-2.96	2
136	Beiwan	501.3	3.79	-1.29	2
137	Beiwan	504	3.66	-4.41	2
138	Beiwan	507	3.58	-2.74	2
139	Beiwan	510	3.43	-3.83	2
140	Beiwan	514	3.25	-3.46	2
141	Beiwan	518.8	2.96	-3.98	2
142	Beiwan	521	3.94	0.04	2
143	Beiwan	524.2	3.70	-2.88	2
144	Beiwan	526.9	2.67	-4.14	2
145	Beiwan	533	2.00	-4.93	2
146	Beiwan	537.5	2.14	-4.15	2
147	Beiwan	543	2.21	-4.30	2
148	Beiwan	546.2	1.79	-5.47	2
149	Beiwan	549.8	1.33	-5.43	2
150	Beiwan	552	2.76	-4.18	2
151	Beiwan	556	2.01	-3.44	2
152	Beiwan	561.5	2.02	-5.16	1
153	Beiwan	564	1.86	-6.37	1
154	Beiwan	565	1.69	-4.32	1
155	Beiwan	569	2.08	-5.63	1
156	Beiwan	574	1.41	-5.97	1

TA.2	Formation	Height (m)	$\delta^{13}C$	$\delta^{18}O$	Replicates
157	Beiwan	579	0.37	-6.22	1
158	Beiwan	584	1.69	-4.63	1
159	Beiwan	589	1.94	-3.42	1
160	Beiwan	593.5	1.64	-5.11	1
161	Beiwan	598	1.69	-5.27	1
162	Beiwan	601	0.62	-6.48	1
163	Beiwan	609	2.01	-3.46	1
164	Beiwan	614	0.61	-8.97	2
165	Beiwan	619	0.44	-4.44	1
166	Beiwan	620.9	-0.89	-10.78	1
167	Beiwan	621.2	-0.25	-10.02	2
168	Beiwan	624	-0.40	-9.96	1
169	Beiwan	626.5	-0.06	-10.18	1
170	Beiwan	628.5	-1.09	-10.07	1

Table A.3. Organic carbon data, sections 0601-A, 0601-B, and 0601-D.

TA.3	Section	Section Height (m)	Correlated Height (m)	%TOC	$\delta^{13}C_{carb}$	$\delta^{13}C_{org}$	$\Delta\delta^{13}C_{carb\text{-}org}$
1	0601-A	0	53	0.15	2.56	-30.22	32.78
2	0601-A	1.83	54.83	0.11	3.3	-31.82	35.12
3	0601-A	2.4	55.4	0.07	3.12	-31.26	34.38
4	0601-A	3.4	56.4	0.24	3.24	-32.05	35.29
5	0601-A	3.5	56.5	0.07	3.32	-31.11	34.43
6	0601-A	4.9	57.9	0.03	3.15	-31.79	34.94
7	0601-A	5.4	58.4	0.15	4.3	-31.76	36.06
8	0601-A	5.5	58.5	0.09	3.85	-30.52	34.37
9	0601-A	6.1	59.1	0.05	3.21	-31.38	34.59
10	0601-A	6.3	59.3	0.03	3.52	-31.91	35.43
11	0601-A	7.4	60.4	0.08	3.51	-31.96	35.47
12	0601-A	7.7	60.7	0.08	3.35	-30.16	33.51
13	0601-A	7.9	60.9	0.09	3.98	-30.92	34.9
14	0601-B	0	54	0.01	3.49	-31.93	35.42
15	0601-B	1	55	0.07	3.57	-32.05	35.62
16	0601-B	2	56	0.11	4.01	-30.94	34.95
17	0601-B	3	57	0.06	2.88	-31.29	34.17
18	0601-B	4	58	0.05	3.13	-31.87	35
19	0601-B	5	59	0.53	3.25	-32.95	36.2
20	0601-B	6	60	0.16	3.26	-32.23	35.49
21	0601-B	7	61	0.13	3.02	-31.03	34.05
22	0601-B	7.1	61.1	0.09	3.37	-30.88	34.25

TA.3	Section	Section Height (m)	Correlated Height (m)	%TOC	$\delta^{13}C_{carb}$	$\delta^{13}C_{org}$	$\Delta\delta^{13}C_{carb-org}$
23	0601-B	7.2	61.2	0.2	3.1	-30.72	33.82
24	0601-B	7.5	61.5	0.1	3.39	-30.62	34.01
25	0601-B	7.9	61.9	0.05	2.99	-27.08	30.07
26	0601-B	8.5	62.5	0.04	2.32	-28.83	31.15
27	0601-B	9.6	63.6	0.06	1.96	-31.15	33.11
28	0601-B	10.7	64.7	0.05	1.11	-31.29	32.4
29	0601-B	11.8	65.8	0.18	1.39	-31.36	32.75
30	0601-B	12.5	66.5	0.22	1.13	-33.23	34.36
31	0601-B	13.7	67.7	0.07	1.59	-28.04	29.63
32	0601-B	14.8	68.8	0.08	1.01	-27.81	28.82
33	0601-B	15	69	0.15	0.53	-27.82	28.35
34	0601-D	-3	70.3	0.27	-4.13	-39.96	35.83
35	0601-D	-2.5	70.8	0.19	-4.43	-38.51	34.08
36	0601-D	-0.6	72.8	0.13	-3.24	-39.31	36.07
37	0601-D	-0.5	72.9	0.07	-4.68	-40.02	35.34
38	0601-D	-0.3	73.1	0.09	-3.84	-38.16	34.32
39	0601-D	0.5	73.7	0.11	-1.58	-38.55	36.97
40	0601-D	1	74.3	0.06	-2.17	-37.24	35.07
41	0601-D	1.5	75	0.11	-4.13	-34.86	30.73
42	0601-D	2.2	75.6	0.21	-1.8	-38.52	36.72
43	0601-D	2.8	76.2	0.11	-1.58	-38.59	37.01
44	0601-D	3.2	77.1	0.42	-0.31	-37.68	37.37
45	0601-D	3.7	77.5	0.49	-2.15	-38.74	36.59
46	0601-D	4.3	77.9	0	-0.97	-39.63	38.66
47	0601-D	6.5	79.5	0.2	-1.51	-40.65	39.14
48	0601-D	7	80.3	0.19	0.93	-40.41	41.34
49	0601-D	7.5	80.8	0.21	-0.22	-39.4	39.18
50	0601-D	8	81.4	0.18	-0.98	-40.3	39.32
51	0601-D	8.4	81.9	0.12	-1.09	-40.43	39.34
52	0601-D	9	82.5	0.07	-0.2	-39.49	39.29
53	0601-D	9.5	83.1	0.04	-0.68	-38.55	37.87
54	0601-D	10	83.7	0.19	0.17	-40.66	40.83
55	0601-D	10.5	84.3	0.09	-0.76	-37.73	36.97
56	0601-D	11	84.9	0.09	2.39	-37.81	40.2
57	0601-D	11.5	85.6	0.14	0.19	-38.3	38.49
58	0601-D	14.5	88.9	0.93	1.17	-38.62	39.79
59	0601-D	15	89.4	1.07	1.5	-39.19	40.69
60	0601-D	17	91.5	0.17	2.11	-37.2	39.31
61	0601-D	18.3	92.8	0.12	1.77	-35.2	36.97
62	0601-D	19.6	94.2	0.19	2.93	-35.86	38.79

TA.3	Section	Section Height (m)	Correlated Height (m)	%TOC	$\delta^{13}C_{carb}$	$\delta^{13}C_{org}$	$\Delta\delta^{13}C_{carb-org}$
63	0601-D	20	94.6	0.06	-0.46	-34.64	34.18
64	0601-D	20.5	95.1	0.06	2.32	-31.01	33.33
65	0601-D	25.5	98.2	0.12	3.24	-30.78	34.02
66	0601-D	25.9	98.6	0.37	1.89	-35.7	37.59
67	0601-D	26.5	99.2	0.1	1.1	-35.66	36.76
68	0601-D	26.6	99.3	0.13	-0.52	-35.52	35
69	0601-D	27.1	99.8	0.13	2.56	-35.66	38.22
70	0601-D	27.6	100.3	0.12	3.17	-35.13	38.3
71	0601-D	28	100.7	0	2.19	-36.07	38.26
72	0601-D	28.5	101.2	0.07	-0.89	-37.68	36.79
73	0601-D	29	101.7	0.15	2.83	-37.87	40.7
74	0601-D	29.5	102.2	0.05	-1.94	-37.71	35.77
75	0601-D	34	105.93	0.1	0.03	-40.23	40.26
76	0601-D	34.5	106.3	0.25	0.67	-40.97	41.64
77	0601-D	34.8	73.7	0.11	-1.37	-35.89	34.52
78	0601-D	35.2	107.15	0.77	1.47	-41.3	42.77
79	0601-D	36.5	108.15	0.18	2.23	-38.95	41.18
80	0601-D	37	108.55	0.09	-2.64	-39.62	36.98
81	0601-D	37.4	108.9	0.41	2.49	-42.79	45.28
82	0601-D	38	109.5	0.15	0.56	-39.51	40.07
83	0601-D	38.5	110	0.18	1.34	-41.54	42.88
84	0601-D	39	110.4	0.12	1.7	-40.85	42.55
85	0601-D	39.5	110.9	0.11	1.86	-41.19	43.05
86	0601-D	40	111.4	0.12	1.67	-40.76	42.43
87	0601-D	44	115.84	0.15	1.21	-41.18	42.39

Table A.4 Leach data for CAS experiments, sections 0601-A, 0601-B, and 0601-D.

TA.4	Section	Section Height (m)	Correlated Height (m)	Leach No.	Precip. Wt. (g)	$\delta^{34}S$
1	0601-A	0	53	1	0.00003	1.87
2	0601-A	0	53	2	0.0019	0.52
3	0601-A	0	53	3	0.00044	2.44
4	0601-A	0	53	4	0.00181	-0.15
5	0601-A	0	53	5	0.00248	0.43
6	0601-A	0	53	6	0.00664	6.79
7	0601-A	0	53	7	0.00404	11.36
8	0601-A	3.5	56.5	1	0.00055	2.66
9	0601-A	3.5	56.5	2	0.00298	3.97
10	0601-A	3.5	56.5	3	0.00067	NA
11	0601-A	3.5	56.5	4	0.00094	NA

TA.4	Section	Section Height (m)	Correlated Height (m)	Leach No.	Precip. Wt. (g)	$\delta^{34}S$
12	0601-A	3.5	56.5	5	0.00068	6.63
13	0601-A	3.5	56.5	6	0.00676	13.16
14	0601-A	3.5	56.5	7	0.00828	11.49
15	0601-A	6.1	59.1	1	0.0048	7.69
16	0601-A	6.1	59.1	2	0.00429	3.36
17	0601-A	6.1	59.1	3	0.00001	9.24
18	0601-A	6.1	59.1	4	0.00001	9.19
19	0601-A	6.1	59.1	5	0.00024	5.51
20	0601-A	6.1	59.1	6	0.0096	16.18
21	0601-A	6.1	59.1	7	0.0097	12.96
22	0601-A	7.7	60.7	1	0.01029	-0.85
23	0601-A	7.7	60.7	2	0.0053	1.25
24	0601-A	7.7	60.7	3	0.00231	0.83
25	0601-A	7.7	60.7	4	0.00141	9.29
26	0601-A	7.7	60.7	5	0.01162	-1.97
27	0601-A	7.7	60.7	6	0.00787	12.41
28	0601-A	7.7	60.7	7	0.00349	15.52
29	0601-B	0	54	1	0.00025	NA
30	0601-B	0	54	2	0.00049	NA
31	0601-B	0	54	3	0.00024	16.55
32	0601-B	0	54	4	0.00009	NA
33	0601-B	0	54	5	0.00024	NA
34	0601-B	0	54	6	0.0086	16.04
35	0601-B	0	54	7	0.01144	16.82
36	0601-B	4	58	1	0.00066	5.25
37	0601-B	4	58	2	0.00686	3.95
38	0601-B	4	58	3	0.00002	7.41
39	0601-B	4	58	4	0.00003	NA
40	0601-B	4	58	5	0.00187	7.43
41	0601-B	4	58	6	0.00724	14.12
42	0601-B	4	58	7	0.00637	15.24
43	0601-B	7	61	1	0.00445	4.21
44	0601-B	7	61	2	0.00311	4.12
45	0601-B	7	61	3	0.00001	10.8
46	0601-B	7	61	4	0.00001	12.61
47	0601-B	7	61	5	0.00008	-2.49
48	0601-B	7	61	6	0.00758	5.46
49	0601-B	7	61	7	0.00432	13.81
50	0601-B	10.7	64.7	1	0.00076	13.25
51	0601-B	10.7	64.7	2	0.00218	11.27
52	0601-B	10.7	64.7	3	0.00108	13.88

TA.4	Section	Section Height (m)	Correlated Height (m)	Leach No.	Precip. Wt. (g)	$\delta^{34}S$
53	0601-B	10.7	64.7	4	0.00001	NA
54	0601-B	10.7	64.7	5	0.00164	12.09
55	0601-B	10.7	64.7	6	0.0043	16.53
56	0601-B	10.7	64.7	7	0.00689	17.89
57	0601-B	13.7	67.7	1	0.00329	-4.03
58	0601-B	13.7	67.7	2	0.00273	-6.91
59	0601-B	13.7	67.7	3	0.0056	-7.34
60	0601-B	13.7	67.7	4	0.00017	-8.92
61	0601-B	13.7	67.7	5	0.00103	-11.42
62	0601-B	13.7	67.7	6	0.01334	-6.68
63	0601-B	13.7	67.7	7	0.01652	-10.77
64	0601-C	-2.5	73.5	1	0.00045	13.37
65	0601-C	-2.5	73.5	2	0.00028	13.27
66	0601-C	-2.5	73.5	3	0.00053	14.73
67	0601-C	-2.5	73.5	4	0.00001	17.31
68	0601-C	-2.5	73.5	5	0.0001	14.01
69	0601-C	-2.5	73.5	6	0.00112	20.97
70	0601-C	-2.5	73.5	7	0.00362	20.49
71	0601-C	-0.6	75.5	1	0.00045	5.55
72	0601-C	-0.6	75.5	2	0.00114	3.71
73	0601-C	-0.6	75.5	3	0.00541	7.81
74	0601-C	-0.6	75.5	4	0.00027	NA
75	0601-C	-0.6	75.5	5	0.00185	7.85
76	0601-C	-0.6	75.5	6	0.00278	NA
77	0601-C	-0.6	75.5	7	0.00608	10.16
78	0601-C	-0.6	75.5	8	0.00595	13.62
79	0601-C	4.9	80.9	1	0.01805	22.18
80	0601-C	4.9	80.9	2	0.00904	33.97
81	0601-C	4.9	80.9	3	0.00627	28.41
82	0601-C	4.9	80.9	4	0.01184	35.58
83	0601-C	4.9	80.9	5	0.01164	30.98
84	0601-C	4.9	80.9	6	0.0073	26.43
85	0601-C	6	82.2	1	0.03329	30.02
86	0601-C	6	82.2	2	0.01495	29.08
87	0601-C	6	82.2	3	0.00029	28.04
88	0601-C	6	82.2	4	0.00493	28.91
89	0601-C	6	82.2	5	0.00635	29.7
90	0601-C	6	82.2	6	0.00653	29.97
91	0601-C	6	82.2	7	0.00619	29.08
92	0601-C	9.5	85.8	2	0.00105	22.94
93	0601-C	9.5	85.8	3	0.00009	17.71

TA.4	Section	Section Height (m)	Correlated Height (m)	Leach No.	Precip. Wt. (g)	$\delta^{34}S$
94	0601-C	9.5	85.8	4	0.00036	15.07
95	0601-C	9.5	85.8	5	0.00071	14.82
96	0601-C	9.5	85.8	6	0.0043	27.24
97	0601-C	9.5	85.8	7	0.00177	24.95
98	0601-C	11.5	88.3	1	0.00028	NA
99	0601-C	11.5	88.3	2	0.00122	21.03
100	0601-C	11.5	88.3	3	0.00017	NA
101	0601-C	11.5	88.3	4	0.00001	NA
102	0601-C	11.5	88.3	5	0.00103	18.71
103	0601-C	11.5	88.3	6	0.0016	NA
104	0601-C	11.5	88.3	7	0.00511	24.89
105	0601-C	17	94.2	1	0.04458	27.74
106	0601-C	17	94.2	2	0.0006	26.09
107	0601-C	17	94.2	3	0.00069	13.07
108	0601-C	17	94.2	4	0.00071	14.99
109	0601-C	17	94.2	5	0.01225	19.94
110	0601-C	17	94.2	6	0.0105	23.85
111	0601-C	20	97.3	1	0.00357	23.8
112	0601-C	20	97.3	2	0.00003	15.43
113	0601-C	20	97.3	3	0.00089	12.99
114	0601-C	20	97.3	4	0.00048	13.44
115	0601-C	20	97.3	5	0.0059	25.78
116	0601-C	20	97.3	6	0.00095	24.45
117	0601-C	26.5	101.9	1	0.00133	24.46
118	0601-C	26.5	101.9	2	0.00218	22.44
119	0601-C	26.5	101.9	3	0.0002	14.85
120	0601-C	26.5	101.9	4	0.00002	14.9
121	0601-C	26.5	101.9	5	0.00367	25.89
122	0601-C	26.5	101.9	6	0.00148	24.36
123	0601-C	28.5	103.9	1	0.05818	32.7
124	0601-C	28.5	103.9	2	0.00466	33.07
125	0601-C	28.5	103.9	3	0.00057	18.24
126	0601-C	28.5	103.9	4	0.0016	21.89
127	0601-C	28.5	103.9	5	0.00925	29.52
128	0601-C	28.5	103.9	6	0.00531	30.11
129	0601-C	34	108.63	1	0.03223	28.43
130	0601-C	34	108.63	2	0.00362	24.88
131	0601-C	34	108.63	3	0.00733	21.8
132	0601-C	34	108.63	4	0.00028	16.54
133	0601-C	34	108.63	5	0.00852	23.15
134	0601-C	34	108.63	6	0.0113	25.63

TA.4	Section	Section Height (m)	Correlated Height (m)	Leach No.	Precip. Wt. (g)	$\delta^{34}S$
135	0601-C	44	118.54	1	0.11312	34.81
136	0601-C	44	118.54	2	0.01812	34.36
137	0601-C	44	118.54	4	0.00505	20.03
138	0601-C	44	118.54	5	0.0137	32.09
139	0601-C	44	118.54	6	0.00648	30.99
140	0601-C	54	127.75	1	0.01568	30.97
141	0601-C	54	127.75	2	0.00254	30.19
142	0601-C	54	127.75	4	0.00492	16.75
143	0601-C	54	127.75	5	0.00285	24.97
144	0601-C	54	127.75	6	0.00034	25.41

Table A.5. Pattern list for XRD analysis of Mattaia sample 0709-60.

No.	Ref. Code	Compound Name	Chemical Formula
1	00-006-0046	Gypsum	$CaSO_4$ - $2H_2O$
2	00-013-0190	Corrensite	$Mg_8Al_3Si_6O_{20}(OH)_{10}$ - $4H_2O$
3	00-007-0025	Muscovite-1M, syn	$KAl_2Si_3AlO_{10}(OH)_2$

Table A.6. Peak list for Mattaia sample 0709-60.

Position (º2θ)	Height (cts)	d-spacing (Å)	Matched by	Rel.Int.[%]
2.8003	956.34	31.55032	N/A	23.17
7.3105	156.31	12.09264	N/A	3.79
8.9717	188.84	9.85695	00-007-0025	4.57
11.617	4127.98	7.61767	00-006-0046	100
13.5001	31.03	6.55903	N/A	0.75
15.0939	49.82	5.86983	00-013-0190	1.21
15.7307	15.69	5.63364	00-013-0190	0.38
17.5569	129.74	5.05155	00-007-0025	3.14
19.7636	997.78	4.49221	00-007-0025	24.17
20.7685	967.96	4.27707	00-006-0046	23.45
23.4466	819.19	3.79426	00-006-0046	19.84
24.3971	148.08	3.64854	00-007-0025	3.59
26.7281	559.83	3.3354	00-007-0025	13.56
27.5928	389.84	3.23282	00-013-0190	9.44
29.136	1280.38	3.06501	00-006-0046	31.02
30.9912	119.41	2.88563	00-006-0046	2.89
32.4041	8.91	2.76297	00-006-0046	0.22
33.4173	105.25	2.68147	00-006-0046	2.55
34.5855	520.77	2.59353	00-006-0046	12.62
35.0362	719.83	2.56119	00-006-0046	17.44

Position (º2θ)	Height (cts)	d-spacing (Å)	Matched by	Rel.Int.[%]
36.5431	119.62	2.45896	00-006-0046	2.9
37.6353	233.72	2.39008	00-006-0046	5.66

Table A.7-1. Datatable for U-Pb geochronologic analyses for Mattaia sample 0709-60, 1 of 2. Analyses of zircon cores in blue.

	Elemental concentrations					Isotope ratios				
Analysis	U	206Pb	U/Th	206Pb*	±	207Pb*	±	206Pb*	±	error
	ppm	204Pb		207Pb*	(%)	235U*	(%)	238U	(%)	corr.
0709-60LG-3C	403	27329	1.2	17.3322	0.9	0.6412	2.1	0.0806	1.9	0.90
0709-60LG-4C	354	68566	1.2	17.2428	0.7	0.6463	2.9	0.0808	2.8	0.97
0709-60LG-5R	244	32794	2.2	17.1757	0.7	0.6671	2.5	0.0831	2.4	0.97
0709-60LG-19C	443	104908	1.0	17.2058	1.0	0.6672	3.3	0.0833	3.2	0.96
0709-60LG-11R	191	14514	1.4	17.3948	0.9	0.6616	2.3	0.0835	2.1	0.92
0709-60LG-6C	112	15291	2.7	17.1609	1.6	0.6730	3.9	0.0838	3.6	0.91
0709-60LG-9BR	89	12975	1.1	17.4618	0.8	0.6622	2.5	0.0839	2.4	0.95
0709-60LG-14R	205	26436	1.5	17.1329	1.2	0.6792	2.7	0.0844	2.4	0.90
0709-60LG-4R	201	23503	1.9	17.2370	0.8	0.6754	2.5	0.0844	2.3	0.95
0709-60LG-7R	149	28283	1.2	17.1522	0.6	0.6829	2.9	0.0850	2.8	0.98
0709-60LG-6R	169	20235	1.6	17.2168	1.3	0.6831	2.3	0.0853	1.9	0.83
0709-60LG-9AC	451	95195	1.2	17.1995	0.7	0.6844	2.0	0.0854	1.9	0.94
0709-60LG-20R	87	17711	1.0	17.1415	0.8	0.6879	2.9	0.0855	2.8	0.96
0709-60LG-12R	275	43328	1.2	17.1352	0.6	0.6904	3.2	0.0858	3.2	0.98
0709-60LG-17R	316	58084	0.9	17.1661	0.6	0.6893	2.9	0.0858	2.9	0.98
0709-60LG-8M	61	7840	1.5	17.2439	1.3	0.6867	3.2	0.0859	2.9	0.92
0709-60LG-13R	89	20515	1.2	17.0703	0.9	0.6962	1.9	0.0862	1.7	0.88
0709-60LG-14C	154	37399	1.6	17.0954	0.9	0.6952	3.4	0.0862	3.3	0.97
0709-60LG-10C	247	28644	1.2	17.1738	1.1	0.6934	2.9	0.0864	2.6	0.92
0709-60LG-20C	112	26248	0.9	17.1547	0.8	0.6962	3.0	0.0866	2.9	0.96
0709-60LG-18MANT.	187	56225	0.9	17.1914	0.6	0.6954	2.8	0.0867	2.7	0.98
0709-60LG-11C	580	81029	0.9	17.1337	0.6	0.6978	2.7	0.0867	2.6	0.98
0709-60LG-12C	240	66138	1.3	17.1633	0.9	0.6984	3.3	0.0869	3.1	0.96
0709-	288	34572	1.2	17.3493	0.7	0.6911	2.5	0.0870	2.4	0.96

	Elemental concentrations					Isotope ratios				
Analysis	U	206Pb	U/Th	206Pb*	±	207Pb*	±	206Pb*	±	error
	ppm	204Pb		207Pb*	(%)	235U*	(%)	238U	(%)	corr.
60LG-16R										
0709-60LG-15R	597	184925	0.9	17.1801	0.9	0.6982	2.9	0.0870	2.8	0.96
0709-60LG-8R	72	19075	1.4	16.8769	1.2	0.7137	2.4	0.0874	2.0	0.86
0709-60LG-1R	68	11675	2.1	16.8456	1.4	0.7164	2.7	0.0875	2.3	0.85
0709-60LG-18C	322	27048	1.1	17.2332	0.9	0.7023	3.2	0.0878	3.1	0.96
0709-60LG-8C	182	16403	1.0	17.1723	1.1	0.7258	2.7	0.0904	2.5	0.92

Table A.7-2			Apparent ages (Ma)						
Analysis	206Pb* 238U*	± (Ma)	207Pb* 235U	± (Ma)	206Pb* 207Pb*	± (Ma)	Best age (Ma)	± (Ma)	Conc (%)
0709-60LG-3C	500	9	503	8	518	21	500	9	96
0709-60LG-4C	501	13	506	12	530	16	501	13	95
0709-60LG-5R	515	12	519	10	538	14	515	12	96
0709-60LG-19C	516	16	519	14	534	21	516	16	96
0709-60LG-11R	517	10	516	9	510	20	517	10	101
0709-60LG-6C	519	18	523	16	540	35	519	18	96
0709-60LG-9BR	519	12	516	10	502	17	519	12	103
0709-60LG-14R	522	12	526	11	544	26	522	12	96
0709-60LG-4R	523	12	524	10	530	17	523	12	99
0709-60LG-7R	526	14	529	12	541	14	526	14	97
0709-60LG-6R	528	10	529	9	533	28	528	10	99
0709-60LG-9AC	528	10	529	8	535	15	528	10	99
0709-60LG-20R	529	14	532	12	542	18	529	14	98
0709-60LG-12R	531	16	533	13	543	13	531	16	98
0709-60LG-17R	531	15	532	12	539	13	531	15	98
0709-60LG-8M	531	15	531	13	529	28	531	15	100
0709-60LG-13R	533	8	537	8	552	19	533	8	97
0709-60LG-14C	533	17	536	14	548	19	533	17	97
0709-60LG-10C	534	14	535	12	538	25	534	14	99
0709-60LG-20C	536	15	537	12	541	18	536	15	99
0709-60LG-18MANTLE	536	14	536	12	536	13	536	14	100
0709-60LG-11C	536	13	537	11	543	13	536	13	99
0709-60LG-12C	537	16	538	14	540	20	537	16	100
0709-60LG-16R	538	13	533	11	516	16	538	13	104
0709-60LG-15R	538	14	538	12	538	19	538	14	100
0709-60LG-8R	540	11	547	10	576	26	540	11	94
0709-60LG-1R	541	12	549	11	580	31	541	12	93
0709-60LG-18C	542	16	540	13	531	19	542	16	102
0709-60LG-8C	558	13	554	12	539	23	558	13	104

Table A.8. Pattern list for Dengying sample 09G-35.3.

No.	Ref. Code	Compound Name	Chemical Formula
1	00-036-0426	Dolomite	$CaMg(CO_3)_2$
2	01-074-9758	Quartz	SiO_2
3	01-074-1392	Muscovite-3T	$Al_3Si_3K(OH)_2O_{10}$

Table A.9. Peak list for Dengying sample 09G-35.3.

Position (°2θ)	Height (cts)	d-spacing (Å)	Matched by	Rel.Int.[%]
2.5266	106.88	34.96812		2.23
4.2527	52.92	20.77811	N/A	1.11
5.8538	32.63	15.09821	N/A	0.68

Position (º2θ)	Height (cts)	d-spacing (Å)	Matched by	Rel.Int.[%]
7.8982	112.33	11.19402	N/A	2.35
8.8305	71.82	10.01424	01-074-1392	1.5
10.2756	39.97	8.60885	N/A	0.84
11.1012	45.51	7.97044	N/A	0.95
12.1419	34.1	7.28951	N/A	0.71
15.6607	27.4	5.65866	N/A	0.57
17.9132	24.03	4.95185	01-074-1392	0.5
19.0587	14.13	4.65673	N/A	0.3
19.689	85.42	4.50908	01-074-1392	1.79
20.852	296.04	4.26012	01-074-9758	6.19
21.5059	22.22	4.13206	00-036-0426	0.46
21.9631	54.4	4.04706	00-036-0426	1.14
23.0924	75.45	3.85164	01-074-1392	1.58
23.9165	275.28	3.72075	00-036-0426	5.76
24.749	49.42	3.59746	01-074-1392	1.03
25.78	92.88	3.45588	N/A	1.94
26.6446	1492.38	3.34566	01-074-9758	31.2
27.6477	46.46	3.22652	N/A	0.97
28.088	47.39	3.17694	N/A	0.99
28.8353	0.75	3.09628	01-074-1392	0.02
29.46	1112.34	3.03202	N/A	23.26
30.7108	4782.65	2.91133	00-036-0426	100
33.2254	93.89	2.69652	00-036-0426	1.96
35.0909	81.47	2.55733	00-036-0426	1.7
36.586	77.38	2.45618	01-074-9758	1.62
37.2346	276.63	2.41487	00-036-0426	5.78
39.4759	185.88	2.28278	01-074-9758	3.89

Table A.10. Pattern list for Dengying sample 09G-37.9.

No.	Ref. Code	Compound Name	Chemical Formula
1	00-034-0517	Dolomite, ferroan	$Ca(Mg,Fe)(CO_3)_2$
2	01-072-4582	Calcite	$Ca(CO_3)$
3	01-075-8320	Quartz	SiO_2

Table A.11. Peak list for Dengying sample 09G-37.9.

Position (º2θ)	Height (cts)	d-spacing (Å)	Matched by	Rel.Int.[%]
7.1632	15.48	12.34097	N/A	0.3
8.7424	78.85	10.11494	N/A	1.53
10.0411	42.12	8.80942	N/A	0.82
13.6336	24.68	6.49511	N/A	0.48

Position (º2θ)	Height (cts)	d-spacing (Å)	Matched by	Rel.Int.[%]
14.7304	18.12	6.01387	N/A	0.35
17.8961	25.79	4.95656	N/A	0.5
19.6826	157.28	4.51053	N/A	3.06
20.8717	250.22	4.25615	01-075-8320	4.86
21.46	37.61	4.14079	N/A	0.73
21.8801	75.99	4.06222	N/A	1.48
23.0987	93.66	3.8506	01-072-4582	1.82
23.919	312.64	3.72038	00-034-0517	6.07
25.0535	46.08	3.55442	N/A	0.9
26.6332	1517.62	3.34707	01-075-8320	29.48
27.572	67.96	3.23521	N/A	1.32
29.4435	1188.7	3.03369	01-072-4582	23.09
30.7003	5147.96	2.9123	00-034-0517	100
32.0744	34.13	2.79061	N/A	0.66
33.1554	94.16	2.70205	00-034-0517	1.83
34.5086	63.36	2.59913	N/A	1.23
35.0472	141.64	2.56041	00-034-0517	2.75
35.9952	102.45	2.49512	01-072-4582	1.99
36.5283	91.81	2.45993	01-075-8320	1.78
37.1624	343.86	2.4194	00-034-0517	6.68
39.4706	255.06	2.28307	01-072-4582	4.95
40.8551	533.8	2.20884	00-034-0517	10.37
42.4053	46.4	2.13162	01-075-8320	0.9
43.175	83.81	2.09538	01-072-4582	1.63
43.6617	31.02	2.07315	00-034-0517	0.6
44.6133	187.48	2.03112	00-034-0517	3.64
45.7478	52.14	1.98335	01-075-8320	1.01
46.6631	19.83	1.94656	N/A	0.39
47.6236	85.25	1.90952	01-072-4582	1.66
48.5779	77.58	1.87421	01-072-4582	1.51
49.0792	26.98	1.85624	00-034-0517	0.52
50.142	309.86	1.81936	00-034-0517	6.02
50.8083	368.61	1.79705	00-034-0517	7.16
53.8033	10.62	1.70388	N/A	0.21
55.0595	8.61	1.66794	01-075-8320	0.17
56.5425	6.82	1.62766	01-072-4582	0.13
57.4854	31.6	1.60319	01-072-4582	0.61
58.7171	45.54	1.57246	00-034-0517	0.88
59.5707	95	1.55195	00-034-0517	1.85
60.7533	22.41	1.52455	01-072-4582	0.44
61.6685	71.42	1.5041	00-034-0517	1.39

Position (º2θ)	Height (cts)	d-spacing (Å)	Matched by	Rel.Int.[%]
63.1821	59.74	1.47167	00-034-0517	1.16
63.9571	15.6	1.45569	00-034-0517	0.3
64.9033	29.22	1.43674	00-034-0517	0.57
65.8189	8.9	1.41896	00-034-0517	0.17
67.1678	64.08	1.39255	00-034-0517	1.24
68.2304	16.7	1.37684	N/A	0.32

Table A.13-1. Datatable for U-Pb geochronologic analyses for Dengying sample 35.3, 1 of 2. Ordered by increasing age.

	Elemental concentrations					Isotope ratios				
Analysis	U	206Pb	U/ Th	206Pb*	±	207Pb*	±	206Pb*	±	error
	ppm	204Pb		207Pb*	(%)	235U*	(%)	238U	(%)	corr.
09G_35.3-35	187	74028	1.3	15.5025	2.2	1.0704	3.5	0.1203	2.7	0.78
09G_35.3-32	144	59902	1.1	15.3032	1.3	1.1439	2.2	0.1270	1.8	0.81
09G_35.3-42	92	60665	1.0	15.3821	2.8	1.1391	3.6	0.1271	2.2	0.62
09G_35.3-25	51	19703	1.0	15.1667	4.6	1.1567	4.9	0.1272	1.7	0.35
09G_35.3-36	125	31363	1.0	15.4463	3.9	1.1440	5.0	0.1282	3.1	0.62
09G_35.3-34	171	257584	1.0	15.2477	1.9	1.1600	2.3	0.1283	1.3	0.57
09G_35.3-18	131	42412	1.1	15.2501	3.7	1.1604	3.9	0.1283	1.3	0.34
09G_35.3-22	48	13274	1.6	15.4505	4.7	1.1523	5.1	0.1291	2.0	0.39
09G_35.3-12	128	68600	0.9	15.6173	4.5	1.1419	4.6	0.1293	1.0	0.21
09G_35.3-16	79	24639	1.2	15.3244	4.4	1.1683	4.8	0.1299	1.9	0.40
09G_35.3-43	77	25745	1.1	15.2255	3.5	1.1798	3.7	0.1303	1.2	0.31
09G_35.3-10	177	69222	1.1	15.3673	2.9	1.1833	3.3	0.1319	1.6	0.48
09G_35.3-9	85	22382	1.3	15.3476	3.6	1.1917	3.9	0.1327	1.5	0.38
09G_35.3-44	118	56773	1.2	15.2220	2.6	1.2063	4.0	0.1332	3.1	0.77
09G_35.3-30	515	119229	1.3	15.0130	0.8	1.2388	1.8	0.1349	1.6	0.90
09G_35.3-26	137	61036	1.1	14.8602	4.7	1.2811	4.8	0.1381	0.8	0.17
09G_35.3-6	418	51343	1.4	14.8177	0.8	1.2864	1.4	0.1382	1.2	0.81
09G_35.3-2	102	67734	0.7	14.6056	4.1	1.3153	4.8	0.1393	2.4	0.50
09G_35.3-8	109	35580	1.4	14.5821	3.1	1.3200	3.4	0.1396	1.5	0.44
09G_35.3-28	170	52415	1.7	15.1371	2.4	1.2799	2.5	0.1405	0.9	0.36
09G_35.3-37	262	284971	0.6	14.7084	1.4	1.3275	1.9	0.1416	1.3	0.66
09G_35.3-19	115	60890	0.9	15.2002	4.3	1.2992	4.8	0.1432	2.0	0.41
09G_35.3-29	86	36224	1.3	14.2682	4.1	1.3841	4.2	0.1432	0.8	0.19
09G_35.3-13	158	80526	1.7	15.0542	2.2	1.3230	2.4	0.1444	1.0	0.42
09G_35.3-11	63	56839	2.1	8.0293	0.9	6.4943	1.3	0.3782	0.9	0.71
09G_35.3-23	59	73444	1.3	6.3439	1.0	10.0847	1.4	0.4640	1.0	0.71

Table A.13-2. Datatable for U-Pb geochronologic analyses for Dengying sample 35.3, 2 of 2. Ordered by increasing age.

Table A.13-2			Apparent ages (Ma)

Analysis	206Pb* 238U*	± (Ma)	207Pb* 235U	± (Ma)	206Pb* 207Pb*	± (Ma)	Best age (Ma)	± (Ma)	Conc (%)
09G_35.3-35	733	19	739	18	758	47	733	19	97
09G_35.3-32	771	13	774	12	785	28	771	13	98
09G_35.3-42	771	16	772	19	775	59	771	16	100
09G_35.3-25	772	12	780	27	804	96	772	12	96
09G_35.3-36	777	23	774	27	766	82	777	23	102
09G_35.3-34	778	10	782	13	793	40	778	10	98
09G_35.3-18	778	10	782	21	793	77	778	10	98
09G_35.3-22	783	15	778	28	765	100	783	15	102
09G_35.3-12	784	7	773	25	743	95	784	7	106
09G_35.3-16	787	14	786	26	783	92	787	14	101
09G_35.3-43	789	9	791	20	796	74	789	9	99
09G_35.3-10	799	12	793	18	777	62	799	12	103
09G_35.3-9	803	11	797	21	779	75	803	11	103
09G_35.3-44	806	23	803	22	797	54	806	23	101
09G_35.3-30	816	12	818	10	826	16	816	12	99
09G_35.3-26	834	6	837	27	847	98	834	6	98
09G_35.3-6	835	9	840	8	853	18	835	9	98
09G_35.3-2	841	19	852	28	883	86	841	19	95
09G_35.3-8	842	12	855	20	886	63	842	12	95
09G_35.3-28	848	7	837	14	808	49	848	7	105
09G_35.3-37	854	10	858	11	868	30	854	10	98
09G_35.3-19	863	16	845	27	800	91	863	16	108
09G_35.3-29	863	6	882	25	931	85	863	6	93
09G_35.3-13	870	8	856	14	820	46	870	8	106
09G_35.3-11	2068	16	2045	11	2022	16	2022	16	102
09G_35.3-23	2457	21	2443	13	2430	17	2430	17	101

Table A.14-1. Datatable for U-Pb geochronologic analyses for Dengying sample 37.9, 1 of 2. Ordered by increasing age.

A.14-1	Elemental concentrations					Isotope ratios				
Analysis	U ppm	206Pb 204Pb	U/ Th	206Pb* 207Pb*	± (%)	207Pb* 235U*	± (%)	206Pb* 238U	± (%)	error corr.
09G_37.9-51	317	11411	1.4	16.7472	2.9	0.6586	3.0	0.0800	0.8	0.25
09G_37.9-92	360	21113	1.1	17.0373	2.1	0.7111	2.7	0.0879	1.8	0.66
09G_37.9-77	122	41578	2.0	17.1322	4.7	0.7145	5.0	0.0888	1.7	0.33
09G_37.9-59	221	81615	1.7	17.0194	1.4	0.7193	2.1	0.0888	1.6	0.75
09G_37.9-85	284	39767	1.7	17.1268	1.5	0.7167	1.8	0.0890	0.9	0.50
09G_37.9-158	260	63375	2.2	16.9812	1.9	0.7316	2.2	0.0901	0.9	0.43
09G_37.9-96	130	15711	1.9	16.9291	4.9	0.7362	5.2	0.0904	1.8	0.34
09G_37.9-167	332	62910	2.5	16.9315	1.9	0.7379	2.0	0.0906	0.8	0.38
09G_37.9-125	291	49358	1.7	17.0983	1.6	0.7314	2.2	0.0907	1.5	0.69
09G_37.9-144	271	52161	1.9	17.2058	2.0	0.7325	2.5	0.0914	1.5	0.60
09G_37.9-131	243	58363	1.8	17.1555	2.6	0.7445	3.3	0.0926	2.0	0.62

A.14-1	Elemental concentrations					Isotope ratios				
Analysis	U	206Pb	U/ Th	206Pb*	±	207Pb*	±	206Pb*	±	error
	ppm	204Pb		207Pb*	(%)	235U*	(%)	238U	(%)	corr.
09G_37.9-94	196	12928	1.6	15.3507	1.8	1.0880	3.5	0.1211	3.0	0.85
09G_37.9-29	124	25676	1.1	15.7387	2.9	1.0683	3.5	0.1219	2.1	0.58
09G_37.9-17	53	9991	1.1	15.3722	4.6	1.0998	4.9	0.1226	1.6	0.34
09G_37.9-93	124	45553	1.4	15.5012	3.3	1.0920	3.5	0.1228	1.3	0.36
09G_37.9-58	107	15638	1.5	15.5722	2.8	1.0880	2.9	0.1229	1.0	0.33
09G_37.9-82	64	13969	1.7	15.2325	4.8	1.1188	5.3	0.1236	2.2	0.42
09G_37.9-60	155	27912	0.7	15.4332	2.1	1.1110	2.3	0.1244	0.9	0.39
09G_37.9-70	87	32639	1.5	15.4545	3.9	1.1156	4.3	0.1250	1.7	0.40
09G_37.9-111	112	30007	1.3	15.7626	4.0	1.0940	4.4	0.1251	1.8	0.40
09G_37.9-120	119	80052	0.9	15.5939	3.2	1.1074	3.4	0.1252	1.2	0.36
09G_37.9-102	67	26990	1.0	15.5405	4.9	1.1196	5.9	0.1262	3.3	0.57
09G_37.9-97	94	52942	0.8	15.1567	4.2	1.1503	4.6	0.1264	1.8	0.40
09G_37.9-126	160	139976	1.0	15.7179	4.1	1.1111	4.1	0.1267	0.8	0.18
09G_37.9-10	120	53650	1.5	15.6171	2.0	1.1196	2.1	0.1268	0.8	0.37
09G_37.9-114	129	37738	0.8	15.3464	3.3	1.1397	3.6	0.1268	1.6	0.44
09G_37.9-100	63	15170	0.9	15.3503	5.0	1.1408	5.2	0.1270	1.6	0.31
09G_37.9-15	68	16871	1.2	15.4148	3.3	1.1395	4.3	0.1274	2.8	0.64
09G_37.9-35	114	31421	1.4	15.2600	2.2	1.1515	3.1	0.1274	2.1	0.68
09G_37.9-110	94	45954	0.9	14.9738	3.3	1.1779	3.7	0.1279	1.7	0.44
09G_37.9-30	89	52146	0.9	15.4982	3.4	1.1431	3.9	0.1285	1.8	0.47
09G_37.9-133	162	66129	0.8	15.5694	2.5	1.1394	2.9	0.1287	1.3	0.46
09G_37.9-105	105	30960	1.4	15.3767	2.9	1.1563	3.4	0.1290	1.8	0.52
09G_37.9-40	135	31818	1.5	15.4301	2.1	1.1541	2.5	0.1292	1.4	0.56
09G_37.9-136	281	44471	0.9	15.5435	1.7	1.1496	2.3	0.1296	1.6	0.70
09G_37.9-151	93	21431	0.7	15.5307	3.7	1.1511	4.2	0.1297	2.1	0.49
09G_37.9-49	123	14915	1.0	15.3874	3.5	1.1634	4.0	0.1298	1.9	0.48
09G_37.9-39	130	41683	1.2	15.3346	2.2	1.1722	2.4	0.1304	0.9	0.37
09G_37.9-160	87	34497	1.0	15.2647	4.7	1.1822	4.9	0.1309	1.4	0.28
09G_37.9-42	158	60480	1.6	15.1031	3.2	1.1969	3.8	0.1311	2.0	0.53
09G_37.9-63	63	24016	1.3	15.3058	2.8	1.1837	3.4	0.1314	1.9	0.56
09G_37.9-45	111	46253	1.4	15.4941	3.0	1.1764	3.7	0.1322	2.2	0.60
09G_37.9-16	106	56054	1.6	14.7395	3.1	1.2507	3.7	0.1337	1.9	0.52
09G_37.9-165	123	37073	0.9	15.0854	3.3	1.2245	4.3	0.1340	2.8	0.65
09G_37.9-41	182	56648	2.3	15.1263	1.8	1.2224	2.1	0.1341	1.1	0.50
09G_37.9-69	140	49302	0.7	15.3658	4.0	1.2043	4.3	0.1342	1.5	0.36
09G_37.9-26	216	71380	1.8	14.9282	1.6	1.2466	2.0	0.1350	1.2	0.60
09G_37.9-65	309	124808	1.5	15.1048	1.1	1.2341	1.3	0.1352	0.6	0.48
09G_37.9-38	88	27100	2.5	14.9723	4.8	1.2476	5.2	0.1355	2.1	0.39
09G_37.9-66	399	167420	0.7	15.1157	1.0	1.2396	1.5	0.1359	1.1	0.74
09G_37.9-47	75	23591	0.9	14.9006	4.9	1.2620	5.2	0.1364	1.7	0.32
09G_37.9-156	243	51173	1.5	14.9863	1.2	1.2584	1.9	0.1368	1.5	0.79
09G_37.9-138	297	95703	0.7	15.1467	1.3	1.2453	2.3	0.1368	1.9	0.83
09G_37.9-1	128	38449	1.0	14.8944	4.1	1.2724	4.3	0.1375	1.1	0.25
09G_37.9-112	60	21429	1.8	14.8312	4.7	1.2847	5.0	0.1382	1.9	0.38
09G_37.9-67	206	112038	2.0	14.9218	1.3	1.2793	1.7	0.1384	1.1	0.64
09G_37.9-109	219	97473	1.3	14.7535	1.5	1.2947	2.0	0.1385	1.3	0.67
09G_37.9-43	82	48027	2.0	14.7533	3.6	1.2986	3.7	0.1389	1.0	0.27
09G_37.9-98	157	68135	1.0	15.1027	2.3	1.2740	2.7	0.1396	1.4	0.53
09G_37.9-74	94	45285	1.0	14.8372	3.7	1.3047	4.0	0.1404	1.4	0.34

A.14-1	Elemental concentrations					Isotope ratios				
Analysis	U	206Pb	U/ Th	206Pb*	±	207Pb*	±	206Pb*	±	error
	ppm	204Pb		207Pb*	(%)	235U*	(%)	238U	(%)	corr.
09G_37.9-5	156	63512	1.3	14.9280	2.2	1.3042	2.9	0.1412	1.8	0.64
09G_37.9-23	122	27348	1.1	14.7203	2.2	1.3227	5.4	0.1412	4.9	0.91
09G_37.9-71	202	50198	1.7	14.7883	1.4	1.3168	2.2	0.1412	1.7	0.77
09G_37.9-107	82	35011	1.1	15.1206	2.9	1.2884	3.3	0.1413	1.6	0.49
09G_37.9-169	88	90624	0.9	14.2735	3.2	1.3700	3.7	0.1418	1.8	0.49
09G_37.9-86	136	76918	1.2	14.9334	2.4	1.3097	2.8	0.1419	1.5	0.51
09G_37.9-104	101	47046	1.5	14.8686	3.5	1.3191	3.6	0.1422	0.9	0.25
09G_37.9-90	91	21547	2.2	14.8517	2.9	1.3282	3.1	0.1431	1.3	0.41
09G_37.9-154	76	21226	1.5	14.6725	4.7	1.3490	4.9	0.1436	1.5	0.30
09G_37.9-61	97	31046	2.4	14.5221	3.1	1.3784	3.6	0.1452	1.7	0.48
09G_37.9-164	146	67948	1.4	14.4182	2.1	1.4226	2.9	0.1488	2.0	0.69
09G_37.9-163	95	13737	2.2	14.7315	2.9	1.4207	3.4	0.1518	1.8	0.52
09G_37.9-56	128	10065	3.0	14.1326	1.6	1.4949	2.6	0.1532	2.0	0.77
09G_37.9-116	93	106525	1.4	14.6757	2.9	1.4422	3.2	0.1535	1.4	0.43
09G_37.9-145	42	53998	1.7	11.2259	4.2	2.9640	4.4	0.2413	1.3	0.29
09G_37.9-84	53	33397	1.1	9.2590	2.0	4.5760	2.3	0.3073	1.0	0.44
09G_37.9-174	75	72434	2.4	9.1495	1.2	4.9204	1.6	0.3265	1.0	0.63
09G_37.9-88	61	17183	1.5	8.4003	1.8	5.4437	3.2	0.3317	2.7	0.84
09G_37.9-27	51	58019	1.3	8.1509	1.2	6.0552	1.8	0.3580	1.4	0.75
09G_37.9-19	166	206903	1.1	8.1236	0.4	6.3105	1.0	0.3718	0.9	0.90
09G_37.9-50	80	77255	0.6	8.1089	0.7	6.3651	1.3	0.3743	1.1	0.83
09G_37.9-153	39	80844	0.9	8.0949	2.5	6.4973	2.7	0.3815	1.1	0.42
09G_37.9-118	151	130666	0.9	8.0486	0.4	6.2363	1.8	0.3640	1.8	0.98
09G_37.9-139	46	64155	0.7	7.8989	1.3	6.7518	1.8	0.3868	1.2	0.67
09G_37.9-57	36	80659	2.2	6.4474	1.6	9.8462	3.0	0.4604	2.6	0.85
09G_37.9-24	65	131852	0.9	6.3972	1.5	9.1725	2.4	0.4256	1.8	0.76
09G_37.9-46	178	357315	1.3	6.3461	0.6	9.7309	1.3	0.4479	1.1	0.89
09G_37.9-101	36	46485	1.3	6.2833	1.0	10.2767	1.6	0.4683	1.2	0.79
09G_37.9-28	49	53175	2.4	6.0652	0.7	10.9307	1.7	0.4808	1.6	0.92
09G_37.9-80	143	210418	2.0	5.7386	0.6	11.4786	1.2	0.4777	1.1	0.88
09G_37.9-130	125	80288	1.5	5.5423	0.4	11.3348	1.8	0.4556	1.8	0.98
09G_37.9-161	274	267903	1.4	5.4500	0.3	13.5735	1.8	0.5365	1.8	0.99

Table A.14-2. Datatable for U-Pb geochronologic analyses for Dengying sample 37.9, 2 of 2. Ordered by increasing age.

Table A.14-2			Apparent ages (Ma)						
Analysis	206Pb*	±	207Pb*	±	206Pb*	±	Best age	±	Conc
	238U*	(Ma)	235U	(Ma)	207Pb*	(Ma)	(Ma)	(Ma)	(%)
09G_37.9-51	496	4	514	12	593	63	496	4	84
09G_37.9-92	543	9	545	12	556	45	543	9	98
09G_37.9-77	548	9	547	21	544	104	548	9	101
09G_37.9-59	548	8	550	9	558	30	548	8	98
09G_37.9-85	550	5	549	7	544	33	550	5	101
09G_37.9-158	556	5	557	9	563	42	556	5	99

Table A.14-2			Apparent ages (Ma)						
Analysis	206Pb*	±	207Pb*	±	206Pb*	±	Best age	±	Conc
	238U*	(Ma)	235U	(Ma)	207Pb*	(Ma)	(Ma)	(Ma)	(%)
09G_37.9-96	558	9	560	22	570	107	558	9	98
09G_37.9-167	559	4	561	9	569	41	559	4	98
09G_37.9-125	560	8	557	10	548	35	560	8	102
09G_37.9-144	564	8	558	11	534	43	564	8	106
09G_37.9-131	571	11	565	14	541	57	571	11	106
09G_37.9-94	737	21	748	19	779	39	737	21	95
09G_37.9-29	742	14	738	19	726	61	742	14	102
09G_37.9-17	746	12	753	26	776	96	746	12	96
09G_37.9-93	747	9	749	19	758	69	747	9	98
09G_37.9-58	747	7	748	16	749	59	747	7	100
09G_37.9-82	751	16	762	29	795	101	751	16	94
09G_37.9-60	756	6	759	12	768	44	756	6	98
09G_37.9-70	760	12	761	23	765	83	760	12	99
09G_37.9-111	760	13	750	23	723	86	760	13	105
09G_37.9-120	761	9	757	18	746	67	761	9	102
09G_37.9-102	766	24	763	32	753	103	766	24	102
09G_37.9-97	768	13	777	25	806	88	768	13	95
09G_37.9-126	769	5	759	22	729	86	769	5	105
09G_37.9-10	770	6	763	11	743	42	770	6	104
09G_37.9-114	770	12	772	20	780	69	770	12	99
09G_37.9-100	771	12	773	28	779	104	771	12	99
09G_37.9-15	773	20	772	23	770	70	773	20	100
09G_37.9-35	773	15	778	17	791	47	773	15	98
09G_37.9-110	776	12	790	20	831	70	776	12	93
09G_37.9-30	779	13	774	21	759	72	779	13	103
09G_37.9-133	780	10	772	15	749	54	780	10	104
09G_37.9-105	782	13	780	19	775	62	782	13	101
09G_37.9-40	783	10	779	14	768	43	783	10	102
09G_37.9-136	786	12	777	13	753	35	786	12	104
09G_37.9-151	786	15	778	23	754	78	786	15	104
09G_37.9-49	787	14	784	22	774	74	787	14	102
09G_37.9-39	790	7	788	13	781	47	790	7	101
09G_37.9-160	793	10	792	27	791	98	793	10	100
09G_37.9-42	794	15	799	21	813	67	794	15	98
09G_37.9-63	796	14	793	19	785	59	796	14	101
09G_37.9-45	800	17	790	20	759	62	800	17	105
09G_37.9-16	809	15	824	21	864	65	809	15	94
09G_37.9-165	810	21	812	24	816	68	810	21	99
09G_37.9-41	811	8	811	12	810	38	811	8	100
09G_37.9-69	812	12	803	24	777	84	812	12	105
09G_37.9-26	816	9	822	11	837	33	816	9	97
09G_37.9-65	817	5	816	7	813	23	817	5	101
09G_37.9-38	819	16	822	30	831	101	819	16	99
09G_37.9-66	821	9	819	9	811	22	821	9	101
09G_37.9-47	824	13	829	29	841	102	824	13	98
09G_37.9-156	826	12	827	11	829	24	826	12	100
09G_37.9-138	827	15	821	13	807	26	827	15	102
09G_37.9-1	830	8	833	24	842	86	830	8	99

Table A.14-2			Apparent ages (Ma)						
Analysis	206Pb*	±	207Pb*	±	206Pb*	±	Best age	±	Conc
	238U*	(Ma)	235U	(Ma)	207Pb*	(Ma)	(Ma)	(Ma)	(%)
09G_37.9-112	834	15	839	29	851	97	834	15	98
09G_37.9-67	836	8	837	9	838	27	836	8	100
09G_37.9-109	836	11	843	12	862	31	836	11	97
09G_37.9-43	839	8	845	21	862	74	839	8	97
09G_37.9-98	842	11	834	15	813	47	842	11	104
09G_37.9-74	847	11	848	23	850	78	847	11	100
09G_37.9-5	851	15	848	16	837	46	851	15	102
09G_37.9-23	852	39	856	31	867	45	852	39	98
09G_37.9-71	852	13	853	13	857	29	852	13	99
09G_37.9-107	852	13	841	19	811	61	852	13	105
09G_37.9-169	855	14	876	21	930	66	855	14	92
09G_37.9-86	855	12	850	16	837	51	855	12	102
09G_37.9-104	857	7	854	21	846	72	857	7	101
09G_37.9-90	862	10	858	18	848	59	862	10	102
09G_37.9-154	865	12	867	29	873	97	865	12	99
09G_37.9-61	874	14	880	21	895	65	874	14	98
09G_37.9-164	894	17	898	17	909	43	894	17	98
09G_37.9-163	911	15	898	20	865	60	911	15	105
09G_37.9-56	919	17	928	16	950	33	919	17	97
09G_37.9-116	921	12	907	19	873	60	921	12	105
09G_37.9-145	1394	16	1398	34	1406	81	1406	81	99
09G_37.9-84	1727	15	1745	19	1766	37	1766	37	98
09G_37.9-174	1821	16	1806	13	1788	22	1788	22	102
09G_37.9-88	1846	43	1892	27	1942	31	1942	31	95
09G_37.9-27	1973	23	1984	16	1996	21	1996	21	99
09G_37.9-19	2038	16	2020	9	2002	8	2002	8	102
09G_37.9-50	2050	19	2027	12	2005	13	2005	13	102
09G_37.9-153	2083	20	2046	24	2008	44	2008	44	104
09G_37.9-118	2001	31	2010	16	2018	7	2018	7	99
09G_37.9-139	2108	21	2079	16	2051	23	2051	23	103
09G_37.9-57	2441	52	2420	28	2403	27	2403	27	102
09G_37.9-24	2286	34	2355	22	2416	26	2416	26	95
09G_37.9-46	2386	23	2410	12	2430	10	2430	10	98
09G_37.9-101	2476	25	2460	14	2447	16	2447	16	101
09G_37.9-28	2531	33	2517	16	2506	11	2506	11	101
09G_37.9-80	2517	22	2563	11	2599	10	2599	10	97
09G_37.9-130	2420	36	2551	17	2657	6	2657	6	91
09G_37.9-161	2769	40	2720	17	2685	5	2685	5	103

Bibliography

1. Anbar, A.D., Duan, Y., Lyons, T. W., Arnold, G. L., Kendall, B., Creaser, R. A., Kaufman, A. J., Gordon, G. W., Scott, C., Garvin, J., Buick, R. (2007) A whiff of oxygen before the Great Oxidation Event? Science 317, 1903-1906.
2. Bartley, J.K., Knoll, A.H., Pope, M., Petrov, P. Yu., Semikhatov, M.A. and Sergeev, V.N. (1998). A Vendian-Cambrian boundary succession from the northwestern margin of the Siberian Platform: stratigraphy, palaeontology, chemostratigraphy and correlation. Geological Magazine 135: 473-494.
3. Bengtson, S.; Zhao, Y. (1992). "Predatorial Borings in Late Precambrian Mineralized Exoskeletons". Science 257 (5068): 367–9.5
4. Bengtson, S. (2004). "Early skeletal fossils". In Lipps, J.H., and Waggoner, B.M. Neoproterozoic- Cambrian Biological Revolutions. 10. 67–78.
5. Bowring, S.A. Grotzinger, J.P., Isachsen, C.E., Knoll, A.H., Pelechaty, S.M., and Kolosov, P. (1993) Calibrating rates of Early Cambrian evolution. Science 261: 1293-1298.
6. Bowring, S., Myrow, P., Landing, E., Ramezani, J., (2003). Geochronological constraints on terminal Neoproterozoic events and the rise of metazoans. Geophysical Research Abstracts 5, 219.
7. Bowring, Samuel A. and Schmitz, Mark D. (2003) High-Precision U-Pb Zircon Geochronology and the Stratigraphic Record. Reviews in Mineralogy and Geochemistry, vol. 53, 305-326.
8. Broecker, W. S. and Peng, T.-H. (1982). Tracers in the Sea. Eldigo Press, Palisades, NY.
9. Burdett, J.W., Arthur, M.A., Richardson, A., 1989. A Neogene seawater sulfate isotope age curve from calcareous pelagic microfossils. Earth Planet. Sci. Lett. 94, 189–198.
10. Canfield, D.E., Poulton, S.W., and Narbonne, G.M. (2007) Late-Neoproterozoic deep-ocean oxygenation and the rise of animal life. Science 315: 92-95.
11. Canfield, D.E., S.W. Poulton, A.H. Knoll, G.M. Narbonne, G. Ross, T. Goldberg and H. Strauss (2008). Ferruginous conditions dominated later Neoproterozoic deep-water chemistry. Science, 321, pp. 949–952.
12. Condon D, et al. (2005) U-Pb ages from the Neoproterozoic Doushantuo Formation, China. Science 308:95–98.
13. Dahl, T. W., Hammarlund, E. U., Anbar, A. D., Bond, D. P. G, Gill, B. C., Gordon, G. W., Knoll, A. H., Nielsen, A. T., Schovsbo, A. H., Canfield, D. E. (2010). Devonian rise in atmospheric oxygen correlated to the radiations of terrestrial plants and large predatory fish. PNAS 107 (42) 17911-17915.
14. Deer, W. A., Howie, R. A., and Zussman, J. (1996) An Introduction to the Rock-Forming Minerals. 2nd Ed. Prentice Hall.
15. Dickin, A. P. (2005) Radiogenic Isotope Geology. 2nd Ed. Cambridge University Press.
16. Dickinson, W. R.,, Gehrels, G. E. (2008) Use of U–Pb ages of detrital zircons to infer maximum depositional ages of strata: A test against a Colorado

Plateau Mesozoic database. Earth and Planetary Science Letters 288, 115–125.
17. Faure, G. (1998) Principles and Applications of Geochemistry. 2nd Ed. Prentice Hall.
18. Fike, D. A., Grotzinger, J. P., Pratt, L. M, and Summons, R. E. (2006) Oxidation of the Ediacaran Ocean. Nature 444: 744 - 747.
19. Fike, D.A. and Grotzinger, J.P. 2007. A paired sulfate-pyrite δ34S approach to understanding the evolution of Ediacaran-Cambrian sulfur cycling. Geochimica et Cosmochimica Acta 72: 2636–2648.
20. Gehrels, G., Kapp, P., DeCelles, P., Pullen, A., Blakey, R., Weislogel, A., Ding, L., Guynn, J., Martin, A., McQuarrie, N., and Yin, A. (2011) Detrital zircon geochronology of pre-Tertiary strata in the Tibetan-Himalayan orogen. Tectonics, Vol. 30. doi:10.1029/2011TC002868
21. Gehrels, G. E., V. Valencia, and J. Ruiz (2008), Enhanced precision, accuracy, efficiency, and spatial resolution of U-Pb ages by laser ablation-multicollector-inductively coupled plasma–mass spectrometry. Geochem. Geophys. Geosyst., 9.
22. Germs, G.J.B. (1972). "New shelly fossils from Nama Group, South West Africa". American Journal of Science 272 (8): 752–761.
23. Gill, B.C., Lyons, T.W., and Frank, T.D., 2008, Behavior of carbonate-associated sulfate during meteoric diagenesis and implications for the sulfur isotope paleoproxy: Geochimica et Cosmochimica Acta, v. 72, p. 4699-4711.
24. Grazhdankin, D. V., Balthasar, U., Nagovitsin, K. E., and Kochnev, B. B., (2008). Carbonate-hosted Avalon-type fossils in arctic Siberia. Geology, v. 36, p. 803-806.
25. Habicht, K. S., Gade, M., Thamdrup, B., Berg, P., and Canfield, D. E. (2002) Calibration of Sulfate Levels in the Archean Ocean. Science 298, 2372.
26. Hayes, J. M., Strauss, H., and Kaufman, A. J. (1999) The abundance of 13C in marine organic matter and isotopic fractionation in the global biogeochemical cycle of carbon during the past 800 Ma. Chemical Geology 161, 103–125
27. Helz, G.R., Miller, C. V., Charnock, J.M., Mosselmans, J. F. W., Parttrick, R. A. D., Garner, C. D., and Vaughn, D. J. (1996). Mechanism of Molybdenum Removal from the Sea and Its Concentration in Black Shales; EX AFS Evidence. Geochimica et Cosmochimica Acta, 60, 3631 - 3642.
28. Kampschulte A., Bruckschen P. and Strauss H. (2001) The sulphur isotopic composition of trace sulphates in Carboniferous brachiopods: implications for coeval seawater, correlation with other geochemical cycles and isotope stratigraphy. Chem. Geol. 175, 149–173.
29. Kampschulte A. and Strauss H. (2004) The sulfur isotopic evolution of Phanerozoic seawater based on the analysis of structurally substituted sulfate in carbonates. Chem. Geol. 204, 255–286.
30. Kaufman, A.J., Corsetti, F.A., and Varni, M.A. (2007) The effect of rising atmospheric oxygen on carbon and sulfur isotope anomalies in the Neoproterozoic Johnnie Formation, Death Valley, USA. Chemical Geology 237: 47-63.

31. Kaufman, A.J., Jacobsen, S.B. and Knoll, A.H. (1993) The Vendian record of C- and Sr-isotopic variations: Implications for tectonics and paleoclimate. Earth and Planetary Science Letters 120: 409-430.
32. Kaufman, A.J. and Knoll, A.H. (1995) Neoproterozoic variations in the carbon isotopic composition of seawater: Stratigraphic and biogeochemical implications. Precambrian Research 73: 27-49.
33. Knauth, L. P., and Kennedy, M. J. (2009). The late Precambrian greening of the Earth. Nature, v. 460, p. 728-732.
34. Knoll, A. H., John P. Grotzinger, Alan J. Kaufman, Petr Kolosov (1995). Integrated approaches to terminal Proterozoic stratigraphy: an example from the Olenek Uplift, northeastern Siberia. Precambrian Research 73: 251-270.
35. Kouchinsky, A., Bengston, S., Pavlov, V. E., Runnegar, B., Torssander, P., Young, E. & Ziegler, K. 2007. Carbon isotope stratigraphy of the Precambrian– Cambrian Sukharikha River section, northwestern Siberian platform. Geological Magazine 144, 1–10.
36. Kouchinsky, A., Bengston, S., , Runnegar, B., Skovsted, C., Steiner, M., and Vendrasco, M. (2011). Chronology of early Cambrian biomineralization. Geological Magazine, 1–31. doi:10.1017/S0016756811000720
37. Ling, H. F., Chen, X., Li, D., Wang, D., Shields-Zhou, G. A., and Zhu, M. (2011) Cerium anomaly variations in Ediacaran–earliest Cambrian carbonates from the Yangtze Gorges area, South China: Implications for oxygenation of coeval shallow seawater, Precambrian Research. Available online 19 October 2011, ISSN 0301-9268, 10.1016/j.precamres.2011.10.011.
38. Lyons TW, Hurtgen MT, Gill BC (2005) New insight into the utility of carbonate-associated sulfate. Geochim Cosmochim Acta 69:A128.
39. Lyons TW, Walter LM, Gellatly AM, Martini AM, Blake RE (2004) in Sulfur Biogeochemistry: Past and Present (GSA Special Paper 379), eds. Amend JP, Edwards KJ, Lyons TW (Geol. Soc. Am., Boulder, CO), pp. 161-176.
40. Maloof, Adam C., Porter, Susannah M., Moore, John L., Dudas, Frank A., Bowring, Samuel A., Higgins, John A., Fike, David A., Eddy, Michael P. (2010) The earliest Cambrian record of animals and ocean geochemical change. Geological Society of America Bulletin, 122, 1731-1774.
41. Marenco, P.J., Corsetti, F.A., Hammond, D.E, Kaufman, A.J., and Bottjer, D.J. (2008a) Oxidation of pyrite during extraction of carbonate associated sulfate. Chemical Geology 247: 124-132.
42. Marenco, P.J., Corsetti, F.A., Kaufman, A.J., and Bottjer, D.J. (2008b) Environmental and diagenetic variations in carbonate associated sulfate: An investigation of CAS in the Lower Triassic of the western USA. Geochimica Cosmochimica Acta 72: 1570-1582.
43. McFadden, K.A., Jing Huang, Xuelei Chu, Ganqing Jiang, Kaufman, A.J., Chuanming Zhou, Xunlai Yuan, and Shuhai Xiao (2008) Pulsed oxidation and biological evolution in the Ediacaran Doushantuo Formation. Proceedings of the National Academy of Sciences of the USA 105: 3197-3202.
44. Narbonne, G. M., Gehling, J. G., (2003). Life after snowball: The oldest complex Ediacaran fossils. Geology 31, 27.

45. Pelechaty, S., Kaufman, A.J. and Grotzinger, J.P. (1996a) Evaluation of $\delta^{13}C$ isotope stratigraphy for intrabasinal correlation: Data from Vendian strata of the Olenek uplift and Kharaulakh Mountains, Siberian platform, Russia. The Bulletin of the Geological Society of America 108: 992-1003.
46. Pelechaty, S.M., Grotzinger, J.P., Kashirtsev, V.A., and Zhernovsky, V.P. (1996b) Chemostratigraphic and sequence stratigraphic constraints on Vendian-Cambrian basin dynamics, northeastern Siberian craton. Journal of Geology 104: 543-564.
47. Ries, J. B., Fike, D. A., Pratt, L. M., Lyons, T. W., and Grotzinger, J. P. (2009) Superheavy pyrite ($\delta^{34}S_{pyr} > \delta^{34}S_{CAS}$) in the terminal Proterozoic Nama Group, southern Namibia: A consequence of low seawater sulfate at the dawn of animal life. Geology, 37; no. 8; p. 743–746.
48. Rogov, V., Marusin, V., Bykova, N., Goy, Y., Nagovitsin, K., Kochnev, B., Karlova, G., and Grazhdankin, D. (2012). The oldest evidence of bioturbation on Earth.
49. Geology, G32807.1, first published on March 19, 2012, doi:10.1130/G32807.1
50. Rothman, D.H., Hayes, J.M., Summons, R.E. (2003). Dynamics of the Neoproterozoic carbon cycle. Proceedings of the National Academy of Sciences, U.S.A. 100 (14): 124-129.
51. Shen, B., Xiao, S, Zhou, C., Kaufman, A. J., and Yuan, X. (2010). Carbon and sulfur isotope chemostratigraphy of the Neoproterozoic Quanji Group of the Chaidam Basin, NW China: Basin stratification in the aftermath of an Ediacaran glaciation postdating the Shuram event? Precambrian Research 177, 241–252
52. Shen, B., Xiao, S, Bao, H., Kaufman, A. J., Zhou, C., and Yuan, X. (2011) Carbon, sulfur, and oxygen isotope evidence for a strong depth gradient and oceanic oxidation after the Ediacaran Hankalchough glaciation. Geochimica et Cosmochimica Acta 75, 1357–1373
53. Waggoner, B. (2003) The Ediacaran biotas in space and time. Integr Comp Biol 43:104 – 113.
54. Xiao, S., Kaufman, A. J., Grazhdankin, D. V., Peek, S., Bykova, N. V., Nagovitsin, K. E., Kochnev, B. B., & Rogov, V. I. (2011). Ediacaran stratigraphic correlation between South China and northern Siberia. Proceedings of the Conference, Neoproterozoic Sedimentary Basins: Stratigraphy, Geodynamics, and Petroleum Potential. Novosibirsk, Russia, 2011. 108-109.
55. Xiao, S., McFadden, K. A., Peek, S., Kaufman, A. J., Zhou, C., Jiang, G., Hu, J. (in press). Integrated chemostratigraphy of the Doushantuo Formation at the northern Xiaofenghe section (Yangtze Gorges, South China) and its implication for Ediacaran stratigraphic correlation and ocean redox models. Precambrian Research, in press.
56. Zhou, C., and S. Xiao (2007) Ediacaran $\delta^{13}C$ chemostratigraphy of South China. Chemical Geology 237: 89-108.